

KNOWLEDGE EXTRACTION FOR ORGANOMETALLIC PEROVSKITE
SOLAR CELLS FROM PUBLISHED DATA IN LITERATURE

by

Çağla Odabaşı Özer

B.S., Chemical Engineering, Hacettepe University, 2010

M.S., Chemical Engineering, Boğaziçi University, 2013

Submitted to the Institute for Graduate Studies in
Science and Engineering in partial fulfillment of
the requirements for the degree of
Doctor of Philosophy

Graduate Program in Chemical Engineering
Boğaziçi University
2019

*Dedicated to my parents
For their endless love, support and encouragement*

ACKNOWLEDGEMENTS

First and foremost, I would like to express my very great appreciation to Prof. Ramazan Yıldırım for his invaluable and constructive suggestions during the planning and development of this research work with his priceless guidance and experience. His willingness to give his time so generously has been very much appreciated. This dissertation would not have been possible without his inspiration and effort.

I would like to express my great appreciations for my dear thesis committee members, Prof. Ahmet Erhan Aksoylu, Assoc. Prof. Hasan Bedir, Assoc. Prof. Tuğba Davran-Candan and Assoc. Prof. Alper Uzun for spending their time and their contributions to my dissertation. I am also grateful to Prof. Zeynep İlsen Önsan, Prof. Ahmet Erhan Aksoylu, Prof. Mehmet Çamurdan, Assoc. Prof. Kerem Uğuz and Assoc. Prof. Burak Alakent for their sincere support and guidance during my PhD education. It was a great opportunity for me to learn from their experience and knowledge. I am also thankful to Assoc. Prof. Erdem Günay for his inspiration and support.

I would like to thank to my friends M. Selcen Başar, Elif Can, Merve Eropak, Aybüke Leba, A. İpek Paksoy, Ali Uzun, and all the other past and present graduate members of Department of Chemical Engineering. I was very lucky to spend many years with them. Also, I would like to thank to A. Sinem Özyurt Uğuz, Şükrü Ordu, Murat Düzgünoğlu, Yakup Bal and Belgin Balkan for their technical aid as well as their friendship.

The financial support provided by Boğaziçi University Research Fund through Project 16A05TUG2 is also gratefully acknowledged.

Finally, I wish to thank to my dearest family members starting from my husband A. Alp Özer; my parents Mustafa Odabaşı and Dilek Odabaşı; my brother Çağrı Odabaşı for their love, support, motivation and encouragement in my whole life. None of this would have been possible without the love and patience of my family.

ABSTRACT

KNOWLEDGE EXTRACTION FOR ORGANOMETALLIC PEROVSKITE SOLAR CELLS FROM PUBLISHED DATA IN LITERATURE

Organolead halide perovskite solar cells (PSCs) have been attracted great attention in recent years. This rapid progress is due to excellent light absorption and charge-carrier mobilities of the perovskite materials besides its low-cost and easy processing conditions. In addition to high power conversion efficiency (PCE), reproducibility, hysteresis and long-term stability of perovskite solar cells are major factors to be solved before commercialization of this technology. The objective of this dissertation is to extract useful knowledge from literature to improve the overall performance of this technology for commercialization. The extensive datasets for PCE, reproducibility, hysteresis and long-term stability of PSCs were constructed from the published papers in literature and analyzed using machine-learning tools to determine the effects of materials and perovskite deposition methods employed during cell manufacturing. The evolution of PCE with time was statistically analyzed under different circumstances (i.e. using different materials types or perovskite deposition methods). Then, the databases for PCE, hysteresis and long-term stability were modeled using random forest, association rule mining and decision tree methods to detect the most effective variables and combinations leading to high performance. For reproducibility, pooled variances of different factors were calculated and compared. The mixed cation perovskites, doped mesoporous TiO_2 (second electron transfer layer) and $\text{LiTFSI}+\text{TBP}+\text{FK209}$ (additive to hole transfer materials) were found to promote high efficiency, reproducibility and stability while they lowered the hysteresis; SnO_2 (compact ETL), $\text{DMF}+\text{DMSO}$ (solvent) and diethyl ether (anti-solvent) also had positive effects on these cell characteristics except hysteresis. Hence, it was concluded that the common factors which led high PCE, also led high reproducibility, low hysteresis and long-term stability. Additionally, our findings were in a reasonable agreement with the literature showing that the data mining and statistics can be used effectively to derive general results and detect trends, which can not be seen by naked eyes.

ÖZET

ORGANOMETALİK PEROVSKİT GÜNEŞ HÜCRELERİ İÇİN LİTERATÜRDEN BİLGİ ÇIKARIMI

Organometalik perovskit güneş hücreleri son yıllarda büyük ilgi görmüş, bu hızlı gelişmeyi, mükemmel ışık absorpsiyonu, yük taşıyıcı hareketlilikleri sahip olmaları, düşük maliyetleri ve kolay işlenebilir olmaları sağlamıştır. Tekrarlanabilirlik, akım-voltaj gecikimi ve uzun süreli kararlılığın sağlanamaması, verimi arttırmanın yanında ticarileşmenin önündeki diğer engellerdir. Tezin amacı, bu teknolojinin gelişmesi ve ticarileşmesi için literatürden yararlı bilgi çıkarımı yapmaktır. Verimlilik, tekrarlanabilirlik, gecikim ve uzun süreli kararlılıkla ilgili yayınlar kullanılarak kapsamlı veri tabanları oluşturulmuş ve yapay öğrenme yöntemleri kullanılarak hücre üretiminde kullanılan malzeme ve perovskit kaplama yöntemlerinin etkileri analiz edilmiştir. Öncelikle verimlilik analizinde, güç dönüşüm verimliliğinin çeşitli koşullar altında (örneğin, değişik malzeme veya perovskit kaplama yöntemleri) zamana göre değişimi istatistiksel olarak analiz edilmiştir. Daha sonra, verimlilik, tekrarlanabilirlik, gecikim ve uzun süreli kararlılık için oluşturulan veri tabanları, yüksek performans için en etkili değişkenleri ve kombinasyonlarını saptamak üzere rastlantısal orman, birliktelik kural çıkarımı ve karar ağaçları yöntemleriyle modellenmiştir. Tekrarlanabilirlik analizinde ise değişik faktörlerin toplu varyansları hesaplanmış ve birbiriyle karşılaştırılmıştır. Birden fazla katyon içeren perovskitler, katkılı gözenekli TiO₂ (ikinci electron taşıyıcı katman) ve LiTFSI+TBP+FK209'un (deşik taşıma katmanı için katkı) gecikimi azaltırken, yüksek verimi, çoğaltılabilirliği ve kararlılığı arttırdığı bulunmuştur; SnO₂ (kompakt elektron taşıma katmanı), DMF+DMSO (çözücü) ve dietil eterin (anti-çözücü) ise gecikim dışındaki faktörler üzerinde olumlu etkisi olduğu saptanmıştır. Sonuç olarak, ortak faktörlerin hem yüksek güç dönüşümünü sağladığı hem de yüksek tekrarlanabilirlik, uzun süreli kararlılık ve düşük gecikime de neden olduğu sonucuna varılmıştır. Ayrıca, bulguların literatürle büyük ölçüde uyumlu olması, yapay öğrenme yöntemlerinin ve istatistiğin çıplak gözle görülemeyen genel sonuçları ve eğilimleri saptamada etkin olarak kullanılabileceğini göstermektedir.

TABLE OF CONTENTS

ABSTRACT	v
ÖZET	vi
LIST OF FIGURES	x
LIST OF TABLES	xv
LIST OF ACRONYMS/ABBREVIATIONS	xx
1. INTRODUCTION	1
2. REVIEW OF THE LITERATURE	4
2.1. Review of Perovskite Solar Cell Performance	5
2.1.1. Effect of Perovskite Type	7
2.1.2. Effect of Perovskite Deposition	10
2.1.3. Effect of Electron Transfer Layer	13
2.1.4. Effect of Hole Transfer Layer	15
2.1.5. Effect of Back Contact	18
2.1.6. Reproducibility	18
2.1.7. Hysteresis	19
2.2. Review of Long-term Stability of Perovskite Solar Cells	20
2.2.1. Effect of Ambient Conditions	21
2.2.2. Effect of Perovskite Type	22
2.2.3. Effect of Perovskite Deposition	23
2.2.4. Effect of Electron Transfer Layer	25
2.2.5. Effect of Hole Transfer Layer	27
2.2.6. Effect of Back Contact	29
2.3. Data Mining and Methods	29
2.3.1. Association Rule Mining	30
2.3.2. Decision Trees	31
2.3.3. Random Forests	33
2.3.4. Data Mining in Field of Solar Energy	33
3. METHODS	36
3.1. Database Construction	36
3.2. Analysis and Computational Methods	44
3.2.1. Analysis of Power Conversion Efficiency	44
3.2.1.1. Descriptive Statistical Analysis	44

3.2.1.2. Random Forest Regression.....	46
3.2.1.3. Association Rule Mining.....	46
3.2.1.4. Decision Tree Analysis.....	46
3.2.2. Analysis of Reproducibility.....	48
3.2.3. Analysis of Hysteresis.....	49
3.2.3.1. Random Forest Regression.....	49
3.2.3.2. Association Rule Mining.....	50
3.2.3.3. Decision Tree Analysis.....	50
3.2.4. Analysis of Long –term Stability.....	50
3.2.4.1. Random Forest Regression.....	51
3.2.4.2. Association Rule Mining.....	51
3.2.4.3. Decision Tree Analysis.....	51
4. RESULTS AND DISCUSSION.....	52
4.1. Analysis of Power Conversion Efficiency.....	52
4.1.1. Comparison of Stabilized Efficiency Dataset with Entire Database.....	52
4.1.2. Descriptive Statistical Analysis of Power Conversion Efficiency.....	54
4.1.2.1. Effect of Perovskite Type.....	55
4.1.2.2. Effect of Perovskite Deposition.....	58
4.1.2.3. Effect of Electron Transfer Layer.....	64
4.1.2.4. Effect of Hole Transfer Layer.....	66
4.1.2.5. Effect of Back Contact.....	69
4.1.2.6. Evolution of Maximum Efficiency.....	69
4.1.3. Predicting the Stabilized Efficiency by Random Forest Analysis.....	72
4.1.4. Analysis of Factor Effects on Power Conversion Efficiency by Association Rule Mining.....	74
4.1.5. Developing Heuristics for High Power Conversion Efficiency by Decision Tree Analysis.....	80
4.2. Analysis of Reproducibility.....	86
4.3. Analysis of Hysteresis.....	91
4.3.1. Predicting the Hysteresis Index by Random Forest Analysis.....	92
4.3.2. Analysis of Factors Effects on Hysteresis by Association Rule Mining.....	93
4.3.3. Developing Heuristics for Low Hysteresis by Decision Tree Analysis.....	101
4.4. Analysis of Long-term Stability.....	102
4.4.1. Predicting the Degradation by Random Forest Analysis.....	103
4.4.2. Analysis of Factor Effects on Stability by Association Rule Mining.....	103
4.4.3. Developing Heuristics for High Stability by Decision Tree Analysis.....	111
5. CONCLUSION.....	114

REFERENCES	119
APPENDIX A: ADDITIONAL INFORMATION ON ANALYSIS OF PCE.....	166
APPENDIX B: ADDITIONAL INFORMATION ON ANALYSIS OF REPRODUCIBILITY	182
APPENDIX C: ADDITIONAL INFORMATION ON ANALYSIS OF HYSTERESIS .	186
APPENDIX D: ADDITIONAL INFORMATION ON ANALYSIS OF LONG-TERM STABILITY	201

LIST OF FIGURES

Figure 2.1. Number of publications on (a) perovskite solar cells (b) perovskite solar cells reporting stabilized efficiencies.	4
Figure 2.2. Commonly studied perovskite cell structures in literature (a) regular mesoporous, (b) regular planar, (c) inverted cell.	6
Figure 2.3. 3D AMX ₃ perovskite structure; A: large cation, B: smaller metal cation, X: anion[33].	8
Figure 2.4. Number of publications on stability of perovskite solar cells.	20
Figure 2.5. Decision tree model.	32
Figure 2.6. Bootstrapping and learning ensembles.	34
Figure 3.1. Comparison of different cell storage conditions (each point represents average of minimum five data points).	39
Figure 4.1. Change in average efficiencies for three cell structure through years (a) regular mesoporous (b) regular planar (c) inverted (blue symbols are overall average for best cell efficiencies, red symbols are for stabilized efficiencies and black symbols are for best cell efficiencies of the cells which the stabilized efficiencies were given).	53
Figure 4.2. Distribution (fractions) of efficiencies in database for three cell structures (a) regular mesoporous (b) regular planar (c) inverted; blue columns show the distribution for entire dataset, red columns are for stabilized efficiencies only, green columns are best cell efficiencies of stabilized data points.	54
Figure 4.4. Comparison of number of papers published (ball size) and average efficiencies (y-axis) obtained with various perovskites through years.	56
Figure 4.5. Comparison of average efficiencies of mixed cation perovskites.	57

- Figure 4.6. Distribution of efficiency in database obtained with different common perovskites in three cell structure (a) regular (n-i-p), (b) inverted (p-i-n), (c) regular (n-i-p) mesoporous, (d) regular (n-i-p) planar.58
- Figure 4.7. Comparison of different perovskite deposition methods (a) change of average efficiencies with one-step (1S) and two-step(2S) procedures through years (b) variation of spin coating methods (spin-spin and spin-dip show sequences in 2S; spin2-3: 2-3 times spin in 1S).....59
- Figure 4.8. Distribution of data in database for one and two step deposition procedure for various cell structures (a) regular (n-i-p), (b) inverted (p-i-n), (c) regular (n-i-p) mesoporous, (d) regular (n-i-p) planar.60
- Figure 4.10. Comparison of the performance of various anti-solvents used (a) average efficiencies obtained with each anti-solvent (b) distribution of data among efficiency ranges.....62
- Figure 4.11. Average efficiencies of MAPbI₃ based cells (coated in one-step) for different thermal annealing conditions (a,b) mesoporous, (c,d) planar, (e,d) inverted cells.....63
- Figure 4.12. Efficiencies values of cells annealed at high temperatures for short time; data obtained from four papers.....64
- Figure 4.13. Comparison of ETL materials in regular (n-i-p) cells, (a) average efficiencies for mesoporous layer (b) distribution of data for mesoporous layer (c) average efficiencies for compact layer for both mesoporous and planar cells; (d) distribution of data for compact layer compact layer for both mesoporous and planar cells.....65
- Figure 4.14. Comparison of ETL materials in inverted (p-i-n) structure (a) average efficiencies, (b) distribution of data (PCBM+C60 shows that mixture of two materials was used).....66

- Figure 4.15. Comparison of common HTLs for regular (n-i-p) cells (a) change of average efficiencies through years, (b) distribution of data (points/lines for inorganic HTL are just for average, not for frequency)..... 67
- Figure 4.16. Comparison of common HTL additives in regular (n-i-p) cells (a) average efficiencies, (b) distribution of data (+ sign in entries shows that the mixture of these material was used)..... 68
- Figure 4.17. Comparison of HTLs for inverted (p-i-n) cells (a) change of average efficiencies of common HTLs through years, (b) distribution of data for common HTLs, (c) comparison of average efficiencies of HTLs including less common materials. 69
- Figure 4.18. Comparison of back contact materials (a) change of average efficiencies of common back contact materials through years for regular cells,(c) for inverted cells; (b) distribution of data for common back contact materials for regular cells, (d) for inverted cells. 70
- Figure 4.19. Evolution of efficiency for regular (n-i-p) structure (a) Logistic growth model (blue points from Ye *et al.* [333]; red data from NREL[1] , (b) successive local s curve structures in data (use of different colors is just to highlight two curve. 71
- Figure 4.20. Actual versus predicted performances by random forest model for stabilized efficiencies (a) training and (b) testing for regular (n-i-p) cells; (c) training and (d) testing for inverted cells; training plots for predictions of data used in model, testing plots for predictions of data not seen before..... 73
- Figure 4.21. Actual versus predicted performances by random forest model for entire dataset of regular cells (a) training (RMSE=2.46) (b) testing (RMSE=3.56); for entire dataset of inverted cells (c) training (RMSE=2.26) (d) testing (RMSE=3.48). 74
- Figure 4.22. Decision tree model for stabilized regular (n-i-p) cells. Percentage at the bottom of nodes is fraction of total data obeying rules imposed up to that

point; numbers in middle line are fraction of A, B and C in that node respectively; letter at the top of the node simply denotes class with the highest fraction. 81

Figure 4.23. Decision tree model of entire regular type cells (minimum split number=10, maximum depth=6, complexity parameter=0). 84

Figure 4.24. Decision tree model of entire dataset of inverted cells(minimum split number=30, maximum depth=5, complexity parameter=0). 85

Figure 4.25. Actual versus predicted hysteresis index by random forest model for (a) training and (b) testing for regular (n-i-p) cells; (c) training and (d) testing for inverted cells. 92

Figure 4.26. Decision tree model for regular (n-i-p) cells in hysteresis analysis (minimum split number=5, maximum depth=4, complexity parameter=0). 102

Figure 4.27. Actual versus predicted hysteresis index by random forest model for (a) training and (b) testing for regular (n-i-p) cells; (c) training and (d) testing for inverted cells. 103

Figure 4.28. Association rule analysis for regular (n-i-p) type cells for (a) perovskite type, (b) deposition procedure, (c) deposition method, (d) precursor solution, (e) anti-solvent treatment, (f) ETL, (g) ETL-2, (h) HTL, (i) HTL additive, (j) back contact (k) stored humidity, (l) stored condition. 106

Figure 4.29. Association rule analysis for inverted (p-i-n) type cells for (a) perovskite type, (b) deposition procedure, (c) deposition method, (d) precursor solution, (e) anti-solvent treatment, (f) ETL, (g) ETL-2, (h) HTL, (i) back contact, (j) stored humidity, (k) stored condition. 109

Figure 4.30. Decision tree model for regular (n-i-p) cells in stability analysis (minimum split number=5, maximum depth=6, complexity parameter=0). 113

Figure C.1. Decision tree model for regular (n-i-p) cells in hysteresis analysis without PCE restriction (minimum split number=5, maximum depth=6, complexity parameter=0)..... 198

Figure D.1. Decision tree model for regular (n-i-p) cells in stability analysis without PCE consideration (minimum split number=5, maximum depth=6, complexity parameter=0)..... 209

LIST OF TABLES

Table 3.1. Details of the Databases Used in Analyses.....	37
Table 3.2. Categorical Variables (Factors) Used in Machine Learning Analyses.....	40
Table 4.1. Association Rule Mining for PCE > 18.0% for Regular (n-i-p) and Inverted (p-i-n) Cells.	76
Table 4.2. Association Rule Mining for PCE > 18% for Regular Cells; Comparing the Results for Best Efficiencies of Stabilized and Entire Dataset	78
Table 4.3. Association Rule Mining for PCE > 18% for Inverted Cells; Comparing the Results for Best Efficiencies of Stabilized and Entire Dataset.	79
Table 4.4. Confusion Matrix of Regular Stabilized Dataset.....	82
Table 4.5. Confusion Matrix of Regular Entire Dataset.	85
Table 4.6. Confusion Matrix of Inverted Entire Dataset.	86
Table 4.7. Reproducibility Analysis of Regular Cells.....	87
Table 4.8. Reproducibility Analysis of Perovskite Types with Different Cell Structures (Mesoporous/Planar) in Regular Cells.	88
Table 4.9. Reproducibility Analysis of Inverted Cells.	90
Table 4.10. Association Rule Mining for HI ≤ 0.01 and PCE ≥ 10% for Regular (n-i-p) Cells with Scan Rate ≤ 0.05 V/s.....	95

Table 4.11. Association Rule Mining for $HI \leq 0.05$ and $PCE \geq 10\%$ for Regular (n-i-p) Cells with Scan Rate ≤ 0.05 V/s.....	96
Table 4.12. Multiple Factor Associations for Regular Cells with $HI \leq 0.01$ and $PCE \geq 10\%$	97
Table 4.13. Association Rule Mining for $HI \leq 0.01$ and $PCE \geq 10\%$ for Inverted (p-i-n) Cells with Scan Rate ≤ 0.05 V/s ($PCE \geq 10\%$ for All Cells).....	99
Table 4.14. Association Rule Mining for $HI \leq 0.05$ for Inverted (p-i-n) Cells with Various Scan Rates (All cells except two have $PCE \geq 10\%$).....	99
Table 4.15. Multiple factor associations for inverted (p-i-n) cells with $HI \leq 0.01$ and $PCE \geq 10\%$	100
Table 4.16. Confusion Matrix of Regular Cells Dataset.....	101
Table 4.17. Multiple Factor Associations for the Regular (n-i-p) Cells Stable More Than 60 Days with $PCE \geq 10\%$	108
Table 4.18. Multiple Factor Associations for Inverted (p-i-n) Cells Stable More Than 60 Days with $PCE \geq 10\%$	111
Table 4.19. Confusion Matrix of Regular Cells Dataset.....	112
Table 5.1. Comparison of Materials and Methods Leading to High PCE, Reproducibility and Stability as well as Low Hysteresis for Regular Cells.	117
Table 5.2. Comparison of Materials and Methods Leading to High PCE, Reproducibility and Stability as well as Low Hysteresis for Inverted Cells.....	117
Table A.1. Explanation for the Term of “others” in Figure 4.21.....	166

Table A.2 Explanation for the Term of “others” in Figure 4.22.....	167
Table A.3 Explanation for the Term of “others” in Figure 4.23.....	178
Table B.1. F-test of Pooled Standard Deviations of Perovskite Layer Related Factors in Regular (n-i-p) Cells.....	182
Table B.2. F-test of Pooled Standard Deviations of Other Layers in Regular Cells.	183
Table B.3. F-test of Pooled Standard Deviations of Perovskite Related Factors in Inverted Cells	184
Table B.4. F-test of Pooled Standard Deviations of Other Layers in Inverted Cells.....	185
Table C.1. Association Rule Mining for $HI \leq 0.01$ and $PCE \geq 10\%$ for Regular (n-i-p) Cells with Scan Rate ≤ 0.05 V/s.....	186
Table C.2. Association Rule Mining for $HI \leq 0.05$ and $PCE \geq 10\%$ for Regular (n-i-p) Cells with Scan Rate ≤ 0.05 V/s.....	187
Table C.3. Association Rule Mining for $HI \leq 0.01$ for Regular (n-i-p) Cells with Scan Rate ≤ 0.05 V/s (without PCE restriction)	188
Table C.4. Association Rule Mining for $HI \leq 0.05$ for Regular (n-i-p) Cells with Scan Rate ≤ 0.05 V/s (without PCE restriction)	189
Table C.5. Association Rule Mining for $HI \leq 0.01$ and $PCE \geq 10\%$ for Regular (n-i-p) Cells with Various Scan Rates	190
Table C.6. Association Rule Mining for $HI \leq 0.05$ and $PCE \geq 10\%$ for Regular (n-i-p) Cells with Various Scan Rates.	191

Table C.7. Association Rule Mining for $HI \leq 0.01$ for Regular (n-i-p) Cells with Various Scan Rates (without PCE restriction).	193
Table C.8. Association Rule Mining for $HI \leq 0.05$ for Regular (n-i-p) Cells with Various Scan Rates (without PCE restriction).	194
Table C.9. Association Rule Mining for $HI \leq 0.01$ and $PCE \geq 10\%$ for Inverted (p-i-n) Cells with Scan Rate ≤ 0.05 V/s ($PCE \geq 10\%$ for All Cells)	196
Table C.10. Association Rule Mining for $HI \leq 0.01$ for Inverted (p-i-n) Cells with Various Scan Rates (all cells except two have $PCE \geq 10\%$).....	197
Table C.11. Confusion Matrix of Hysteresis Analysis of Regular Cells without PCE Restriction	199
Table C.12. Explanation for the Term of “others” in Figure 4.25.....	199
Table C.13. Explanation for the Term of “others” in Figure C.1.	200
Table D.1. Association Rule Mining for Regular (n-i-p) Cells with $PCE \geq 10\%$ Stable More Than 15 Days	201
Table D.2. Association Rule Mining For Regular (n-i-p) Cells Stable More Than 30 Days.....	203
Table D.3. Association Rule Mining for Regular (n-i-p) Cells Stable More Than 60 Days.....	204
Table D.4. Association Rule Mining for Inverted (p-i-n) Cells Stable More Than 15 Days.....	205
Table D.5. Association Rule Mining for Inverted (p-i-n) Cells Stable More Than 30 Days.....	207

Table D.6. Association Rule Mining for Inverted (p-i-n) Cells Stable More Than 60 Days.....208

Table D.7. Confusion Matrix of Regular Cells Without PCE Consideration.....210

Table D.8. Explanation for the Term of “others” in Figure 4.29.....210

Table D.9. Explanation for the Term of “others” in Figure D.1.....210

LIST OF ACRONYMS/ABBREVIATIONS

2D	Two Dimensional
3D	Three Dimensional
ETL	Electron Transport Layer
FA	Formamidinium
FTO	Fluorine doped Tin Oxide
HTL	Hole Transport Layer
ITO	Indium Tin Oxide
MA	Methylammonium
NREL	National Renewable Energy Laboratory
PCE	Power Conversion Efficiency
PSC	Perovskite Solar Cell

1. INTRODUCTION

The metal halide perovskite solar cells (PSCs) have been among the most popular research topics in recent years; the power conversion efficiency rose to 23.7% in a few years making this potentially low cost device a serious alternative for the current solar technologies[1]. This remarkable success came from the contributions of hundreds of researchers around the world, then in return attracted more attention creating a virtuous cycle. Indeed, the number of research articles listed by Web of Science was exceeded 10000 within a decade (with the keyword search of perovskite solar in topic segment on 16.01.2019), and these efforts seem to be continued in the future since there are still significant obstacles to overcome to commercialize this promising technology.

Perovskite based solar cells have emerged from the dye sensitized solar cells; first perovskite solar cells were created with a motivation to find better absorbers than conventional dyes. Organolead perovskite materials have a suitable band gap, high light absorption coefficient, long electron and hole diffusion lengths, easy processing conditions and low cost[2]; these properties made the perovskite solar cells the most promising solar technology of recent years.

However, the challenges in long term stability remained unsolved preventing the commercialization of this promising technology; consequently, there has been a considerable shift in research focus to stability, which has been also improved, in recent years. For example, Grancini *et al.*[3] achieved stability of solar modules more than 10000 hours without PCE loss using 2D/3D perovskites. Additionally, the hysteresis, which complicates PCE measurement, and reproducibility, which is essential for large-scale fabrication, should be also understood because all these three cell characteristics are affected from the morphology of the cells and crystallization process that are highly dependent on materials and deposition methods[4-6]; hence, they may be linked. Indeed, Saliba *et al.*[7] argued that the hysteresis, which has significant effects on efficiency measurement, may also influence the reliability of aging tests, may also influence the reliability of aging tests (i.e.

test for long term stability) suggesting a new testing protocol involving maximum power point tracking.

When the huge amount of experimental research on organic solar cells is considered, it can be concluded that a significant amount of knowledge has been accumulated in the literature over the years. However, this accumulation is difficult to be utilized effectively by naked eyes because it was distributed over a very large number of publications and different parameters were studied in each publication. Hence, some data mining tools can be used in order to extract knowledge from these data and feed the results to the experimental works to help to develop more effective solar cells. Data mining can help to have a better understanding of results by discovering patterns and make useful predictions; the functions like classification, clustering, description, estimation and prediction can be performed using data mining tools. Some of the common data mining tools are multiple linear regression, multiple logistic regression, decision trees, random forests, association rule mining and artificial neural networks.

In this dissertation, the power conversion efficiency (PCE), reproducibility, hysteresis and long-term stability aspects of perovskite solar cells are analyzed using various data mining methods. Evolution of PCE and factors affecting PCE are given in the first part of Literature Survey (Section 2.1). The developments on long-term stability as well as some remarks on cell reproducibility and hysteresis are introduced in the second part of Literature Survey (Section 2.2). A general information on data mining methods are also presented in Section 2.3. In Section 3, all detailed procedures for analyses are explained including database construction, analysis and computational methods.

The analysis of power conversion efficiency is presented in the first part of Results and Discussion (Section 4.1). The difference between stabilized and best efficiencies reported in articles are compared in a statistical point of view in Section 4.1.1. Section 4.1.2 presents a review and statistical analysis of a database containing 1921 solar cell device performance data points extracted from 800 publications on the organo-lead halide perovskite solar cell published between 2013-2018. The aim is to review the literature to capture the major patterns in cell performance in the past and compare the effect of factors affecting efficiency. In Section 4.1.3, Section 4.1.4 and Section 4.1.5, the database is

analyzed using machine learning tools to develop heuristics and models to predict the cell performance. The maximum efficiencies reported each year were also modelled using logistic growth curve to check if the PCE evolution obeyed the classical logistic curve behavior, which is common in the development of new technologies.

In Section 4.2, the reproducibility dataset having 838 cases (samples) containing 24142 cells from 439 papers was analyzed to compare factors affecting cell reproducibility using pooled variances. The hysteresis data for 387 cells from 194 papers and stability profiles (power conversion efficiency versus time plots) for 404 cells from 181 papers were analyzed using random forest, association rule mining and decision trees similar to PCE analysis to determine the effects of materials and perovskite deposition methods employed during cell manufacturing and their results are given in Section 4.3 and Section 4.4, respectively.

2. REVIEW OF THE LITERATURE

The metal halide perovskite solar cells (PSCs) have been among the most popular research topics in recent years since perovskite based solar cells were selected as one of the Breakthrough of the Year by both Science and Nature magazine in 2013. The power conversion efficiency rose to 23.7% in less than 10 years [1]. In this short period of time, the number of research articles listed by Web of Science was exceeded 10000 as given in Figure 1a (with the keyword search of perovskite solar in topic segment on 16.01.2019); Figure 1b shows the number of papers reporting stabilized efficiencies (with the keywords of perovskite solar and stabilized efficiency or steady state efficiency) as it will be discussed later.

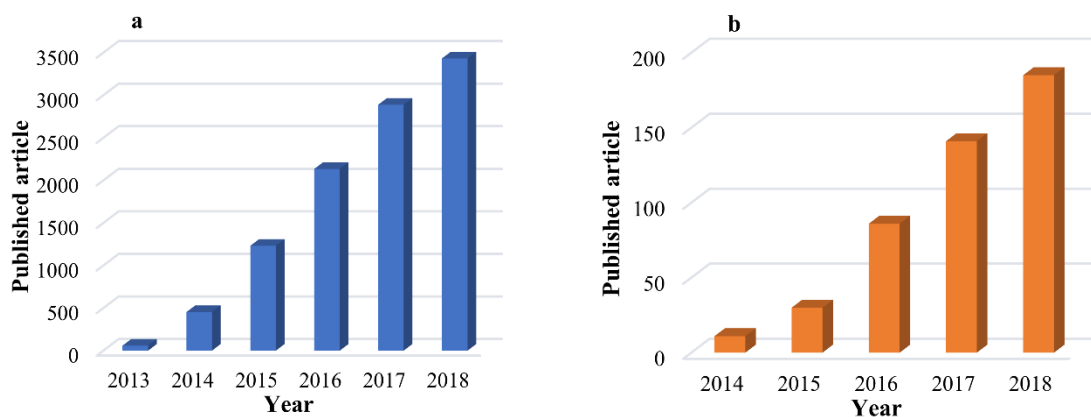


Figure 2.1. Number of publications on (a) perovskite solar cells (b) perovskite solar cells reporting stabilized efficiencies.

These efforts seem to be continued in the future since there are still significant obstacles to overcome to commercialize this promising technology. The main bottlenecks of the perovskite solar cell technology are long-term stability and degradation. Many factors such as environmental conditions and the defects on the surfaces might increase degradation and reduce the stability; hence a great amount of publications have been published in the literature to solve these issues. Although, there is a significant improvement on perovskite stability, this issue is still unsolved for the commercialization of this technology.

2.1. Review of Perovskite Solar Cell Performance

Originally, perovskite solar cells emerged from dye-sensitized cells in the pursuit of finding better absorbers. MAPbI₃ and MAPbBr₃ were initially employed with liquid electrolyte cell replacing dyes, and their initial efficiencies were found as 0.4% and 2.2% [8], [9]. Although MAPbI₃ initially resulted in lower conversion efficiency than MAPbBr₃, it was proven to be better in later works. Progress in the field had continued and Im *et al.* reached to the PCE of 6.5% in 2011 [10]. However, the perovskite was degraded by the liquid electrolyte and this problem was solved by replacing it with a solid-state hole conducting material, spiro-OMeTAD, which was a turning point in the field. Kim *et al.* has reached to the PCE of 9.7% in solid state cell by depositing perovskite on mesoporous TiO₂ layer and using spiro-OMeTAD as hole conducting layer [11]; a cell with typical mesoporous structure was shown in Figure 2.2a. In the same year, Lee *et al.* reached to 10.9 % efficiency using MAPbI_{3-x}Cl_x; they also replaced mesoporous TiO₂ with mesoporous Al₂O₃, which acts as a scaffold to perovskite (not an electron transfer layer) [12]. The PCE of 15.0% (14.1% certified) was achieved by introducing a sequential deposition of perovskite film instead of one step solution based coating; this was reported to prevent the uncontrolled precipitation of perovskite and non-homogenous surface morphology [13]. Later, the mesoporous layer was eliminated, and a simple planar architecture perovskite solar cell (Figure 2.2b) with PCE of 15.4% was introduced by Liu *et al.* by depositing perovskite layer by two-source thermal evaporation method that is suitable to deposit highly uniform films [14]. Jeon *et al.* obtained a highly uniform and dense perovskite layer with improved PCE of 16.2% by solvent modifications in 2014 [15]. In the same year, Zhou *et al.* reached to the PCE of 19.3% in planar configuration with yttrium doped compact TiO₂ layer [16]. The hysteresis also started to be considered in characterization of cells in 2014, and since then, the stabilized power conversion efficiencies has been also reported in some publications [10,11]. The 20.0 % limits for PCE was reached in 2015; Yang *et al.* obtained a PCE of 20.2 % using formamidinium based solar cells and improving perovskite crystallization [18]. Saliba *et al.* reported a PCE value for 21.1% using a more stable triple cation perovskite by adding cesium [19]. The PCE was further improved to 22.1% by forming the perovskite by intramolecular exchanging process [20]. Afterwards, the highest power conversion efficiency of 22.7% and 23.3% were published by NREL[1]; recently, Jeon *et al.* also reported a best efficiency of 23.2% under reverse scan with a steady state efficiency of 22.85% by employing a fluorene-

terminated hole-transporting material [21]. Lastly, Oxford PV set last record to 23.7% using a tandem perovskite-silicon architecture[1].

Although regular structure is the first and still the most commonly used PSC design (the record efficiencies also belong to this structure), the inverted structure cells (Figure 2.2c) had also attracted attention since 2013 due to their potential lower processing cost and flexibility. These cells are prepared starting from the transparent front electrode, and they are deposited in the order of HTL-Perovskite-ETL layers as opposite to the regular cells; their materials are cheaper, have lower sintering temperatures, and more convenient for the flexible substrates [22].

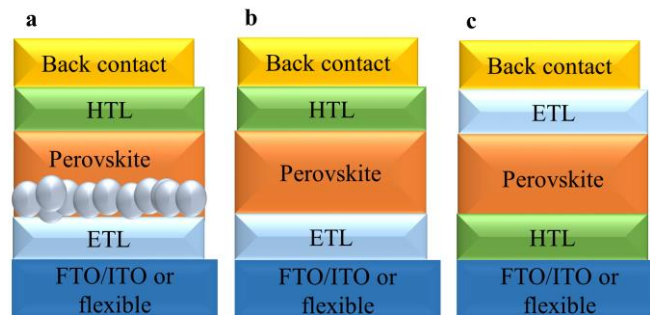


Figure 2.2. Commonly studied perovskite cell structures in literature (a) regular mesoporous, (b) regular planar, (c) inverted cell.

The first study on inverted cells achieved a PCE of 3.9% by Jeng *et al.* using the most common HTL, PEDOT:PSS, and a fullerene derivative ETL [23]. Liang *et al.* reached a PCE of 11.8% by using additives in perovskite precursor solution, which enhanced crystallization [24]; the efficiency was improved to 15.4% in the same period by depositing the perovskite layer using interdiffusion method [25]. In another study in 2014, PCE reached to 16.3% with the application of two-step spin coating of perovskite again between an optimized PEDOT:PSS and PCBM layer [26]. In 2015, the morphology of the perovskite was improved further by using solution processed hot casting technique and a pinhole free perovskite layer with millimeter scale grains was synthesized; the efficiency was 17.7% [27]. Bi *et al.* also synthesized large grain sized perovskite layer using a non-wetting hole transport layer, and PCE was improved to 18.3% [28]. Then, by employing SnO₂ as an effective electron transfer layer and a robust barrier for oxygen and moisture, Zhu *et al.* fabricated a high efficiency

inverted type cell (PCE of 18.8%) with high stability [29]. In the same year, Rao *et al.* synthesized an inverted cell with the efficiency of 19.0% by employing Cl incorporation during the $\text{MAPbI}_{3-x}\text{Cl}_x$ preparation with CuO_x as HTL [30]. In 2017, the efficiency of 20.2% was achieved by employing dual source precursor solution for mixed cation perovskite by Luo *et al.*[31]. Recently, Luo *et al.* achieved 20.9% certified efficiency in inverted cells by proposing a solution-processed secondary growth method which reduced nonradiative recombination [32].

The first PSC design, which is usually called as mesoporous regular structure, involved the deposition of an electron transport layer (ETL) over a transparent front electrode followed by perovskite active layer, hole transport layer (HTL) and metal back electrode; some other cell structures (like planar and inverted cells) have been also evolved with time. There are numerous options for the materials, solvents and deposition methods used for each layer creating a vast experimental domain involving large number of factors. For example, the perovskite layer has been improved through the past five years by modifying the perovskite structure itself by doping or replacing the halide, metal and organic parts with various options, improving the deposition strategies and techniques (one-step, two-step, spin coating, dip coating vapor deposition and so on) and testing numerous solvent combinations, anti-solvents and additives. The situation is not any different for ETL and HTL. If all options for the material and the methods are considered, the number of configurations one can use to create a PSC is almost endless. This wide and versatile experimental domain is one of the main reasons for the remarkable progress in the performance, which is usually measured by power conversion efficiency (stability has been also attracting more attention in recent publications), and inconceivable number of paper published in last few years creating a massive accumulation of experience in the literature.

2.1.1. Effect of Perovskite Type

Perovskite were named by Lev Perovski who first characterized its unique AMX_3 structure. In organolead halide perovskites, A is an organic cation (mostly organic methylammonium (MA), formamidinium (FA) or inorganic Cs), M represents a smaller cation (mostly Pb^{2+}) and X site is halide part (typically I, Br, or Cl) (Figure 2.3). As mentioned above, MAPbBr_3 performed better in the initial trials; however, MAPbI_3 took the

lead in a short time, and since then it has been the most commonly studied perovskite. A simple search in Web of Science (09.06.2018) using keywords of perovskite solar and names of the most commonly used perovskites with various possible names and synonyms (like perovskite solar $\text{CH}_3\text{NH}_3\text{PbI}_3$, perovskite solar MAPbI_3 , or perovskite solar methylammonium lead iodide) revealed that 64 % of the articles published in this subject involved the use of MAPbI_3 . The remaining 36% was shared by $\text{MAPbI}_{3-x}\text{Cl}_x$ (5%), MAPbBr_3 (6%), Cs based cells (9%), formamidinium cells (8%) and mixed cation cells (4%) and lead-free cells (4%). Although the performance with all these perovskites increased with time because the skills and experience of the researchers as well as the material and deposition methods have been improved, some perovskites still resulted higher average efficiencies than the others did.

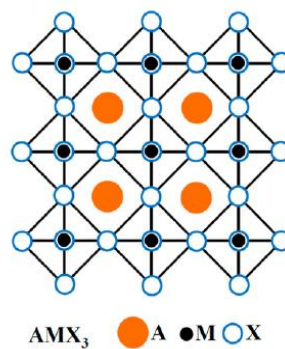


Figure 2.3. 3D AMX₃ perovskite structure; A: large cation, B: smaller metal cation, X: anion[33].

The Cl^- addition in perovskite cells was first studied by Lee *et al.* in 2012, and the performance was reached to 10.9 % in mesoporous cells; they claimed that Cl^- addition made the perovskite a better light absorber and more stable than MAPbI_3 [12]. Stranks *et al.* also tested $\text{MAPbI}_{3-x}\text{Cl}_x$ in planar structure, and they obtained a PCE of 12.0% higher than PCE of 4.0% obtained with MAPbI_3 perovskite. They reported that the electron-hole diffusion length of $\text{MAPbI}_{3-x}\text{Cl}_x$ was exceeding one micrometer which was 10 times higher than MAPbI_3 as the cause of higher efficiency [34]. Some efforts on changing or modifying the deposition method of $\text{MAPbI}_{3-x}\text{Cl}_x$ layer further improved the efficiency[30,31]. There have been also several other attempts to improve the performance of $\text{MAPbI}_{3-x}\text{Cl}_x$ by using different precursors like $\text{Pb}(\text{Ac})_2$ as Pb source[37] and modifications involving solvents. However, there is also reports suggesting that Cl only play a role during film formation

leading to a better film morphology and hence opto-electronic properties of MAPbI₃ but to a different structure [38].

Replacing MA with FA was another effective modification as introduced in 2014; in general, the efficiency seemed to be higher than those obtained over MA based cells; this was attributed to its band gap of 1.43 eV, which was lower than MAPbI₃ [39]. In 2014, Eperon *et al.* showed that the performance could reach to 14.2% using FAPbI₃ absorber[40]. Later, Wang *et al.*, improved PCE to 17.5% by replacing PbI₂ in formamidinium halide perovskite with a new precursor, HPbI, in one step spin coating process, and they obtained more uniform and thermally more stable FAPbI₃ perovskite[41]. Yang *et al.* has reached PCE of 20.2% by depositing high quality layer of FAPbI₃ via intramolecular exchange[18]. The power conversion efficiencies for FA/MA mixed cation perovskites were also tested and reported to be superior to single cation perovskites[42], [43].

Since the perovskites degraded mostly because of their organic parts, some researchers studied the doping or replacing that part to improve stability as well as the performance. One of the most common modifications for this purpose has been the partial or complete replacement of MA by Cs. Although the Cs-based cells have not resulted as high power conversion efficiencies as MA or FA based perovskites, their stability was reported to be significantly better[44-46]. However, the partial replacement of the organic cation with Cs was found to improve the performance as well as the photo-stability and moisture resistance of the perovskite film[47], [48]. Indeed, the cells with the mixed Cs-FA-MA cations showed the best average efficiency due to the shift of tolerance factor to a cubic phase region and eliminating the yellow phase impurities in perovskite films. Additionally, the higher thermal stability and humidity resistance was also reported [49],[50]. Incorporating Cs with FA cation only was more beneficial than doping MA only due to its narrower band gap and a more stable perovskite phase than FAPbI₃ alone [51], [52]. The FA-MA cations, which is quite common combination in the literature, also improved performance; for example, MAPbBr₃ incorporation in FAPbI₃ was reported to increase the performance and prevent the phase instability of FAPbI₃ [43].

In order to improve the performances and the stability of 3D perovskites, 2D perovskite materials such as ammonium valeric acid (AVA)[53] or phenyl ethyl ammonium (PEA)[54]

were also employed. 2D/3D perovskite engineering enabled more moisture resistant perovskite cells by acting of 2D layer as a protective window while the 3D layer supports the high charge transport. Although the average performances of 2D-3D mixed perovskites are slightly lower than other mixed cation perovskites, they are promising due to their high stability.

With the consideration that the solar cell is supposed to be an environmentally friendly, some researchers have been working on replacing the lead in perovskite with a less toxic alternative such as Sn^{2+} . Initially, lead-free perovskite cells were employed by replacing Pb^{2+} with Sn^{2+} , which is also a group 14 element. However, the chemical stability and the power conversion efficiency of MASnI_3 based cells have been always lower than those containing Pb [55], [56]. Partial insertion of Sn^{2+} to Pb^{2+} resulted more stable material and provided wider light absorbance range; however the PCE obtained was still lower than that of MAPbI_3 [57]. Bi^{+2} , Ge^{2+} , Ca^{2+} and Sr^{2+} were also used for replacing Pb^{2+} but the performance was still much lower than the cells with Pb^{2+} [58-61].

2.1.2. Effect of Perovskite Deposition

Morphological properties (such as film thickness, surface coverage, crystallinity etc.) of the perovskite layer are highly dependent on the preparation procedures, which have to be optimized. The solvents types and ratios, other additives, experimental variables and conditions during deposition process (like spinning rate and time, any extra treatments, humidity etc.) and pre/post treatment steps (like annealing temperature and time, additional treatments after deposition etc.) may have significant effects on PCE through morphological properties. As the result, significant amount of efforts has been devoted to improve the procedures and methods to control the morphology of the perovskite films.

The most important distinction in perovskite deposition procedure is whether the process was implemented in one or two steps. First and still the most common method is one-step spin coating, which is a low cost and easily applicable method; however, it was not easy to control the crystallization and obtain homogenous perovskite films with this method. Hence, many researchers have studied to improve the procedure, and these efforts led to two major directions: (1) replacing it with two-step process, and (2) improving it by

optimizing the solvent and anti-solvent use (as some named as solvent engineering). These efforts seem to be paid off. The two-step deposition procedure, which involves the sequential deposition of Pb and MA precursors, was developed to control of the crystallization and precipitation of perovskites. This technique was first introduced in 2013 by Burschka *et al.* [13]; they first coated the lead halide by spin coating and they dipped the lead halide coated surface into MAI solution; hence the perovskite was formed within the pores of TiO₂. The power conversion efficiency achieved was as high as 15.0%, which was among the highest at that time. Since then, various investigators have implemented this technique. It was argued that the perovskite coated with sequential deposition had stronger absorption capacity and higher performance [39], [62]. The perovskite penetration could also be controlled through optimizing factors like the solution concentrations and the dipping time. Although the most common way of implementing this process is spin-dip configuration, the spin-spin configuration was also tested and found to be a good candidate for perovskite deposition[63]. There are also other modifications of two-step process such as pre-heating of substrate before PbI₂ deposition, depositing PbO film instead of PbI₂, vapor treatment of coated PbI₂ films with various organic solvents such as toluene or chlorobenzene[64].

One-step procedure has also been improved much better in later years. The major cause of this change should be the efforts involving the more effective use of solvent and anti-solvent in this approach. The most common solvent types for perovskite deposition are dimethylformamide (DMF), γ -butyrolactone (GBL) and dimethyl sulfoxide (DMSO); DMF was utilized more than any other listed. Mixtures of these solvents were also used. For example, Kim *et al.* used the mixture of DMF and GBL to increase the surface coverage and uniformity of MAPbI₃ and the performance has increased[65]. Similarly, Jeon *et al.* used mixed solvent of GBL and DMSO for MAPbI_{3-x}Br_x with toluene treatment afterwards, and obtained a dense and uniform perovskite layer with a power conversion efficiency of 16.2% without any hysteresis[15]. In another work, the solution of PbI₂, DMF, DMSO and MAI was spin coated (accompanied with diethyl ether dripping) and the power conversion efficiency has reached to 19.7% with average efficiency of 18.3% [66]. Some additives such as 1,8-diiodooctane (DIO)[24], poly(ethylene glycol) (PEG)[67], low volatility components such as FACl and MACl [68], HI[69] and Pb(SCN)₂ [70] were also used. Similar solvents were also utilized in in two-step processes.

The role of the anti-solvent treatment is to reduce the solubility of perovskite in precursor solution and to speed up the crystallization and nucleation. For example, Xiao *et al.* employed various anti-solvents to control the grain growth and nucleation of MAPbI₃. They reported that the performance improved significantly from 1.5% to 13.9% by employing chlorobenzene; a high-quality film without any grain boundaries and defects was formed. Benzene, xylene and toluene were also observed to give uniform grain morphologies [71]. In another study, Jung *et al.* revealed that chlorobenzene was superior to dichlorobenzene and toluene. They observed that the high temperature annealing process became less necessary to obtain highly crystalline and uniform structure if optimum anti-solvents were employed [72]. Later, diethyl ether was found to be superior to chlorobenzene and toluene [66]. Some other anti-solvents such as acetonitrile in chlorobenzene also used and found to be effective [73].

Thermal annealing of perovskite after deposition also has an effect on performance. The aims of thermal annealing are to facilitate perovskite formation, evaporate residual solvent and improve crystallization [6]. Various researchers have investigated the effects of annealing variables such as temperature, time and ambience; however, the annealing conditions differ for different perovskite and cell types [74–76] and the optimum annealing conditions may also depend on the annealing environment [77].

The annealing temperature has a strong effect on morphology and grain size. Su *et al.* showed that, as annealing temperature increased, the grain size of MAPbI₃ film also increased. However, when the temperature exceeded 120 °C, the perovskite decomposed to PbI₂ [78]. During thermal annealing, the evolution of secondary phase plays an important role; it was found that pure perovskite phase without secondary phase formation resulted better performance [79], [80]. Chen *et al.* investigated the annealing temperature (80-140 °C) in MAPbI₃ based inverted cells for five minutes and revealed that annealing perovskite at 100 °C extend the exciton lifetime and performance [81].

It was reported in the literature that the annealing environment has also profound effect on performance; an improved morphology with larger grains was observed when the perovskite film annealed in a moisture environment with relative humidity of 30-40%. However, degradation occurs at high humidity levels greater than 80% [82], [83]. It was also

reported by various investigators that annealing in air environment produced higher efficiencies than in glovebox [82], [84], [85].

In contrary to the common belief that perovskite decompose at higher annealing temperatures than 120 °C[78], [86], Kim *et al.* proposed another approach involving very high temperature and short time annealing process. For example, the annealing at 400 °C for four seconds also caused a larger grain formation of perovskite and more uniform morphology than that could be obtained at lower temperatures[87]. Cao *et al.* also reported grain coarsening and reduced recombination with increasing annealing temperature from 100 °C to 250 °C [88].

2.1.3. Effect of Electron Transfer Layer

Basically, the perovskite active layer is sandwiched between electron transport layer (ETL) and hole transport layer (HTL). When the active layer is excited by photon energy in the sunlight, electron-hole pair occurs. The electrons are injected to electron transfer layer and then transferred to electrode. The first criteria that both ETL and HTL should obey is the band gap alignment of the solar cells that electron could pass through easily. Different materials which satisfy the band gap alignment with perovskite could be employed as ETL and HTL (such as metal oxides, organic and inorganic materials).

As the perovskite solar cells were first derived from dye sensitized solar cells in which mesoporous TiO₂ structure was employed as a scaffold for electron transfer, it has been a common practice to employ the same mesoporous TiO₂ layer in the early perovskite cell as well [89]. The porous structure of the ETL provides a larger surface area for the absorber material resulting in more incident light absorption. However, nearly at the same period, mesoporous TiO₂ was replaced with an insulating mesoporous Al₂O₃ which acted just as a passive scaffolds [6] for the perovskite rather than an ETL; in this design, perovskite behaved as both absorber and electron transfer material. The power conversion efficiency was improved from 8.0% to 10.9% by replacing mesoporous TiO₂ with Al₂O₃, and it was found that the electron transfer in perovskite layer was faster than TiO₂ [12]. Later, Ball *et al.* achieved even higher PCE (above 12.0%) by lowering the annealing temperature of Al₂O₃. The same group also designed a cell by removing mesoporous scaffold and using a

thin porous compact Al_2O_3 layer, and they obtained the power conversion efficiency of 9.1% with an internal quantum efficiency of nearly 100% [90]; this was also the introduction of planar configuration in perovskite solar cells.

The performance of the cells with the mesoporous structure has been continued to improve with various modifications. For example, various forms of TiO_2 structures (such as nanorods) were also investigated through years[91]. Doping TiO_2 with various dopants such as Al, Mg and reduced graphene oxide were also used [92–94]. In other works, TiO_2 was completely replaced by new materials such as SrTiO_3 [95], ZnSnO_4 [96] and SnO_2 [68]; similarly, the other passive mesoporous scaffold such as ZrO_2 [62] and SiO_2 [97] were also tested as replacement of Al_2O_3 , and they were found to be effective.

The compact layer, which is deposited before the mesoporous layer for blocking the electrons and avoiding the contact between front electrode and perovskite, does not only improve the performance of mesoporous cells, but also serves as the electron transfer layers in planar cells. The compact TiO_2 has been the first and the most commonly used material, and it has been studied and modified through years in various ways. For example, doping of compact TiO_2 with some of dopants like yttrium [98], zirconia[99] and niobium[100] were reported to improve morphology and electron transfer. ZnO was employed as another compact layer material in planar solar cell to reduce the high processing temperature of TiO_2 . The required thickness was also thinner than TiO_2 and no sintering was required. Some modifications were reported to improve the performance of ZnO compact layer as well [101]. Other alternatives such as C_60 [102], [103], Nb_2O_5 [104], CdS [105], WO_x [106] and SnO_2 [107] were also reported. Additionally, the complete elimination of ETL is an increasing trend in literature to simplify the structure further[108].

The fullerene derivatives were the most commonly used ETL material for the inverted cells due to their high electron mobility and room temperature processability; among them the phenyl-C61-butyric acid methyl ester (PCBM) is the most widely used. In some studies, doping of PCBM with various materials (such as oleamide[109], reduced graphene oxide[110] or polystyrene[111]) were also tested to improve morphology and electron transfer of PCBM layer.

The C60, which is another fullerene derivative, was also tested as ETL in inverted cells and found to be effective; its higher electron mobility, higher performance, better conductivity, and lower price has made it more preferable than PCBM[112]. Other fullerene derivatives and organic materials such as ICBA[113], tris(2,4,6-trimethyl-3-(pyridin-3-yl)phenyl) borane (3TPYMB)[114] and azaacene derivatives[115], [116] were also employed.

2.1.4. Effect of Hole Transfer Layer

The initial studies on perovskite solar cells have employed liquid electrolyte as a hole transporting material until 2012[10], [117]. However, the instability, leakage problems and dissolution of perovskite in liquid electrolyte have limited the performance of this new solar cell technology. Spiro-OMeTAD was used as a solid state hole conductor to solve these limitations [11]. Due to its suitable energy levels, high hole conductivity, high mobility and possibility of use without any post annealing process, the spiro-OMeTAD has been the most commonly used hole transport material in regular cells.

The spiro-OMeTAD had become the preferred HTL as the result of some additives; otherwise its pristine form actually had low conductivity and hole mobility. Lithium bis(trifluoromethylsulfonyl)- imide salt (LiTFSI) and 4-tert-butylpyridine (TBP) together are the most commonly used additives; they increase the conductivity and improve the properties of HTL[118]. In addition, Co(III) complexes such as tris(2-(1H-pyrazol-1-yl)pyridine) cobalt(III) (FK102)[119], tris(2-(1H-pyrazol-1-yl)-4-tert-butylpyridine) cobalt(III) tris-(bis(trifluoromethylsulfonyl)imide)) (FK209)[120], [121] and tris[2-(1H-pyrazol-1-yl)pyrimidine]cobalt(III) tris [bis(trifluoromethylsulfonyl)- imide] (MY11)[122] were also used together with LiTFSI+TBP. Using some additional novel dopants such as Ir complex or Cu(bpcm)₂ have also resulted higher efficiency[123], [124].

The structure of spiro-OMeTAD has been also modified to make it cheaper and more efficient. For example the methoxy groups (OMe), which plays an important role in controlling the electronic properties of HTL, was substituted with its derivative o-OMe and was reported to result higher performance by lowering series resistance and increasing fill factor[125]. Similarly the spirobifluorene core, which is an expensive material due to its

highly complex synthetic process, was replaced by cheaper alternatives as pyrene[126], triptycene [127], 1,3,5-triazine [128], a fused quinolizino arcidine[129] and triphenylamine[130].

Some cheaper polymeric alternatives for spiro-OMeTAD have been also studied. For example, poly-3-hexylthiophene (P3HT) is another common polymeric hole transport material used in regular cells. Even though P3HT based devices could not reach to the high efficiencies of spiro-OMeTAD based devices in the literature, they are still investigated as cheaper and convenient alternative[128], [131]. The performance of P3HT was also improved through the use of some additives like D-TBP[132], Au nanoparticles[133] and tetrafluoro-tetracyano-quinodimethane (F4TCNQ)[134]. LiTFSI+TBP is also used with P3HT as additive similar to spiro-OMeTAD. A polymeric hole conductor, poly-triarylamine (PTAA) is another polymeric HTL resulting high efficiencies. PTAA was found to be superior to other polymeric HTLs and quite compatible with spiro-OMeTAD[135]. However, its high production cost (due to its complex synthesis procedure) constitutes a major drawback. PEDOT was employed as another high conductivity polymeric HTL due to its promising efficiency, simple synthesis steps and low price; however, its stability is an issue to be solved[136], [137]. Other polymeric alternatives such as PDPPDBTE[138], DR3TBDTT[139], TFB[140] and PNBA[141] for HTL were also reported.

Additionally, some inorganic materials have been also gained attention as HTL due to their simpler nature, easier synthesis procedure, low cost, durability and stability. For example, cupric oxide (CuO), cuprous oxide (Cu₂O), copper iodide (CuI), and thiocyanate (CuSCN) were widely implemented inorganic HTLs[142–144].

Finally, hole transport layer free cells have been also studied in recent years due to their simpler structure, improved stability and lower cost [145]. Etgar *et al.* first introduced HTL-free cells with PCE of 5.5% using a gold back contact[146]. Although the work function of gold is well matched with perovskite and gold has a high conductivity, its high cost and complex deposition method (thermal evaporation) are not feasible[147]. Hence, carbon back contact was also studied for HTL-free cells by various researchers because of its low cost, suitable work function, high conductivity and moisture resistance[148–150].

The HTLs used in inverted structure can be divided into two groups as organic and inorganic materials. The PEDOT: PSS is the most commonly used organic polymeric HTL because of its excellent conductivity, suitable band gap alignment, low temperature annealing process and suitability for flexible devices; it is usually used with PCBM as the ETL layer. It was initially reported by Chen *et al.* with the PCE of 3.9% [23]. Then, Docampo *et al.* improved the PCE to 10% by sandwiching MAPbI_{3-x}Cl_x perovskite between PEDOT:PSS and PCBM while the same configuration resulted 6.3% efficiency on flexible substrate [151]. In the same year, the efficiency reached to 17.1% by annealing perovskite in a mild environment using PEDOT:PSS as HTL and PCBM as ETL [82]. In 2015, the PCE of 18.1% had already achieved by controlling the perovskite morphology with PEDOT:PSS [152]. Some modifications have been also performed on PEDOT:PSS to improve its low work function; for example, Tae-Woo *et al.* increased the work function of PEDOT:PSS by using a perfluorinated ionomer (PFI) layer [153]. Doping with GeO₂ [154], Ag-nanoparticles [155] or GO [156] also improved the hole conductivity of PEDOT:PSS.

Beside its lower work function, PEDOT: PSS could also slightly decompose in perovskite precursor solution (especially in DMF or DMSO) in the presence of water or humidity. Hence, some novel polymeric alternatives with simple synthesis procedures were also employed; the examples are polythiophene (PT), poly(p-phenylene) (PPP), poly(4,4'-bis(N-carbazolyl)-1,1'-biphenyl)(PPN), poly[N,N'-bis(4-butylphenyl)-N,N'-bis(phenyl)benzidine] (Poly-TPD), and poly[bis(4-phenyl)(2,4,6-trimethylphenyl)amine] (PTAA) [28], [157], [158]. PTAA appears to be an effective organic material as HTL gaining more interest in recent years [32], [159], [160].

Inorganic HTLs were also employed because of their high chemical stability, durability, wide band gap, high hole mobility and low fabrication cost. NiO_x, as the most common inorganic HTL, was initially introduced by Docampo *et al.* [151] with a very poor efficiency (lower than 0.1%). Later, Hu *et al.* improved perovskite film morphology on NiO_x by employing two step dipping technique and improved PCE to 7.6% [161]. Li *et al.* further improved PCE to 13.6% by employing a one-step fast crystallization-deposition method for perovskite [162]. Later, Park *et al.* introduced an inverted cell with pulse laser deposited NiO_x layer and achieved a PCE of 17.3% [163]. Doping of NiO_x layer with highly conductive

metal ions such as Cu, Li and Mg was reported to enhance the conductivity and performance significantly [162], [164], [165].

The other inorganic materials like CuSCN [166], CuI [167] and graphene oxide (GO) [168] were also employed in inverted structures. Additionally, similar to regular cells, HTL free inverted structure were also studied to reduce cost and fabricate simpler devices with comparable efficiencies [166], [169].

2.1.5. Effect of Back Contact

Au is the most common back contact material and it was also found to be optimum among Pt, Ag, Cu, Ni and Cr. Besides, Pt was also found to be better due to its low internal resistance between HTL and high stability. Although Ag also leded compatible performance with Au, its photodecomposition is a major drawback [170]. Due to being a low cost and abundant material, carbon could be a good alternative as a back electrode especially for HTL-free cells. Direct preparation of carbon electrode requires high temperature but the perovskite absorber is sensitive to high temperatures. Hence, Zhou *et al.* developed a fully low temperature and solution processed method for TiO₂/MAPbI₃ structured cell with carbon back electrode and PCE was measured as 9% with a good stability. Implementing low temperature solution method reduced the cost and simplified the process [171]. The limitation of carbon back electrodes in HTL-free cells is the poor contact at perovskite/carbon interface. Hence, perovskite with such a good morphology should be fabricated to prevent good contact with carbon electrode [172], [173].

2.1.6. Reproducibility

Besides the efforts on performance improvement, reproducibility also plays an important role on commercialization of this technology for large scale production. Many efforts have been made in literature to overcome the reproducibility problem. Perovskite morphology and crystallization, which were determined by perovskite type and deposition conditions, play an important role on cell reproducibility. Wu *et al.* [174] and Ahn *et al.* [66] produced reproducible and pin-hole free perovskite cells employing DMSO which formed a Lewis base adduct with PbI₂ and retarded crystallization. Employing a sequential spin

coating method also reported to increase the quality of perovskite layer, its morphology and reproducibility[175]. Liu *et al.* reported that spin coating of $\text{MAPbI}_{3-x}\text{Cl}_x$ with high concentration also leded reproducible cells with better uniformity and coverage[176]. Besides perovskite morphology, some other modifications also studied to enhance the reproducibility. For example, Pae *et al.* [177] produced reproducible cells using e-beam evaporation technique for low-temperature deposition of uniform charge transport layers. Higgings *et al.* reported that including Ag nanoparticles at low concentration in PCBM in inverted cells also improved reproducibility[178].

2.1.7. Hysteresis

Hysteresis, which is the difference between forward and reverse scan during J–V characterization, is a drawback of this technology for fabricating commercial cells and complicates the determination of the actual performance of the solar cells enormously. Although the origin of J-V hysteresis is still unknown, there are some hypotheses on the mechanism of hysteresis such as ion migration, charge trapping, capacitive effects or ferroelectric polarization[2], [60]. The hysteretic behavior depends on various parameters such as scan rate, scan direction, voltage range and perovskite morphology and solar cell architecture[2]. Kim *et al.* reported that the hysteresis decreased in the presence of mesoporous layer and perovskite with larger crystal size[179]. Some modifications on charge transport layers also decreased hysteresis due to enhanced charge transport from perovskite whereas the absence of charge transport layers such as TiO_2 compact layer as ETL or spiro-OMeTAD as HTL was reported to increase hysteresis in regular cells[180-183].

As the hysteresis complicates the actual performance measurement of a solar cell, stabilized power conversion efficiencies were reported in some publications since 2014 as better measures of the real performance because they are more representative of the steady-state performance of perovskite solar cells, as J-V measurements are strongly influenced by the transient effects[2], [17]. The hysteresis should be eliminated to report stabilized efficiencies. Measuring at slow scan rates were suggested for this purpose, as well as adjusting scan range with different initial biases. However, a more standard protocol is needed to measure stabilized PCE such as maximum power point(MPP) tracking using a

perturb and observe method[184]. Maximum power point tracking is the most reliable method to measure stabilized efficiencies of hysteretic cells[185]. Perturb and observe method is a control process that is used for adjusting operating voltage to obtain maximum power. Once, maximum power is reached, the voltage is adjusted again to keep the cell stable at this point. The maximum power oscillates around the maximum power value until it stabilizes.

2.2. Review of Long-term Stability of Perovskite Solar Cells

Although the efficiency of perovskite solar cells has been increased remarkably in a few years, the long term cell stability is still a challenge that prevents the commercialization of this technology. Consequently, the research focus seems to be shifted to this issue in recent publications due to the fact it became the bottleneck after the efficiency reached top a certain level. Indeed, not only the number of research articles involving the stability increased as evident from Figure 2.4 (from Web of Science search with the keyword search of perovskite solar and stability in topic segment on 16.01.2019), but also there has been some considerable progress in the field.

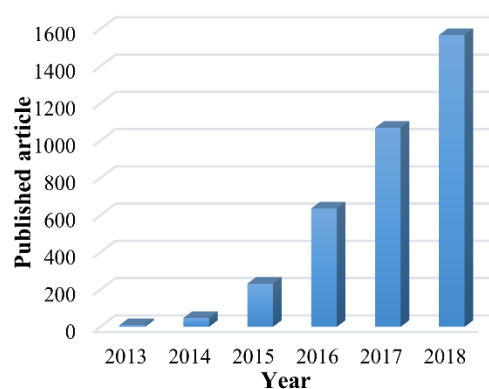


Figure 2.4. Number of publications on stability of perovskite solar cells.

Most of the studies have concentrated on the stability of regular type cells[186]; some recent articles that reported cells with high stability, have also employed regular structured cells as well[3], [187], [188]. On the other hand, Heo *et al.* reported that the inverted ITO/PEDOT:PSS/MAPbI₃/PCBM/Au cell was more stable than regular

FTO/TiO₂/MAPbI₃/PTAA:tBP + LiTFSI/Au cell due to better electron transfer capacity and hydrophobicity of PCBM than TiO₂ and lack of corrosive additives of HTL[152].

2.2.1. Effect of Ambient Conditions

The moisture, oxygen, ambient temperature and light were found to affect the device stability by various investigators. It is well known that the perovskite layer is very sensitive to moisture because its alkylammonium salts are hygroscopic[189]; even this is sufficient to say that moisture may have significant impact on stability. Tai *et al.* stated that the intrinsic stability of the perovskite material was more dominant than the morphology of the films in air under high relative humidity[190]. Indeed, there are numerous works on testing and commenting on the effects of humidity in the ambient air on cell stability. For example, it was reported that a regular type cell with MAPbI₃ perovskite was stable more than 10 days at the RH of 50% and below, whereas the same cell could resist for maximum four days at the RH of 80% and above[191]. In another study, a significant decay in performance of MAPbI₃ based cell was observed after exposure to RH of 55%[192]. In accordance with Leguy *et al.*[193] suggested that the band gap of the perovskite could change upon high RH exposure (70%); the reason was attributed to the transformation of the perovskite to monohydrate (MAPbI₃.H₂O). Although the monohydrate phase could return to its initial structure at dry atmosphere, the reaction became irreversible upon longer humidity exposure. Christians *et al.* reported that the cells were stable at RH 0% and 50% in dark, whereas decomposition occurred at high RH of 90%. They also investigated the stability under illumination and revealed that illumination caused additional decomposition under the humid conditions indicating that there are also interactions among the ambient related factors[194]. Rajan Jose *et al.* also investigated the effect of humidity and light exposure together, and they found that perovskite showed a minor degradation under dark condition with a humidity level above 70% whereas upon light exposure, the degradation rate increased significantly[195]. The interactions among various ambient factor were also confirmed by the work of Ashgar *et al.*[196]; no significant decay in performance was observed if the perovskite cells were stored in dark and dry air because oxygen cannot degrade the perovskite cell under dark. The oxygen was reported to cause photo-oxidation in the presence of light[197], [198].

The ambient temperature is also influential and interacting with the other factors. Misra *et al.*[199] exposed encapsulated MAPbI₃ devices to 100 suns for 60 min at different temperatures; the cell stored at 45-55 °C degraded and caused PbI₂ crystallization while the cell stored at 25 °C hasn't showed any degradation. It was found that the degradation occurred by photoinduced decomposition was thermally enhanced. Changing temperature causes some structural phase transitions in perovskites[200]. Brunetti *et al.*[201] studied the thermal and thermodynamic stability of MAPbX₃(X=I, Cl or Br) perovskites in inert atmosphere and found out that all these perovskites decomposed to solid lead (II) halide, gaseous methylamine and hydrogen halide even at moderate temperatures of 60 °C. On the other hand, MAPbI₃ was found to be more resistant to temperature of 90 °C, which is the temperature of the solar cell reach at harsh conditions. Beside the ambient temperature, temperature-annealing was also found to accelerate decomposition in the presence of humidity[202].

As the result, different decomposition pathways might occur under different sets of ambient conditions. For example, the perovskite was detected to decompose to elemental lead and iodine and might form PbI₂ agglomeration on FTO surface under inert conditions at high temperatures whereas the elemental species were seen to diffuse from perovskite to HTL in air[203]. Abdelmageed *et al.*[204] conducted another study and revealed that MAPbI₃ perovskite started to degrade at 75 °C under light to elemental Pb and PbI₂ and 85 °C under dark to PbI₂. Consequently, the effects of these entire factors as well as their interactions should be investigated together to see the whole picture.

2.2.2. Effect of Perovskite Type

Perovskite composition is another factor that strongly affects the stability. It was reported that the stability of MAPbI₃, which is the most commonly used perovskite, can be enhanced by replacing I with Cl or Br, Pb with Sn or organic part (MA) with inorganic Cs was reported to enhance stability[205]. MAPbI₃ perovskite showed cubic to tetragonal phase transition approximately at 57 °C; however, no phase transitions were observed for MAPbBr₃ and MAPbCl₃ perovskites in the temperature range of -40 °C to 85 °C[206]. Consequently, these perovskites could be regarded as structurally more stable than MAPbI₃ at the temperatures up to 85 °C [196]; actually MAPbBr₃ perovskite was found to be more

stable than MAPbI₃, and this was attributed to the differences in bond strengths and crystalline forms[199], [207]. Even, MAPb(I_{1-x}Br_x)₃ perovskite (with x=0.2 or 0.29) showed better stability than MAPbI₃ under high humidity conditions with its compact and stable structure[192]. MAPbI_{3-x}Cl_x was also found to be more thermally stable than MAPbI₃ because no phase transition occurred between 25-100 °C unlikely to MAPbI₃ (50 °C) [208].

Replacing cation part with FA also affected stability. Due to higher phase transition temperature of FAPbI₃ (at 150 °C), FAPbI₃ was found to be more stable than MAPbI₃ in air. However, FAPbI₃ degraded at moist atmosphere at a rate similar with MAPbI₃ [40], [209]. Cesium was another cation replaced with MA and studies have already confirmed their enhanced thermal stability, humidity resistance, and photostability due to its inorganic nature [44], [210].

Incorporating two or more cations together was also found to improve the stability significantly. For example, employing MA and FA cations together improved both performance, thermal and long-term and stability[211]. In another study, doping of FAPbI₃ with MABr or Cs resulted better stability than FAPbI₃ alone[48], [212], [213]. However, using triple cation perovskite (including MA, FA and Cs cations together) was found to improve stability much more by hindering yellow phase impurities and forming uniform perovskite grains[19].

2.2.3. Effect of Perovskite Deposition

Perovskite deposition procedure (more specifically one or two step deposition) influence the quality, homogeneity and surface coverage of the perovskite film, and consequently may played a significant role in stability in air by resisting the moisture in the environment[6], [214], [215]. The two-step deposition technique has been considered as the one that result in stable cells since it was introduced by Burschka *et al.*[13]. For example, Yang *et al.*[216] stated that layer by layer vacuum deposition of perovskite (PbI₂ and MAI were coated separately) provided a cell with a good stability in air due to uniform morphology with full surface coverage and controlled environment provided a pure perovskite layer that is more robust to moisture. A good stability using two-step deposition method was also provided by adding DMF solvent to MAI/FAI cation solution of FA_xMA₁₋

$x\text{PbI}_{2.55}\text{Br}_{0.45}$ perovskite[217]. One-step deposition was also used in cells with high stability. For example, the modules which were stable more than 10 000 hours, were prepared by one-step deposition. Koushik *et al.*[187] and Arora *et al.*[188] also employed one-step deposition to produce stable cells in their studies.

The technique employed for deposition may be also influential. Different from the most common spin coating technique, some other deposition techniques were also found to be effective on high stability. For example, Kim *et al.* [214] found that blade coating resulted more homogenous perovskite layer with large and compact crystalline domains which acted like an air-protection barrier, and led to high stability cells while the cell prepared by spin coating degraded in air. Even Deng *et al.*[218] modified this technique by adding a small amount of surfactant to perovskite solution and enhanced stability. Similarly, chemical vapor deposition is another technique to deposit high quality perovskite layer with high stability. This promising stability was related to evaporation of the excess MAI and incorporated water at temperatures above 160 °C during deposition[219]. Vacuum deposition of perovskite was found to be another technique to produce stable cells [216], [220].

Perovskite precursor solution has also effect on stability because the composition and structure of the precursor solution directly affects the perovskite morphology and crystallization[221]. For example, employing different lead source[222], type of solvents[223] or using additives into conventional precursor solutions such as water [224] PDMS–urea (a hydrophobic polymer) [225], polyethylene glycol (PEG) [226], polyvinylpyrrolidone (PVP) [227], polyvinyl alcohol (PVA)[228] or C70 fullerene[229] were found to affect stability of the perovskite cells. Similarly, anti-solvent treatment has an effect on stability as well due to the similar reasons with precursor solution[230–234].

Another modification to improve stability was adding extra layer on top of the perovskite layer to protect the perovskite film. For example, Koushik *et al.*[187] coated an ultra thin Al_2O_3 layer and reduced hysteresis beside enhanced long term stability in air. Similarly, Su *et al.*[235] employed poly-N-vinylcarbazole (PVK) which is a hydrophobic and conductive polymer between perovskite and HTL. This interlayer not only enhanced stability and protected the perovskite layer from moisture and degradation, but also reduced

recombination within the cell. Li *et al.*[236] improved light and moisture stability using hydrophobic alkyl bisphosphonic molecules on perovskite layer in inverted type cell.

2.2.4. Effect of Electron Transfer Layer

Charge transport layers in perovskite cells also affect the stability. In regular cells, in order to investigate the effect of TiO₂ architecture as ETL, Fakharuddin *et al.*[237] employed planar and nanorod TiO₂, and it was found that although planar cells gave higher initial efficiency, using a scaffold provided longer term durability. The reason was attributed to larger exposure area of the planar devices to ambient atmosphere where perovskite interacted with moisture faster. Hence, it was reported that stability of the cells was also affected by the morphology, porosity and the chemical stability of the electron transport layer. However, in another work, the stability of mesoporous or planar architectures were compared and they were found to be comparable with each other[6]. They argued that there was no superiority among the architectures; the perovskite solar cell performance was reported to be independent from the device architecture (mesoporous, planar, regular, inverted etc.) and highly dependent on film morphology that affected by deposition method, material composition, additives and film treatment. On the other hand, mesoporous TiO₂ was also considered unstable due to light-induced desorption of surface-adsorbed oxygen when the cell was encapsulated in nitrogen environment, and numerous solutions were implemented to overcome this limitation such as the passivation of the TiO₂ surface in the solid state, prevention of the mesoporous TiO₂ from the UV light during operation or removal of the mesoporous TiO₂[238]. In order to passivate the TiO₂ surface, a uniform CdS shell was coated onto the surface of a TiO₂ layer and the light stability of the cell improved significantly[239]. When CdS layer was employed as ETL and TiO₂ was eliminated, the photostability was reported to be enhanced. The cell with CdS layer conserved its 90% of the initial efficiency under continuous illumination while the cell with TiO₂ conserved only 18%[240]. Using interlayers such as CsCl[241], CsBr[242] or aminoacids[243] between ETL and perovskite was also beneficial for stability. Interlayers could reduce the reactivity of TiO₂, defect density at the interface and improve the surface coverage of the perovskite. Doping of mesoporous TiO₂ layer with Al or Nd also passivated the surface defects and contributed stability[92], [244]. Different structures of TiO₂ such as nanocolumnar

structures[245], nanorods[237], [246] and nanotubes[247] were also reported to enhance stability.

The other alternative like SnO₂ was also employed as ETL to replace TiO₂ due to its wide band gap, high electron mobility and low chemical and photocatalytic reactivity. An improved stability was observed in most of the studies[248–251]. The improved stability was attributed to the remnant PbI₂ between SnO₂ and perovskite interface which passivated the surface. Besides, SnO₂ was reported to be less hygroscopic than TiO₂ that might contribute to improve stability[252]. Liu *et al.*[248] employed a mesoporous layer of SnO₂ nanosheets above compact SnO₂ layer and the stability was improved to a higher level than compact SnO₂ alone. The hierarchical SnO₂ layer provided an excellent charge transport pathway besides inhibited the degradation of the perovskite from moisture in air. ZnO is another type of ETL which has higher conductivity, lower cost and simpler synthesis besides requiring lower temperatures for processing than conventional TiO₂. However, it was found that the stability of MAPbI₃ perovskite was lower on ZnO than on TiO₂ layer under ambient conditions. The reason was attributed to the heat treatment of perovskite layer (110 °C, 5 minutes), after the heat treatment of perovskite, it was seen that MAPbI₃ was degraded rapidly on ZnO layer whereas no degradation was observed on TiO₂ layer[253]. However, an insertion of an ultra-thin Al₂O₃ insulating layer between ZnO and perovskite enhanced both efficiency, thermal stability and suppress the photocatalytic degradation of perovskites[254], [255]. Aluminum doping of ZnO was reported to synthesize extraordinarily thermally stable perovskite layers by hindering the Lewis acid–base chemical reaction between perovskite and ETL[256]. Hence, more simplified cell structure was obtained. In another study, triple cation perovskite, Cs₆(MA_{0.17}FA_{0.83})₉₄Pb(I_{0.83}Br_{0.17})₃, with the annealing temperature of 95 °C, was found to be stable on low temperature processed ZnO as ETL[257]. Excess PbI₂ was reported to passivate the traps in perovskite layer and fabricated ZnO based perovskite cell showed excellent durability and photostability.

Although the PCBM is the most commonly used ETL in inverted cells, it was reported to have low solubility in toluene and chlorobenzene; hence it was difficult to fabricate a uniform PCBM film without pin holes on perovskite layer by one-step spin coating method. Besides, the crystallinity and morphology of PCBM layer was found to change with aging time. Hence, the stability of PCBM cells were quite low. To overcome this problem, Heo *et*

al. employed N,N'-bis(phenylmethyl)naphthalene-1,4,5,8-tetracarboxylic diimide (NDI-PM)-based electron transporting material which was a more stable and robust ETL; the improved thermal stability was attributed to much stronger hydrogen bonds in the NDI-PM molecular crystals than the PCBM crystals[258]. Kim *et al.* used edged-selectively fluorine (F) functionalized graphene nanoplatelets (EFGnPs-F) as ETL which has superhydrophobic properties and a robust material that protected perovskite layer from air degradation[259]. Doping of PCBM with reduced graphene oxide[110] or with surfactant CTAB[260] improved the stability of the devices in ambient air. Coating an extra layer on PCBM layer such as ZnO[261], TiO_x[151], ZrO_x[262] and Cr₂O₃[263] also enhanced air stability of the device. A highly crystalline SnO₂ was also reported to enhance stability as an ETL in inverted cells in ambient air due to its stable and robust structure[264].

2.2.5. Effect of Hole Transfer Layer

As mentioned in previous sections, the most common HTL was spiro-MeOTAD. However, according to Sanchez *et al.*[265], one of the main limiting factor for long term stability of the perovskite solar cells was the photo-oxidation of spiro-MeOTAD under inert or air environment. Even, using dopants (LiTFSI and tBP) with spiro-MeOTAD and the presence of any contact with the ETL (TiO₂) contributed to degradation. In addition, as spiro-MeOTAD is one of the organic semiconductors, it was reported that the carbon-carbon double bonds tended to break up upon exposure to long term illumination in oxygen environment, hence the conductivity of the material decreases resulting decaying performance. Although employing dopants such as Li-TFSI and tBP was reported to improve hole conductivity of spiro-MeOTAD, Li-TFSI requires oxygen from the air even in encapsulation or N₂ environment which can lead degradation. Besides, Li-TFSI was reported to be highly hygroscopic, hence water molecules could penetrate into HTL and then to perovskite surface which causes degradation[266]. In order to improve stability, Li-TFSI was replaced with some non-hygroscopic dopants such as Ag-TFSI[267] and F4-TCNQ[268] or some dopant free HTLs were employed such as tetrathiafulvalene derivative (TTF-1: 4-(4-(bis(4-(4-(dibutylamino)styryl)phenyl)-amino)styryl)-N,N-dibutylaniline) [269], triphenylamine (TPA)-based HTL (Z1011)[270] or N₂,N₂,N₂',N₂',N₇,N₇'N₇'-octakis(4-methoxyphenyl)-10-phenyl-10H-spiro[acridine-9,9'-fluorene]-2,2',7,7'-tetraamine (SAF-OMe)[271].

P3HT is a widely used alternative for spiro-OMeTAD with its dopant free structure and easier synthesis[272], [273]. The stability of a P3HT based cells were found to be better than conventional spiro-OMeTAD[274]. As parallel to this case, Kim *et al.*[275] reported that the device stability was improved moisture stability by using mixed spiro-OMeTAD and P3HT as HTL. PTAA is another polymeric HTL used and it was reported that the stability also enhanced by replacing spiro-MeOTAD with PTAA[276].

Using a hydrophobic semiconductor material as HTL could protect the perovskite layer from moisture and water-induced degradation. Polymer-functionalized single-walled carbon nanotubes (SWNTs) embedded in an insulating polymer matrix[277], 7-(9,9'-spirobifluorene-2-yl)-N-(7-(9,9'-spirobifluorene-2-yl)-9,9-dioctyl-9H-fluorene-2-yl)-N-(4-(9H-carbazol-9-yl)phenyl)-9,9-dioctyl-9H-fluorene-2-amine(CzPAF-SBF)[278], an oligothiophene derivative named DR3TBDTT[139], 4,4'-(4,8-bis((2-ethylhexyl)oxy)benzo[1,2-b:4,5-b']dithiophene-2,6-diyl) bis(N,N-bis(4-methoxyphenyl)aniline) (OMeTPA-BDT)[279] and poly[2,5-bis(2-decyldodecyl)pyrrolo[3,4-c]pyrrole-1,4(2H,5H)-dione-(E)-1,2-di(2,2'-bithiophen-5-yl) ethene] (PDPPDBTE)[138] were some of the hydrophobic HTLs that improved long term stability. Inorganic HTLs such as CuI[280] were also employed to eliminate the disadvantages of using organic compounds as HTL and improved long term stability.

PEDOT:PSS is the most common HTL type used in inverted perovskite cells due to its high conductivity and good transparency in the visible range. However, its inability to block electrons, the hygroscopic and acidic nature of PEDOT:PSS limits the stability of the inverted cells[281]; hence some modifications were made to improve the device stability of PEDOT:PSS based cells. For example, Huang *et al.* doped PEDOT:PSS with dopamine and the stability of the device enhanced by reducing the acidity of PEDOT:PSS[282]. Changing pH or using an organic solvent to enhance morphology also reported to improve the stability of the cell[283], [284].

The replacing PEDOT:PSS with metal oxide NiO_x and CuSCN as the hole transport layer can also improve the stability as well as the the hole extraction capacity of the cell[285–287]. Graphene oxide is another stable HTL synthesized with a simple solution-based process and with cost-effective raw materials. Yang *et al.*[288] studied the light soaking and

shelf-lifetime stabilities of GO and PEDOT:PSS, and the stability was reported to enhance by using GO due to its higher work function and formation of larger perovskite crystals above; the hole extraction capacity was also reported to be enhanced.

2.2.6. Effect of Back Contact

Au, Al and Ag are the most commonly used back contact materials. However, the diffusion of Au through HTL causes degradation. Besides, the high cost of Au makes this material completely unpromising. Ag, which is a cheaper alternative for back contact, also causes degradation by reacting with halide ions in humid environment. Low cost Cu was found to be a promising alternative for high stability as no reaction occurred between Cu and perovskite and high PCE was achieved[289]. Another promising alternative is low cost carbon back contact. Mei *et al.*[290] achieved excellent stability using carbon as back contact in a fully printable perovskite solar cell. Carbon layer was found to protect the perovskite from moisture. Single walled carbon nanotube was also employed as back contact and showed negligible degradation under high temperature and illumination[291]. Carbon back contact also found to be suitable for large area deposition. Priyadarshi *et al.*[292] obtained high stability and a moderate PCE (10.74%) in large area (70 cm²) module using carbon back contact.

2.3. Data Mining and Methods

According to Hand *et al.*[293], “Data mining is the analysis of (often large) observational data sets to find unsuspected relationships and to summarize the data in novel ways that are both understandable and useful to the data owner.” Another definition is, “Data mining is an interdisciplinary field bringing together techniques from machine learning, pattern recognition, statistics, databases and visualization to address the issue of information extraction from large data bases.”[294]. As the large amount of data is being generated in research and business area, data mining becomes an important field of research in order to have a better understanding of data by discovering patterns and make useful predictions. Some of the applications of data mining that is used for prediction are flooding, speech recognition, machine learning and pattern recognition[295].

Data mining is an application of machine learning to large databases; there are various methodologies to extract knowledge from the databases. These methods can be analyzed in four main categories: classification, clustering, regression and association. Classification is used to separate data into predefined groups or classes. It can be referred as a supervised learning because the classes should be determined before examining the data. Clustering is a machine learning technique used to place data elements into related groups without advance knowledge of the group definitions. It is an unsupervised learning technique because the groups are not predefined but rather defined by the data themselves. The grouping is accomplished by finding similarities between data points according to characteristics found in actual data [295]. The groups are called clusters and the similar data are grouped into the same clusters. Popular clustering techniques include k-means clustering and expectation maximization (EM) clustering. Regression is a statistical tool for the investigation of relationships between variables. The aim is to fit the target data into some known type of function that is created from a known data. It deals with estimation of an output value based on input values. Association rule mining determines the most frequent patterns, combinations and associations in database which can not be seen by naked eyes using statistics.

2.3.1. Association Rule Mining

Association rule mining is used to determine frequent combinations, patterns, rules and associations. Association rule mining creates associations between item sets (i.e. A and B) in a form of if A, then B ($A \Rightarrow B$) where A is antecedent and B is consequent. There are three parameters that are used to interpret and make decision in this technique: support, confidence and lift. Support indicates the frequency of the occurrence of two item sets together in database (Equation 2.1). Confidence defines the ratio of number of data points in which two item sets are found together to number of data points in item set A (Equation 2.2). This value provides information on the validity of this combination in item set A. Lift is the ratio of how much an item set B is found with item set A over item set A to the ratio of the frequency of item set B in overall database, hence we understand if the occurrence of B with A is more frequent than its occurrence in overall database; hence, lift value is greater than one if the occurrence of these two item sets together is significant (Equation 2.3).

$$\text{support} = \frac{\text{number of data points containing both A and B}}{\text{total number of data points}} \quad (2.1)$$

$$\text{confidence} = \frac{\text{number of data points containing both A and B}}{\text{number of data points containing A}} \quad (2.2)$$

$$\text{lift} = \frac{\frac{\text{number of data points containing both A and B}}{\text{number of data points containing A}}}{\frac{\text{number of data points containing B}}{\text{total number of data points}}} \quad (2.3)$$

A priori algorithm is used in association rule mining which narrows down the search space by determining priori properties. Hence, computation of this method gets easier. This algorithm assumes that if an item set Z is not frequent alone, so adding another item set A to Z will not make neither Z nor A and Z together frequent; hence any combination containing Z will not be frequent. Then, Z is not considered in association analysis according to a priori algorithm[296].

2.3.2. Decision Trees

Decision trees method is one of the most used data mining technique that extracts rules from the database. It is a supervised method that classify or predict data according to the rules derived. The rules are easy to understand and help user to have a better idea on the dataset. It provides conditional control statements and give a tree-like structure. The rules are decided by purifying data using nodes and branches.

A decision tree is a composed of a collection of decision nodes, connected by branches (Figure 2.5). Related class or value is located at the end of each branch. A decision tree starts from the root node and branches out. Attributes are tested and the possible outcome is calculated[296].

The main issue is to decide how to split a root to branches, or a branch to other sub-branches. Two branches are created in each decision node. A database should contain enough data points and the boundaries should be clear. The classification and regression trees (CART) method is one of the main algorithms for decision tree construction. The data is separated in order to give the similar outputs at the final node. The CART algorithm selects

the optimum split for tree construction by evaluating all possibilities (all variables and splitting values).

The optimum split is selected upon which split maximizes the goodness of split (Equation 2.4)[296]

$$\text{Goodness of Split} = 2P_L P_R \sum_{j=1}^{\# \text{ classes}} |P(j|t_L) - P(j|t_R)| \quad (2.4)$$

where t_L = left child node, t_R = right child node,

$$P_L = \frac{\text{number of data points at } t_L}{\text{number of data points in database}}, \quad P_R = \frac{\text{number of data points at } t_R}{\text{number of data points in database}}$$

$$P(j | t_L) = \frac{\text{number of class } j \text{ at } t_L}{\text{number of data points in } t_L}, \quad P(j | t_R) = \frac{\text{number of class } j \text{ at } t_R}{\text{number of data points in } t_R}$$

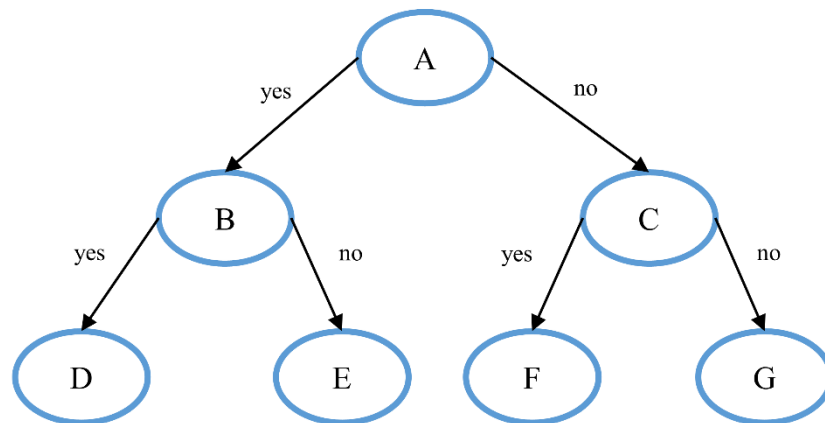


Figure 2.5. Decision tree model.

Another main algorithm used in decision trees is C4.5 algorithm. In C4.5 algorithm, the concept of entropy reduction is used to select the optimal split. First several candidate splits are created and a variable X having k possible values have probabilities of p_1, p_2, \dots, p_k and the entropy of X is defined as:[296]

$$H(X) = - \sum_j p_j \log_2(p_j) \quad (2.5)$$

The candidate split S , which divides the training set into T subsets (T_1, T_2, \dots, T_k) has a total entropy calculated as:

$$H_s(T) = \sum_{i=1}^k P_i H_s(T_i) \quad (2.6)$$

where P_i represents the proportion of the records in subset i and the main aim is find an optimum split that minimizes H_s .

Various values of the minimum number of split (the minimum number of data needed in each split to continue dividing into rules), depth of the tree (maximum length of the branches) and complexity parameter (the measure of the minimum increase of R^2 to model continue splitting,) are used to represent the data best with the maximum prediction accuracy. These parameters should be adjusted carefully to prevent overfitting as much as possible to detect generalizable rules.

2.3.3. Random Forests

Random forest is another common supervised method used for both classification and regression. It creates an ensemble of decision trees (CART model) to produce more accurate predictions. The combination of various learning models increases the performance of the method. This method adds randomness to the model while training using a random subset of variables each time, which is called bootstrap aggregation or bagging (Figure 2.6). Then, best split is decided among them for each tree; hence, random forest usually prevents overfitting of the data.

2.3.4. Data Mining in Field of Solar Energy

Data mining techniques have been used in the field of solar energy for many years by various researchers to extract valuable information from the experimental data. Different techniques have been applied to various areas in solar energy. For example, prediction of

solar radiation and solar power using data-mining tools is a quite popular field and many publications were published in the literature[297–300].

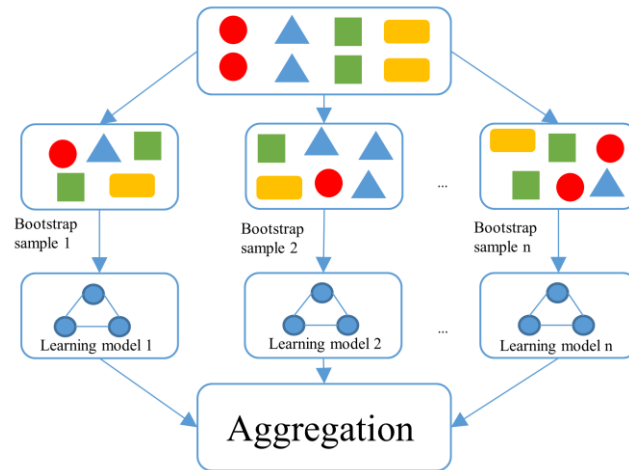


Figure 2.6. Bootstrapping and learning ensembles.

Almonacid *et al.*[301] predicted the electrical characteristics of Si-crystalline modules using module temperature and irradiance values as input. Evans *et al.*[302] studied multi-crystalline silicon cells to understand the effects of manufacturing conditions and material quality variations on the cell performance using data-mining approach.

Data-mining approach was also studied in organic cells. The preparation conditions such as materials' concentration in the absorber solution and the spin coating speed of the absorber solution of organic solar cells were analyzed and the effects of them were investigated[303]. In another study, Sue *et al.* [304] constructed various machine learning models successfully to predict efficiency of organic solar cells using microscopic properties of organic materials. There are also some studies on dye sensitized cells. New classes of dyes were tried to be predicted using data-mining tools[305], [306].

There are not much publications on data-mining in perovskite solar cell field recently, however, this field is becoming more popular. For example, Kim *et al.*[307] published a dataset of hybrid organic-inorganic perovskites to be used in data-mining efforts. Other study was conducted by Li *et al.*[305], in which they investigated the development trends of perovskite solar cell technology based on patent analysis and Twitter data mining. Recently, Odabaşı and Yıldırım investigated the factors affecting efficiency of perovskite solar cells

using various data-mining methods and determined the material and perovskite deposition types leading high efficiency cells[308].

3. METHODS

3.1. Database Construction

The database for PCE analysis was constructed using 800 articles published in various journals from ACS, Elsevier, Wiley and RSC databases as well as Nature and Science in 2013 and 2018 (until May 31 of 2018) and 1921 experimental data from these articles were extracted (Table 3.1). The articles were selected based on relevance search for “*perovskite solar*” as a topic; we tried to take the number of papers from each database as proportional to total publications as possible. Although the relevance sorting may not be the best way to rank the papers based on the quality of results, it is the only practical option to extract random data from large number of publications; the results should represent the literature well considering that the sample size (800 papers) is quite large. Hence, the number of articles used in database is 10% of the articles according to Web of Science search (with the keyword search of “*perovskite solar*” in topic segment at 16.07.2018).

The datasets for reproducibility, hysteresis and long-term stability were also created from research articles published in various journals from ACS, Elsevier, Wiley and RSC databases as well as Nature Group and Science; between 2015-2018 for reproducibility and hysteresis, and 2016-2018 for stability because it had been studied more frequently in these years (all until August 2, 2018). The keywords of *perovskite solar* for reproducibility and hysteresis, *perovskite solar* and *stability* for stability were used to list the related papers by relevance.

For PCE analysis, total 1407 data points from 585 articles belonged to regular structure (n-i-p) cells while 514 data points from 216 articles were involved inverted structure (p-i-n) cells (one paper had both regular and inverted cell data). The data belonging to flexible cells were not taken because this design is not well established yet; the papers published before 2013 were also excluded because the efficiencies of that time do not represent the same level of expertise of the later years. We manually extracted the data from the papers as they were given in the text or tables. We used best and stabilized PCE values to evaluate performance of the cells.

Table 3.1. Details of the Databases Used in Analyses.

PCE analysis				
	Stabilized PCE		Best PCE	
	Articles	Data number	Articles	Data number
Regular (n-i-p)	153	249	585	1407
Inverted (p-i-n)	59	74	216	514
Reproducibility analysis				
	Articles	Data number	Sample	
Regular (n-i-p)	292	547	15446	
Inverted (p-i-n)	147	291	8696	
Hysteresis analysis				
	PCE \geq 10%		Without PCE restriction	
	Articles	Data number	Articles	Data number
Regular (n-i-p) cells with scan rate \leq 0.05 V/s	64	110	67	129
Inverted (p-i-n) cells with scan rate \leq 0.05 V/s	18	35	18	35
Regular (n-i-p) cells	137	245	145	294
Inverted (p-i-n) cells	47	91	49	93
Stability Analysis				
	PCE \geq 10%		Without PCE restriction	
	Articles	Data number	Articles	Data number
Regular (n-i-p) cells stable more than 15 days	115	232	130	288
Regular (n-i-p) cells stable more than 30 days	106	203	122	253
Regular (n-i-p) cells stable more than 60 days	96	166	111	211
Inverted (p-i-n) cells stable more than 15 days	47	99	51	116
Inverted (p-i-n) cells stable more than 30 days	44	92	48	108
Inverted (p-i-n) cells stable more than 60 days	42	77	47	91

For the reproducibility analysis of regular cells, 547 samples containing 15446 cells from 292 articles were used while these numbers were 291 samples containing 8696 cells from 147 articles for inverted cells. The analyses for hysteresis were performed on a data set containing 295 regular cells from 146 articles and 93 inverted cells from 49 articles. The long-term stability was analyzed using the performance (% PCE) versus time (days) plots. However, in some articles, the stability has not been observed until the PCE decreased to 80% of its initial PCE (selected as stability criterion); in such cases, we used the data for only the period in which it operated (for example, if test stopped in 35th days even though PCE was not decrease to %80 of its initial value yet, we used that for 15 days and 30 days

data but not for 60 days because we could not be sure if it will reach to 60th day). For the largest data set, which was for 15 days, we used 288 stability plot from 130 papers for regular cells and 116 plots from 51 papers for inverted cells. For the PCE values, we considered the best PCE values reported in publications. However, if it was not reported, we considered average PCE or initial PCE shown in plots. More details for the data sets used were given in Table 3.1.

478 data points from 185 articles were collected for stability analysis between 2016 and 2018 (until August 2nd of 2018) with the keywords of perovskite solar and stability on topic section based on relevance search using various journals (ACS, Elsevier, Wiley and RSC databases as well as Nature and Science). However, the cells which were encapsulated (40 data points) or stored under extreme conditions such as illumination (63 data points) or higher temperatures than 30 °C (43 data points) were eliminated to prevent complexity of the model. In some articles, cell storage temperature, ambiance and humidity values were not reported. We assumed the cells were stored at room temperature (25 °C) if the temperature was not reported and represent it with 'na' sign in Data files. We also eliminated the data points where stored humidity values were not reported. If the environment where a cell was stored not determined clearly, we assumed they stored under room-light in analysis and represent them as not specified ('ns' sign). In order to check if there is any significant stability difference between storing the cells under dark or room-light, we compared the trend of average of normalized efficiencies of the cells. (Figure 3.1) We limit this comparison for the cells which were stored under zero-humidity and maximum temperature of 30 °C. As we cannot see any significant difference between room-light and dark conditions, we continued our analysis using both of them.

The data points were collected manually as they were given in the text, tables or the plots in which the data were extracted using Digitizelt software[309]. Most of the works in the literature have focused on increasing the power conversion efficiency (PCE) as the measure of progress; hence, this variable was taken as the output (performance) variable in analyses. The pooled variance, hysteresis index and the period in which the cell preserved more than 80% of its initial PCE were used as the output variables for reproducibility, hysteresis and stability, respectively. The type of the major materials in all layers (perovskite, ETL, HTL and back contact) as well as perovskite deposition techniques (one

or two-step deposition procedures and techniques used during the deposition), which affect the performance of the cell (PCE, hysteresis, stability and reproducibility), were used as the input variables as they are clearly reported in publications (Table 3.2). These are categorical variables that are key to describe the cell, hence they are decided first in research and clearly communicated in publications; most of the times, they have clear, standard and comparable meanings; hence, we used these as the input variables in our analysis. The variables used in the analyses and their most common alternatives are presented in Table 3.2.

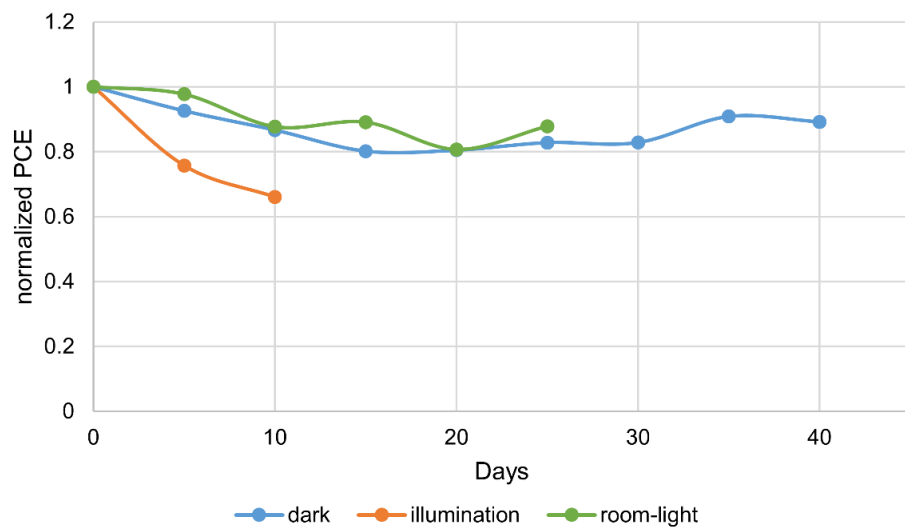


Figure 3.1. Comparison of different cell storage conditions (each point represents average of minimum five data points).

There are also continuous variables like speed and duration of coating, concentration of materials, temperature and time of annealing and so on. These variables also affect the performance significantly. However, the available data related to these variables are not always suitable for modeling because they are not always comparable due to the small variations in implementation. Indeed, our initial attempts showed that no reliable models could be developed from these variables with the data from many different sources. Hence, we omitted these variables from our analysis (with the expense of information loss on their effects) so that we can develop reliable models for the major categorical variables. Various values (levels) of omitted variables will be evenly distributed over the entire experimental domain, and their effects on the categorical variables will be balanced due to the large number of data points (like large number of experiments in statistical experimental design).

Table 3.2. Categorical Variables (Factors) Used in Machine Learning Analyses.

Factor	Alternatives
Perovskite type	MAPbI ₃ , MAPbBr ₃ , MAPbBr _{3-x} Cl _x , MAPbI _{3-x} Br _x , MAPbI _{3-x} Cl _x , MASn _{1-x} Pb _x I ₃ , FA based, Cs based, Sn based, mixed cation, mixed halide perovskites (MA=CH ₃ NH ₃ , FA=CH(NH ₂) ₂)
Perovskite deposition procedure	one-step, two-step
Perovskite deposition method	spin, spin 2-3, spin-dip, spin 2-3-dip, dip coating, VASP, CVD, evaporation-spin, spin-spray, spray, spin-dripping
Precursor solution	DMF, DMA, DMF+DMSO, DMF+CHP, DMF+DIO, DMF+GBL, DMF+H3P, DMF+HI, DMSO, DMSO+GBL, DMSO+SnF ₂ , GBL, 2-methoxyethanol+CHP
Anti-solvent treatment	chlorobenzene, toluene, diethyl ether, trifluorotoluene, ethyl acetate, ethanol, without anti-solvent treatment
ETL	Regular: (as compact layer) C60, SnO ₂ , TiO ₂ , TiO ₂ -doped, ZnO, ZnO-doped, Fe ₂ O ₃ , graphene, PCBM, without ETL Inverted: PCBM, doped PCBM, C60, PCBM+C60, ZnO, without ETL
Second layer of ETL/ETL interlayer (ETL-2)	Regular: C60, PCBM, mTiO ₂ , doped mTiO ₂ , mAl ₂ O ₃ , TiO ₂ -ns, ZnO-ns, without ETL-2 layer (m-mesoporous, ns-nanostructure) Inverted: ZnO, TiO _x , PEI, LiF, Ca, Bphen, BCP, Ba, AZO
HTL	Regular: spiro-OMeTAD, CuSCN, P3HT, PEDOT, PTAA, SWNT, without HTL Inverted: PEDOT:PSS, PEDOT:PSS-doped, CuSCN, GO, NiO _x , doped NiO _x , PTAA, without HTL
Second layer of HTL (HTL-2) (for inverted cells only)	Inverted: mAl ₂ O ₃ , polyTPD, without HTL-2
HTL additive (for regular cells only)	LiTFSI+TBP, LiTFSI+TBP+FK102, LiTFSI +TBP+FK209, LiTFSI, LiTFSI +2,6lutidine, without additive
Back contact	Carbon, Au, Ag, Al

Consequently, the analyzing and modelling the effects of the major categorical variables will be still possible.

On the other hand, the effects of thermal annealing seem to be too vital to exclude from such an analysis; hence, we also reviewed and analyzed the effects of annealing temperature, time and environment on PCE. Although this attempt helped to extract some valuable information on this issue, it also verified the difficulties dealing with such variables with data from multiple sources.

As early as 2014, it was highlighted that reported power conversion metrics might be strongly afflicted by a discrepancy in current-voltage measurements in different scan directions (hysteresis)[2], [17], and since then, the stabilized power conversion efficiencies has been also reported in some publications. There are 323 cases (17% of entire data) reporting stabilized efficiencies while the others report only the initial efficiencies as a single value for a single cell or the average and/or the best initial efficiencies of more than one cell prepared at the same conditions. Normally, the stabilized efficiencies should represent the actual performance more realistically than the initial efficiencies (even though the way to measure the stabilized efficiencies are not yet fully standardized). However, the number of papers reporting the stabilized efficiencies is still lower even though it also increases with time as it is given in Figure 2.1. Hence, the use of entire dataset for the review may give a better picture for the progress in the field because it will also cover the changes before 2014 and hundreds of works that may still contain valuable information even though they do not contain information for hysteresis. To decide for the course of action, we first analyzed and compared the dataset with stabilized efficiencies and the entire set with the best initial efficiencies (Section 4.1.1).

The “na” sign in data points represents the absence of any information in related publication. We represented the less commonly used material types or additives as others to simplify the databases. For the variable of perovskite deposition step, two-step deposition was defined to generalize the all deposition methods where halide part (ie. PbI_2) and cation part (MAI) were deposited separately and perovskite form on the surface. One-step deposition was used for the perovskite deposition methods where the perovskite was formed first in a different place, then deposited on substrate. As considering the deposition methods,

some abbreviations for vapor-assisted solution process and chemical vapor deposition were written as VASP and CVD, respectively. Spin 2-3 represents multi times spin coating of perovskite, generally two or three times repeatedly in single-step procedure. For two-step deposition methods, the steps of deposition were written with using “-” between such as spin-spray, spin-dip or spin-spin. In some rare cases, the halide part was deposited multiple times before spinning of cation part or dipping into cation solution.

For the perovskite type, in the case of perovskite contains more than one cation, it was called as mixed cation perovskite. In the case of a one cation perovskite contains more than two halides, it was called as mixed halide perovskite. If a perovskite contains Sn and does not have any Pb, it was called Sn based perovskite. One cation perovskites which have FA or Cs cation were called as FA or Cs based perovskites. The perovskites synthesized using lead (II) thiocyanate ($\text{Pb}(\text{SCN})_2$) as a precursor solution were named as “ $\text{MAPb}(\text{SCN})_x\text{I}_{3-x}$ ” [190], [310], on the other hand, in some other studies, $\text{Pb}(\text{SCN})_2$ was mentioned as a precursor solution additive [70], [311]; hence we used the exact names given in publications in PCE analysis. However, we named them as MAPbI_3 to prevent complexity in other analyses.

For regular structure, in order to identify the mesoporous structures in ETL-2 (second layer of ETL), “m” was written at the beginning of the material names such as mAl_2O_3 , mTiO_2 etc. For determining the structures of nanorod(nr), nanowire(nw), nanocone(nc), nanoflower(nfl), nanoflake(nfl), nanocolumnar(ncl), nanosheet(ns), nanotubes(nt) and nanofiber(nf), we named them as nanostructures (ns) (TiO_2 -ns, ZnO -ns etc.) for generalization. For ETL (compact layer), ETL-2, HTL and HTL-2, some variables were defined as “0” or “no”. 0 was used to represent the absence of one of those whereas no were used for the absence of entire layer (like HTL free cells). Some of the most common ETL or HTL materials were doped with various dopants to improve performance. Instead defining all these variables as a new variable, we gave a common name such as TiO_2 -doped to simplify the database for analysis. For the other materials except TiO_2 in PCE analysis, the name of the material was used only in ETL or ETL-2 columns even they were doped or not, because we had less data points for other ETL materials (ZnO -doped was used for entire dataset modeling because we had enough data points for this variable, but it was named as ZnO for modelling of stabilized database). For the hysteresis analysis of inverted cells only,

all PTAA containing cells (doped or not) in were labeled as PTAA due to the low number of cases. Similarly, in reproducibility analysis, there was only one data point for doped P3HT as HTL in regular cells, and we also labeled this point as P3HT in our analysis. For ETL and ETL-2 in inverted and regular cells, we took all C60 derivatives (except PCBM) as C60; we labeled PCBM as separately due to its frequent use.

For inverted cells, PEDOT:PSS and NiO_x were separated as doped or undoped in HTL column. Although we had data points using doped PTAA, we did not consider it as another variable to have enough data points. For the second layer of HTL, “m” was written at the beginning of the mesoporous materials similar . Similar to PTAA, data points with doped mNiO_x were not indicated as “doped” due to lack of enough data points.

Some common HTL additives were named as following: Lithium bis(trifluoromethylsulfonyl)-imide salt (Li), 4-tert-butylpyridine (TBP), Co(III) complexes such as tris(2-(1H-pyrazol-1-yl)pyridine)cobalt(III) (FK102), 106 tris(2-(1H-pyrazol-1-yl)-4-tert-butylpyridine) cobalt(III) tris-(bis(trifluoromethylsulfonyl)imide)) (FK209) and tris[2-(1H-pyrazol-1-yl)pyrimidine]cobalt(III) tris[bis(trifluoromethylsulfonyl)- imide] (MY11). In two articles, the exact structure of Co(II)TFSI was not indicated (as FK102, FK209 etc); hence we also used Co(II)TFSI for his material as in the articles. In reproducibility, hysteresis and long-term stability analyses, we named all inorganic materials as inorganic HTL.

We represented all carbon containing back contact types (such as graphene, graphite) or different carbon structures (such as nanotubes, porous structure, cloth) as carbon. In inverted cells, Ag nanowire (Ag-nw) also assumed as Ag back contact material.

For the annealing conditions, one-step deposited MAPbI₃ based perovskite cells were considered only.

In reproducibility analysis, some articles did not contain the exact number of cells of which the standard deviation was calculated, instead they mentioned “more than xx”; we used xx as the sample size in pooled standard deviation analysis. If any article reports the cell number is between two numbers, we took the average of it.

In stability analysis, the ambient humidity was divided into three parts, 0-30% RH, 30-60% RH and humidity above 60% RH. The temperature was assumed to be room temperature (25 °C) if the publications did not report the ambient temperature where perovskite cells were stored. The data of the cells stored in extreme conditions (under illumination, at high temperatures or in special encapsulation) or if the storage conditions are not clearly explained were not used in analysis.

3.2. Analysis and Computational Methods

Descriptive statistical analysis was conducted on Excel. Data mining analyses were performed using R Studio software[312]. Random forest regression was performed using randomForest package[313], association rule mining analyses were performed using arules package[314] where apriori algorithm was employed and decision trees were built using rpart package[315] of RStudio where CART algorithm was employed. Random sampling of classes was implemented using dplyr package[316] of RStudio.

3.2.1. Analysis of Power Conversion Efficiency

3.2.1.1. Descriptive Statistical Analysis. First, the data were analyzed using simple descriptive statistics like annual change in average (mean) efficiencies and distribution of data among the efficiency levels for each specific factor so that the change of trends with time could be seen in Section 4.1.2. The data range (0-23.3%) was divided into five equal parts (0%-4.5%, 4.5%-9.0%, 9.0%-13.5%, 13.5%-18.0%, 18.0%-23.3%; efficiencies equal to exactly 4.5%, 9.0%, 13.5% and 18.0% were put into the lower classes) creating five subsets to draw distribution of data to make sure that the averaging efficiencies are meaningful (i.e. whether the data distributed normally around its own mean or not). It should be noted that the record efficiency of perovskite solar cells was 23.3% when the analysis was made, but it increased to 23.7% in later works[1]. Although there are some slightly skewed distributions in Section 4.1.2, almost all distributions are quite close to normal; hence, the arithmetical mean was used as the indicator of the average performance for simplicity.

The ball size (and the numbers) in Figure 4.4 (perovskite materials) shows the number of publications found in Web of Science search involving the perovskite material in a given

year. However, in other figures in Section 4.1.2, the ball size shows the fraction of data points in our database for the material or method of interest because an accurate search in Web of Science for other variables could not be possible. Considering the large size of the database, these fractions can be assumed to reflect the actual status in literature reasonable well. The plots for the time changes for the variables (like Figure 4.3a) were constructed with minimum five data points for each year (20-25 in total) while the distribution plots (like Figure 4.3b) were constructed only the variables having more than 20 data points. If the average of two alternatives of a variable were compared (like Figure 4.5), minimum 10 data points for each were required. However, the number of cases in database for less frequently used but promising factors (like Cs based perovskites, some of mixed cation perovskites, some inorganic and some organic HTLs) were not sufficient for statistical analysis (as the consequence of random data extraction process). Hence, the additional data points were extracted to calculate the averages for these variables if the number is close to the limits described above. However, the new data points were not used in other analyses to keep the randomly created structure of the database.

The certified record efficiencies reported by NREL were also modelled using S shaped logistic growth curve presented in Equation 3.1,

$$\frac{\text{PCE}}{(\text{PCE})_{\text{limit}}} = \frac{1}{1 + ae^{-bt}} \quad (3.1)$$

$(\text{PCE})_{\text{limit}}$ is the upper limit of efficiency and assumed to be 27% [317] (31 % could be also used without changing the result significantly [318]), a and b are constant to be determined while t represent time as years. The equation was linearized first as

$$\ln\left(\frac{1 - \text{PCE}/(\text{PCE})_{\text{limit}}}{\text{PCE}/(\text{PCE})_{\text{limit}}}\right) = \ln(a) - bt \quad (3.2)$$

Then, constants $\ln(a)$ and (b) were determined from $\ln\left(\frac{1 - \text{PCE}/(\text{PCE})_{\text{limit}}}{\text{PCE}/(\text{PCE})_{\text{limit}}}\right)$ versus time t plot as 848.35 and 0.4213 respectively with the R^2 value of 0.98.

3.2.1.2. Random Forest Regression. The random forest regression model was built to test the predictability of power conversion efficiency; the root mean square error (RMSE) was used as the indicator of the prediction capacity of the model. Basically, random forest model is an ensemble method that creates multiple decision trees and predicts a new data point by the majority vote. The number of the trees was optimized by 5-fold cross validation. The dataset was divided into 5 equal parts and different number of trees were implemented for each fold. Then, the average RMSE value of each tree number within each fold was listed, the tree number with the minimum average RMSE was considered in model. 110 and 30 trees were used for stabilized dataset of regular and inverted cells whereas 600 and 250 number of trees were generated for the entire dataset of regular and inverted cells.

3.2.1.3. Association Rule Mining. Association rule mining is used to determine frequent combinations, patterns, rules and associations. There are three parameters that are used to interpret and make decision in this technique: support, confidence and lift. Support indicates the frequency of the occurrence of two itemsets together. Confidence is the ratio of how much a specific item found with another specific item. Lift is the ratio of how much a specific item found with another specific item to the ratio of this specific item found in overall database, hence it shows if the occurrence of this item with another specific item is significant and more frequent. An example was given in Section 4.1.4 to understand these terms better. The lift value was used for the detection of any patterns or rules in this part. Support value was adjusted as any condition should fulfill at least 5 data points. 5 data points may be slightly low but we wanted to extract any less common patterns as well. Confidence values were set to 0.1. The rule deduction was performed only for the highest efficiency class (above 18.0%) for each dataset since one usually seeks to know what to do to achieve high efficiency. We selected this limit considering both number of data points and decision tree classification which gave us the best split.

3.2.1.4. Decision Tree Analysis. The decision tree analysis was performed by using rpart package in RStudio. Database was classified into three groups as high (A), intermediate (B) and low (C) efficiency groups for regular structure. In decision tree analysis, the database should be normally divided into certain number of approximately equal size classes to prevent the class imbalance problem may occur (even the small fraction of incorrectly classified data from large classes may reduce the accuracy rate of neighbouring small

classes). If three equal size classes were created from our databases, the minimum level for the high efficiency class would be 16.5% for stabilized ; 14% for entire datasets of regular and inverted cells. However, in order to extract rules compatible with association rule mining analysis, the limits of the highest (18.0%) and the lowest (4.5 %) groups used in distribution plots were selected to represent Class A and Class C considering that one really prefer to know the rules and conditions for significantly high conversion such as 18.0%. However, the stabilized efficiency dataset is much smaller and the data are mostly located at higher efficiencies; there are only 5 data points at 4.5% and below for the regular cells, which is clearly not sufficient for the decision tree analysis (there are only 2 cases for inverted cells). Hence, we had to change the limits of low (C) class from 4.5% to 9 % (also covering the second lowest parts in distribution analysis) for regular and inverted cells (number of data points for C classes increased to 25 for regular cells, which were sufficient). Even this change was not sufficient for the stabilized efficiency dataset for the inverted cells; consequently, we decided not to perform decision tree analysis for this set.

We had only 38 data points (111 data points in entire dataset) in Class A and 25 data points (411 data points in entire dataset) in Class C while the remaining 186 data points (885 data points in entire database) remained in class B in regular stabilized database; this is definitely a class imbalance situation. In such situations, the data points in small classes are duplicated by random sampling until they reach the size of large sample if the number of data points in small sample is large enough to have a similar statistical distribution with its enlarged version. In regular cells, the number of data points in Class A and C are sufficiently large to apply random sampling; hence the data points in Class A were replicated for 4.9 times to have 186 data points (8 times to have 888 data points in entire dataset) and data in class C for 7.4 times to have 185 data points (2.2 times to have 904 data points) to have a balanced class structure. Similarly, in the entire dataset of inverted case, the number of data points in Class A and Class C were 37 and 123, respectively and they were replicated for 9.6 and 2.9 times (355 and 356 data points were obtained for Class A and C, respectively).

Various values of the minimum number of split, depth of the tree and complexity parameter were tested with the class structure described above. 5 fold cross validation procedure was employed to optimize the minimum number of split, depth of the tree and complexity parameter. Then, the parameters were fine-tuned to have a tree not only with the

highest classification accuracy but also to with reasonable generalizable results in the terminal nodes.

The performance of the classification of decision tree model was evaluated using two measures. First, the overall classification accuracy of the model (ratio of correctly classified data points to the total number of data points in database) was considered. Second measure was the precision of each class. (ratio of the correctly classified data points which belonged to Class A to number of the data points predicted as Class A) Although the accuracy (ratio of the correctly classified data points which belonged to Class A to total data number of Class A) is also an important measure for classification, this measure was more important for us than accuracy of each class because we tried to get the purest branches and nodes to implement better rules. The most of the data predicted as Class A should be pure as much as possible. Hence, the model should not predict other classes as A.

As mentioned before, for the stabilized dataset of regular cells, the low efficiency upper limit was changed to 9% for decision tree modelling due to lack of enough data points below 4.5%. Hence, this case should be taken in account while interpreting the rules.

3.2.2. Analysis of Reproducibility

The standard deviations for sample (batches) were obtained from the papers or calculated from Equation (1) using the PCE distribution given for that batch:

$$S = \sqrt{\frac{1}{N-1} \sum_{i=1}^N (x_i - \bar{x})^2} \quad (3.3)$$

where N is total number of data points in sample while x_i and \bar{x} are the individual PCEs and their sample mean respectively. Then, the pooled standard deviation (S_p) or variance (S_p^2), which can be used as the measure of reproducibility[319], was computed for the samples containing the same factor (material or method):

$$S_p = \sqrt{\frac{(n_1 - 1)S_1^2 + (n_2 - 1)S_2^2 + \dots + (n_k - 1)S_k^2}{(n_1 + n_2 + \dots + n_k - k)}} \quad (3.4)$$

The F-test was performed for pairwise comparison of S_p^2 to assess whether the differences in pooled variances are statistically significant or not for the use as the measure of reproducibility[319]; the confidence level was taken as % 95.

We used only the batches having minimum five cells in reproducibility calculations to capture the variability in each work sufficiently. We also considered material types and techniques reported by minimum five publications.

3.2.3. Analysis of Hysteresis

Hysteresis index (HI) as performance measure for analysis was calculated from Equation 3.5 [320]

$$HI = \frac{|PCE_{reverse} - PCE_{forward}|}{PCE_{reverse}} \quad (3.5)$$

where $PCE_{forward}$ and $PCE_{reverse}$ are the power conversion efficiencies obtained using forward and reverse scan respectively. Mostly, the higher efficiency values are obtained under reverse scan conditions[60] while the efficiency under forward scan can be also higher in some cases; hence, we took the absolute value of $(PCE_{forward} - PCE_{reverse})$. Although some other HI formulations were also proposed for more accurate representation of hysteresis[179]; the one in Equation 3.5 was chosen for its simplicity for the construction and interpretation of the model.

3.2.3.1. Random Forest Regression. Since the scan rate has a significant impact on hysteresis measurements and it should be as low as possible for accurate measurement, we used only the data obtained under maximum scan rate of 0.05 V/s for regression. The number of trees generated was optimized using entire dataset using 5 fold cross validation. 15 and 10 trees were generated for regular (n-i-p) and inverted (p-i-n) cells, respectively. 5-fold cross

validation was implemented to check the reliability of the model. Average RMSE of training and testing were considered. The analysis was performed by using rpart package in RStudio.

3.2.3.2. Association Rule Mining. In order to detect the most significant factors for low hysteresis, we again used the data measured under the maximum scan rate of 0.05 V/s. We also performed the analysis covering all scan rates for comparison. The analyses for hysteresis was performed for $HI \leq 0.01$ as the criterion for low hysteresis; the analysis was also repeated for $HI \leq 0.05$ for additional information because the results may be slightly more reliable for this case due to the larger number of data points. We also restricted our analysis to the cells having $PCE \geq 10\%$ to capture the hysteresis trends for high PCE cells but again we also provided the results for entire data set.

The association rule mining was used to analyze the impact of input variables and find the most frequently used factors leading low hysteresis cells. Three parameters were used for the analysis; support, confidence and lift; all are explained in Section 3.2.1.3 and Table 4.1; while the lift was also discussed in detail in Results and Discussion (Section 4.1.4).

3.2.3.3. Decision Tree Analysis. We splitted the the dataset into three classes; the cells with $HI \leq 0.01$ (Class A), $0.01 < HI \leq 0.1$ (Class B) and $HI > 0.1$ (Class C). We performed analysis with the cells which have $PCE \geq 10\%$ because we are not just looking for factors leading low hysteresis but also cells with a considerable PCE. The number of classes in database of regular cells are 18, 54 and 38 for Class A, B and C, respectively. Hence, the data points were randomly sampled to prevent class imbalance (Class A and C were sampled three and 1.4 times, respectively). For the inverted cells, there were no cells which have HI larger than 0.1, hence database was divided into two classes. The minimum split number, maximum depth and complexity parameter were optimized as explained in Section 3.2.1.4. We also did same analyses without considering PCE limitation.

3.2.4. Analysis of Long –term Stability

The PCE versus time values were extracted from the stability plots in the papers for 15, 30 and 60 days period using Digitizelt software[309]. The performance measure was

selected as the number of days in which cell can preserve more than 80% of its initial PCE. Normalized PCE values were used in the analyses.

3.2.4.1. Random Forest Regression. Random forest regression was employed to predict the exact time when the cells have dropped to 80% of their initial PCE. The number of trees generated was optimized using entire dataset using average RMSE of 5 fold cross validation. 65 and 20 trees were generated for regular (n-i-p) and inverted (p-i-n) cells, respectively. The models were checked by using 5-fold cross validation and average RMSE of training and testing were considered.

3.2.4.2. Association Rule Mining. Association rule mining was performed to capture the most effective factors for long-stability. We repeated the analysis for 15 days, 30 days and 60 days cumulatively (15 days data covers 30 and 60 days while 30 days data covers 30 and 60 days). However, considering that the absolute value of PCE is also important to see the potential of the cell, we also performed the same analyses covering only the cells having the initial $PCE \geq 10\%$. The y-axis of bubble plots represents the lift values and bubble size gives the number of data points provides this condition. These numbers were also written on bubbles whereas the numbers in parenthesis represents how many of them have initial $PCE \geq 10\%$. In bubble plots, we included the variables which have at least 5 data points in analysis of 15 days. However, the analysis for all cases can be seen in Appendix D.

3.2.4.3. Decision Tree Analysis. In order to determine the heuristics for high stability, the data was divided into three classes; cells stable more than 60 days (Class A), cells degraded within 7-60 days (Class B) and cells degraded within 6 days (Class C). This division (except Class A) was decided depending on data distribution. We divided the remaining data from Class A into two equal part. One can use different class limits and do the same analysis as well. For regular cells, we performed random sampling of Class A to prevent class imbalance (Class A was sampled 3.5 times). In database of inverted cells, we did not have enough data points for Class A for both $PCE \geq 10$ (only 8 in 77 data points) and without PCE consideration (only 8 in 91 data points), we could not construct a decision tree.

4. RESULTS AND DISCUSSION

4.1. Analysis of Power Conversion Efficiency

4.1.1. Comparison of Stabilized Efficiency Dataset with Entire Database

As mentioned in computational details, the hysteresis was taken into consideration, and the stabilized efficiencies have been reported in some of the articles since 2014. The stabilized efficiencies are better measures of the real performances because they are usually lower than the initial efficiencies, which are directly computed from J-V curves. As the result, we also analysed the dataset containing only the data extracted from these articles to see if there are significant differences in the patterns of this subset from the entire database. Figure 4.1 shows the change of average efficiencies computed from the entire database and stabilized efficiency subset for three cell structures through the years starting from 2015 to 2017. The data belonging to these years were used in both datasets; 2014 was excluded due to the insufficient number of stabilized efficiency data while 2018 was not taken because it is not yet completed. It should be also noted that the entire database contained stabilized efficiencies as well because the other data points in the database do not necessarily have hysteresis; simple, they are not checked for that. Surprisingly, the averages of stabilized efficiencies are slightly higher than those for the entire database for all three structures but they seem to follow exactly the same trend with the entire dataset; the difference is slightly higher for the inverted cells in recent years.

To understand the differences between the stabilized efficiencies only and the entire databases better, we also plot the distribution of data in two groups for all three cell designs. As seen in Figure 4.2, the distributions for the stabilized efficiencies are narrower and shifted to the higher efficiency sides with very small fractions (even none) in the very low efficiencies. Probably, these differences come from the fact that the experienced groups, whose initial efficiencies are also higher than the average, report the stabilized efficiencies more often. The analyses presented in Section 4.1.3 also seem to support this argument; the statistical fitness of the models developed by the stabilized efficiencies are also higher (indicating higher reproducibility) than the models from the entire database. Consequently,

we built and presented our machine learning models derived from the stabilized efficiencies in Section 4.1.4 and Section 4.1.5 while occasionally comparing them with the models of entire dataset.

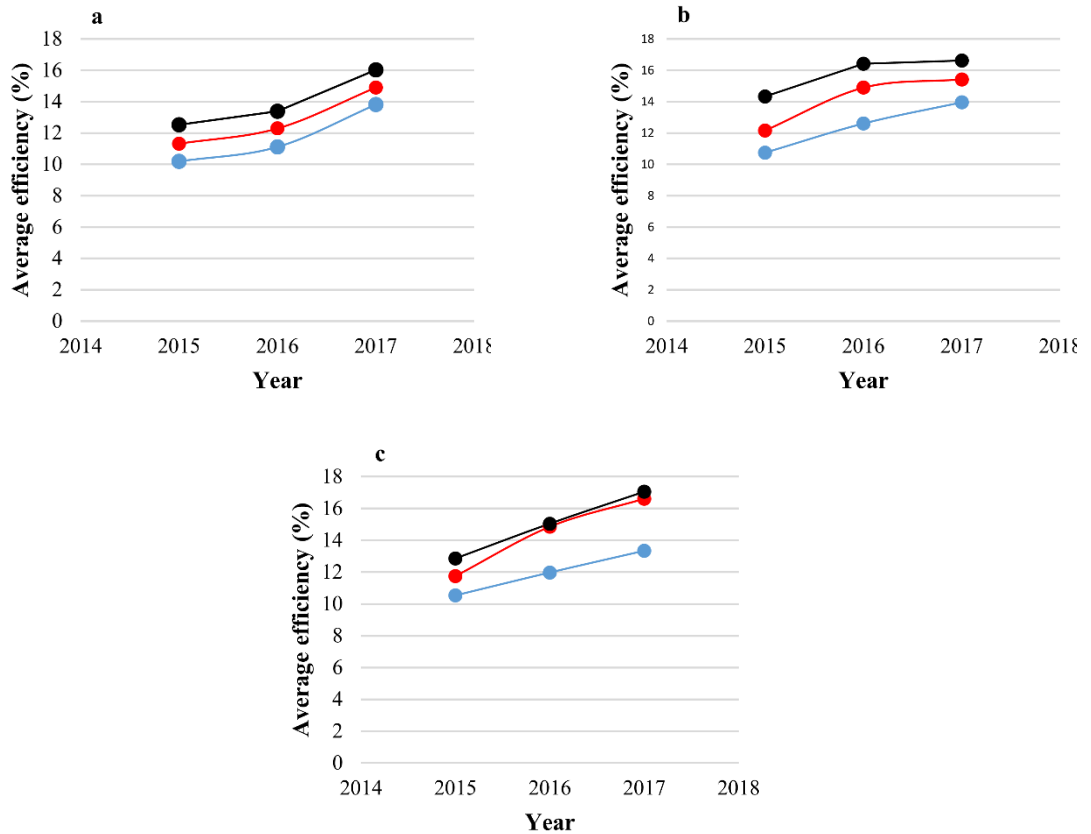


Figure 4.1. Change in average efficiencies for three cell structure through years (a) regular mesoporous (b) regular planar (c) inverted (blue symbols are overall average for best cell efficiencies, red symbols are for stabilized efficiencies and black symbols are for best cell efficiencies of the cells which the stabilized efficiencies were given).

On the other hand, the stabilized efficiencies data are not sufficient to appreciate the progress in the field because it does not contain the works before 2014, and only partially cover the results reported since 2014. Considering that the papers in which the hysteresis is not checked, are also the valuable parts of the experience in the field, and the two datasets follow similar trends (see Figure 4.1 and association rule mining results in Section 4.1.4); we decided to use the entire database in the part of Section 4.1.2 for the review of progress.

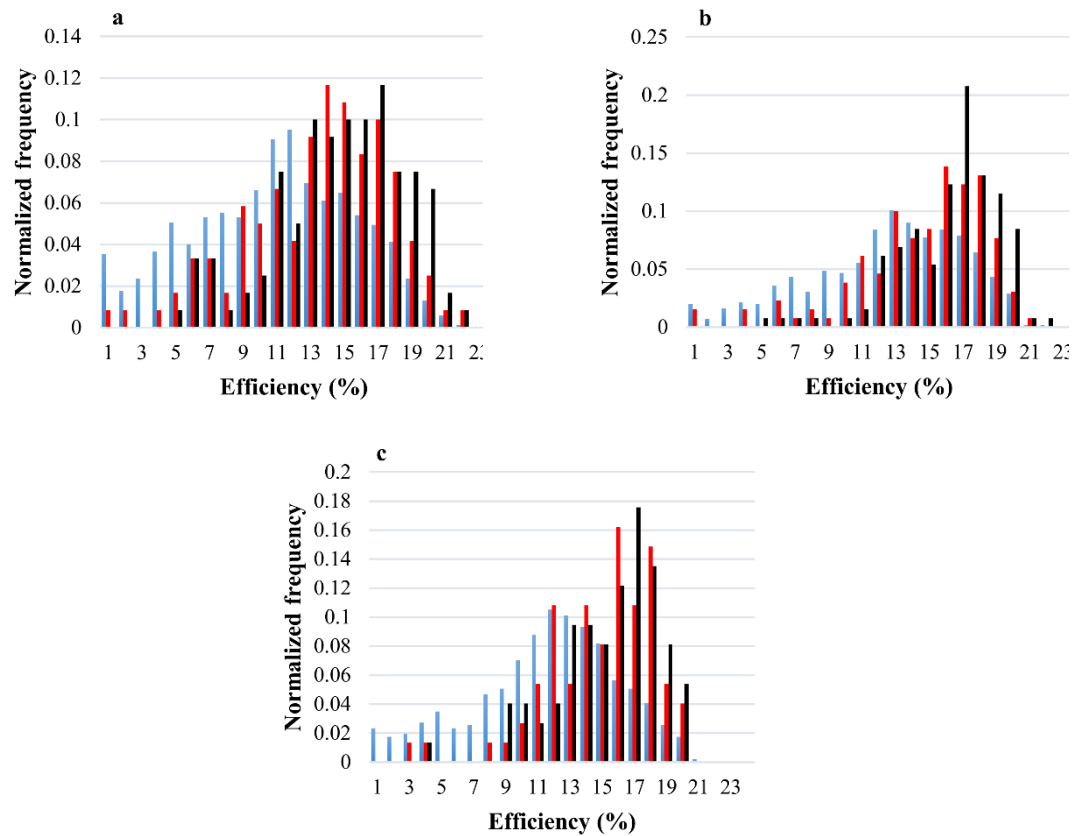


Figure 4.2. Distribution (fractions) of efficiencies in database for three cell structures (a) regular mesoporous (b) regular planar (c) inverted; blue columns show the distribution for entire dataset, red columns are for stabilized efficiencies only, green columns are best cell efficiencies of stabilized data points.

4.1.2. Descriptive Statistical Analysis of Power Conversion Efficiency

Although the popularity of inverted structure has been increased in recent years, the number of data points in regular structure (sum of planar and mesoporous) is still larger (73 % of total data in database). Figure 4.3a shows the average efficiencies (y-axis), which were obtained from the averaging the data for regular (mesoporous and planar) and inverted structures in the database. Although, our database contains data points for the inverted cells in 2013 with the average efficiency of 3.4%, which is consistent with the annual efficiency trend, the average was not included in Figure 4.3a, because the data points were less than five.

The average efficiency obtained with regular planar structure has been generally higher than mesoporous and inverted structure slightly. However, the gap seems to be closed in recent years. Figure 4.3b shows the distribution of data points among the efficiency levels. The data for the regular mesoporous and inverted structures are almost normally distributed while the curve for regular planar cells is slightly shifted to the right; although the 9.0-13.5% efficiency range has the highest fraction of data points for planar mesoporous and inverted cells, the most crowded group for regular planar cells is 13.5-18.0% data range.

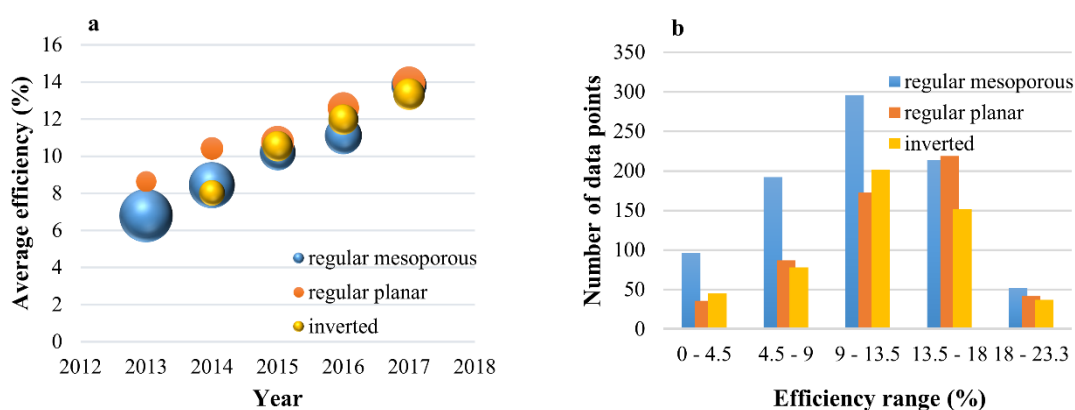


Figure 4.3. Performance of common cell structures through years (a) change of average efficiencies (ball size shows fraction of data in each year) (b) distribution of data over the efficiency levels.

4.1.2.1. Effect of Perovskite Type. In Figure 4.4, the bubble size (with number in the same color) indicates the number of publications involving that perovskite in Web of Science search while the y-axis indicates the average efficiencies, which is computed from our database (we could not do that from Web of Science data). However, as we mentioned above, our database contains sufficiently large number of points; hence, the averages computed from our data should represent the entire literature reasonable well.

As Cl⁻ addition to the most common MAPbI₃ perovskite reported to improve performance[12], [34], [36], the average efficiencies obtained with this perovskite seems to be also slightly higher than MAPbI₃. On the other hand, the study of Stone *et al.*[38] should also be considered which reported that Cl addition only enhanced morphology of the MAPbI₃ perovskite but did not take part in the structure; this case is also possible due to similar average efficiencies and trends of these two perovskites. Also, Figure 4.4 seems to

verify the claims that FA based and mixed cation perovskite solar cells are generally more efficient than MAPbI_3 and $\text{MAPbI}_{3-x}\text{Cl}_x$. Although, our database also contains data points for mixed cation in 2014 with average efficiency of 10.2%, we did not plot it in Figure 4.4 because we had four data points (<five data points) for this year.

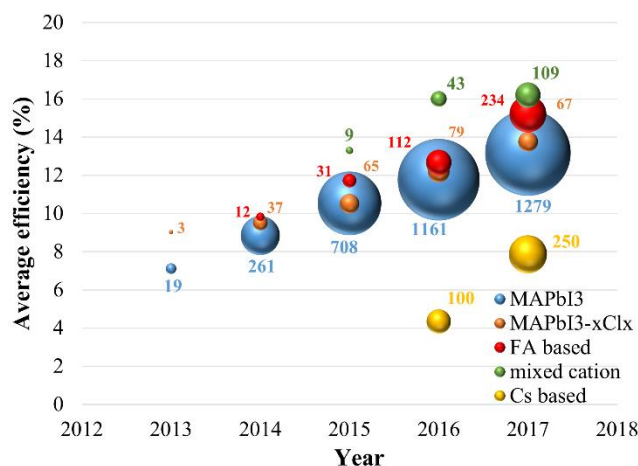


Figure 4.4. Comparison of number of papers published (ball size) and average efficiencies (y-axis) obtained with various perovskites through years.

The highest average efficiencies in Figure 4.4 belongs to mixed cation cells, which are made of perovskites with the combinations of two or three different cations. Hence, the performances of individual combinations were also analyzed separately so that the best combinations could be identified.

The cells with the mixed Cs-FA-MA cations showed the best average efficiency in Figure 4.5 due to the shifted tolerance factor to a cubic phase region and eliminated yellow phase impurities in perovskite films[50]. Incorporating Cs with FA cation was found to perform second best option due to its narrower band gap and a more stable perovskite phase than FAPbI_3 alone[51], [52]. The FA-MA cations have also a high average efficiency of 15% (even though it is not the highest); this combination was reported to increase the performance and prevent the phase instability of FAPbI_3 alone[43]. Although the average performances of 2D-3D mixed perovskites (AVA-MA, PEA-MA) are slightly lower than other mixed cation perovskites, they are promising due to their high stability[53], [54].

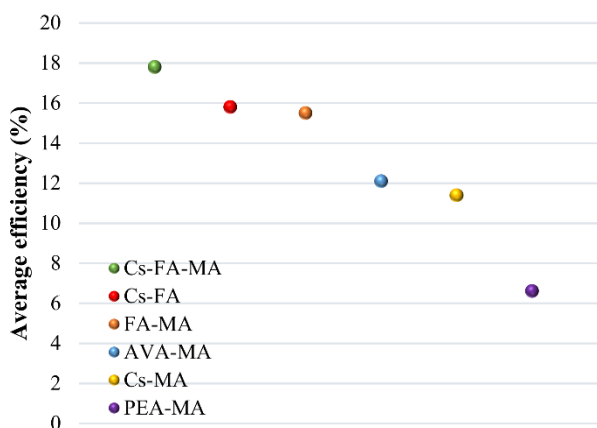


Figure 4.5. Comparison of average efficiencies of mixed cation perovskites.

Although the average efficiencies presented in Figure 4.4 provide valuable information for the performance of perovskite material, inspection of the efficiency distribution in the entire range of 0% to maximum 23.3% may also provide some additional information (Figure 4.6). For the regular structure (Figure 4.6a), the data points for MAPbI_3 and $\text{MAPbI}_{3-x}\text{Cl}_x$ almost normally distributed around the mean efficiency values by covering the entire range of literature. The efficiencies of FA based and mixed cation perovskite, on the other hand, distributed to narrower (and higher) ranges, and they negatively skewed indicating that the high efficiency cells with these perovskites are more probable.

The pattern for inverted cell (Figure 4.6b) is quite similar to regular cell for MAPbI_3 and $\text{MAPbI}_{3-x}\text{Cl}_x$ in both shape and the location of the average distribution. However, the number of mixed cation cells are small to have generalization (even though they show some pattern); the data for FA based cells were even smaller to show a distribution in the figure.

Then we analyzed regular structure in more detail by separating data for mesoporous and planar structure (Figure 4.6c and Figure 4.6d). The average efficiency for MAPbI_3 and $\text{MAPbI}_{3-x}\text{Cl}_x$ are same in mesoporous cell structure whereas the average was slightly better for MAPbI_3 in planar structure; the highest number of cells were obtained in 13.5-18.0 % efficiency range in planar cells while this range was 9.0-13.5% in mesoporous cells. Shi *et al.* reported that MAPbI_3 gave higher performance in mesoporous cells while $\text{MAPbI}_{3-x}\text{Cl}_x$ is better in planar structures[321]; however, the distribution curves in Figure 4.6c and Figure 4.6d shows that both perovskites (especially MAPbI_3) performed better in planar structure.

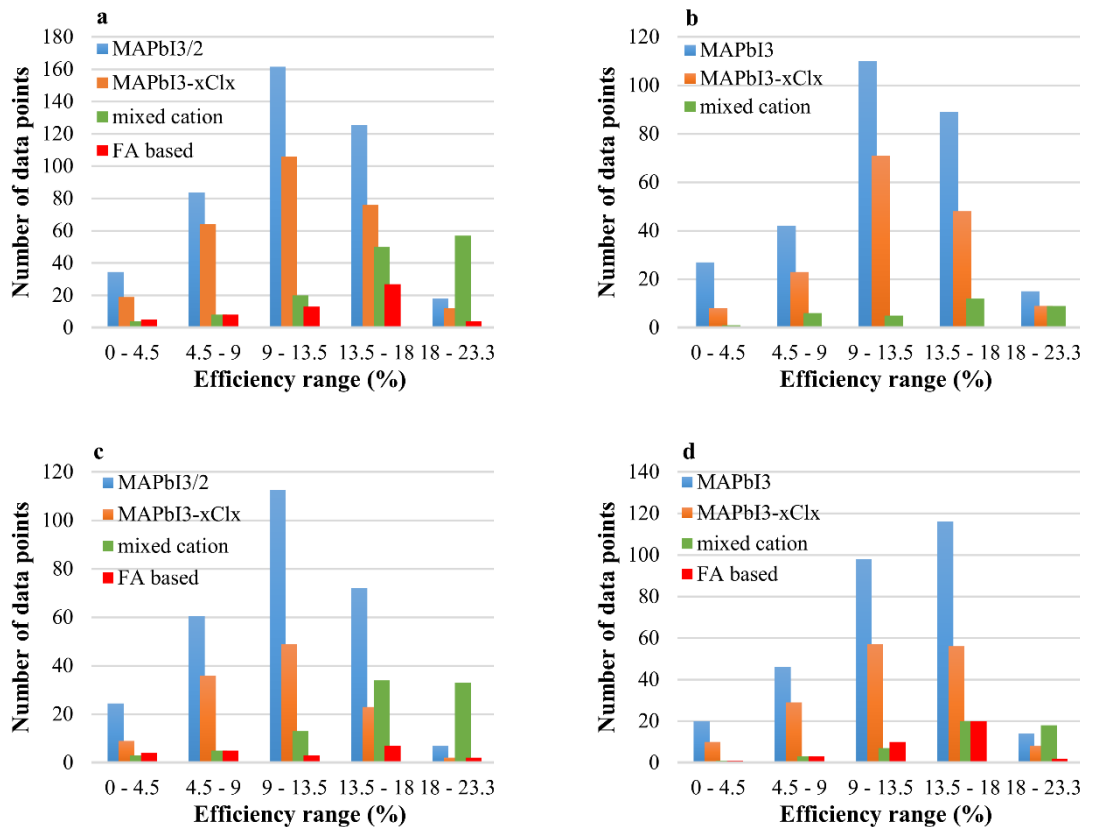


Figure 4.6. Distribution of efficiency in database obtained with different common perovskites in three cell structure (a) regular (n-i-p), (b) inverted (p-i-n), (c) regular (n-i-p) mesoporous, (d) regular (n-i-p) planar.

4.1.2.2. Effect of Perovskite Deposition. Perovskite deposition procedure (one or two step deposition) has an effect on performance because it affects the perovskite morphology. First and the most common method is one-step spin coating (64.7% of experimental data points in our database were obtained with this method). However, two step procedure is employed because of the challenges in controlling the crystallization and obtaining homogenous perovskite films using one-step method. As Figure 4.7a shows, the average efficiency obtained with both procedures continuously increased with time; the two-step procedure indeed resulted in better power conversion efficiencies in early years (Figure 4.7a). On the other hand, one-step procedure has been improved much better in later years as it is clearly observable from Figure 4.7a because of the efforts involving the more effective use of solvent and anti-solvent in this approach. In Figure 4.7b, the trends in various version of spin coating methods for perovskite deposition were also given. Similar to Figure 4.7a, one-step

deposition methods (spin and spin 2-3) were seemed to result higher efficiencies in recent years.

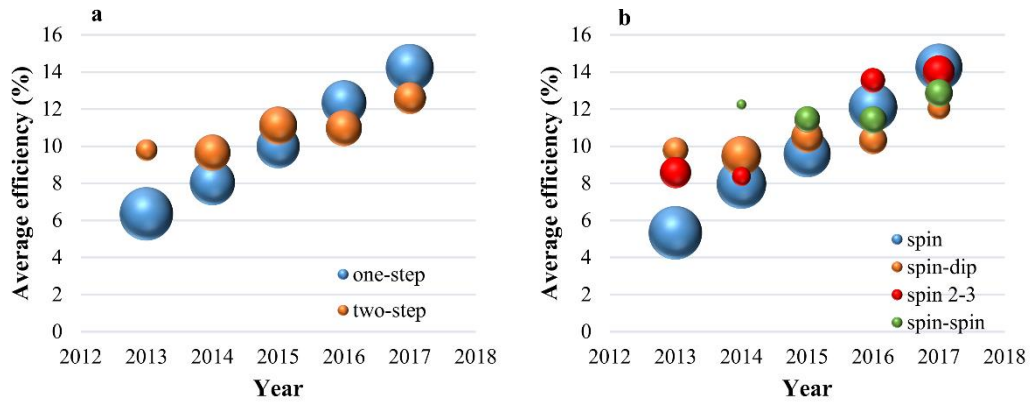


Figure 4.7. Comparison of different perovskite deposition methods (a) change of average efficiencies with one-step (1S) and two-step(2S) procedures through years (b) variation of spin coating methods (spin-spin and spin-dip show sequences in 2S; spin 2-3: 2-3 times spin in 1S)

The distribution of the data points among various efficiency levels for different cell structure verifies this argument (Figure 4.8). In regular structure (Figure 4.8a), the one-step method has been implemented more often especially at high efficiency cells while the two-step method has been also used significantly; however, one-step method was overwhelmingly more preferred than two-step procedures in inverted cells (Figure 4.8b). The difference between two deposition methods becomes more obvious if the regular cell data are divided into mesoporous and planar structures (Figure 4.8c and Figure 4.8d). The one-step procedure has been clearly more preferred for the planar cells while both methods seems to be used almost equally in mesoporous structure; this may be due to the belief that two-step procedure aids the perovskite penetrate to the pores of mesoporous structure. However, one-step procedure seems to result in higher average efficiencies in both types of regular cell.

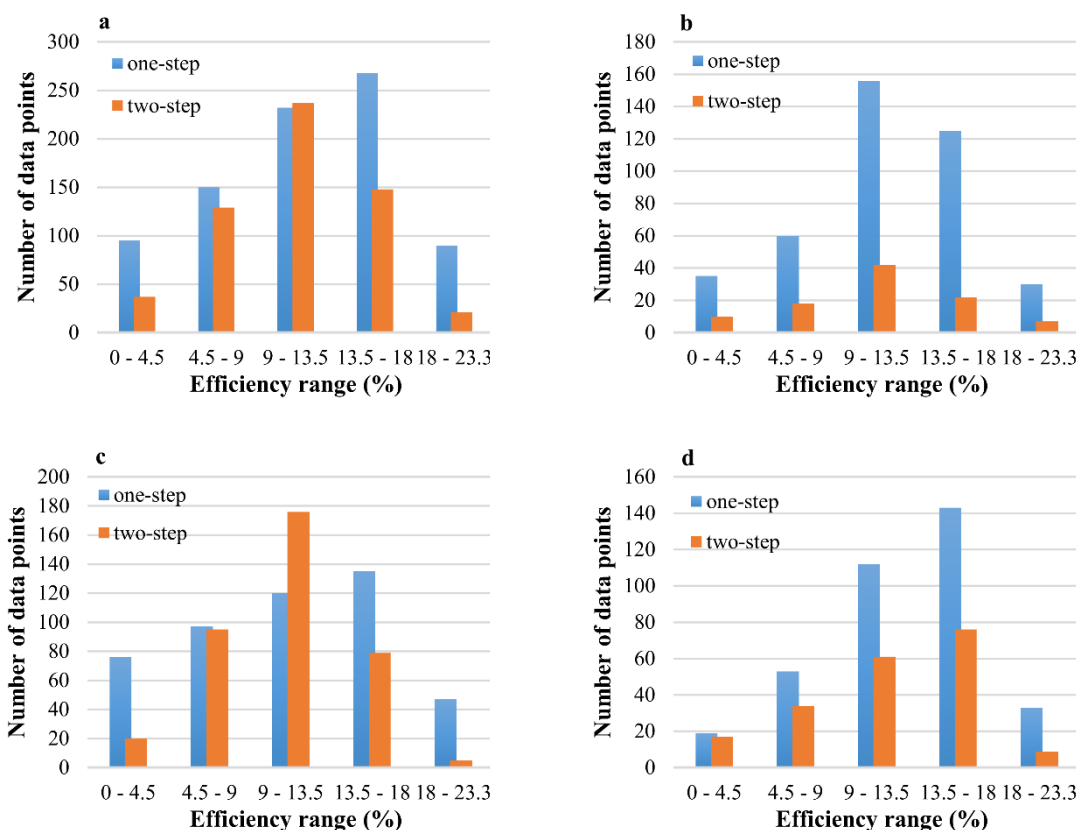


Figure 4.8. Distribution of data in database for one and two step deposition procedure for various cell structures (a) regular (n-i-p), (b) inverted (p-i-n), (c) regular (n-i-p) mesoporous, (d) regular (n-i-p) planar.

The effects of solvents and anti-solvents were also analyzed in detail since various sources in the literature have been discussed the importance of this issue for the better control of crystallization. Figure 4.9a shows the frequency of the solvents and average efficiencies obtained (in both one-step and two-step procedures). DMF is the most common solvent used in both method (although it gives the fourth highest average efficiency); DMSO or DMSO addition to other solvents also improved the efficiency. For example, DMF+DMSO mixture seems to be the most effective solvent; this was attributed to the fact that DMSO coordinates PbI_2 with covalent bonds and forms PbI_2 -DMSO complex for MAPbI_3 coating; then, by the interaction of this complex with MAI, a flat and homogenous films occur by an intramolecular exchange and retarded crystallization of PbI_2 in DMF[322]. Besides the controlled crystallization of the perovskite by DMF+DMSO, the surface coverage better than using DMSO alone was also provided. The role of DMSO was found to retard crystallization whereas DMF was found to improve surface coverage by increasing the surface tension of the solution and decreasing the polarity[323]. When employing GBL as the solvent, a rapid

crystallization of perovskite was observed; this resulted inhomogeneous surface structure and poor coverage of perovskite. However, when GBL solvent was used with DMSO, an intermediate phase occurred (MAI–PbI₂–DMSO) and the crystallization was slowed down. As a result, a homogenous flat surface of perovskite was formed[15].

The distribution of data among the efficiency levels is also given in Figure 4.9b; all the solvents (except GBL) exhibited almost normal like distribution around their own means (DMSO, DMF+DMSO and DMSO+GBL showed higher frequencies at high efficiencies verifying their superiority as discussed above). We also tried to distinct the situations in one and two-step procedure, but we could not; the most common solvent (DMF) resulted almost the same average in both procedure, and there were not sufficient number of data to compare the others.

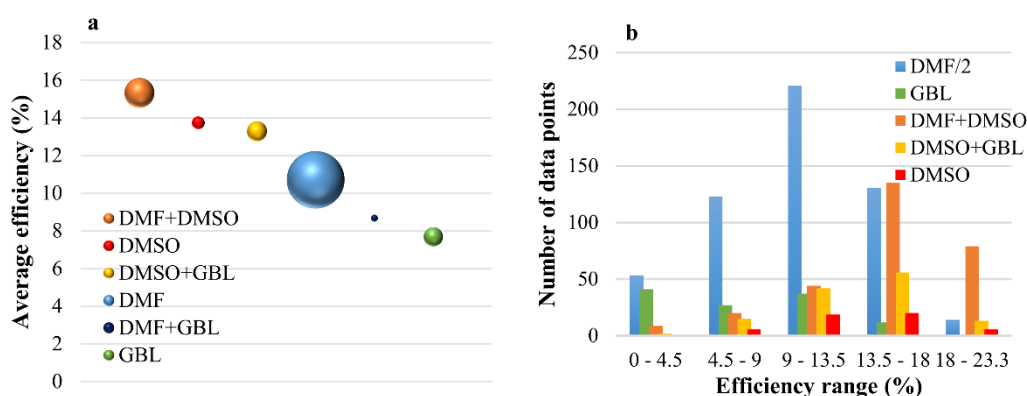


Figure 4.9. Comparison of efficiencies resulted by use of different solvents (a) average efficiencies of solvents (b) distribution of data among efficiency ranges.

The average efficiencies obtained with three most commonly used anti-solvent were compared with the results obtained without any in Figure 4.10a. The data of diethyl ether in 2015 and chlorobenzene in 2014 were not included because the data points were less than five. Diethyl ether and chlorobenzene have the highest positive effect on average efficiency as reported by various investigators while the average efficiency obtained with toluene was comparable lower. As Figure 4.10b shows, the data for all anti-solvents are well distributed their own means.

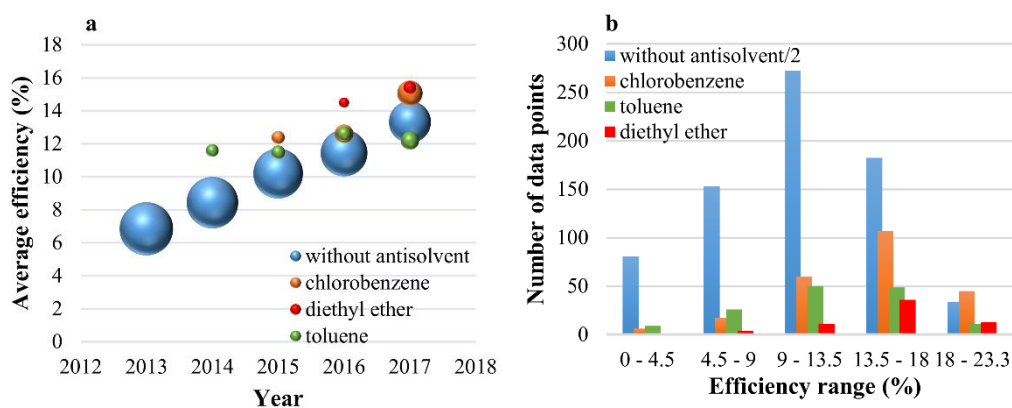


Figure 4.10. Comparison of the performance of various anti-solvents used (a) average efficiencies obtained with each anti-solvent (b) distribution of data among efficiency ranges.

The conditions of thermal annealing of perovskite layer and consequently film formation kinetics may vary depending on the laboratory, in which the samples are prepared. This was also apparent from the fact that the analysis performed for thermal treatment was less conclusive than the other factors. Therefore, we will just summarize some major results that we found together with some experimental results reported in the literature.

We analyzed the effects of annealing temperature for all three cell types (mesoporous/planar regular cells, inverted cells) by fixing the perovskite to MAPbI₃ and coating method to one-step; this way we obtained sufficiently high number of data points (31.2% of all data) to see the temperature effect. The average efficiencies obtained at 100 °C seems to be higher than those at lower and higher temperatures. The 100 °C was also reported as the optimum by Chen *et al.*[81] investigated the annealing temperature (80-140 °C) in MAPbI₃ based inverted cells for five minutes and revealed that annealing perovskite at 100 °C extend the exciton lifetime and performance. Then, we analyzed the effect of annealing time by fixing the temperature at 100 °C for MAPbI₃ cells (Figure 4.11). The most frequently employed period for all three cell structure is 10 minutes. The efficiency increases with increasing annealing time in regular planar cells while it seems to be almost constant in inverted cells; no specific trend could be observed in regular mesoporous cells.

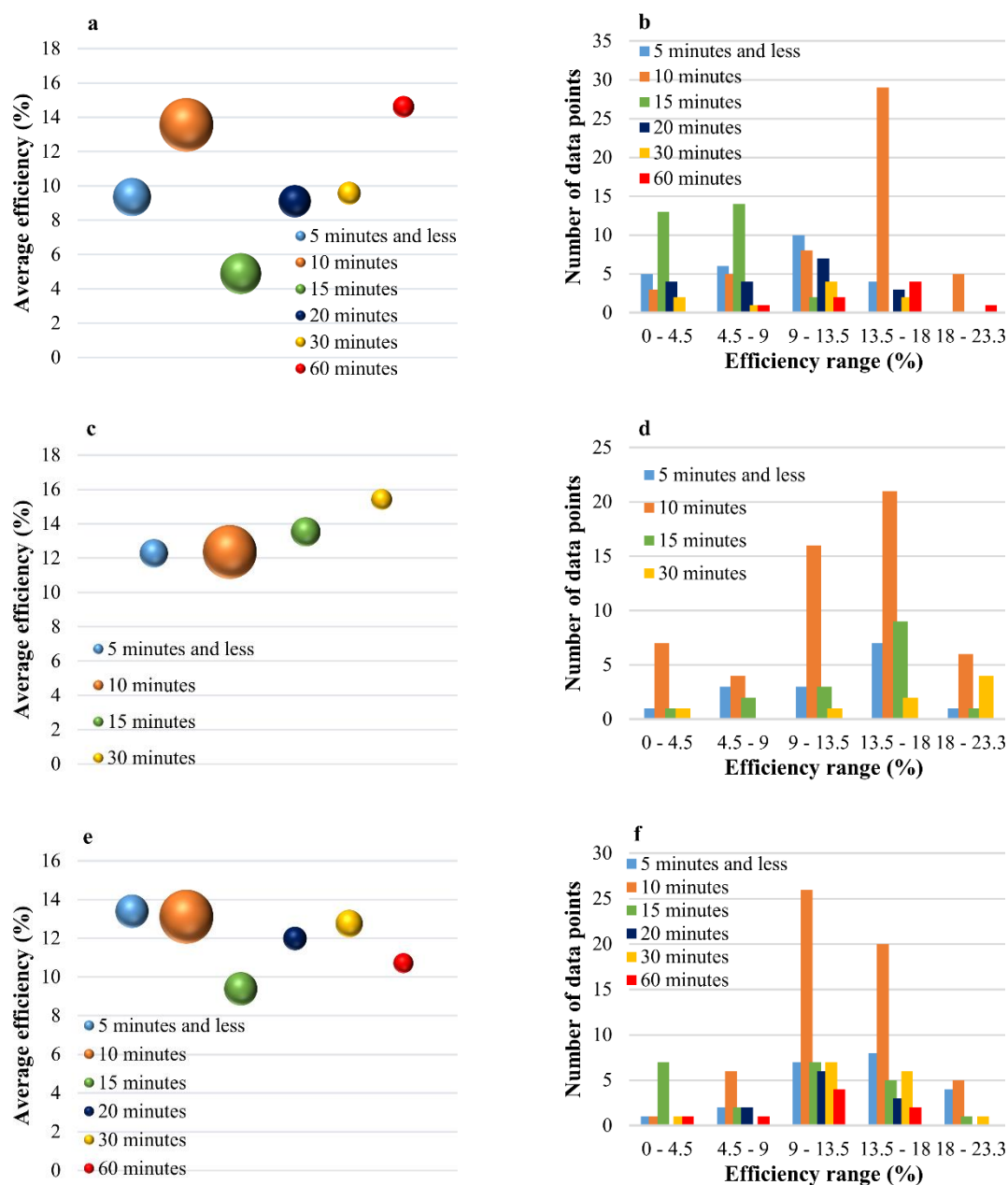


Figure 4.11. Average efficiencies of MAPbI₃ based cells (coated in one-step) for different thermal annealing conditions (a,b) mesoporous, (c,d) planar, (e,d) inverted cells.

We also analyzed the database to test the generalizability of these reports and found that the cells annealed in glovebox produced higher average efficiencies for regular cells while the ambient conditions seem to be better for inverted cells. For example, for mesoporous MAPbI₃ cells, the average efficiency for the cells annealed in glovebox (64 cases) is 10.7 % while this value is 7.2 % for the cells annealed in the air (24 cases). The cells annealed in dry air conditions also show higher efficiencies but their frequency in the

database are quite small for generalization compared to the cases with ambient air or glovebox conditions.

Then we tried to analyze the possible advantages or disadvantages of multi-step (MS) thermal annealing procedure, which is a common modification of annealing process to deposit more uniform and well crystallized perovskite films[324], [325]. The average efficiencies of the cells annealed in multi-steps were indeed higher than one-step annealed cell for MAPbI₃; the average PCEs of planar regular cells were 16.8% and 12.6% if they were annealed in multi and single steps respectively. These values were 13.3% for multi-step and 10.9% for single step in mesoporous regular cells, and 13.8% and 12.2% respectively for the inverted cells.

Lastly, we compare the high temperature-short time annealed cells with conventional annealing (100 °C); we found that high temperature-short time annealing indeed produced cells with higher efficiencies (Figure 4.12).

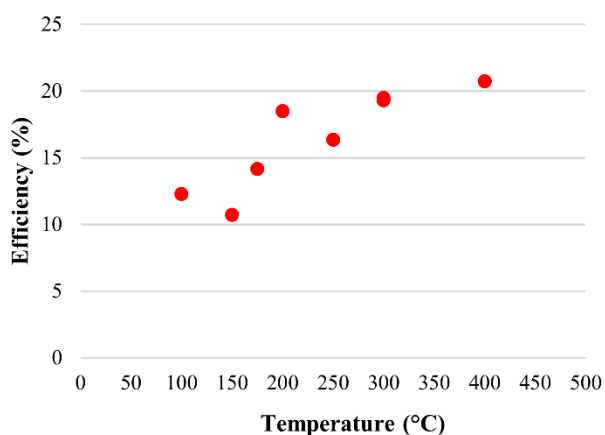


Figure 4.12. Efficiencies values of cells annealed at high temperatures for short time; data obtained from four papers.

4.1.2.3. Effect of Electron Transfer Layer. Investigating the ETL in regular cells, mesoporous TiO₂ was found to be the dominant ETL choice in literature (84.2% of regular mesoporous cells and 50.9% of entire regular cells) and it is more effective than most of the other materials (Figure 4.13a); the only alternative that leads higher average efficiency is still TiO₂ doped by various metals or using various forms. The efficiencies for all alternative

presented are almost normally distributed around their own mean with (Figure 4.13b) while the distribution of $m\text{Al}_2\text{O}_3$ does not seem to be normal.

The average performance of the most common compact layer material and distribution of efficiencies are given in Figure 4.13c and Figure 4.13d, respectively. Although TiO_2 was also found to be the most commonly used material as compact layer (83.6% of data points in the database of regular cells), SnO_2 seems to result in higher performances; the cells with ZnO and without any ETL also have performances comparable to TiO_2 .

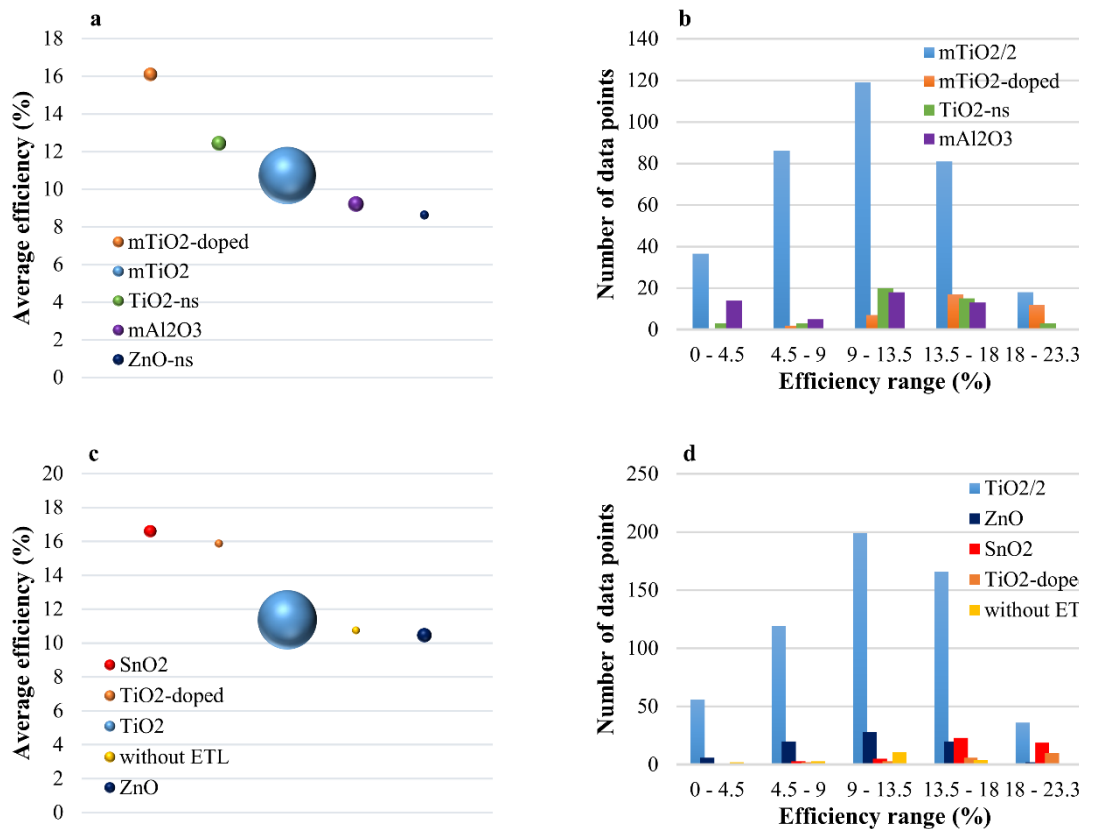


Figure 4.13. Comparison of ETL materials in regular (n-i-p) cells, (a) average efficiencies for mesoporous layer (b) distribution of data for mesoporous layer (c) average efficiencies for compact layer for both mesoporous and planar cells; (d) distribution of data for compact layer compact layer for both mesoporous and planar cells.

The performance of ETL in inverted cells was investigated in Figure 4.14a, the performance of cells made of PCBM, C60 or both PCBM and C60 have been increased through years. The average performance of PCBM and C60 are quite close, and the

performance becomes higher when they are employed together. The available data for the other ETL materials were not sufficient to have a statistical analysis. As Figure 4.14b indicates, the PCBM data were normally distributed while C60 and PCBM+C60 seems to shift slightly to the right as their average was also high.

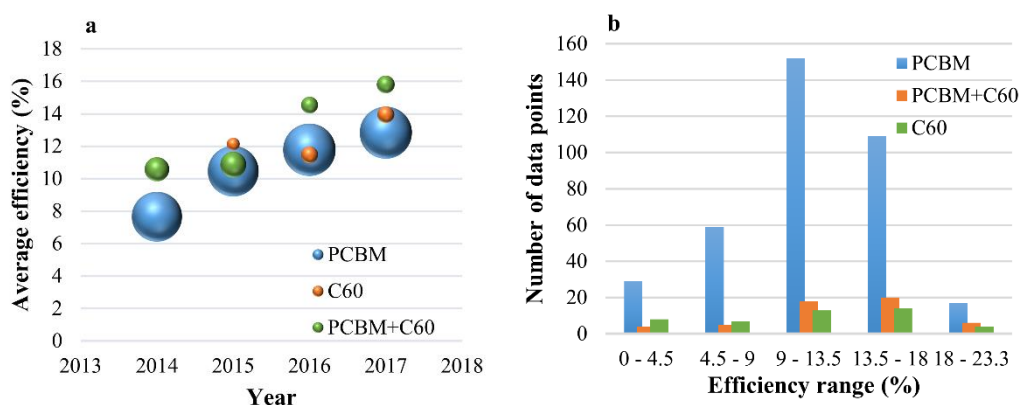


Figure 4.14. Comparison of ETL materials in inverted (p-i-n) structure (a) average efficiencies, (b) distribution of data (PCBM+C60 shows that mixture of two materials was used).

4.1.2.4. Effect of Hole Transfer Layer. The performance analysis of HTL in regular cells is presented in Figure 4.15. Due to its suitable energy levels, high hole conductivity, high mobility and possibility of use without any post annealing process, the spiro-OMeTAD has been the most commonly used hole transport material in regular cells. Poly-3-hexylthiophene (P3HT) is another common polymeric hole transport material used in regular cells. Even though P3HT based devices could not reach to the high efficiencies of spiro-OMeTAD based devices in the literature, they are still investigated as cheaper and convenient alternative. Poly-triarylamine (PTAA) is another polymeric HTL resulting high efficiencies. PTAA was found to be superior to other polymeric HTLs and quite compatible with spiro-OMeTAD[135]; this is also evident from Figure 4.15a.

Although inorganic HTL materials were initially studied for their high stability, their performances have been also improved through years. The time change of average efficiency of inorganic materials was compared with the performance of spiro-OMeTAD in Figure 4.15a; the plot for inorganic materials is presented as line (not ball graphs) because the additional data were collected to compute the averages and these data were not added to the

database as explained in Section 3.1.2; hence the ball graph representation will not be meaningful. As Figure 4.15a shows, the curve for the inorganic HTLs follow almost the same trend with spiro-OMeTAD, and their performance seems to be catching up. The average efficiency obtained with CuSCN is found to be 8.7 % while this was 7.8% for CuI. Rajeswari *et al.*[326] also showed that the CuSCN has better performance than CuI in their review covering 2012-2016. Although, the average efficiencies are relatively low, the maximum PCEs in the database for CuSCN and CuI are 17.1 % [144] and 17.6% [143] respectively, and these performance levels are high enough to make these materials promising alternatives.

There are less number of cases containing CuO and Cu₂O, and some of these cases involved doping by various elements; hence, their performances cannot be generalized at this stage. However, there are works reporting high performance with these materials (or their derivatives); for example, 15.7 % efficiency was obtained with CuO_xN_y [327]. The cell with CuGaO₂ as HTL, also resulted high efficiency (18.5%)[328]. Additionally, Cu₂O was computationally found to be a more promising HTL than CuSCN and CuI[329]. Yu *et al.* also reported that the hole mobility of Cu₂O was higher than CuSCN and CuI[330]. Finally, Rajeswari *et al.*[326] stated that CuO_x has the highest performance among the inorganic HTLs in their previously mentioned review.

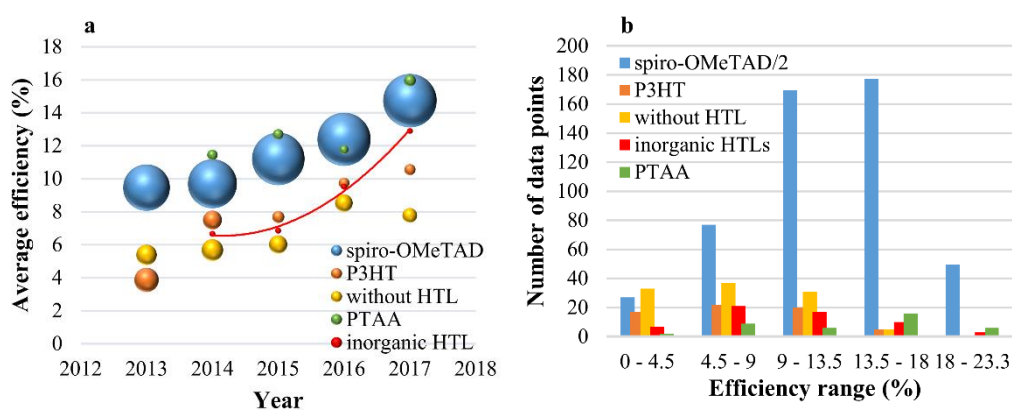


Figure 4.15. Comparison of common HTLs for regular (n-i-p) cells (a) change of average efficiencies through years, (b) distribution of data (points/lines for inorganic HTL are just for average, not for frequency).

Finally, hole transport layer free cells have been also studied in recent years due to their simpler structure, improved stability and lower cost[145]; although their average performance is also low, they have been improved continuously as it is seen in Figure 4.15a.

As presented in Figure 4.16, the use of all these additives improved the performance (especially cobalt complexes) of cells containing spiro-OMeTAD. The cells that used FK209 dopant with the commonly used LiTFSI+TBP gave the highest average performance.

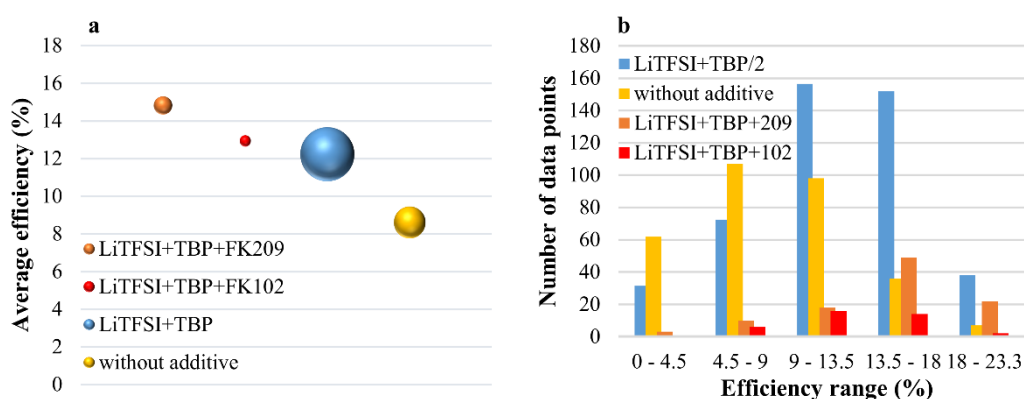


Figure 4.16. Comparison of common HTL additives in regular (n-i-p) cells (a) average efficiencies, (b) distribution of data (+ sign in entries shows that the mixture of these material was used).

The average efficiencies and distribution of data points among the efficiency levels for HTL materials in inverted cells are given in Figure 4.17a and Figure 4.15b. PTAA appears to be an effective organic material as HTL gaining more interest in recent years; and it has the highest average in 2017 (the previous years and the distribution could not be presented because of insufficient number of data points in database). As shown in Figure 4.17a, the average efficiencies obtained over NiO_x are considerably higher than PEDOT:PSS in recent years.

The average efficiency of PEDOT:PSS and NiO_x were also compared with other less common but still significant HTL (including plain and doped PTAA) materials in Figure 4.17c. The plain and doped PTAA gave the highest average PCE; the average for the plain PTAA was computed to be higher even though the doping reported to improve device

efficiency[331], [332]. Doping of PEDOT:PSS leded better performance than PEDOT:PSS evident from Figure 4.17b and Figure 4.17c.

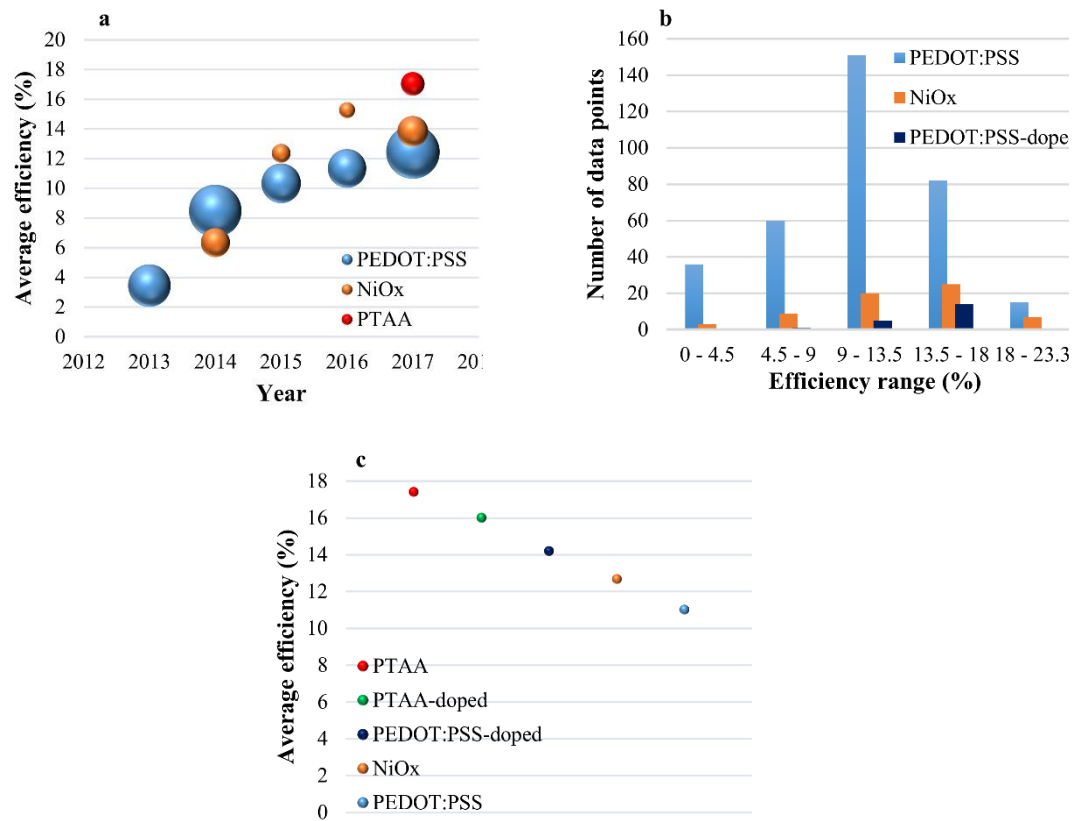


Figure 4.17. Comparison of HTLs for inverted (p-i-n) cells (a) change of average efficiencies of common HTLs through years, (b) distribution of data for common HTLs, (c) comparison of average efficiencies of HTLs including less common materials.

4.1.2.5. Effect of Back Contact. The averages and performance distribution of different back contacts were also compared. Au is the most commonly used back contact material in regular cells whereas it also gives higher average performance than Ag and carbon (Figure 4.18a). Au was also found to be the optimum back contact[170]. In inverted cells, Ag and Al were found to be used in common and their average performances are compatible. (Figure 4.18c)

4.1.2.6. Evolution of Maximum Efficiency. The limits of maximum achievable power conversion efficiencies for perovskite cells have been determined using different models in the literature. Sha *et al.*[318] predicted the limit for MAPbI₃ perovskite solar cells as 31.0% by using a detailed balance model. Later, Grånäs *et al.*[317] reported the theoretical

performance limit for metal halide perovskite cells as in the range of 25.0-27.0 % by using first-principles calculations and thermodynamic modelling. Considering that the certified efficiencies reported by NREL seems to obey S shaped logistic growth curve presented in Equation 3.1, we fitted the NREL data and tried to explain the pattern with the guide of results presented in Section 4.1. The upper limit of efficiency and assumed to be 27% (31 % could be also used), a and b are constant to be determined while t represent time as years.

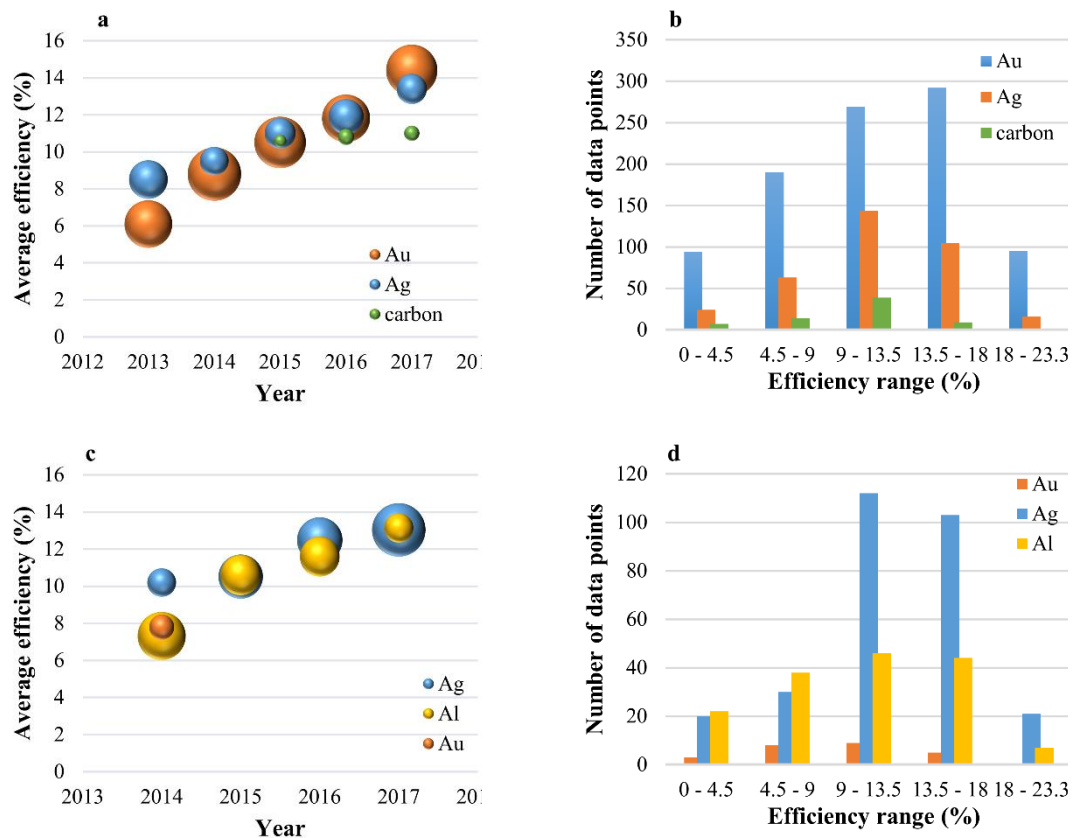


Figure 4.18. Comparison of back contact materials (a) change of average efficiencies of common back contact materials through years for regular cells,(c) for inverted cells; (b) distribution of data for common back contact materials for regular cells, (d) for inverted cells.

As can be clearly seen in Figure 4.19a, the evolution of PCE efficiency for regular cells follow the classical logistic curve behavior, which is common in the development of new technologies; R^2 of linearized model is 0.98, which is quite satisfactory for a dataset collected from various sources. In such curve, the initial slow progress, which may be attributed to the problems and difficulties of early years, is replaced by a fast growth phase together with accumulation of knowledge and experience as well as contributions of

increasing number of researchers and funds as the result of growing interest in the field. Then the progress slows down again as the technology is approaching to its theoretical limits because not only the increase of performance become more difficult, but also some researchers and fund migrate to new areas; this phase is generally known as maturity. These patterns seem to be also true for organolead perovskite cells at the initial and the growth phase. If the current progress continues, the limits seems to be approached in the next few years.

However, a closer inspection of experimental data also reveals some local S-curve patterns; the data from 2007-2015, and 2014-2017 seems to form two overlapping S-shape curves themselves as illustrated in Figure 4.19b, which is the same curve with narrower time frame. The data points in 2012-2014 seems to form the maturity of phase of first curve (blue) while they also represent the initial stage of the second curve (red). This behavior is also observed occasionally in the development of new technologies; S-shape development cycle repeats itself a few times as one is completed while the new one is started (due to some major changes in design, material or methods) until it reaches to the final limits. The growth phase of the first curve was in 2012-2014 and appears to be result of serious developments such as the use spiro-OMeTAD as HTL, two step perovskite deposition and modifications in perovskites. The second acceleration started in 2015, and the analysis in Section 3 and 4 suggests that the major factors were the effective utilization of solvents and anti-solvents in this new trend.

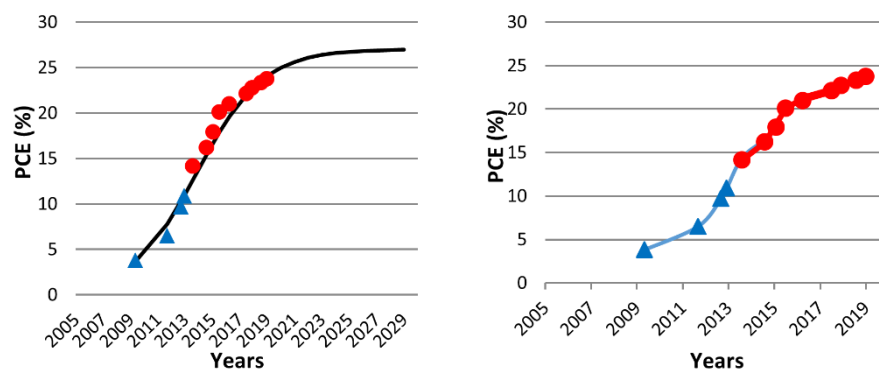


Figure 4.19. Evolution of efficiency for regular (n-i-p) structure (a) Logistic growth model (blue points from Ye *et al.* [333]; red data from NREL[1] , (b) successive local s curve structures in data (use of different colors is just to highlight two curve.

4.1.3. Predicting the Stabilized Efficiency by Random Forest Analysis

First, the predictability of stabilized PCEs was checked by constructing and testing a model using random forest techniques. The stabilized efficiency data for regular and inverted cells were modelled using random forest regression to test the predictability of performance and use the results to deduce some conclusions if it is possible. The stabilized PCE was used as the performance variable while the cell properties given in Table 3.1 were used as input variables. The 5-fold cross validation procedure was implemented; the database was randomly divided into five parts; the four parts (80% of data) was used for training (model building) and remaining set (20% of data) set was used for testing. This was repeated five times to cover the entire dataset to see the strength of model in full data range.

The plot of actual versus predicted stabilized power conversion efficiencies for training and testing of regular and inverted cells are presented in Figure 4.20. The average root mean square error (RMSE) for training and testing were 1.70 and 3.29 for regular, 1.51 and 2.91 for the inverted cells respectively. The model fitness for training is sufficiently high for both regular and inverted cells to conclude that the data can be modelled, and the variation in efficiencies can be explained by the change of input variables in Table 1. However, the true indicator of the predictive strength of the model is its performance in testing in which the model is forced to predict the data unseen before. As Figure 4.20b and Figure 4.20d indicate, both models have some predictive power; nevertheless, the goodness of the fit is not sufficient for both of them to be used for the practical purposes like planning an experiment.

When the models were built using the best efficiencies of entire database (including the cases in which the hysteresis was not considered), the RMSE became 2.46 (training) and 3.56 (testing) for regular cells while they were 2.26 (training) and 3.38 (testing) for inverted cells. The plots for these models are given in Figure 4.21. Although, the statistical fitness of models for stabilized efficiencies are slightly higher (indicating better reproducibility of data), the differences (especially in testing) are not significant indicating that the basic natures of the datasets are the same; this will be more apparent and informative in the association rule mining analysis in next section.

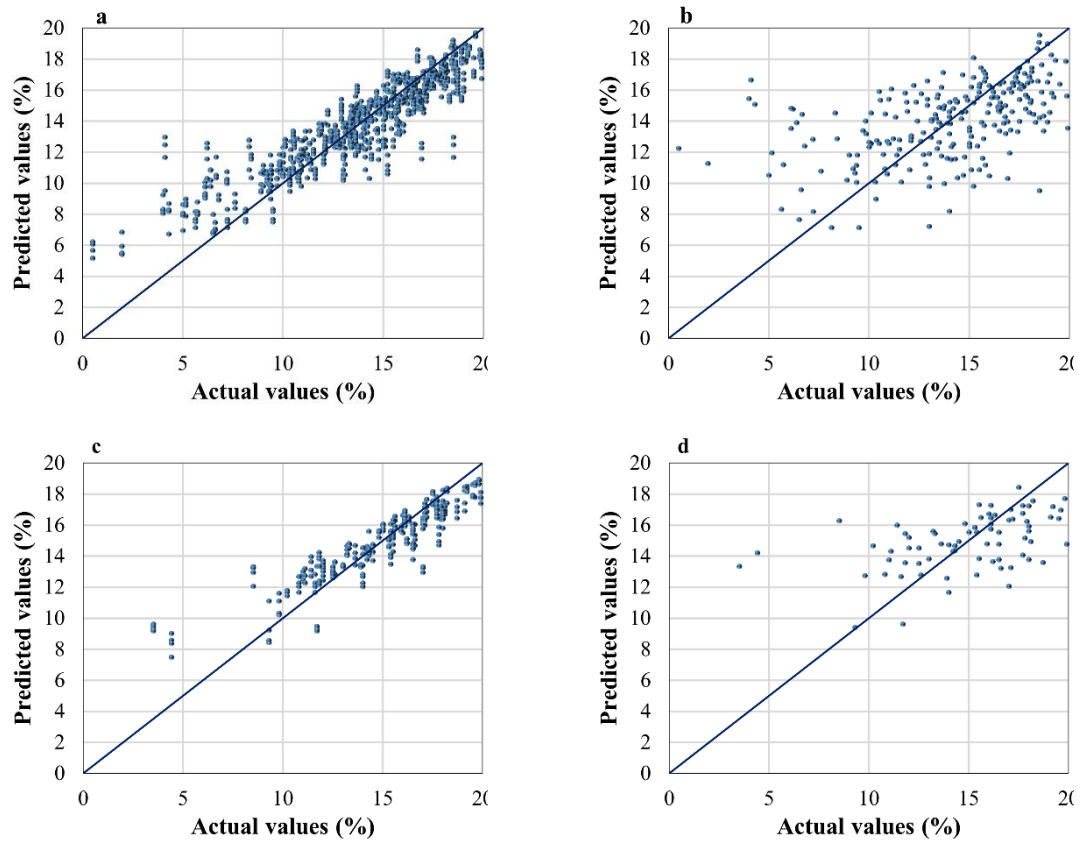


Figure 4.20. Actual versus predicted performances by random forest model for stabilized efficiencies (a) training and (b) testing for regular (n-i-p) cells; (c) training and (d) testing for inverted cells; training plots for predictions of data used in model, testing plots for predictions of data not seen before.

It can be concluded from above results that predicting the efficiency with a practical accuracy level was not possible at this stage. We decided to construct classification-based models to predict the possible range of efficiency as presented in the following sections; this way, a less accurate but more reliable models could be build.

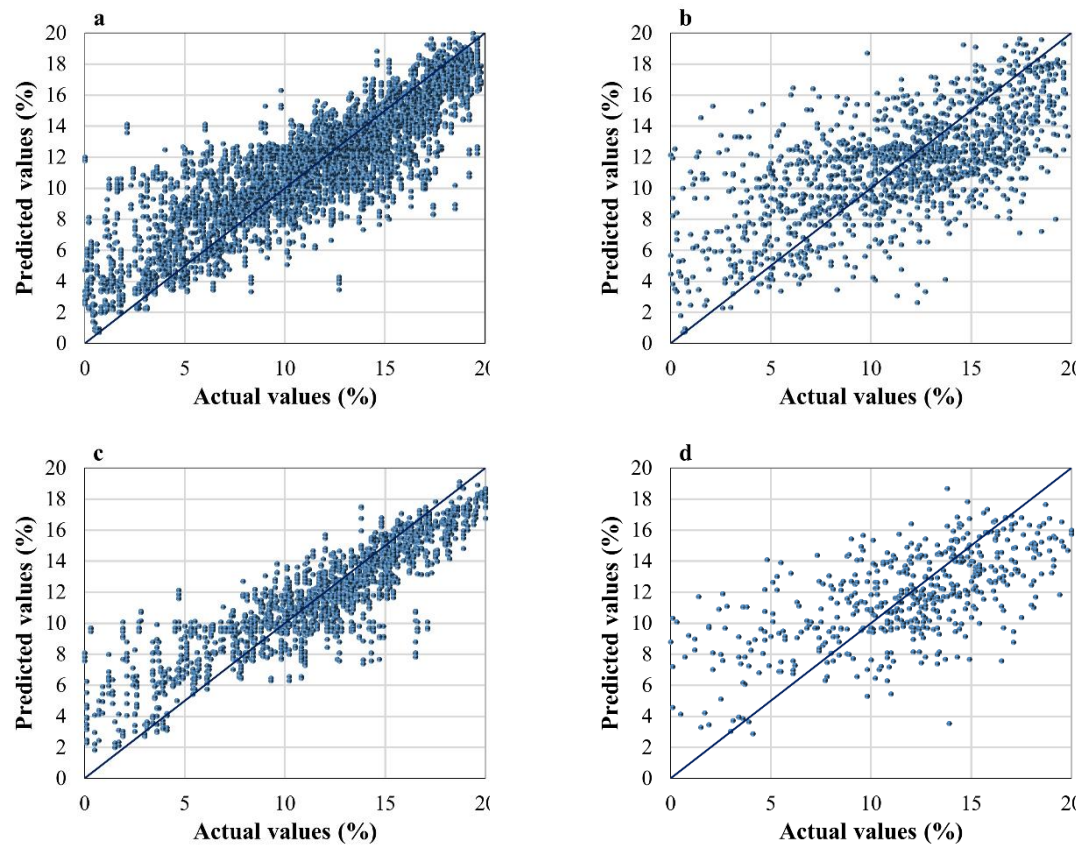


Figure 4.21. Actual versus predicted performances by random forest model for entire dataset of regular cells (a) training (RMSE=2.46) (b) testing (RMSE=3.56); for entire dataset of inverted cells (c) training (RMSE=2.26) (d) testing (RMSE=3.48).

4.1.4. Analysis of Factor Effects on Power Conversion Efficiency by Association Rule Mining

Association rule mining was implemented to determine the key variables (if there are any) leading to high efficiency in perovskite cells; the one-factor associations were studied to obtain simple easy to follow rules. The efficiency levels were divided into five equal classes as used in Section 4.1.2 for distributions, and the conditions leading to the highest efficiency class (named as class A to use the same notation in decision tree analysis in next section) were analyzed; since there are no physical reasons behind this choice, one can repeat the same analysis by changing the limits. However, increasing upper limit too much may decrease the number of data points in class A in a way that the results may not be generalized. The opposite of this, on the other hand, will make the distinction harder (this is more important for decision tree as will be apparent in the next section).

The results of one-factor associations are given in Table 4.1 for stabilized efficiencies datasets of regular and inverted cells. There are three parameters that are used to interpret and make decision in this technique: support, confidence and lift; all are explained in Table 4.1 as well as through examples below.

As seen from Table 4.1, the highest lift ratio (3.09) was obtained for the mixed cation perovskites for high efficiency class (A); this indicate that the use of mixed cations is the best way to obtain a cell that has higher than 18.0% stabilized efficiency. Support of this factor is $(25/249) = 0.10$ meaning that 25 out of total 249 data points have the efficiency values higher than 18.0% and they were produced using mixed cation perovskites (higher support means higher reliability to generalize the effect of that factor) The total number of data points in class A is 38. Then the confidence is $(25/38) = 0.658$; in another word, 65.8 % of high efficiency regular cells are produced with mixed cation perovskites (higher confidence also means higher reliability). If the ratio of mixed cation perovskite cells in the total database was also about 65.8 %, we would conclude that the use mixed cation has no effect on efficiency (lift value would be one). However, this is not the case; the fraction of the cells containing mixed cation perovskites in the entire database is only 21.3 % ($53/249=0.213$) indicating that this material indeed tendency to give high efficiency cells. Then the lift value for mixed cation perovskites can be computed as $65.8/21.3=3.09$, which can be also stated as the fraction of mixed cation perovskites containing cells in class A is 3.09 times higher than that in the entire database.

It is clear from the above example that the lift value should be minimum one, and higher values shows higher probability to obtain high class cells with that factor; consequently, only the factors having the lift values higher than one are presented in Table 4.1, and only the ones that have significantly higher lifts are discussed. The support (fraction of A class cells made with that factor in total data) and confidence (fraction of cells made with that factor in A class) should be as high as possible for high reliability but they should be low enough to capture the less frequently used but effective items. Usually, minimum values for support and confidence are defined, and the list of factors are ranked by the lift. We set the minimum support to 0.02 (2% of 249 corresponding to five cells) and the confidence to 0.1 (10% of 38 corresponding four cells) for stabilized dataset of regular cells. We did not present the factors with lower support and confidence values than these values

(even if their lifts are high) because the reliability of the such result would be too low; the most of the factors with the lift value higher than one already have higher supports and confidence than those minimums.

Table 4.1. Association Rule Mining for PCE > 18.0% for Regular (n-i-p) and Inverted (p-i-n) Cells.

Antecedent	Consequent	Support	Confidence	Lift	Data count
We are interested in these performance criteria	This feature was used in cells belonging to efficiency levels in A	This is fraction of all data belonging to class in A and has feature in B	This fraction of data in A has feature in B	(This fraction of data in A has feature in B) / (This fraction of data in all data has feature in B)	Number of data points provides this condition
PCE>18% For regular (n-i-p) cells (Support=0.02, Confidence= 0.1)	Perovskite=mixed cation	0.10	0.66	3.09	25
	HTL additive= LiTFSI+TBP+FK209	0.03	0.21	2.76	8
	Perovskite deposition method=spin 2-3	0.05	0.34	2.37	13
	Anti-solvent treatment=chlorobenzene	0.06	0.39	1.79	15
	Perovskite solution = DMF+DMSO	0.07	0.47	1.55	18
	ETL= SnO ₂	0.02	0.13	1.17	5
	Perovskite deposition procedure= one-step	0.12	0.82	1.14	31
	ETL-2= 0	0.07	0.45	1.10	17
	HTL= spiro-OMeTAD	0.13	0.87	1.07	33
	ETL= TiO ₂	0.11	0.74	1.03	28
PCE>18% For inverted (p-i-n) cells (Support= 0.05 Confidence=0.1)	HTL= PTAA	0.05	0.44	3.65	4
	Perovskite=mixed cation	0.05	0.44	3.29	4
	ETL-2= BCP	0.08	0.67	1.70	6
	Anti-solvent treatment= no	0.07	0.56	1.08	5
	Perovskite deposition method=spin	0.08	0.67	1.07	6

The lift value of 3.09 for mixed cation perovskites is a strong indicator for the positive effects of this factor; however, it is rather predictable from the discussion in Section 4.1.2. This is simply because there are many cases (the fraction of mixed cation cells in A class is 66 percent). This may be also the case for DMF+DMSO in the fifth rank (and partially for chlorobenzene in the fourth rank) because both support and confidence values are also high. However; the results found for HTL additive of LiTFSI +TBP+FK209 and two or three time

spinning in one-step procedure, both of which have high lift ratios, were less obvious in a first look. For example, there are 8 A class cases with LiTFSI+TBP+FK209 and they form 21% of all A class cells; however, the total data set has 19 such cases corresponding to 8% (19/249), which is much smaller fraction showing the high potential of this factor for high efficiency. Similarly, the appearance of SnO₂ as a potential ETL is also important (lift value of 1.17 is low but still notable because the number of cases involving this material is also low).

There are also factors with high support and confidence but low lift in the table. For example, 33 of 38 A class cases (confidence of $33/38=0.87$, which is remarkably high) was produced with spiro-OMeTAD; however, this ratio is almost the same in the total data ($0.87/1.07=0.81$) showing that high fraction of B and C class cells were also produced with spiro-OMeTAD. As the results, the support, confidence and lift values should be treated together to benefit from the techniques like association rule mining.

We repeated the same analysis for the stabilized inverted cells and presented in Table 4.1. We had to decrease the support for this analysis in a way that the minimum number of data points required for the rule to be reliable from five to four due to the relatively smaller size of this database. The use of PTAA as the HTL, mixed cation as the perovskite and BCP as ETL interlayer appeared as the most significant factors for high efficiencies with the lift values of 3.65, 3.29 and 1.70 with the relatively high confidence values.

Most of the factors appeared in association rule mining analysis in Table 4.1 strengthen the analysis presented in Section 4.1.2 and they are in accordance with the suggestions recently made by Saliba *et al.*[334] for high efficiency cells. We also compared the association rule mining results for stabilized efficiencies set and entire dataset for both regular and inverted cells as well. The stabilized efficiencies are naturally lower than the best efficiencies of the same cells, and the entire database contains only the best efficiencies. Consequently, we compared the models for the best efficiencies of the cells in stabilized efficiencies dataset and the best efficiencies in the entire database. Similarities between the results of stabilized efficiencies subsets and the entire database for both structures were remarkable (Table 4.2 and Table 4.3). Although the numerical values of support, confidence and lift are different as expected (different sets with different sizes), the most influential

factors are similar in two sets This is the strongest evidence for the fact that two sets have similar characters and the review in Section 3 and models in Section 4 can complement each other reasonably well.

Table 4.2. Association Rule Mining for PCE > 18% for Regular Cells; Comparing the Results for Best Efficiencies of Stabilized and Entire Dataset.

Antecedent	Consequent	Support (%)	Confidence	Lift	Data Count
PCE>18% for stabilized efficiency database with best cell efficiencies (Support= 0.02, Confidence=0.1)	ETL=TiO ₂ -doped	0.03	0.11	4.08	7
	Perovskite=mixed cation	0.13	0.52	2.46	32
	Perovskite deposition method=spin 2-3	0.07	0.28	1.88	17
	Perovskite solution = DMF+DMSO	0.14	0.56	1.83	34
	HTL additive= Li+TBP+FK209	0.03	0.13	1.72	8
	Antisolvent treatment= diethyl ether	0.03	0.13	1.72	8
	Antisolvent treatment=chlorobenzene	0.09	0.36	1.63	22
	ETL= SnO ₂	0.04	0.18	1.60	11
	HTL= spiro-OMeTAD	0.22	0.92	1.13	56
	Perovskite deposition procedure = one-step	0.20	0.80	1.12	49
PCE>18% for entire database with best cell efficiencies (Support= 0.0035, Confidence=0.1)	HTL additive= LiTFSI+TBP	0.19	0.77	1.04	47
	ETL-2= 0	0.10	0.41	1.01	25
	Perovskite=mixed cation	0.04	0.51	5.20	57
	ETL= SnO ₂	0.01	0.17	4.82	19
	ETL-2= mTiO ₂ -doped	0.01	0.13	4.23	14
	Perovskite solution = DMF+DMSO	0.05	0.60	3.84	67
	Antisolvent treatment= diethyl ether	0.01	0.11	2.93	12
	Antisolvent treatment=chlorobenzene	0.03	0.32	2.82	36
	HTL additive= Li+TBP+FK209	0.02	0.20	2.73	22
	Perovskite deposition method =spin 2-3	0.02	0.30	2.10	33
PCE>18% for entire database with best cell efficiencies (Support= 0.0035, Confidence=0.1)	Perovskite deposition procedure = one-step	0.06	0.81	1.37	90
	HTL= spiro-OMeTAD	0.07	0.89	1.25	99
	Perovskite deposition method =spin	0.05	0.62	1.11	69
	ETL-2= 0	0.03	0.35	1.07	39
	HTL additive= LiTFSI+TBP	0.05	0.68	1.07	76

Table 4.3. Association Rule Mining for PCE > 18% for Inverted Cells; Comparing the Results for Best Efficiencies of Stabilized and Entire Dataset.

Antecedent	Consequent	Support (%)	Confidence	Lift	Data Count
PCE>18% for stabilized efficiency database with best cell efficiencies (Support= 0.05, Confidence=0.1)	ETL= others	0.05	0.24	2.49	4
	Perovskite=mixed cation	0.07	0.29	2.18	5
	HTL= PTAA	0.05	0.24	1.93	4
	ETL= PCBM+C60	0.05	0.24	1.45	4
	Perovskite solution = DMSO+GBL	0.05	0.24	1.45	4
	Antisolvent treatment=toluene	0.05	0.24	1.45	4
	Perovskite deposition method=spin 2-3	0.09	0.41	1.27	7
	ETL interlayer= BCP	0.11	0.47	1.20	8
	Antisolvent treatment= chlorobenzene	0.07	0.29	1.09	5
	HTL-2= 0	0.22	0.94	1.02	16
PCE>18% for entire database with best cell efficiencies (Support= 0.008, Confidence=0.1)	HTL= PTAA	0.01	0.19	5.72	7
	ETL=others	0.02	0.22	3.59	8
	Perovskite=mixed cation	0.02	0.22	3.47	8
	Perovskite solution = DMF+DMSO	0.02	0.32	2.53	12
	HTL= others	0.01	0.14	1.83	5
	Perovskite deposition method =spin 2-3	0.02	0.32	1.68	12
	ETL interlayer= BCP	0.03	0.41	1.65	15
	ETL= PCBM+C60	0.01	0.16	1.57	6
	Antisolvent treatment= chlorobenzene	0.02	0.22	1.52	8
	Perovskite solution = DMSO+GBL	0.01	0.19	1.52	7
HTL= NiO _x	0.01	0.19	1.52	7	
Antisolvent treatment= toluene	0.02	0.22	1.37	8	
Perovskite deposition procedure= one-step	0.06	0.81	1.02	30	

4.1.5. Developing Heuristics for High Power Conversion Efficiency by Decision Tree Analysis

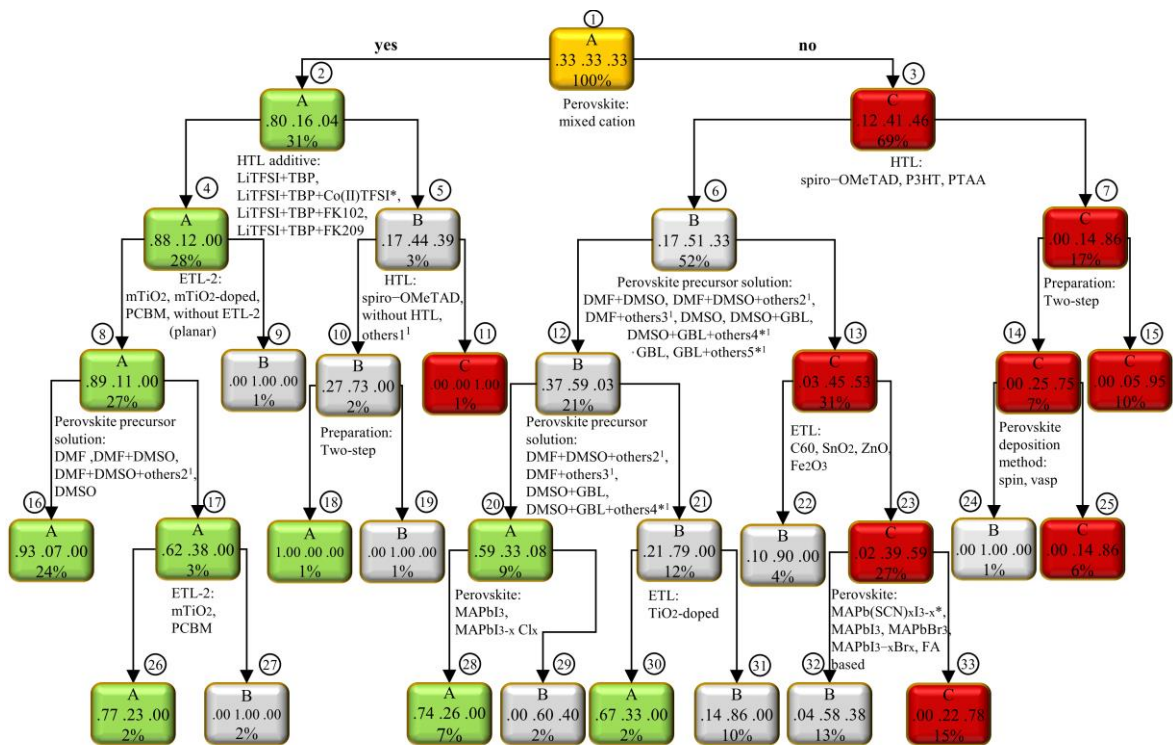
The decision tree analysis, which is an effective classification method, was performed to identify the factors and conditions leading high efficiency cells and develop some heuristics if it is possible. The database was split into three classes as Class A (high efficiency), Class B (intermediate efficiency) and Class C (low efficiency). As explained in Section 3.1.5, the limits of the low class were set as 9.0% while the high efficiency class (A) was made of the cells with efficiencies higher than 18.0%; this way the results for high efficiency (A) class should be comparable with those in association rule mining analysis and reviews in Section 3.

The database should be normally divided into approximately equal size classes in decision tree (not required in association rule mining), otherwise class imbalance problem may occur (even the small fraction of incorrectly classified data from large classes may spoil and reduce the accuracy rate of neighboring small classes). However, if three equal size classes were created from our database, the low and high performance classes would lose their meaning because the vast majority of the data points are in intermediate efficiencies. In such situation, one can create unequal size classes, and then implement random sampling method to avoid class imbalance problem involving the duplicating the data points of small classes to the level of large classes[335]; however, the present number of data points should be still large enough to make a reliable sampling. This is definitely the case for the entire dataset considering that the number of data points for A and C classes are 111 and 411 for the regular cells (885 data points in B class) respectively while they are 37 and 123 for the inverted cells (354 data points in B class). The number of data points in the stabilized efficiencies dataset for the regular cells were also sufficient for sampling; the data points for A, B and C classes are 38, 186 and 25, respectively. The number of data points in the stabilized efficiency dataset for inverted cells, however, was not even sufficient for sampling (only 9 data points for A class and 3 data points for C class); hence, we did not construct a decision tree for this subset.

The decision tree constructed for the stabilized efficiencies of regular cells is presented in Figure 4.22 (minimum split number=10, maximum depth=5, complexity parameter=0).

The classification accuracy of the tree was found as 83% (tree classified 83% of the data points correctly) which is quite high. The accuracies for individual classes (as confusion matrix) are given in Table 4.4.

The percentage at the bottom of each node in Figure 4.22 shows the fraction of total data obeying that rule while the fractions in the middle line, from left to right, represent the fractions of A, B and C in that node respectively; the letter at the top of the node simply denotes the class with the highest fraction. The percentage written inside the first node is 100% because it is the root node and the fractions of classes are equal. As splitting the tree from root node, the percentages inside the nodes decreases and the class fractions increases in the sake of the dominant class for purification. To have a reliable rule or heuristics, the number of cases in a terminal node (bottom percent) should be sufficiently large and the purity of the node (i.e. fraction of one class) should be as high as possible.



¹ Term of "others" were explained in Table A.1.

Figure 4.22. Decision tree model for stabilized regular (n-i-p) cells. Percentage at the bottom of nodes is fraction of total data obeying rules imposed up to that point; numbers in middle line are fraction of A, B and C in that node respectively; letter at the top of the node simply denotes class with the highest fraction.

One can increase the size (complexity of the tree) to have better classification and high purity nodes; however, the number of data points in these nodes would be too small for generalization. On the other hand, the tree can be reduced to have larger number of data points in the terminal nodes for better generalization; nevertheless, the purity of the nodes will be lower this time decreasing the reliability of the rules deduced. The tree presented in Figure 4.22 was optimized to have not only the highest classification accuracy but also to have reasonable generalizable results in the terminal nodes.

Table 4.4. Confusion Matrix of Regular Stabilized Dataset.

		Actual Class			Precision
		Class A	Class B	Class C	
Predicted Class	Class A	173	26	0	87%
	Class B	13	134	31	75%
	Class C	0	26	154	86%
	Accuracy	93%	72%	83%	
Overall accuracy			83%		

The tree divided the data by perovskite first and sent the cells containing mixed cation perovskites to the left branch, which lead to the leftmost node in the second line; this node contains 31% of data ($557 \times 0.31 = 173$ data points), and 80% of them ($173 \times 0.80 = 138$ cases) are A class cells. Then, the tree purified this node further based on HTL additive, ETL-2 and precursor solution used during perovskite coating; the leftmost terminal nodes at the bottom contains 24% ($557 \times 0.24 = 134$ data points) of the data with 93% purity A (remaining 7 percent is B). In other words, 24% of the data are obeying the line of rules described in the leftmost branch, and 93 % of them are A class cells. This is a highly reliable result that can be generalized as a heuristic, and the rules set by the tree for high efficiencies.

If the perovskite is other than one of those mixed cation structures (69 % of the data), tree continues on right to make the further discrimination based on HTL type, and separates 17% of cases ($557 \times 0.17 = 95$ cases). Then it further proceeds with the preparation procedure

reaching to the rightmost terminal node. The rules described by these two steps can be also used as a heuristic (to avoid low efficiency cells) considering that 10% of the data are obeying them with 95 % probability of obtaining C class cell.

Similar analysis can be repeated by all branches, and the rules and the heuristics can be developed as long as the number of data points and the purity of one class are sufficiently high in terminal nodes. There are also nodes with large number of data points and high purity in B; they are, in principle, also eligible for generalization. However, there may not be any practical value of knowing the conditions for intermediate efficiencies considering that one usually need to know the rules or heuristics for high performance to follow or for low performance to avoid. The entry named as others in the tree represents the collection of cells that were built with rarely employed alternatives (like HTL material) having less than three instances each; these data were not eliminated because they also contained information for other variables. Similarly, the variables with (*) sign has small number of points in database (due to the random sampling). Consequently, the results related to these two types of factors in the tree cannot be generalized.

The decision tree for the regular and inverted cells were also built using the entire database and presented in Figure 4.23 and Figure 4.24; their confusion matrices were given in Table 4.5 and Table 4.6, respectively.

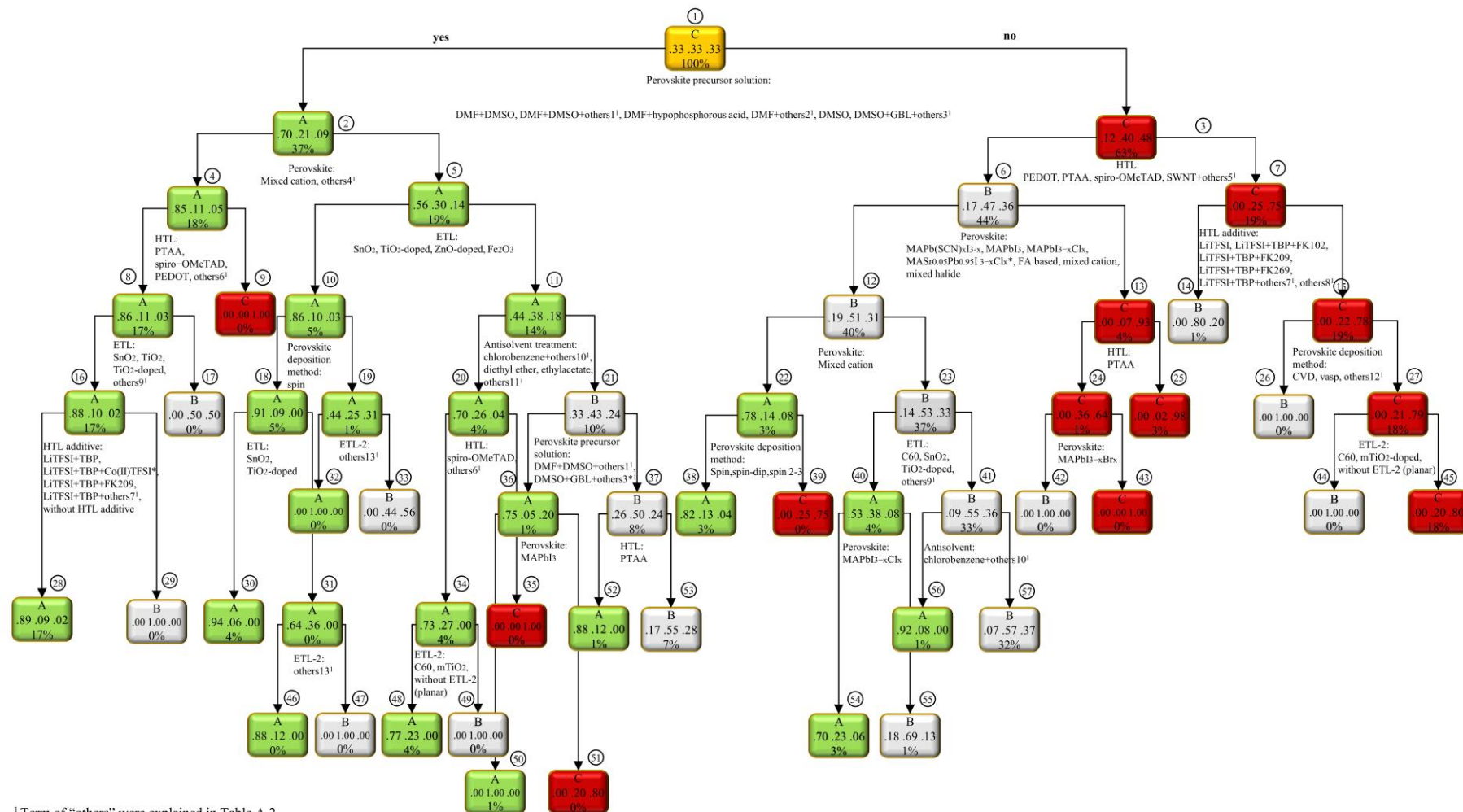
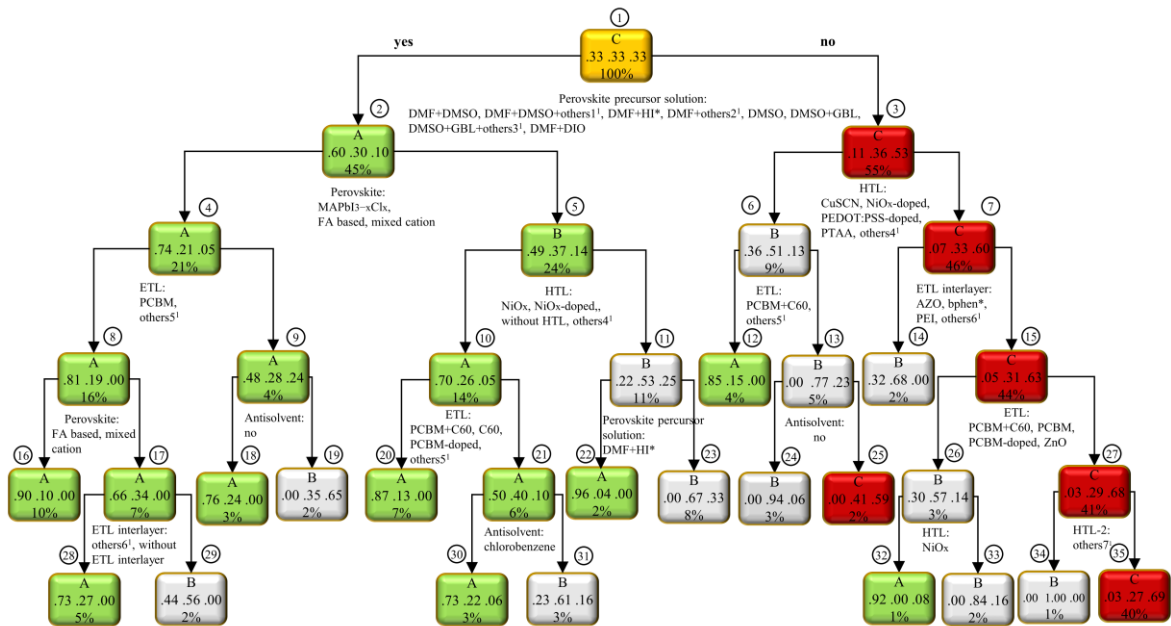


Figure 4.23. Decision tree model of entire regular type cells (minimum split number=10, maximum depth=6, complexity parameter=0).

Table 4.5. Confusion Matrix of Regular Entire Dataset.

		Actual Class			
		Class A	Class B	Class C	Precision
Predicted Class	Class A	791	106	17	87%
	Class B	97	672	383	58%
	Class C	0	107	504	82%
Accuracy		89%	76%	56%	
Overall accuracy		73%			



¹ Term of "others" were explained in Table A.3.

Figure 4.24. Decision tree model of entire dataset of inverted cells (minimum split number=30, maximum depth=5, complexity parameter=0).

Table 4.6. Confusion Matrix of Inverted Entire Dataset.

		Actual Class			
		Class A	Class B	Class C	Precision
Predicted Class	Class A	318	56	3	84%
	Class B	23	169	39	73%
	Class C	14	129	314	69%
	Accuracy	90%	48%	88%	
Overall accuracy		75%			

4.2. Analysis of Reproducibility

The papers on the efficiency of PSCs usually report the best and/or average PCE from large number of cells manufactured in the same batch (sample) together with the distribution or standard deviation of PCEs for that batch. We computed pooled variances (S_p^2) for each material or deposition method using the variances of batches in all papers, in which that material or method was used (see Section 3.2.2). Then, we compared S_p^2 for alternative materials (or method) used for the same purpose as the measure of reproducibility of process when that alternative was utilized. Although the materials for all cell layers are changing in all samples, the difference in S_p^2 of two data subsets containing two different alternatives for the same layer will reflect the difference between the effects of these two materials because all the other factors will be distributed in two subsets randomly, and their effects will be balanced due to the large number of random repeats.

In overall, the inverted (p-i-n) cells were found to have lower pooled variance (0.78) than regular (n-i-p) structure (1.14). We did not observe a statistically significant difference in reproducibility of mesoporous and planar structures of regular (n-i-p) cells; they resulted in S_p^2 of 1.16 and 1.13, respectively. S_p^2 values for individual factors are presented in Table 4.7 for the regular (n-i-p) cells while F-test performed to check the significance of S_p^2 differences are given in Appendix. (Table B.1, Table B.2, Table B.3 and Table B.4); the results for inverted (p-i-n) cells are also shown in Table 4.9.

Table 4.7. Reproducibility Analysis of Regular Cells.

Factor name		# of articles	# of samples	# of cells	S_p^2	S_p
Perovskite	MAPbI _{3-x} Br _x	5	6	108	0.46 ^x	0.68
	Cs based	6	8	129	0.48 ^x	0.69
	mixed cation	52	87	2190	0.75	0.87
	MAPbI ₃	174	320	9112	1.00	1.00
	FA based	17	26	843	1.59	1.26
	MAPbI _{3-x} Cl _x	51	97	2918	1.86	1.36
Deposition steps	two-step planar	47	81	2421	0.83	0.91
	two-step mesoporous	66	116	3182	0.96	0.98
	one-step planar	111	204	5742	1.26 ^y	1.12
	one-step mesoporous	82	146	4101	1.31 ^y	1.14
Deposition method	spin-spin (two-step)	37	71	2173	0.54	0.73
	spin 2-3 (one-step)	61	108	3179	1.05 ^z	1.03
	vasp (two-step)	6	8	244	1.10 ^z	1.05
	spin-dip (two-step)	49	91	2170	1.11 ^z	1.05
	spin (one-step)	125	237	6499	1.39	1.18
Precursor solution	DMF+DMSO+others*	9	9	315	0.56 ^k	0.75
	DMSO+GBL	13	24	471	0.59 ^k	0.77
	DMF+DMSO	50	91	2538	0.60 ^k	0.78
	DMSO	15	22	559	0.71	0.84
	GBL	9	19	875	0.96	0.98
	DMF	157	281	7231	1.40	1.18
	DMF+others**	22	34	1416	1.90	1.38
Anti-solvent treatment	diethyl ether	17	27	848	0.65	0.81
	toluene	14	24	693	0.76 ^l	0.87
	chlorobenzene	51	100	2058	0.78 ^l	0.88
	w/o anti-solvent	209	375	11214	1.30	1.14
ETL	SnO ₂	22	39	1283	0.55 ^m	0.74
	w/o ETL	6	8	119	0.57 ^m	0.75
	doped-TiO ₂	7	8	577	0.74	0.86
	ZnO	14	20	666	1.17 ⁿ	1.08
	TiO ₂	237	421	11596	1.20 ⁿ	1.10
Second layer of ETL/ETL interlayer (ETL-2)	PCBM	13	19	596	0.81 ^p	0.90
	TiO ₂ -ns	12	23	931	0.86 ^p	0.92
	doped-mTiO ₂	12	23	655	0.90 ^p	0.95
	mTiO ₂	116	205	5137	1.01	1.01
	ETL-2=0	139	239	6776	1.11	1.06
HTL	P3HT	8	11	190	0.68	0.82
	PTAA	15	24	817	0.82	0.91
	w/o HTL	18	29	699	1.02	1.01
	spiro-MeOTAD	234	420	12396	1.20 ^f	1.10
	inorganic HTL	11	16	384	1.25 ^f	1.12
HTL additive	LiTFSI+TBP+FK102	9	17	291	0.27	0.52
	LiTFSI+TBP+FK209	29	45	1285	0.56	0.75
	LiTFSI+TBP	196	354	10345	1.18	1.09
	w/o additive	109	63	3001	1.41	1.19

Table 4.7. Reproducibility Analysis of Regular Cells(cont.).

Factor name		# of articles	# of samples	# of cells	S_p^2	S_p
Back contact	carbon	24	41	817	0.85	0.92
	Au	198	365	10475	0.95	0.98
	Ag	67	130	3843	1.69	1.30
^{x, y, z, k, l, m, n, p, r} The differences are not significant according to F-test. *others: terephthalic acid (TPA), IPA, N-methyl-2-pyrrolidone (NMP), LiI, poly-vinylpyrrolidone (PVP), thiourea, SnF ₂ -pyrazine, Pb(SCN) ₂ **others: H ₂ O, HCl, HI, HP, IPA, NH ₄ SCN, HBr, TBP, tert-butyl substituted copper phthalocyanine (CuPc(tBu) ₄), polyacrylic acid (PAA), PDMS-urea, PEG, PEI, PVP, carbon nanotubes (CNT), 4-methylbenzenesulfonic acid (4-MSA), thiourea, IPA/Cyclohexane (CYHEX)						

As it is shown in Table 4.7, Cs based perovskites and MAPbI_{3-x}Br_x have the lowest pooled variance (difference between two is not statistically significant). These are followed by mixed cation perovskites, which can be also considered as reproducible if the most commonly studied MAPbI₃ is taken as reference; FAPbI₃ and MAPbI_{3-x}Cl_x resulted in higher pooled variances. Cs based perovskites are already known to be stable[210], which may be linked to reproducibility; similarly MAPbI_{3-x}Br_x and mixed cation perovskites are also reported to be reproducible[19],[336]. However, the high pooled variance for MAPbI_{3-x}Cl_x was somehow unexpected because the film morphology and reproducibility was reported to be improved with Cl⁻ addition[176]. In a more detailed analysis, MAPbI_{3-x}Cl_x was found to have lower S_p^2 in planar structures (still higher than others) while the other perovskites performed better in mesoporous cells (Table 4.8).

Table 4.8. Reproducibility Analysis of Perovskite Types with Different Cell Structures (Mesoporous/Planar) in Regular Cells.

Factor name		# of articles	# of samples	# of cells	S_p^2	S_p	F	$F_{critical}$
Perovskite type	mixed cation- mesoporous	28	49	987	0.64	0.80	1.34	1.11
	mixed cation-planar	24	38	1203	0.85	0.92		
	MAPbI ₃ -mesoporous	92	165	4743	0.98 ^x	0.99	1.03	1.05
	MAPbI ₃ -planar	88	155	4369	1.01 ^x	1.01		
	MAPbI _{3-x} Cl _x - mesoporous	18	30	960	2.94	1.72	2.22	1.10
	MAPbI _{3-x} Cl _x -planar	38	67	1958	1.32	1.15		
	FA based- mesoporous	4	5	310	0.54	0.73	4.11	1.18
	FA based-planar	13	21	533	2.21	1.49		
^x The difference is not significant according to F-test.								

Two-step perovskite deposition seems to produce slightly more reproducible cells in both planar and mesoporous structure probably due to controlled precipitation of perovskite[13] (however, the one-step procedure had lower pooled variance for inverted cells as given in Table 4.9). Among the techniques used in two step deposition, the spin-spin configuration was slightly better as it was also reported by Shen *et al.*[63]. Multiple spin coating (spin 2-3) technique has the lowest Sp^2 among one-step deposition methods. The perovskite precursor solutions containing DMSO were more reproducible than the others, and this can be attributed to better morphology by slow crystallization of perovskite in the presence of DMSO[337],[338]; DMSO was also better for PCE in our previous work[308]. The use of all major anti-solvents decreased Sp^2 indicating their positive effects on reproducibility; indeed, Xiao *et al.*[71] attributed high reproducibility obtained with chlorobenzene treatment to the improved morphology of the perovskite layer.

Compact SnO_2 was found to be the most reproducible ETL as it was first introduced by Dong *et al.*[339] for the same reason while the cell without compact layer were also reproducible; the doping of compact TiO_2 enhances the reproducibility as well. PCBM insertion between the compact layer and perovskite was observed to increase reproducibility, which may be linked to enhancement of performance, charge transfer and lower hysteresis as reported by Chen *et al.*[340]. The use of porous TiO_2 (nanostructured TiO_2 , doped and un-doped mesoporous TiO_2) as the second ETL is also better than using none (i.e. planar structure) for higher reproducibility. This may be due to the difficult control of crystal size of perovskite on planar surface[338].

P3HT and PTAA have smaller Sp^2 (more reproducible) than spiro-OMeTAD, which is the most common HTL; HTL-free cells also resulted smaller Sp^2 . The HTL additives of LiTFSI+TBP+FK102 and LiTFSI+TBP+FK209, which enhanced PCE[308], also improved the reproducibility of cell that are manufactured with spiro-OMeTAD as it was also reported by Ye *et al.*[341].

Finally, carbon back contact was found to result more reproducible cells (lower Sp^2) as Hashmi *et al.*[342] reported while Sp^2 of Au was also low. Ag, on the other hand, has the highest variation; however, Ag is more reproducible in inverted cell (Supplementary Table 3).

Different than regular structure, although MAPbI_{3-x}Cl_x based perovskite solar cells are seemed to be less reproducible in regular structure, it was found to be the most reproducible perovskite type in inverted cells; as Cl addition was reported to improve the perovskite morphology[343].(Table 4.9) In inverted cells, using PCBM with C60 as ETL and employing an ETL interlayer also found to be in more reproducible for inverted cells. As investigating the reproducibility of the HTL in inverted structure, doped PEDOT:PSS resulted best reproducibility. Liu *et al.*[344] reported that doping of PEDOT:PSS with F4-TCNQ increased performance, stability, reproducibility and reduced hysteresis with a better conductivity, favorable energy level alignment and reduced charge accumulation.

To conclude, the pooled variance of PCE for the cells manufactured with some materials (or methods) are significantly lower than those for the other alternatives used for the same purpose; although these results may not be exactly valid for large scale applications, they can be used as initial indicators for the relative reproducibility of the process when these materials or methods are used.

Table 4.9. Reproducibility Analysis of Inverted Cells.

Factor name		# of articles	# of samples	# of cells	S _p ²	S _p
Perovskite	MAPbI _{3-x} Cl _x	44	79	2716	0.69 ^x	0.83
	MAPbI _{3-x} Br _x	6	10	327	0.71 ^x	0.84
	mixed cation	17	24	649	0.74 ^x	0.86
	MAPbI ₃	90	161	4482	0.85	0.92
Deposition steps	one-step	122	240	7238	0.72	0.85
	two-step	29	51	1463	1.10	1.05
Deposition method	spin-spin (two-step)	17	34	908	0.51 ^y	0.72
	spin 2-3 (one-step)	34	66	2133	0.55 ^y	0.74
	Spin (one-step)	86	168	4846	0.75	0.87
	spin-dip (two-step)	6	7	281	2.96	1.72
Precursor solution	DMF+DMSO	33	48	1377	0.61 ^z	0.78
	DMSO	7	13	382	0.63 ^z	0.80
	DMSO+GBL	22	49	1335	0.68 ^z	0.83
	DMF	70	130	3980	0.86	0.93
	DMF+others*	17	27	742	1.00	1.00
Anti-solvent treatment	toluene	29	57	1211	0.43	0.65
	chlorobenzene	30	62	1857	0.66	0.81
	w/o anti-solvent	83	159	5238	0.88	0.94
	diethylether	8	11	347	1.08	1.04
ETL	PCBM+C60	9	19	417	0.53	0.73
	C60	29	40	1148	0.67	0.82

Table 4.9. Reproducibility Analysis of Inverted Cells (cont.).

Factor name		# of articles	# of samples	# of cells	S_p^2	S_p
ETL	PCBM	108	213	6588	0.81	0.90
Second layer of ETL/ETL interlayer (ETL-2)	ZnO	6	12	395	0.39	0.62
	PEI	5	13	381	0.70	0.84
	BCP	39	66	1806	0.84	0.92
	ETL-2=0	71	135	4213	0.91	0.95
HTL	doped-PEDOT:PSS	7	10	356	0.44 ^k	0.66
	w/o HTL	5	7	194	0.53 ^k	0.73
	PEDOT:PSS	99	187	5487	0.68 ^l	0.82
	NiO _x	23	40	1067	0.69 ^l	0.83
	PTAA	5	6	365	0.98	0.99
	inorganic HTL (including NiO _x)	37	62	1807	1.17	1.08
HTL-2	present	144	270	8081	0.75	0.87
	absent	17	21	615	1.15	1.07
Back contact	Ag	88	183	5231	0.72	0.85
	Al	47	87	2916	0.80 ^m	0.89
	Cu	6	8	392	0.88 ^m	0.94
	Au	6	11	108	2.91	1.70
^{x,y,z,k,l,m} The differences are not significant according to F-test. *others:tetraphenylphosphonium iodide (TPPI), 1,8-diiodooctane (DIO), V ₂ O ₅ , H ₂ O, HI, F4TCNQ, PbAc ₂ +H ₂ O, GO, NH ₄ Cl, PVP, hypophosphorous acid (HPA), PCBM						

4.3. Analysis of Hysteresis

Hysteresis complicates the characterization of solar cells, and it is generally lower at slow scan rates (or long delay times). As the starting point, we computed the hysteresis index (HI) as defined in Equation 3.5 using the data obtained with the low scan rates (≤ 0.05 V/s) for low hysteresis ($HI \leq 0.01$) and analyzed using random forest, association rule mining and decision tree techniques; we also restricted our analysis to the cells with $PCE \geq 10\%$ to capture the factors leading to low hysteresis with a reasonable cell performance. As can be expected, every restriction (low scan rate, low HI and high PCE) decreases the number of available data and reduced the reliability of the analyses. Hence, we performed hysteresis analysis also for all combinations of HI (≤ 0.01 or 0.05), PCE (higher than 10% or all values) and scan rates (low or all values). We observed that all these analyses suggest almost the same materials for low hysteresis with some minor changes in their ranking.

4.3.1. Predicting the Hysteresis Index by Random Forest Analysis

Similar to PCE analysis (Section 4.1.3.), the predictability of hysteresis index was checked using random forest technique. The data measured at the low scan rates (≤ 0.05 V/s) was modeled to check if data have some predictive power for low hysteresis ($HI \leq 0.01$). The 5-fold cross validation procedure was again implemented. The overall actual versus predicted hysteresis index values for five folds were plotted for regular and inverted cells and presented in Figure 4.25. The average RMSE for training and testing for regular cells are 0.07 and 0.12 for regular structure; 0.01 and 0.02 for inverted structure, respectively. Although, these models were seemed to have some predictive power, they are not sufficient to estimate the exact hysteresis index of the cells. Hence, classification will be more reliable in this case.

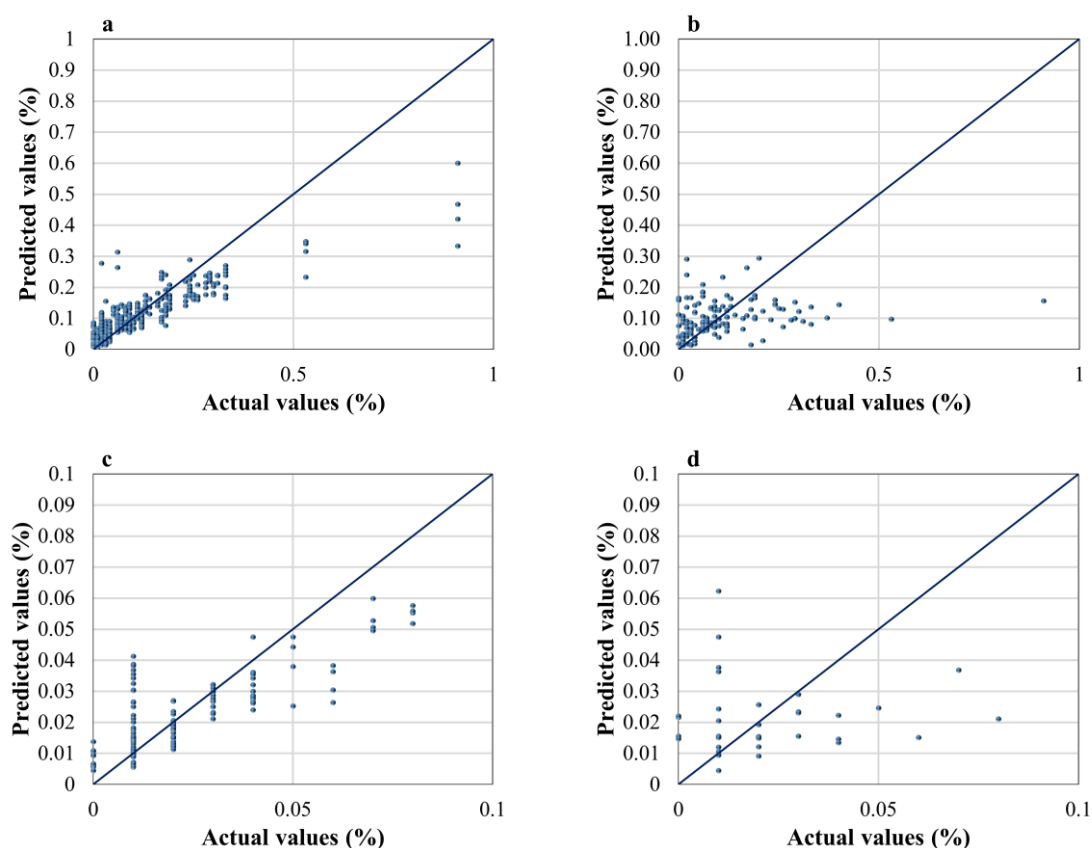


Figure 4.25. Actual versus predicted hysteresis index by random forest model for (a) training and (b) testing for regular (n-i-p) cells; (c) training and (d) testing for inverted cells.

4.3.2. Analysis of Factors Effects on Hysteresis by Association Rule Mining

We summarized the results of $HI \leq 0.01$ and $HI \leq 0.05$ for regular and inverted cells with $PCE \geq 10\%$ tested under low scan conditions in Table 4.10, Table 4.11, Table 4.13 and Table 4.14, respectively. All the other analyses as well as the detailed version of the tables given in this section (without restriction of minimum data count) are given in Appendix B with their full details.

As explained in Table 4.1 (in headings), the higher lift in association rule mining shows the higher positive impact of a factor. For example, in Table 4.10, the lift of cells having doped- $mTiO_2$ (m: mesoporous) as second layer of ETL is 2.52 for $HI \leq 0.01$. There are 17 cells made of doped- $mTiO_2$ in the dataset containing 110 cells; while 18 of 110 cells have $HI \leq 0.01$, this number is seven out of 17 for the doped- $mTiO_2$ cells. Then, the lift is $(7/18)/(17/110) = 2.52$ meaning that the fraction of doped- $mTiO_2$ cells with $HI \leq 0.01$ is 2.52 times higher than the fraction of the doped- $mTiO_2$ in the entire database; this is a strong indicator that doped- $mTiO_2$ favors lower hysteresis. On the other hand, only five cells out of 46 prepared with undoped $mTiO_2$ has $HI \leq 0.01$ resulting the low lift of $(5/18)/(46/110) = 0.66$; consequently we can conclude that doping to $mTiO_2$ generally reduces hysteresis.

Although the lift is a good indicator for the factor effect, it is not sufficient because there should be certain number of cells supporting the lift for reliable conclusion (see for the parameter support and confidence in Table 4.10). For example, if a material tested only twice and resulted $PCE \geq 10\%$ and $HI \leq 0.01$, its lift would be $(2/18)/(2/110) = 6.11$, which is quite high. However, there are only two cases meeting these conditions; hence, this result is not statistically reliable. On the other hand, new but promising materials will also initially appear like this. Hence, one should rely on the factors with high support for reliable generalization while carefully watching the factors with high lift for possible early warnings for new alternatives even though their support is low. Here, we restrict our discussion with the materials and methods having both high lifts and sufficiently high number of cells. We took minimum five cells for $HI \leq 0.05$ to have an acceptable generalization and listed the same factors for $HI \leq 0.01$ for continuation in Table 4.10 even if the number decreased; we also considered ZnO (ETL) and PTAA (HTL) because both have high lifts for $HI \leq 0.05$

(ZnO also has the highest $HI \leq 0.01$), and both have four data points, which is close to our limit of five. We presented the number of data points (satisfying the conditions) for each factor in the last column of Table 4.10 and Table 4.11 because it is much easier to follow number of data points than support and confidence.

The mixed cation perovskites were the only perovskites with high lift (1.25) as they also reported to cause less hysteresis in literature[19][345]; Jacobsson *et al.*[346] also stated that changing cation and halide ratios affect hysteresis. Indeed, six out of eight mixed cation perovskite are Cs-FA-MA perovskites in Table 4.10 (10 out 18 for $HI \leq 0.05$) while the effect of changing halide ratio was not observable in our work. Two-step perovskite deposition procedure also has better lift (1.58) than one step (0.68) probably due to easier control of crystallization[13][63]; this is more apparent in the cells prepared with spin-spin configuration (lift is 2.35). DMF seems to be the best solvent for low hysteresis; we could not see the positive effect of DMSO containing solvents even though it was suggested so by Seo *et al.*[347]. The anti-solvent treatment was also found to suppress hysteresis as suggested (by improving film morphology)[348][349], and the trifluorotoluene (lift=2.35) was found to lead the lowest hysteresis in accordance with Paek *et al.*[348].

Although Cai *et al.*[350] and Kim *et al.*[351] reported that doped compact TiO_2 lowered hysteresis, we did not observe such results (it may be due to the small number of cases). ZnO appeared with a high lift (although there are only four cells); a similar results were also reported for ZnO in literature with the explanation that it has longer charge carrier lifetime and higher electron conductivity than compact TiO_2 [352],[353]. We could not obtain any conclusive results for SnO_2 , which was the most reproducible ETL. For the second ETL, we found that doped mesoporous TiO_2 reduced hysteresis significantly (highest lift for $HI \leq 0.05$) as the doping was reported to passivate the electronic trap states or defects that causes hysteresis [354],[355].

The best HTL materials for $HI \leq 0.01$ were found to be various types of diphenylamine substituted carbazole fragments linked by a nonconjugated methylenebenzene unit studied by Magomedov *et al.*[356] which labeled as others in Table 4.10 with the lift of 1.39. The lift of spiro-OMeTAD, which is the most common material, is 0.76 indicating that it does not favor low hysteresis even though Salado *et al.* stated otherwise; they found it better than

PTAA[357]. However, although PTAA did not appear in a $HI \leq 0.01$ analysis, it was found to be much better than spiro-OMeTAD in our analysis for $HI \leq 0.05$ (with four cases). For $HI \leq 0.05$, the positive effects of other HTLs were also conclusive (details are given in Table 4.11).

Table 4.10. Association Rule Mining for $HI \leq 0.01$ and $PCE \geq 10\%$ for Regular (n-i-p) Cells with Scan Rate ≤ 0.05 V/s.

Antecedent	Consequent	Support	Confidence	Lift	Data count
$HI \leq 0.01$ $PCE \geq 10\%$ Scan rate \leq 0.05 V/s	ETL=ZnO	0.04	0.22	4.07	4
	ETL-2=doped-mTiO ₂	0.06	0.39	2.52	7
	Deposition method=spin-spin	0.05	0.28	2.35	5
	Anti-solvent treatment=trifluorotoluene	0.05	0.28	2.35	5
	HTL additive=no	0.03	0.17	1.83	3
	Deposition procedure=two-step	0.06	0.39	1.58	7
	HTL additive=LiTFSI+TBP+FK209	0.06	0.39	1.53	7
	HTL=others*	0.05	0.28	1.39	5
	Precursor solution=DMF	0.07	0.44	1.29	8
	Perovskite=mixed cation	0.07	0.44	1.25	8
	Back contact=Ag	0.05	0.33	1.22	6
	Anti-solvent treatment=no	0.09	0.56	1.18	10
	HTL=PTAA	0.01	0.06	1.02	1
	Perovskite=MAPbI ₃	0.08	0.50	0.95	9
	Deposition method=spin	0.07	0.44	0.94	8
	Precursor solution=DMF+DMSO	0.06	0.39	0.86	7
	Preparation=one-step	0.10	0.61	0.81	11
	ETL=TiO ₂	0.10	0.61	0.77	11
	HTL=spiro-OMeTAD	0.09	0.56	0.76	10
	Back contact=Au	0.08	0.50	0.75	9
HTL additive=LiTFSI+TBP	0.07	0.44	0.73	8	
ETL-2=mTiO ₂	0.05	0.28	0.66	5	
Deposition method=spin 2-3	0.03	0.17	0.63	3	
ETL-2=0	0.04	0.22	0.58	4	

*others: Diphenylamine-substituted carbazole-based derivatives (V885, V886, V908, V911, V946)

Additives to HTL also seem to have large impact on hysteresis. For example, LiTFSI+TBP was reported to increase hysteresis due to Li⁺ ion migration [358],[359] as we also found in our analysis (lift is 0.73); the cells without HTL additive were found to be

better (with lift of 1.83) even though there are only three such cases. However, adding FK209 to LiTFSI+TBP decreased hysteresis significantly (lift is 1.53), and this may be attributed to the increasing conductivity of HTL by FK209 addition[341].

Finally, Ag back contact seems to decrease hysteresis slightly (lift is 1.22) while the effect of Au was found to be negative (0.75). No sufficient data were available for the carbon back contact, which was found to be the most reproducible materials in previous section.

Table 4.11. Association Rule Mining for $HI \leq 0.05$ and $PCE \geq 10\%$ for Regular (n-i-p) Cells with Scan Rate ≤ 0.05 V/s.

Antecedent	Consequent	Support	Confidence	Lift	Data count
$HI \leq 0.05$ $PCE \geq 10\%$ $Scan\ rate \leq 0.05\ V/s$	ETL-2=doped-mTiO ₂	0.13	0.34	2.21	14
	Anti-solvent treatment=trifluorotoluene	0.09	0.24	2.06	10
	HTL=PTAA	0.04	0.08	1.79	4
	ETL=ZnO	0.04	0.10	1.79	4
	Deposition method=spin-spin	0.07	0.20	1.65	8
	HTL=others*	0.11	0.29	1.46	12
	HTL additive=LiTFSI+TBP+FK209	0.14	0.37	1.44	15
	HTL additive=no	0.05	0.12	1.34	5
	Perovskite=mixed cation	0.16	0.44	1.24	18
	Anti-solvent treatment=no	0.21	0.56	1.19	23
	Deposition procedure=two-step	0.10	0.27	1.09	11
	Precursor solution= DMF	0.14	0.37	1.06	15
	Back contact= Au	0.25	0.68	1.03	28
	ETL=TiO ₂	0.30	0.80	1.02	33
	Deposition method=spin	0.17	0.46	0.98	19
	Deposition procedure=one-step	0.27	0.73	0.97	30
	Deposition method=spin 2-3	0.09	0.24	0.93	10
	Precursor solution=DMF+DMSO	0.15	0.41	0.91	17
	Back contact=Ag	0.09	0.24	0.89	10
	Perovskite=MAPbI ₃	0.17	0.46	0.88	19
	HTL additive=LiTFSI+TBP	0.18	0.49	0.80	20
	HTL=spiro-OMeTAD	0.21	0.56	0.77	23
	ETL-2=0	0.11	0.29	0.77	12
ETL-2=mTiO ₂	0.12	0.32	0.76	13	

*others: poly[(2,5-bis(2-hexyldecyloxy)phenylene)-alt-(5,6-difluoro-4,7-di(thiophen-2-yl)benzo[c][1,2,5]-thiadiazole) (PPDT2FBT), a novel N-phenylindole-diketopyrrolopyrrole-containing narrow band-gap materials (DPIO), Dimethoxydiphenylamine-substituted dispiro-oxepine derivative 2,2',7,7'-tetrakis-(N,N'-di-4-methoxyphenylamine)dispiro-[fluorene-9,4'-dithieno[3,2-c:2',3'-e]oxepine-6',9''-fluorene] (DDOF), Diphenylamine-substituted carbazole-based derivatives (V885, V886, V908, V911, V928, V931, V946, V957, V1039)

It is also possible to analyze multi factor associations to find the possible combinations of factors leading low hysteresis with a feasible PCE; such combinations may not only offer a good starting point to manufacture low hysteresis cells, but may also provide some evidences for the presence of interactions (factors enhancing the effects of each other) and confounding (causing insignificant factors to appear significant because they happen to be used together with significant factor). Indeed, we found only one combination having nine factors with high lifts as given in Table 4.12. There are also some derivatives of these combinations obtained by removing one or two factors but we did not discuss them because they do not contain additional information.

Table 4.12. Multiple Factor Associations for Regular Cells with $HI \leq 0.01$ and $PCE \geq 10\%$.

Antecedent	Consequent	Support	Confidence	Lift	Data count
$HI \leq 0.01$ $PCE \geq 10\%$ Scan rate \leq 0.05 V/s	ETL=TiO ₂ ,	0.05	0.56	3.40	5
	ETL-2= doped-mTiO ₂ ,				
	Perovskite=mixed cation,				
	Deposition procedure=one-step,				
	Deposition method=spin,				
	Anti-solvent treatment=trifluorotoluene,				
	Precursor solution=DMF+DMSO,				
	HTL=others*,				
	HTL additive= LiTFSI+TBP+FK209,				
Back contact = Au					
*others: Diphenylamine-substituted carbazole-based derivatives (V885, V886, V908, V911, V946)					

This combination represents five of 18 cells with $HI \leq 0.01$; the common high lift elements are mixed cations perovskites (eight counts), doped mTiO₂ (seven counts), trifluorotoluene (five counts), diphenylamine substitutes as HTL (five counts) and LiTFSI+TB+FK209 (seven counts) as given Table 4.10. The lift indicates the fraction of cells having this seven factors with low hysteresis is 3.04 times higher than their fraction in entire dataset. Such results should be inspected more carefully for the potential risks of interaction and confounding among the factors because the five cells are coming from the same source[356], and all of HTL materials and most of the other high lift materials seem to be used in these cells; we cannot know whether all these factors are indeed effective or just happen to be used with effective materials for low hysteresis. However, these five factors are actually utilized in large number of cells in other papers as well, and they resulted in high

lifts for $HI \leq 0.05$ (Table 4.11); this indicates that they may be also effective by themselves. Although the HTL materials (diphenylamine substitutes) seems to be too specific for generalization, there are some other new HTL alternatives in others group in Table 4.11 indicating that search for a new and better HTL alternatives seems to work. Consequently, we can use this combination as a good starting points while we can still make generalization for the individual effects of involving factors.

The result of hysteresis analysis for inverted cells were given in Table 4.13 and Table 4.14. Different than the regular structure, multiple spin coating of perovskite (spin 2-3) which is a one-step deposition procedure has the highest lift in inverted structure and the anti-solvent treatment with toluene was found to be present in cells with less hysteresis. Toluene was also found to lead more reproducible cells in Section 4.2. Although we could not observe the positive effect of mixed cation perovskite due to less number of data points in inverted cells compared to regular structure, the lift of four cells with $HI \leq 0.01$ and $PCE \geq 10\%$ was found to be 1.72. (Table C.10). Using PCBM as ETL, and an ETL interlayer (such as BCP, PEI or LiF) were found to reduce hysteresis. Heo *et al.*[152] reported the advantages of using a PCBM as ETL; i) good electron transfer from perovskite to ETL due to high electron conductivity of PCBM, ii) better charge injection/separation efficiency between $MAPbI_3$ and iii) increased resistance to air and humidity due to hydrophobic nature of PCBM. The reduced hysteresis in the presence of PCBM was attributed to balanced electron and hole flux and reduced trap states. This property of PCBM was also confirmed by Xu *et al.*[360], even they employed PCBM directly in perovskite layer. However, although using BCP as an ETL interlayer was found to cause less hysteresis, Yoon *et al.*[103] observed more hysteresis in the presence of BCP due to unnecessary trap states causing hysteresis besides decreased performance. NiO_x was found to be a good HTL material for low hysteresis which was also suggested by Yin *et al.* [361]. Lastly, similar to reproducibility analysis, Ag back contact was found to lead the cells with less hysteresis.

Table 4.13. Association Rule Mining for $HI \leq 0.01$ and $PCE \geq 10\%$ for Inverted (p-i-n) Cells with Scan Rate ≤ 0.05 V/s ($PCE \geq 10\%$ for All Cells).

Antecedent	Consequent	Support	Confidence	Lift	Data count
$HI \leq 0.01$ $PCE \geq 10\%$ Scan rate \leq 0.05 V/s	Deposition method=spin2-3	0.23	0.47	1.65	8
	Anti-solventtreatment=toluene	0.26	0.53	1.43	9
	HTL= NiO_x	0.17	0.35	1.24	6
	Perovskite=MAPbI ₃	0.34	0.71	1.18	12
	ETL=PCBM	0.40	0.82	1.15	14
	Deposition procedure=one-step	0.46	0.94	1.14	16
	ETL-2=BCP	0.17	0.35	1.12	6
	BC=Ag	0.31	0.65	1.08	11
	Back contact=Al	0.17	0.35	0.95	6
	Precursor solution=DMF+DMSO	0.17	0.35	0.95	6
	HTL-2=0	0.37	0.76	0.92	13
	HTL=PEDOT:PSS	0.20	0.41	0.85	7
	ETL-2=0	0.20	0.41	0.80	7
	Deposition method=spin	0.20	0.41	0.80	7
	Anti-solventtreatment=no	0.17	0.35	0.69	6
	*masp: meniscus asisted spin coating **DEA: diethanolamine ***PN4N: polymeric interfacial modification layer to improve the cathode interface ****DIO: 1,8-diiodooctane				

Table 4.14. Association Rule Mining for $HI \leq 0.05$ for Inverted (p-i-n) Cells with Various Scan Rates (All cells except two have $PCE \geq 10\%$).

Antecedent	Consequent	Support	Confidence	Lift	Data count
$HI \leq 0.05$ $PCE \geq 10\%$ Scan rate \leq 0.05 V/s	Anti-solvent treatment=toluene	0.14	0.48	1.95	13
	ETL-2=BCP	0.10	0.33	1.72	9
	Deposition method=spin 2-3	0.11	0.37	1.72	10
	Scan rate=0-0.05 V/s	0.18	0.63	1.67	17
	Precursor solution=DMSO+GBL	0.09	0.30	1.62	8
	HTL-2=others (mNiO _x -Cu, PEDOT:PSS, DEA****)	0.08	0.26	1.61	7
	ETL-2=others****	0.08	0.26	1.42	7
	ETL=PCBM	0.23	0.78	1.29	21
	Back contact=Ag	0.23	0.78	1.17	21
	HTL= NiO_x	0.09	0.30	1.15	8
	Deposition procedure=one-step	0.28	0.96	1.12	26
	Scan rate=0.05-0.1 V/s	0.06	0.22	1.09	6
	Perovskite=MAPbI ₃	0.19	0.67	1.02	18
	Precursor solution=DMF+DMSO	0.11	0.37	1.01	10
	HTL=PEDOT:PSS	0.14	0.48	1.00	13

Table 4.14. Association Rule Mining for $HI \leq 0.05$ for Inverted (p-i-n) Cells with Various Scan Rates (All cells except two have $PCE \geq 10\%$) (cont.).

Antecedent	Consequent	Support	Confidence	Lift	Data count
$HI \leq 0.05$	HTL-2=0	0.22	0.74	0.88	20
	Deposition method=spin	0.16	0.56	0.88	15
$PCE \geq 10\%$	Perovskite=MAPbI _{3-x} Cl _x	0.05	0.19	0.82	5
Scan rate \leq 0.05 V/s	Back contact=Al	0.06	0.22	0.74	6
	Anti-solvent treatment=no	0.08	0.26	0.69	7
	ETL-2=0	0.12	0.41	0.65	11
*masp: meniscus asisted spin coating **others: 2-aminoethanesulfonamide hydrochloride (ASCI), Ag ***DEA: diethanolamine ****others: polymeric interfacial modification layer to improve the cathode interface (PN4N), TiO _x , LiF, rhodamine 101/LiF, aluminium-doped ZnO (AZO)/SnO _x , PEI					

For the inverted structure, we could detect only one combination with five of 17 cells (from three different publications) [362–364] (Table 4.15). All factors are high lift elements; NiO_x (six counts), MAPbI₃ (12 counts), one-step (16 counts), spin 2-3 (eight counts), toluene (nine counts), PCBM (14 counts) and Ag (11 counts). Except MAPbI₃, these seven factors are actually utilized in large number of cells in other papers as well, and they resulted in high lifts for $HI \leq 0.05$ (Table 4.14). Hence, this combination can also be used as a good starting point while we can still make generalization for the individual effects of involving factors.

Table 4.15. Multiple factor associations for inverted (p-i-n) cells with $HI \leq 0.01$ and $PCE \geq 10\%$.

Antecedent	Consequent	Support	Confidence	Lift	Data count
$HI \leq 0.01$	HTL=NiO _x , Perovskite=MAPbI ₃ , Deposition procedure=one-step,	0.14	0.83	1.72	5
$PCE \geq 10\%$	Deposition method=spin 2-3,				
Scan rate \leq 0.05 V/s	Anti-solvent treatment=toluene, ETL= PCBM, Back contact = Ag				

To summarize, the materials causing the low hysteresis could be identified in general using association rule mining. The number of data points was not as large as those for reproducibility; hence, only the most effective factors could be identified for low hysteresis in contrast to reproducibility analysis in which all the alternatives could be compared.

However, most of our findings are in agreement with the literature, and they may still contribute to the efforts to minimize the hysteresis in perovskite cells.

4.3.3. Developing Heuristics for Low Hysteresis by Decision Tree Analysis

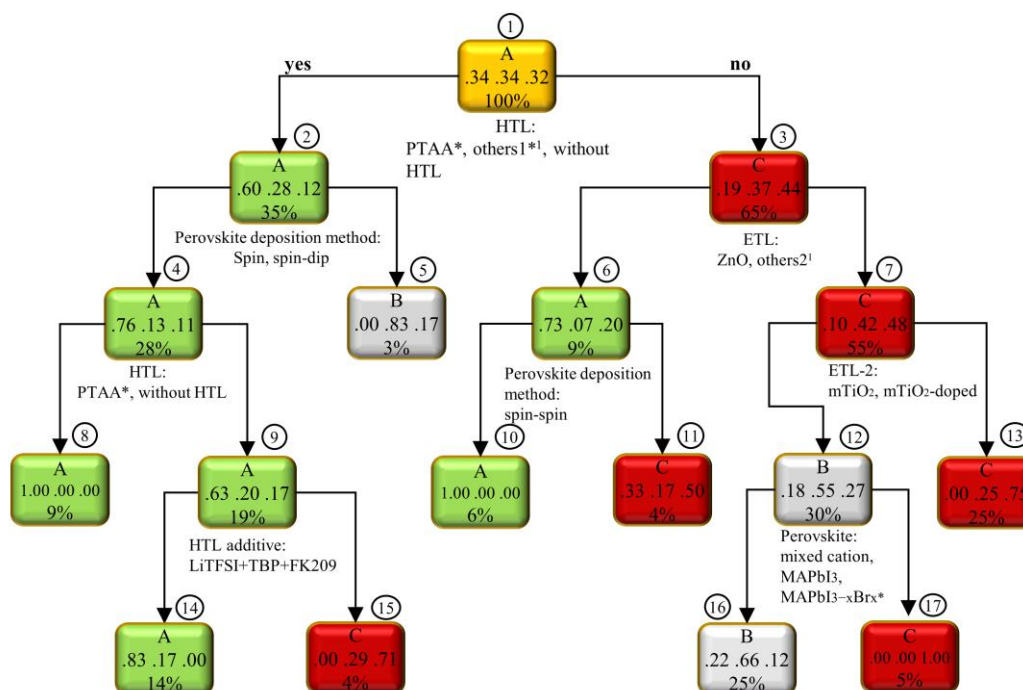
The decision tree classification was employed to develop heuristics for low hysteresis if it is possible. The HI limit for low hysteresis was again taken as maximum of 0.01 (Class A) and the cells which have $HI > 0.1$ were considered as high hysteresis cells (Class C). We wanted to analyze the cells with $PCE \geq 10\%$ as well as low hysteresis because we are also seeking the rules for the cells with considerable PCE. Unfortunately, we could not build a successful decision tree model for inverted structure for this case. For regular cells, the accuracy of the decision tree was 78% and the confusion matrix was given in Table 4.16. As we are seeking rules for low hysteresis (Class A), the precision is quite high (91%) as well as accuracy (80%). We also built decision tree without PCE restriction for regular cells. The details were given in Appendix C (Figure C.1. and Table C.11).

Table 4.16. Confusion Matrix of Regular Cells Dataset.

		Actual Class			Precision
		Class A	Class B	Class C	
Predicted Class	Class A	43	4	0	91%
	Class B	9	37	7	70%
	Class C	2	13	46	75%
Accuracy		80%	69%	87%	
Overall accuracy					78%

The decision tree model for regular (n-i-p) cells was presented in Figure 4.26. The root node was splitted by HTL type selection followed by perovskite deposition method. This rule led to Node 8 that contains only Class A cells. In addition to these rules, HTL additive selection was also founded to lead low hysteresis cells (Node 14). Another rule for low

hysteresis was based upon HTL type, ETL type and perovskite deposition method and this final node (Node 10) also contains completely Class A cells.



¹ Term of "others" were explained in Table C.12.

Figure 4.26. Decision tree model for regular (n-i-p) cells in hysteresis analysis (minimum split number=5, maximum depth=4, complexity parameter=0).

4.4. Analysis of Long-term Stability

In this part of the communication, we present our analysis on the long-term stability of perovskite solar cells manufactured using different materials and procedures. We used number of days passed for a cell to reach to 80% of its initial PCE as the stability criterion. Firstly, we employed random forest regression to see whether the number of days which the PCE dropped to its 80% could be predicted. Then, we performed the association rule mining analysis for three periods leading three stability criteria: stable more than 15 days, stable more than 30 days and stable more than 60 days; these criterias were defined cumulatively (for example, more than 15 days class also covers 30 and 60 days data); the analyses for 15 and 30 days were used to follow the trends in time and obtain some additional evidences to back up the analysis for 60 days, which was the longest practical period that we could analyze. We also constructed decision trees to deduce rules for the cells stable more than 60 days with a considerable initial PCE ($PCE \geq 10\%$).

4.4.1. Predicting the Degradation by Random Forest Analysis

The random forest regression was performed to predict the number of days when the PCE has dropped to its 80%. The RMSE of training and testing was found to be 15.6 and 37.4 for regular cells; 6.1 and 11.4 for inverted cells, respectively. Although RMSEs of the models were quite high (especially for testing), we detected that the model has some predictive power similar to PCE and hysteresis analysis (Figure 4.27). Hence, we continued to our analysis by classifying our output into various ranges.

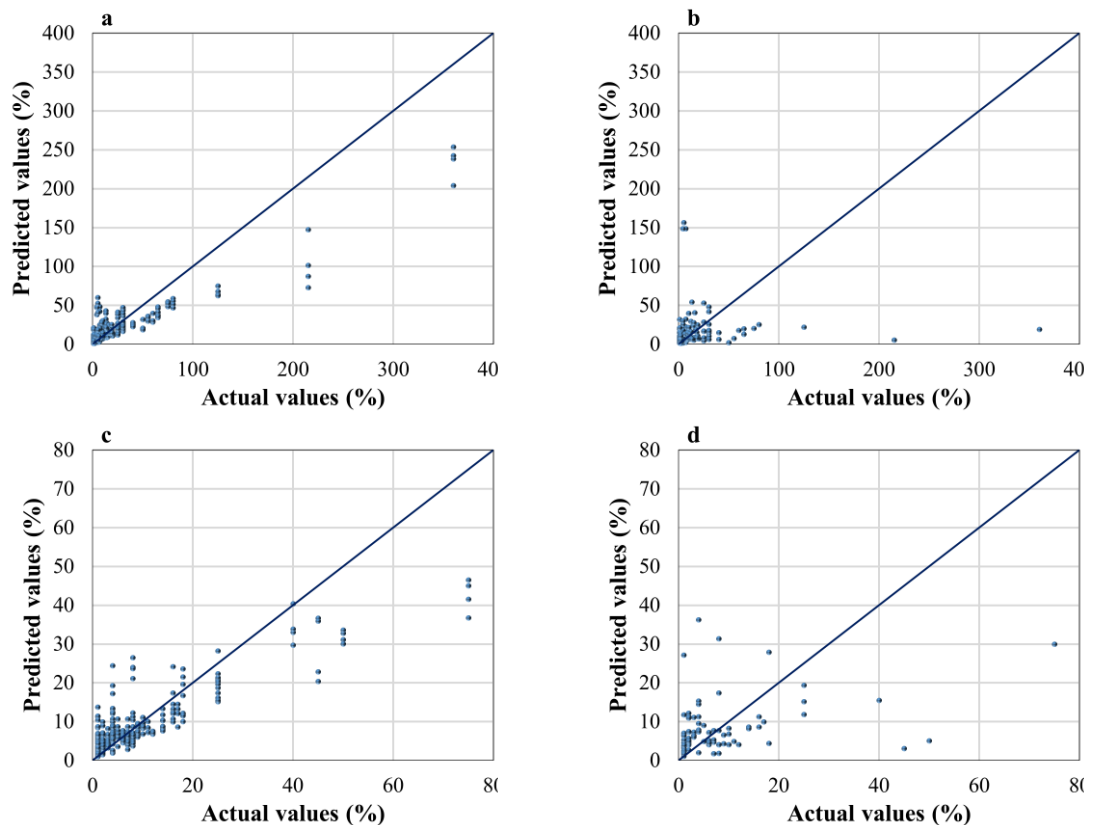


Figure 4.27. Actual versus predicted hysteresis index by random forest model for (a) training and (b) testing for regular (n-i-p) cells; (c) training and (d) testing for inverted cells.

4.4.2. Analysis of Factor Effects on Stability by Association Rule Mining

We presented the lift versus time plots in Figure 4.28; the x-axis represents the days (as 15, 30 and 60) for stable operation whereas the y-axis shows the lift values for individual factors with the same definition used in hysteresis analysis above. The size and the adjacent

numbers shows the number of cases fulfilling the time requirement stated in x-axis. The numbers in parenthesis are for the cells with the initial PCE of more than 10% to show both efficient and stable cells. As Figure 4.28a shows, the most stable cells were found to be made of mixed cation perovskites (mostly with MA-FA cations, as the most common combination, together with few Cs-MA-FA, MA or FA cations and perovskites with 2D structures); the lift of 1.42 for the stability criterion for 15 days states that the probability of having stable mixed cation perovskite cell for more than 15 days has 1.42 times higher than the probability of finding a mixed cation cell in entire database. The lift of mixed cation perovskite cells increases with the increasing time period (1.58 and 1.73 for 30 and 60 days, respectively) as a clear indicator of stability. This result is also consistent with the literature[365]. Although the number of stable cells made of MAPbI₃ is still higher than those made of mixed cation cells, its lift is lower because the number of unstable cells made of this perovskite is much larger. MAPbI_{3-x}Cl_x was stated to be thermally more stable than MAPbI₃ because no phase transition occurred between 25-100 °C[208], and this hypothesis is supported by the enhanced crystallinity and morphology of MAPbI_{3-x}Cl_x[343]. However, we found that this perovskite is less stable than MAPbI₃ even though the number of instances involving MAPbI_{3-x}Cl_x is rather small for a definitive conclusion (there are also reports stating that Cl⁻ addition does not necessary result in a different composition than MAPbI₃[38]).

The morphology and crystallinity of the perovskite film, which were highly dependent on the deposition procedures, plays an important role on both performance and stability[6],[215],[366]: One-step procedure appears to be slightly more stable in Figure 4.28b (the difference diminishes at 60 days); however, a more significant difference occurs in the selection of specific deposition techniques as it is given in Figure 4.28c. Most of the stable cells, produced using one-step procedure, were made by multiple spinning (spin 2-3) of the perovskite solution. The solvent used during perovskite deposition were also stated to affect the stability through morphology[367]. Indeed, the DMF+DMSO mixture (themselves of together with some additives such as benzoquinone[368]) improves stability significantly (Figure 4.28d). The use of anti-solvent also seems to affect the stability of the cell (Figure 4.28e). The chlorobenzene, especially with some additives (such as acetonitrile[73] or some p-type polymers[369]) and diethyl ether (only for 15 days data), seems to improve stability as it was reported and attributed to the improving the crystallization and morphology

[234],[370] while the toluene was found to decrease stability even though the numbers of cases are rather small to be conclusive.

Only the SnO₂ appears as a more stable alternative to the commonly used TiO₂ as the ETL compact layers for the 15 and 30 days data. (Figure 4.28f); Jiang *et al.*[371] also reported that SnO₂ was much more stable than TiO₂ under ambient conditions and illumination. Our analysis was not conclusive for ZnO due to the small number of cases. The effects of second ETL materials seems to be more significant, even though no significant difference observed between the cells without second ETL layer (planar) and with mesoporous TiO₂ as the most definitive trend in Figure 4.28g. Doped-mTiO₂, PCBM insertion and some other ETL interlayer materials (like [6,6]-phenyl-C61-butyric acid (PCBA)[372], passivated tin oxide (PTO)[373] and mesostructured ZnO[374]) seem to enhance the stability.

We found that HTL-free cells and cells with inorganic HTLs were more stable than spiro-OMeTAD even though their numbers in Figure 4.28h are low. HTL-free cells not only have simpler structures but they may also decrease the probability of negative effect of (organic) HTL materials on stability; for example, the most common HTL, spiro-OMeTAD, was found to play role in degradation of the cell at high temperatures[375]. However, all of three cells stable more than 60 days (four of five HTL-free stable more than 30 days) in Figure 4.28h also have carbon back contact confounding the effects of these two variables)

The most common HTL dopant, Li-TFSI, oxidizes HTL material in the presence of light and air which also causes degradation[376] whereas Lee *et al.*[377] attributed this behavior to the hygroscopic nature of Li-TFSI. A chemical interaction between oxidized HTL and TBP was also found to cause degradation[378]. However, LiTFSI+TBP+FK209 combination (Figure 4.28i) resulted in more stable cells; apparently, FK209 dopant has strong positive effect on the stability. The cells without HTL additives were also found to be stable than those used LiTFSI+TBP, which is the most common additive. F4CQN addition also appears to increase stability as consistent with the in results reported literature[268].



Figure 4.28. Association rule analysis for regular (n-i-p) type cells for (a) perovskite type, (b) deposition procedure, (c) deposition method, (d) precursor solution, (e) anti-solvent treatment, (f) ETL, (g) ETL-2, (h) HTL, (i) HTL additive, (j) back contact (k) stored humidity, (l) stored condition.

The cells with carbon back contact appear to be more stable (Figure 4.28j). However, as mentioned above, three of four cells stable more than 60 days are also HTL-free (four out of five for 30 days); hence it is not clear whether this effect comes from the carbon back contact or HTL-free structure. The silver back contact based cells were detected to be less stable probably due to silver oxidation to silver iodide as a result of the reaction with iodine in perovskite[379].

The moisture, oxygen, temperature and light were reported to affect the device stability by various investigators. Different decomposition pathways might occur under different sets of ambient conditions[203],[204]. Unfortunately, the analysis of all cell storage conditions in full details was not possible. Hence, we removed the cells stored in extreme conditions (under illumination, at high temperatures or in special encapsulation); we also excluded the data if the storage conditions are not clearly explained. At the end, we could only analyze the effect of humidity and oxygen. Our analysis for the humidity effect was quite conclusive; as it is clearly seen from Figure 4.28k, storing the cells under low humidity conditions (RH of 0-30%) clearly enables longer cell lifetime (27% of the cells in this groups actually tested under zero humidity condition). However, we could not obtain any conclusive results for oxygen probably due to the small number of data obtained under zero oxygen level (Figure 4.28l) even though the presence of oxygen and light together were reported to be the main reason of cell degradation, and the oxygen degradation was reported to be the dominant factor in long term stability rather than moisture degradation[380].

We also performed multiple factor association for the same purpose discussed for hysteresis (to find good combinations as starting points and check possible interactions or confounding). The four combinations of factors (one with eight factors and three with seven factors) for high stability (with $PCE \geq 10\%$) are originated from the various combinations of five articles[144], [368], [381–383] (usually three or four papers are common in all while one or two are changed from case to case) and given in Table 4.17. The one-step deposition, multiple spin (spin 2-3), chlorobenzene as anti-solvent and low humidity conditions as the test environment are the four common high lift elements. However, there are much larger number of cases involving all these factors (15 for one step, 11 for multiple spin, seven for chlorobenzene and 18 for low humidity) for 60 days data set and much more for 30 and 15 day with high lift; consequently, we can use these combinations as good starting points for

high stability cells, and we can also assume that these factors are effective themselves as well.

Table 4.17. Multiple Factor Associations for the Regular (n-i-p) Cells Stable More Than 60 Days with $PCE \geq 10\%$.

Antecedent	Consequent	Support	Confidence	Lift	Data count
Stable more than 60 days $PCE \geq 10\%$	ETL=TiO ₂ , Perovskite=MAPbI ₃ , Deposition procedure=one-step, Back contact=Au, O ₂ exists=yes, Stored condition= room-light, Stored humidity=0-30% RH	0.04	0.60	4.74	6
	ETL=TiO ₂ , Perovskite=MAPbI ₃ , Deposition procedure=one-step, HTL=spiro-OMeTAD, Back contact=Au, O ₂ exists=yes, Stored condition= room-light, Stored humidity=0-30% RH	0.03	0.56	4.39	5
	ETL=TiO ₂ , Deposition procedure=one-step, Deposition method=spin 2-3, Anti-solvent treatment=chlorobenzene, HTL=spiro-OMeTAD, Back contact=Au, O ₂ exists=yes, Stored humidity=0-30% RH	0.03	0.42	3.29	5
	ETL=TiO ₂ , ETL-2=0, Deposition procedure=one-step, HTL=spiro-OMeTAD, Back contact=Au, O ₂ exists=yes, Stored condition= room-light, Stored humidity=0-30% RH	0.03	0.38	3.04	5

Different than the regular cells, long term stability of MAPbI_{3-x}Cl_x was found to be superior to MAPbI₃ for inverted structures according to Figure 4.29. Although, this hypothesis is correct due to enhanced crystallinity and better morphology of MAPbI_{3-x}Cl_x[343], it is advised to be cautious because MAPbI_{3-x}Cl_x contains less data points than others. Besides, the difference in stability between MAPbI₃ and MAPbI_{3-x}Cl_x may support

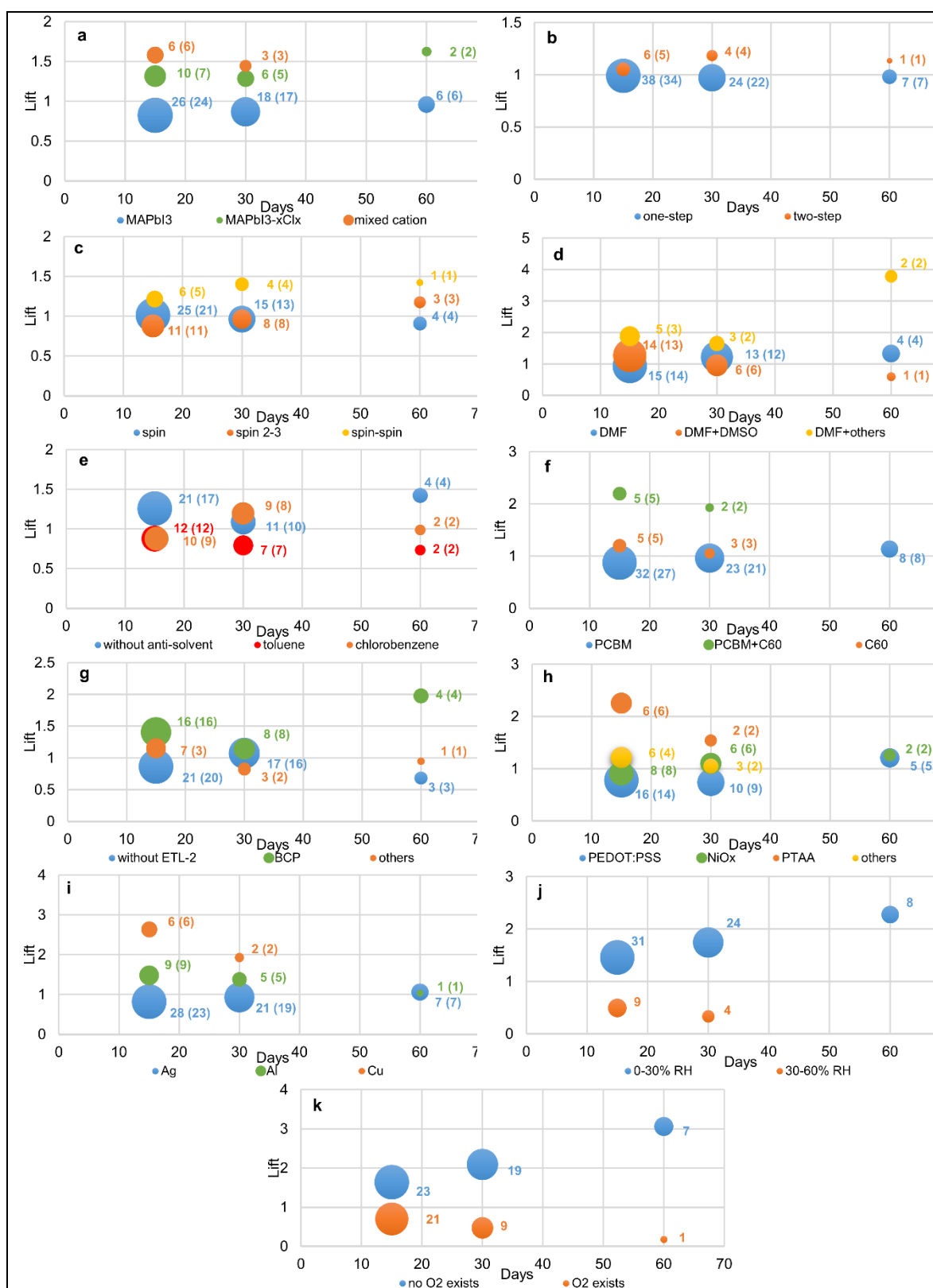


Figure 4.29. Association rule analysis for inverted (p-i-n) type cells for (a) perovskite type, (b) deposition procedure, (c) deposition method, (d) precursor solution, (e) anti-solvent treatment, (f) ETL, (g) ETL-2, (h) HTL, (i) back contact, (j) stored humidity, (k) stored condition.

that the presence of Cl ion in $\text{MAPbI}_{3-x}\text{Cl}_x$ perovskite despite the opponent publications [384], [385].

We could not detect any strong result for material type selection for ETL and HTL in order to achieve long term stability. However, PCBM with C60 as ETL and PTAA as HTL seem to lead more stable cells. Besides, using BCP as an interlayer between ETL and back contact was found to enhance stability as well as performance[386].

For the inverted type cells, the stability of the cells that employed Al was detected to be better than Ag despite to its unstable interfacial contact[387]. Regarding the data number of Al based cells, this result may not be strongly considered.

The humidity has also a significant effect on performance. For inverted cells, non-humid conditions were dominant for long term stability. Yang *et al.* [191] studied the dependence of relative humidity on degradation rate and found out that the perovskite layer degraded faster at higher humidity rates. The MAPbI_3 perovskite transforms into MAI and halide in the presence of humidity[366].The lift value of the cells stored under inert conditions are quite high for inverted cells as expected. Bryant *et al.* also found that MAPbI_3 perovskite cells degrade in the presence of oxygen under dark in the presence of an external bias whereas no degradation occurs in the inert condition[380].

Multiple factor association was performed for inverted cells which were stable more than 60 days with initial PCE $\geq 10\%$ (Table 4.18). Seven factors were detected from five of 21 cells with high stability (from three different publications[363], [388], [389]). The common high lift elements are PCBM (eight counts), Ag (seven counts), no O_2 condition (seven counts), stored humidity 0-30% RH (eight counts), room-light condition (eight counts). Although, the numbers of high lift factors aren't much greater than five, it is questionable to indicate their effects on long term stability individually. However, using these factors together was found to be common for high stability.

Table 4.18. Multiple Factor Associations for Inverted (p-i-n) Cells Stable More Than 60 Days with PCE \geq 10%.

Antecedent	Consequent	Support	Confidence	Lift	Data count
Inverted (p-i-n) cells stable more than 60 days PCE \geq 10%	HTL-2=0, Perovskite=MAPbI ₃ , ETL= PCBM, Back contact = Ag, O ₂ exists=no, Stored humidity=0-30% RH, Stored condition=room-light	0.065	0.45	4.38	5

As the result, the stability trends for most of the materials and methods are quite clear; if the lift is high for a factor (favoring the stability) for 15 days, it usually increases with increasing time period to 30 and 60 days. Considering these trends and the large number of data supporting the analysis, it can be concluded that the results obtained may be quite reliable, and they may be used to improve long-term stability of the perovskite cells.

4.4.3. Developing Heuristics for High Stability by Decision Tree Analysis

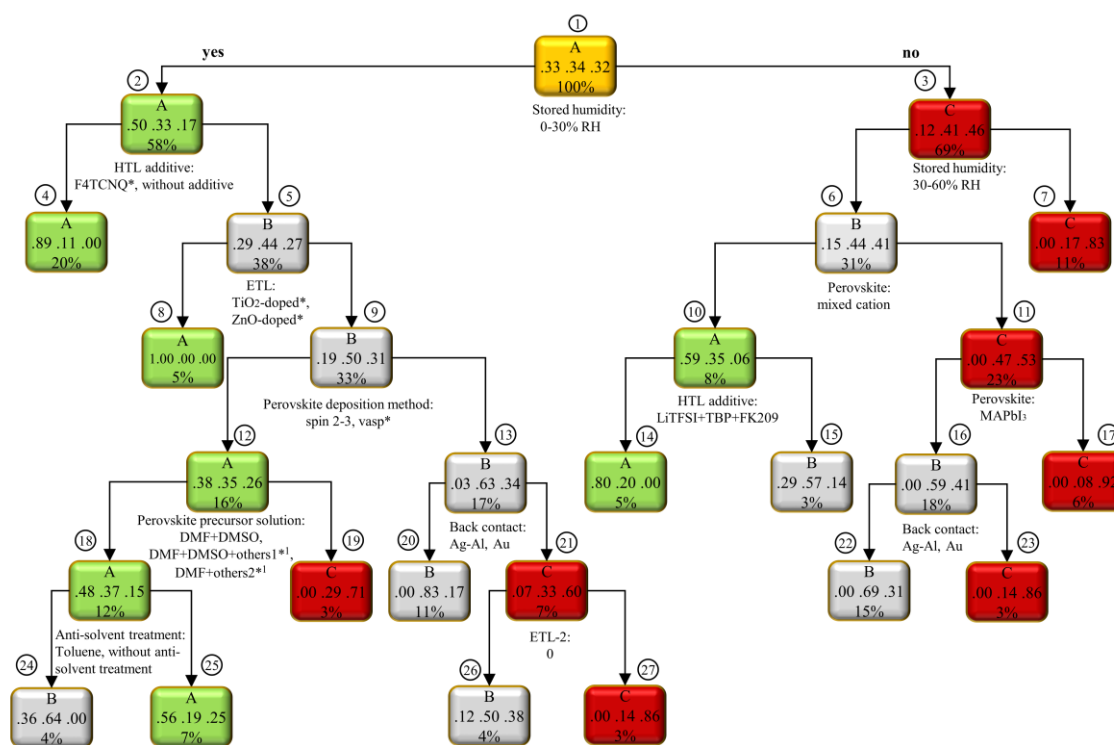
Decision tree classification was used to obtain set of rules leading high stability of the cells. For this purpose, the data was divided into three classes; cells stable more than 60 days (Class A), cells degraded within 7-60 days (Class B) and cells degraded within 6 days (Class C). We could not construct decision tree for inverted structure due to less data points of Class A. Hence, we constructed decision tree for stable regular (n-i-p) cells with initial PCE \geq 10%. The accuracy of the decision tree for regular cells was found to be 78% and the precision of Class A was 83% (Table 4.19). However, we had slightly less data points for this case than stability analysis without PCE consideration. Hence, we also gave the decision trees and confusion matrices for all data points (Figure D.1 and Table D.7), because one may want to look at the rules for high stability only.

As presented in Figure 4.30, the first split was made upon the stored humidity of the cells. Then, the cells provide low humidity conditions again divided based on HTL additive type (Node 2). Although, the dopants for the most common HTL, LiTFSI and TBP, improve PCE, they found to lead degradation because of hygroscopic nature of LiTFSI[266].

Table 4.19. Confusion Matrix of Regular Cells Dataset

		Actual Class			Precision
		Class A	Class B	Class C	
Predicted Class	Class A	66	10	4	83%
	Class B	7	56	18	69%
	Class C	0	9	48	84%
	Accuracy	90%	13%	6%	
Overall accuracy		78%			

Hence, using HTL without dopants are preferred for high stability. Although the cells with F4TCNQ additive in Node 4 were reported in only one paper (not generalizable), F4TCNQ was reported to enhance stability significantly[268]. Beside stored humidity and HTL additive type, ETL type selection leded a pure Class A node (Node 8); doping of TiO₂ and ZnO improves performance. Another heuristics is splitted based on stored humidity, perovskite type and HTL additive type (Node 14).



¹ Term of "others" were explained in Table D.8.

Figure 4.30. Decision tree model for regular (n-i-p) cells in stability analysis (minimum split number=5, maximum depth=6, complexity parameter=0).

5. CONCLUSION

The database (and the literature) has many non-comparable (even erroneous) data points due to the nonstandard testing procedures; this may even be true for stabilized efficiencies or maximum power point tracking of long-term stability, which have been reported in recent publications as the better measure of true performance due to the hysteresis consideration. However, as the benefit of having a large database, even the simple statistical analysis showed the effects of different materials and methods in statistically more significant way while the analysis of data with machine learning tools provided more detailed heuristics and models for high performance.

In PCE analysis, it was clearly seen that the average efficiencies obtained with MAPbI₃ and MAPbI_{3-x}Cl_x were nearly the same while FA based and mixed cation cells gave higher efficiency. Similarly, the data showed that, although the use of two-step deposition method had initially increased the average efficiency, the one-step procedure has been improved better in recent years with the improvements in solvent and anti-solvent treatments. Additionally, the potential of some rarely used materials (like Cs containing triple cation perovskites), inorganic HTLs and PTAA as HTL alternative for both regular and inverted cells were also emerged in simple statistical analysis. The association rule mining analysis of the stabilized efficiencies of regular cells revealed that the factors such as mixed cation perovskites, DMF+DMSO as solvent, chlorobenzene as anti-solvent and two or three times spinning as the one-step coating technique emerged as the effective ways of obtaining cells with PCE higher than 18.0%. Similarly, relatively less frequently used factors like LiTFSI+TBP+FK209 as HTL additive and SnO₂ as ETL layer were also detected as the alternatives for the high efficiency cells. The use of PTAA as HTL, mixed cation perovskite and BCP as ETL interlayer also appeared as the significant factors for high efficiency in inverted cells. The significance of factors mentioned above were also verified by the decision tree analysis; for example, the statistically most significant route leading to the high efficiency regular cells are separated from the others with the selection of perovskite, some alternatives for HTL additives, ETL, and precursor solution. The maximum efficiencies reported by NREL was also analyzed, and it was found that the evolution of maximum efficiency obeyed S-shape logistic pattern.

In reproducibility analysis, the samples were sufficiently large and differences among the pooled variances of factors are statistically significant in general; hence, the results should be quite reliable. Mixed cation perovskites, Cs based perovskites and $\text{MAPbI}_{3-x}\text{Br}_x$ perovskites were found to be more reproducible than other perovskites. Two step spin coating method (also multi-spin coating as one-step method) with use of DMSO containing precursor solutions and antisolvent treatment (diethyl ether, toluene, chlorobenzene) increased reproducibility. In regular structure, employing SnO_2 and doped TiO_2 as ETL compact layer; PCBM, TiO_2 -nanostructure and doped mesoporous TiO_2 as second layer of ETL; P3HT, PTAA as HTL or HTL-free structure; HTL dopants especially FK209 and FK102 with LiTFSI+TBP and carbon back contact were found to favored high reproducibility. For inverted structure, employing PCBM and C60 together as ETL; using an ETL interlayer (ZnO, PEI, BCP); doping of PEDOT:PSS or HTL-free cells and Ag as back contact were found for high reproducibility.

In hysteresis analysis, although the dataset for $\text{HI} \leq 0.01$ (due to the scan rate and PCE constraints) was relatively small creating difficulties in isolating individual factor effects for hysteresis, the analysis for $\text{HI} \leq 0.05$ also provided some additional evidence to resolve those difficulties. Associating rule mining results justified that mixed cation perovskites; two-step spin coating of perovskite, multiple spin coating as one-step coating; BCP as ETL interlayer; PTAA as HTL; using LiTFSI+TBP+FK209 as HTL dopant also reduced hysteresis as they were found to increase reproducibility. Besides, employing trifluorotoluene as anti-solvent treatment, DMF as precursor solution, ZnO as compact ETL layer and cells without anti-solvent treatment were also found to be effective to suppress hysteresis in regular cells. In inverted structure, using toluene as anti-solvent (similar to reproducibility), PCBM as ETL, NiO_x as HTL and Ag as back contact were found to suppress hysteresis. Decision tree analysis supported the findings given above for both regular and inverted structure.

In the dataset for stability (even for the 60 days) was sufficiently large; additionally, plotting the lifts for 15, 30 and 60 days together made the trend more apparent and helped to make reliable generalizations. Association rule mining revealed that mixed cation perovskites, multi-spin coating method as one-step deposition, DMF+DMSO as precursor

solution, LiTFSI+TBP+FK209 as HTL additive were found to have a positive effect on stability similar to reproducibility and hysteresis in regular structure. Besides, using chlorobenzene as anti-solvent, SnO₂ as ETL compact layer, PCBM as second ETL, HTL-free cells and carbon as back contact were common with reproducibility in regular structure. Employing inorganic HTLs and F4TCNQ as HTL dopant were found to improve stability. In inverted cells, mixed cation perovskites, two-step spin coating of perovskite, BCP interlayer, PTAA as HTL were found to be common effective elements for stability, reproducibility and hysteresis. Using PCBM and C60 together was also found to have a positive effect on high stability similar to high reproducibility; whereas, using NiO_x as HTL were found to be in common for high stability and low hysteresis. Apart from these results, employing DMF and some novel additives(such as N-cyclohexyl-2-pyrrolidone or GO) as perovskite precursor solution and not using an anti-solvent may also resulted high stability in inverted cells. Storing cells at low humidity, under O₂ free and dark conditions were found to be significant for high stability as expected. In addition to the factors mentioned above, using doped TiO₂ or doped ZnO as compact layer also improved stability of regular cells according to decision tree analysis for high stability.

We summarized the most effective factors for high PCE, reproducibility, hysteresis and stability for regular and inverted cells in Table 5.1 and Table 5.2, respectively. The materials leading to high efficiency, high reproducibility, low hysteresis and long term stability were quite similar while high PCE, reproducibility and stability seem to have more common elements than they have with low hysteresis. In regular cells, the mixed cation perovskites, doped mesoporous TiO₂ as second ETL layer and HTL additive of LiTFSI+TBP+FK209 have the positive effects on all; SnO₂ compact layer, one-step multiple spin coating (spin 2-3), DMF+DMSO solvent and diethyl ether anti-solvent are also common for all except hysteresis. Spin-spin coating of perovskite was detected to be useful for reproducibility and low hysteresis. For inverted cells, the results were slightly less conclusive. Using a second ETL layer (especially BCP) has the positive effects on all; the mixed cation perovskites, chlorobenzene as anti-solvent, PCBM+C60 as ETL are found to be in common for all except hysteresis. One-step multiple spin coating of perovskite is useful for all except stability. Although it is not presented in Table 5.1, the low humidity is also clearly required for high stability.

Table 5.1. Comparison of Materials and Methods Leading to High PCE, Reproducibility and Stability as well as Low Hysteresis for Regular Cells.

Material/method	Efficiency	Reproducibility	Hysteresis*	Stability**
Perovskite	Mixed cation (also FA based perovskites)	MAPbI_{3-x}Br_x (also Cs based & mixed cation perovskites)	Mixed cation	Mixed cation
Perovskite Deposition	One-step: spin 2-3	Two-step: spin-spin (also one-step: spin 2-3)	Two-step: spin-spin	One-step: spin 2-3
Solvent	DMF+DMSO (also DMSO & DMSO+GBL)	DMF+DMSO+others⁺ (also DMSO+GBL, DMF+DMSO& DMSO)	DMF	DMF+DMSO+others⁺⁺ (also DMF+DMSO)
Anti-solvent	Diethyl ether, chlorobenzene	Diethyl ether (also toluene & chlorobenzene)	Trifluorotoluene (or without anti-solvent treatment)	Chlorobenzene +others⁺⁺⁺ (also chlorobenzene & diethyl ether)
ETL	SnO₂ (also doped-TiO ₂)	SnO₂ (also doped-cTiO ₂ , without ETL)	ZnO	SnO₂
ETL second layer/interlayer	doped mTiO₂ (also TiO ₂ -ns)	PCBM (also TiO ₂ -ns & doped-mTiO ₂)	doped-mTiO₂	PCBM (also doped-mTiO ₂)
HTL	PTAA	P3HT (also PTAA, HTL-free)	PTAA (for HI 0.05 only) (also diphenylamine substituted carbazole based HTLs)	Inorganic HTLS (and HTL-free)
HTL additive	LiTFSI+TBP+FK209 (also LiTFSI+TBP+FK102)	LiTFSI+TBP+FK102 (also LiTFSI+TBP+FK209)	LiTFSI+TBP+FK209	F4TCNQ (also LiTFSI+TBP+FK209 & no HTL additive)
Back contact	Au (also Ag)	Carbon	Ag	Carbon
<small>*for HI ≤ 0.01) with scan rates ≤ 0.05 V/s and PCE ≥ 10 %; **For cells stable more than 60 days +others include Pb(SCN)₂, SnF₂-pyrazine, thiourea, polyvinylpyrrolidone (PVP), LiI, N-Methyl-2-Pyrrolidone (NMP), IPA, terephthalic acid (TPA) ++others include benzoquinone (BQ) for 60 days, 2-pyridylthiourea, N-Methyl-2-Pyrrolidone (NMP), Pb(SCN)₂ for 30 days +++others include acetonitrile for 60 days, toluene, p-type polymer with or without (w/wo) molecular fluorination (PF-0, PF-1), n-type polymer w/wo molecular fluorination (N2200, F-N2200) for 30 days</small>				

Finally, this work revealed that this type of analysis may be beneficial to review and understand the literature better, see the overall picture and draw some valuable conclusions for the future works. This type of analyses will be likely more reliable in the future with the increasing number of data points and with a better standardization of procedures and parameters for cell preparation, characterization and reporting. However, it should be remembered that these methods were designed to draw generalizable conclusions from the large data sets, and in some sense, convert the experiences of large groups into comprehensible knowledge. Hence, by their nature, they may not capture the emerging promising alternatives due to their insufficient number of data points or lower initial (immature) performances against the more established competitors. Some additional analysis may be needed as we did for Cs based cells, individual combinations of mixed cations cells and some HTL materials in performance analysis.

Table 5.2. Comparison of Materials and Methods Leading to High PCE, Reproducibility and Stability as well as Low Hysteresis for Inverted Cells.

Material/method	Efficiency	Reproducibility	Hysteresis*	Stability**
Perovskite	Mixed cation (also FA based perovskites)	MAPbI_{3-x}Br_x, MAPbI_{3-x}Cl_x & mixed cation perovskites)	MAPbI3	Mixed cation (also MAPbI _{3-x} Cl _x)
Perovskite Deposition	One-step: spin2-3	One-step: spin 2-3 (also two-step: spin-spin)	One-step: spin 2-3	Spin-spin
Solvent	DMF+DMSO (also all DMSO containing solvents or DMSO, DMSO+GBL)	DMF+DMSO (also DMSO & DMSO+GBL)	DMSO+GBL (for HI ≤ 0.05)	DMF+others
Anti-solvent	Diethyl ether, chlorobenzene	Toluene (also chlorobenzene)	toluene	Without anti-solvent (also chlorobenzene)
ETL	PCBM+C60	PCBM+C60	PCBM	PCBM+C60
ETL second layer/interlayer	BCP	ZnO (also PEI & BCP)	BCP	BCP
HTL	PTAA	doped-PEDOT:PSS (or HTL free)	NiOx	PTAA (also NiO _x)
HTL-2	Not applicable	present	--	--
Back contact	Ag, Al	Ag (also Al and Cu)	--	Cu, Al

REFERENCES

1. “NREL Best Research-Cell Efficiencies Chart.”, <https://www.nrel.gov/pv/assets/pdfs/pv-efficiency-chart.20181221.pdf>, accessed at December 2018.
2. B. Chen, M. Yang, S. Priya, and K. Zhu, “Origin of J-V Hysteresis in Perovskite Solar Cells,” *J. Phys. Chem. Lett.*, vol. 7, no. 5, pp. 905–917, March 2016.
3. G. Grancini *et al.*, “One-Year stable perovskite solar cells by 2D/3D interface engineering,” *Nat. Commun.*, vol. 8, p. 15684, June 2017.
4. Y. Wu *et al.*, “Perovskite solar cells with 18.21% efficiency and area over 1 cm² fabricated by heterojunction engineering,” *Nat. Energy*, vol. 1, no. 11, p. 16148, November 2016.
5. J. Luo *et al.*, “Toward high-efficiency, hysteresis-less, stable perovskite solar cells: Unusual doping of a hole-transporting material using a fluorine-containing hydrophobic Lewis acid,” *Energy Environ. Sci.*, vol. 11, no. 8, pp. 2035–2045, August 2018.
6. T. Salim, S. Sun, Y. Abe, A. Krishna, A. C. Grimsdale, and Y. M. Lam, “Perovskite-based solar cells: impact of morphology and device architecture on device performance,” *J. Mater. Chem. A*, vol. 3, no. 17, pp. 8943–8969, April 2015.
7. M. Saliba, M. Stollerfoht, C. M. Wolff, D. Neher, and A. Abate, “Measuring Aging Stability of Perovskite Solar Cells,” *Joule*, vol. 2, no. 6. Cell Press, pp. 1019–1024, June 2018.
8. A. Kojima, K. Teshima, T. Miyasaka, and Y. Shirai, “Novel Photoelectrochemical Cell with Mesoscopic Electrodes Sensitized by Lead-Halide Compounds (2),” *Meet. Abstr.*, vol. MA2006-02, no. 7, pp. 397–397, June 2006.
9. A. Kojima, K. Teshima, Y. Shirai, and T. Miyasaka, “Novel Photoelectrochemical

- Cell with Mesoscopic Electrodes Sensitized by Lead-halide Compounds (5),” *Meet. Abstr.*, vol. MA2007-02, no. 8, pp. 352–352, September 2007.
10. J. H. Im, C. R. Lee, J. W. Lee, S. W. Park, and N. G. Park, “6.5% efficient perovskite quantum-dot-sensitized solar cell,” *Nanoscale*, vol. 3, no. 10, pp. 4088–4093, October 2011.
 11. H.S. Kim *et al.*, “Lead iodide perovskite sensitized all-solid-state submicron thin film mesoscopic solar cell with efficiency exceeding 9%,” *Sci. Rep.*, vol. 2, p. 591, 2012.
 12. M. M. Lee, J. Teuscher, T. Miyasaka, T. N. Murakami, and H. J. Snaith, “Efficient hybrid solar cells based on meso-superstructured organometal halide perovskites,” *Science (80-.)*, vol. 338, no. 6107, pp. 643–647, November 2012.
 13. J. Burschka *et al.*, “Sequential deposition as a route to high-performance perovskite-sensitized solar cells,” *Nature*, vol. 499, no. 7458, pp. 316–319, July 2013.
 14. M. Liu, M. B. Johnston, and H. J. Snaith, “Efficient planar heterojunction perovskite solar cells by vapour deposition,” *Nature*, vol. 501, no. 7467, pp. 395–398, September 2013.
 15. N. J. Jeon, J. H. Noh, Y. C. Kim, W. S. Yang, S. Ryu, and S. Il Seok, “Solvent engineering for high-performance inorganic-organic hybrid perovskite solar cells,” *Nat. Mater.*, vol. 13, no. 9, pp. 897–903, September 2014.
 16. H. Zhou *et al.*, “Interface engineering of highly efficient perovskite solar cells,” *Science (80-.)*, vol. 345, no. 6196, pp. 542–546, 2014.
 17. E. Zimmermann *et al.*, “Characterization of perovskite solar cells: Towards a reliable measurement protocol,” *APL Mater.*, vol. 4, no. 9, p. 091901, September 2016.
 18. W. S. Yang *et al.*, “High-performance photovoltaic perovskite layers fabricated through intramolecular exchange,” *Science (80-.)*, vol. 348, no. 6240, pp. 1234–

1237, June 2015.

19. M. Saliba *et al.*, “Cesium-containing triple cation perovskite solar cells: improved stability, reproducibility and high efficiency,” *Energy Environ. Sci.*, vol. 9, no. 6, pp. 1989–1997, June 2016.
20. W. S. Yang *et al.*, “Iodide management in formamidinium-lead-halide-based perovskite layers for efficient solar cells,” *Science*, vol. 356, no. 6345, pp. 1376–1379, June 2017.
21. N. J. Jeon *et al.*, “A fluorene-terminated hole-transporting material for highly efficient and stable perovskite solar cells,” *Nat. Energy*, vol. 3, no. 8, pp. 682–689, August 2018.
22. L. Meng, J. You, T.-F. Guo, and Y. Yang, “Recent Advances in the Inverted Planar Structure of Perovskite Solar Cells,” *Acc. Chem. Res.*, vol. 49, no. 1, pp. 155–165, January 2016.
23. J. Y. Jeng *et al.*, “CH₃NH₃PbI₃ perovskite/fullerene planar-heterojunction hybrid solar cells,” *Adv. Mater.*, vol. 25, no. 27, pp. 3727–3732, July 2013.
24. P.-W. Liang *et al.*, “Additive Enhanced Crystallization of Solution-Processed Perovskite for Highly Efficient Planar-Heterojunction Solar Cells,” *Adv. Mater.*, vol. 26, no. 22, pp. 3748–3754, June 2014.
25. Z. Xiao *et al.*, “Efficient, high yield perovskite photovoltaic devices grown by interdiffusion of solution-processed precursor stacking layers,” *Energy Environ. Sci.*, vol. 7, no. 8, pp. 2619–2623, July 2014.
26. C.-H. Chiang, Z.-L. Tseng, and C.-G. Wu, “Planar heterojunction perovskite/PC₇₁ BM solar cells with enhanced open-circuit voltage via a (2/1)-step spin-coating process,” *J. Mater. Chem. A*, vol. 2, no. 38, pp. 15897–15903, September 2014.
27. W. Nie *et al.*, “High-efficiency solution-processed perovskite solar cells with

- millimeter-scale grains,” *Science*, vol. 347, no. 6221, pp. 522–5, January 2015.
28. C. Bi, Q. Wang, Y. Shao, Y. Yuan, Z. Xiao, and J. Huang, “Non-wetting surface-driven high-aspect-ratio crystalline grain growth for efficient hybrid perovskite solar cells,” *Nat. Commun.*, vol. 6, no. 1, p. 7747, December 2015.
 29. Z. Zhu, Y. Bai, X. Liu, C. C. Chueh, S. Yang, and A. K.-Y. Jen, “Enhanced Efficiency and Stability of Inverted Perovskite Solar Cells Using Highly Crystalline SnO₂ Nanocrystals as the Robust Electron-Transporting Layer,” *Adv. Mater.*, vol. 28, no. 30, pp. 6478–6484, August 2016.
 30. H. Rao *et al.*, “Solution-Processed CuS NPs as an Inorganic Hole-Selective Contact Material for Inverted Planar Perovskite Solar Cells,” *ACS Appl. Mater. Interfaces*, vol. 8, no. 12, pp. 7800–7805, March 2016.
 31. D. Luo *et al.*, “Dual-Source Precursor Approach for Highly Efficient Inverted Planar Heterojunction Perovskite Solar Cells,” *Adv. Mater.*, vol. 29, no. 19, p. 1604758, May 2017.
 32. D. Luo *et al.*, “Enhanced photovoltage for inverted planar heterojunction perovskite solar cells,” *Science*, vol. 360, no. 6396, pp. 1442–1446, June 2018.
 33. N. G. Park, “Organometal perovskite light absorbers toward a 20% efficiency low-cost solid-state mesoscopic solar cell,” *J. Phys. Chem. Lett.*, vol. 4, no. 15, pp. 2423–2429, August 2013.
 34. S. D. Stranks *et al.*, “Electron-hole diffusion lengths exceeding 1 micrometer in an organometal trihalide perovskite absorber,” *Science* (80-.), vol. 342, no. 6156, pp. 341–344, October 2013.
 35. A. T. Barrows, A. J. Pearson, C. K. Kwak, A. D. F. Dunbar, A. R. Buckley, and D. G. Lidzey, “Efficient planar heterojunction mixed-halide perovskite solar cells deposited via spray-deposition,” *Energy Environ. Sci.*, vol. 7, no. 9, pp. 2944–2950,

August 2014.

36. P. Docampo *et al.*, “Solution deposition-conversion for planar heterojunction mixed halide perovskite solar cells,” *Adv. Energy Mater.*, vol. 4, no. 14, p. 1400355, October 2014.
37. J. Qing *et al.*, “Chlorine Incorporation for Enhanced Performance of Planar Perovskite Solar Cell Based on Lead Acetate Precursor,” *ACS Appl. Mater. Interfaces*, vol. 7, no. 41, pp. 23110–23116, October 2015.
38. K. H. Stone *et al.*, “Transformation from crystalline precursor to perovskite in PbCl₂-derived MAPbI₃” *Nat. Commun.*, vol. 9, no. 1, p. 3458, December 2018.
39. S. Pang *et al.*, “NH₂CH=NH₂PbI₃: An alternative organolead iodide perovskite sensitizer for mesoscopic solar cells,” *Chem. Mater.*, vol. 26, no. 3, pp. 1485–1491, February 2014.
40. G. E. Eperon, S. D. Stranks, C. Menelaou, M. B. Johnston, L. M. Herz, and H. J. Snaith, “Formamidinium lead trihalide: a broadly tunable perovskite for efficient planar heterojunction solar cells,” *Energy Environ. Sci.*, vol. 7, no. 3, p. 982, February 2014.
41. F. Wang, H. Yu, H. Xu, and N. Zhao, “HPbI₃: A new precursor compound for highly efficient solution-processed perovskite solar cells,” *Adv. Funct. Mater.*, vol. 25, no. 7, pp. 1120–1126, February 2015.
42. N. Pellet *et al.*, “Mixed-organic-cation perovskite photovoltaics for enhanced solar-light harvesting,” *Angew. Chemie - Int. Ed.*, vol. 53, no. 12, pp. 3151–3157, March 2014.
43. N. J. Jeon *et al.*, “Compositional engineering of perovskite materials for high-performance solar cells,” *Nature*, vol. 517, no. 7535, pp. 476–480, January 2015.
44. M. Kulbak *et al.*, “Cesium Enhances Long-Term Stability of Lead Bromide

- Perovskite-Based Solar Cells,” *J. Phys. Chem. Lett.*, vol. 7, no. 1, pp. 167–172, January 2016.
45. X. Chang *et al.*, “Carbon-Based CsPbBr₃ Perovskite Solar Cells: All-Ambient Processes and High Thermal Stability,” *ACS Appl. Mater. Interfaces*, vol. 8, no. 49, pp. 33649–33655, December 2016.
 46. A. Swarnkar *et al.*, “Quantum dot-induced phase stabilization of α -CsPbI₃ perovskite for high-efficiency photovoltaics,” *Science (80-.)*, vol. 354, no. 6308, pp. 92–95, October 2016.
 47. H. Choi *et al.*, “Cesium-doped methylammonium lead iodide perovskite light absorber for hybrid solar cells,” *Nano Energy*, vol. 7, pp. 80–85, July 2014.
 48. J. W. Lee, D. H. Kim, H. S. Kim, S. W. Seo, S. M. Cho, and N. G. Park, “Formamidinium and cesium hybridization for photo- and moisture-stable perovskite solar cell,” *Adv. Energy Mater.*, vol. 5, no. 20, p. 1501310, October 2015.
 49. G. Niu, H. Yu, J. Li, D. Wang, and L. Wang, “Controlled orientation of perovskite films through mixed cations toward high performance perovskite solar cells,” *Nano Energy*, vol. 27, pp. 87–94, September 2016.
 50. R. Zhang *et al.*, “Theoretical lifetime extraction and experimental demonstration of stable cesium-containing tri-cation perovskite solar cells with high efficiency,” *Electrochim. Acta*, vol. 265, pp. 98–106, March 2018.
 51. D. P. McMeekin *et al.*, “A mixed-cation lead mixed-halide perovskite absorber for tandem solar cells,” *Science (80-.)*, vol. 351, no. 6269, pp. 151–155, January 2016.
 52. F. Ye, W. Yang, D. Luo, R. Zhu, and Q. Gong, “Applications of cesium in the perovskite solar cells,” *J. Semicond.*, vol. 38, no. 1, p. 011003, January 2017.
 53. Y. Sheng *et al.*, “Mixed (5-AVA)_xMA_{1-x}PbI_{3-y}(BF₄)_yperovskites enhance the

- photovoltaic performance of hole-conductor-free printable mesoscopic solar cells,” *J. Mater. Chem. A*, vol. 6, no. 5, pp. 2360–2364, January 2018.
54. B.-E. Cohen, M. Wierzbowska, and L. Etgar, “High Efficiency and High Open Circuit Voltage in Quasi 2D Perovskite Based Solar Cells,” *Adv. Funct. Mater.*, vol. 27, no. 5, p. 1604733, February 2017.
 55. S. Yang, W. Fu, Z. Zhang, H. Chen, and C. Z. Li, “Recent advances in perovskite solar cells: Efficiency, stability and lead-free perovskite,” *Journal of Materials Chemistry A*, vol. 5, no. 23. The Royal Society of Chemistry, pp. 11462–11482, 13-June 2017.
 56. M. Konstantakou and T. Stergiopoulos, “A critical review on tin halide perovskite solar cells,” *J. Mater. Chem. A*, vol. 5, no. 23, pp. 11518–11549, June 2017.
 57. F. Hao, C. C. Stoumpos, R. P. H. Chang, and M. G. Kanatzidis, “Anomalous band gap behavior in mixed Sn and Pb perovskites enables broadening of absorption spectrum in solar cells,” *J. Am. Chem. Soc.*, vol. 136, no. 22, pp. 8094–8099, June 2014.
 58. B. W. Park, B. Philippe, X. Zhang, H. Rensmo, G. Boschloo, and E. M. J. Johansson, “Bismuth Based Hybrid Perovskites $A_3Bi_2I_9$ (A: Methylammonium or Cesium) for Solar Cell Application,” *Adv. Mater.*, vol. 27, no. 43, pp. 6806–6813, November 2015.
 59. P. P. Sun, Q. S. Li, L. N. Yang, and Z. S. Li, “Theoretical insights into a potential lead-free hybrid perovskite: Substituting Pb^{2+} with Ge^{2+} ,” *Nanoscale*, vol. 8, no. 3, pp. 1503–1512, January 2016.
 60. Z. Shi and A. H. Jayatissa, “Perovskites-based solar cells: A review of recent progress, materials and processing methods,” *Materials*, vol. 11, no. 5. Multidisciplinary Digital Publishing Institute (MDPI), May 2018.
 61. J. I. Uribe, D. Ramirez, J. M. Osorio-Guillén, J. Osorio, and F. Jaramillo,

- “CH₃NH₃CaI₃ perovskite: Synthesis, characterization, and first-principles studies,” *J. Phys. Chem. C*, vol. 120, no. 30, pp. 16393–16398, August 2016.
62. D. Bi *et al.*, “Using a two-step deposition technique to prepare perovskite (CH₃NH₃PbI₃) for thin film solar cells based on ZrO₂ and TiO₂ mesostructures,” *RSC Adv.*, vol. 3, no. 41, p. 18762, September 2013.
63. H. Shen *et al.*, “Improved Reproducibility for Perovskite Solar Cells with 1 cm² Active Area by a Modified Two-Step Process,” *ACS Appl. Mater. Interfaces*, vol. 9, no. 7, pp. 5974–5981, February 2017.
64. N.-G. Park, “Methodologies for high efficiency perovskite solar cells,” *Nano Converg.*, vol. 3, no. 1, p. 15, December 2016.
65. H.-B. Kim *et al.*, “Mixed solvents for the optimization of morphology in solution-processed, inverted-type perovskite/fullerene hybrid solar cells,” *Nanoscale*, vol. 6, no. 12, p. 6679, May 2014.
66. N. Ahn, D. Y. Son, I. H. Jang, S. M. Kang, M. Choi, and N. G. Park, “Highly Reproducible Perovskite Solar Cells with Average Efficiency of 18.3% and Best Efficiency of 19.7% Fabricated via Lewis Base Adduct of Lead(II) Iodide,” *J. Am. Chem. Soc.*, vol. 137, no. 27, pp. 8696–8699, July 2015.
67. S. S. Mali, C. S. Shim, and C. K. Hong, “Highly porous Zinc Stannate (Zn₂SnO₄) nanofibers scaffold photoelectrodes for efficient methyl ammonium halide perovskite solar cells,” *Sci. Rep.*, vol. 5, no. 1, p. 11424, September 2015.
68. Y. Li *et al.*, “Mesoporous SnO₂ nanoparticle films as electron-transporting material in perovskite solar cells,” *RSC Adv.*, vol. 5, no. 36, pp. 28424–28429, March 2015.
69. J. Kim *et al.*, “Nucleation and Growth Control of HC(NH₂)₂PbI₃ for Planar Perovskite Solar Cell,” *J. Phys. Chem. C*, vol. 120, no. 20, pp. 11262–11267, May 2016.

70. W. Ke *et al.*, “Employing Lead Thiocyanate Additive to Reduce the Hysteresis and Boost the Fill Factor of Planar Perovskite Solar Cells,” *Adv. Mater.*, vol. 28, no. 26, pp. 5214–5221, July 2016.
71. M. Xiao *et al.*, “A Fast Deposition-Crystallization Procedure for Highly Efficient Lead Iodide Perovskite Thin-Film Solar Cells,” *Angew. Chemie*, vol. 126, no. 37, pp. 10056–10061, September 2014.
72. J. W. Jung, S. T. Williams, and A. K.-Y. Jen, “Low-temperature processed high-performance flexible perovskite solar cells via rationally optimized solvent washing treatments,” *RSC Adv.*, vol. 4, no. 108, pp. 62971–62977, November 2014.
73. J. Ye *et al.*, “Effective and reproducible method for preparing low defects perovskite film toward highly photoelectric properties with large fill factor by shaping capping layer,” *Sol. Energy*, vol. 136, pp. 505–514, October 2016.
74. M. Saliba *et al.*, “Influence of thermal processing protocol upon the crystallization and photovoltaic performance of organic-inorganic lead trihalide perovskites,” *J. Phys. Chem. C*, vol. 118, no. 30, pp. 17171–17177, July 2014.
75. S. Aharon, A. Dymshits, A. Rotem, and L. Etgar, “Temperature dependence of hole conductor free formamidinium lead iodide perovskite based solar cells,” *J. Mater. Chem. A*, vol. 3, no. 17, pp. 9171–9178, April 2015.
76. D. Khatiwada *et al.*, “Efficient Perovskite Solar Cells by Temperature Control in Single and Mixed Halide Precursor Solutions and Films,” *J. Phys. Chem. C*, vol. 119, no. 46, pp. 25747–25753, November 2015.
77. H. M. Cronin, K. D. G. I. Jayawardena, Z. Stoeva, M. Shkunov, and S. R. P. Silva, “Effects of ambient humidity on the optimum annealing time of mixed-halide Perovskite solar cells,” *Nanotechnology*, vol. 28, no. 11, p. 114004, March 2017.
78. T. Su, X. Li, Y. Zhang, F. Zhang, and Z. Sheng, “Temperature-modulated crystal

- growth and performance for highly reproducible and efficient perovskite solar cells,” *Phys. Chem. Chem. Phys.*, vol. 19, no. 20, pp. 13147–13152, May 2017.
79. T. Bin Song *et al.*, “Unraveling film transformations and device performance of planar perovskite solar cells,” *Nano Energy*, vol. 12, pp. 494–500, March 2015.
 80. Y. Z. Zheng *et al.*, “Effects of precursor concentration and annealing temperature on CH₃NH₃PbI₃ film crystallization and photovoltaic performance,” *J. Phys. Chem. Solids*, vol. 107, pp. 55–61, August 2017.
 81. L. C. Chen, C. C. Chen, J. C. Chen, and C. G. Wu, “Annealing effects on high-performance CH₃NH₃PbI₃ perovskite solar cells prepared by solution-process,” *Sol. Energy*, vol. 122, pp. 1047–1051, December 2015.
 82. J. You *et al.*, “Moisture assisted perovskite film growth for high performance solar cells,” *Appl. Phys. Lett.*, vol. 105, no. 18, p. 183902, November 2014.
 83. M. K. Gangishetty, R. W. J. Scott, and T. L. Kelly, “Effect of relative humidity on crystal growth, device performance and hysteresis in planar heterojunction perovskite solar cells,” *Nanoscale*, vol. 8, no. 12, pp. 6300–6307, March 2016.
 84. S. R. Raga, M. C. Jung, M. V. Lee, M. R. Leyden, Y. Kato, and Y. Qi, “Influence of air annealing on high efficiency planar structure perovskite solar cells,” *Chem. Mater.*, vol. 27, no. 5, pp. 1597–1603, March 2015.
 85. G. E. Eperon *et al.*, “The Importance of Moisture in Hybrid Lead Halide Perovskite Thin Film Fabrication,” *ACS Nano*, vol. 9, no. 9, pp. 9380–9393, September 2015.
 86. A. Dualeh, N. Tétreault, T. Moehl, P. Gao, M. K. Nazeeruddin, and M. Grätzel, “Effect of annealing temperature on film morphology of organic-inorganic hybrid perovskite solid-state solar cells,” *Adv. Funct. Mater.*, vol. 24, no. 21, pp. 3250–3258, June 2014.
 87. M. Kim *et al.*, “High-Temperature-Short-Time Annealing Process for High-

- Performance Large-Area Perovskite Solar Cells,” *ACS Nano*, vol. 11, no. 6, pp. 6057–6064, June 2017.
88. X. Cao *et al.*, “High annealing temperature induced rapid grain coarsening for efficient perovskite solar cells,” *J. Colloid Interface Sci.*, vol. 524, pp. 483–489, August 2018.
 89. H. S. Kim *et al.*, “Mechanism of carrier accumulation in perovskite thin-absorber solar cells,” *Nat. Commun.*, vol. 4, no. 1, p. 2242, December 2013.
 90. J. M. Ball, M. M. Lee, A. Hey, and H. J. Snaith, “Low-temperature processed meso-structured to thin-film perovskite solar cells,” *Energy Environ. Sci.*, vol. 6, no. 6, p. 1739, May 2013.
 91. U. K. Thakur, A. M. Askar, R. Kisslinger, B. D. Wiltshire, P. Kar, and K. Shankar, “Halide perovskite solar cells using monocryalline TiO₂nanorod arrays as electron transport layers: Impact of nanorod morphology,” *Nanotechnology*, vol. 28, no. 27, p. 274001, July 2017.
 92. S. K. Pathak *et al.*, “Performance and Stability Enhancement of Dye-Sensitized and Perovskite Solar Cells by Al Doping of TiO₂,” *Adv. Funct. Mater.*, vol. 24, no. 38, pp. 6046–6055, October 2014.
 93. K. Manseki, T. Ikeya, A. Tamura, T. Ban, T. Sugiura, and T. Yoshida, “Mg-doped TiO₂ nanorods improving open-circuit voltages of ammonium lead halide perovskite solar cells,” *RSC Adv.*, vol. 4, no. 19, pp. 9652–9655, February 2014.
 94. G. S. Han *et al.*, “Reduced Graphene Oxide/Mesoporous TiO₂Nanocomposite Based Perovskite Solar Cells,” *ACS Appl. Mater. Interfaces*, vol. 7, no. 42, pp. 23521–23526, October 2015.
 95. A. Bera, K. Wu, A. Sheikh, E. Alarousu, O. F. Mohammed, and T. Wu, “Perovskite oxide SrTiO₃as an efficient electron transporter for hybrid perovskite solar cells,” *J.*

- Phys. Chem. C*, vol. 118, no. 49, pp. 28494–28501, December 2014.
96. A. Bera *et al.*, “Fast Crystallization and Improved Stability of Perovskite Solar Cells with Zn₂SnO₄ Electron Transporting Layer: Interface Matters,” *ACS Appl. Mater. Interfaces*, vol. 7, no. 51, pp. 12404–12411, December 2015.
 97. X. Yu *et al.*, “Enhanced photovoltaic performance of perovskite solar cells with mesoporous SiO₂scaffolds,” *J. Power Sources*, vol. 325, pp. 534–540, September 2016.
 98. P. Qin *et al.*, “Yttrium-substituted nanocrystalline TiO₂ photoanodes for perovskite based heterojunction solar cells,” *Nanoscale*, vol. 6, no. 3, pp. 1508–1514, January 2014.
 99. H. Nagaoka *et al.*, “Zr incorporation into TiO₂electrodes reduces hysteresis and improves performance in hybrid perovskite solar cells while increasing carrier lifetimes,” *J. Phys. Chem. Lett.*, vol. 6, no. 4, pp. 669–675, February 2015.
 100. I. Jeong *et al.*, “A tailored TiO₂electron selective layer for high-performance flexible perovskite solar cells via low temperature UV process,” *Nano Energy*, vol. 28, pp. 380–389, October 2016.
 101. L. Zuo *et al.*, “Enhanced Photovoltaic Performance of CH₃NH₃PbI₃ Perovskite Solar Cells through Interfacial Engineering Using Self-Assembling Monolayer,” *J. Am. Chem. Soc.*, vol. 137, no. 7, pp. 2674–2679, February 2015.
 102. K. Wojciechowski *et al.*, “C₆₀ as an efficient n-type compact layer in perovskite solar cells,” *J. Phys. Chem. Lett.*, vol. 6, no. 12, pp. 2399–2405, June 2015.
 103. H. Yoon, S. M. Kang, J. K. Lee, and M. Choi, “Hysteresis-free low-temperature-processed planar perovskite solar cells with 19.1% efficiency,” *Energy Environ. Sci.*, vol. 9, no. 7, pp. 2262–2266, July 2016.
 104. S. L. Fernandes *et al.*, “Nb₂O₅ hole blocking layer for hysteresis-free perovskite solar

- cells,” *Mater. Lett.*, vol. 181, pp. 103–107, October 2016.
105. J. Liu *et al.*, “Low-temperature, solution processed metal sulfide as an electron transport layer for efficient planar perovskite solar cells,” *J. Mater. Chem. A*, vol. 3, no. 22, pp. 11750–11755, May 2015.
 106. K. Wang *et al.*, “Low-temperature and solution-processed amorphous WO_x as electron-selective layer for perovskite solar cells,” *J. Phys. Chem. Lett.*, vol. 6, no. 5, pp. 755–759, March 2015.
 107. W. Ke *et al.*, “Cooperative tin oxide fullerene electron selective layers for high-performance planar perovskite solar cells,” *J. Mater. Chem. A*, vol. 4, no. 37, pp. 14276–14283, September 2016.
 108. W. Ke *et al.*, “Efficient hole-blocking layer-free planar halide perovskite thin-film solar cells,” *Nat. Commun.*, vol. 6, no. 1, p. 6700, December 2015.
 109. F. Xia *et al.*, “Efficiency Enhancement of Inverted Structure Perovskite Solar Cells via Oleamide Doping of PCBM Electron Transport Layer,” *ACS Appl. Mater. Interfaces*, vol. 7, no. 24, pp. 13659–13665, June 2015.
 110. G. Kakavelakis *et al.*, “Efficient and Highly Air Stable Planar Inverted Perovskite Solar Cells with Reduced Graphene Oxide Doped PCBM Electron Transporting Layer,” *Adv. Energy Mater.*, vol. 7, no. 7, p. 1602120, April 2017.
 111. Y. Bai *et al.*, “High performance inverted structure perovskite solar cells based on a PCBM: Polystyrene blend electron transport layer,” *J. Mater. Chem. A*, vol. 3, no. 17, pp. 9098–9102, April 2015.
 112. P.-W. Liang, C.-C. Chueh, S. T. Williams, and A. K.-Y. Jen, “Roles of Fullerene-Based Interlayers in Enhancing the Performance of Organometal Perovskite Thin-Film Solar Cells,” *Adv. Energy Mater.*, vol. 5, no. 10, p. 1402321, May 2015.
 113. Q. Wang, Y. Shao, Q. Dong, Z. Xiao, Y. Yuan, and J. Huang, “Large fill-factor bilayer

- iodine perovskite solar cells fabricated by a low-temperature solution-process,” *Energy Environ. Sci.*, vol. 7, no. 7, pp. 2359–2365, June 2014.
114. O. Malinkiewicz *et al.*, “Metal-Oxide-Free Methylammonium Lead Iodide Perovskite-Based Solar Cells: The Influence of Organic Charge Transport Layers,” *Adv. Energy Mater.*, vol. 4, no. 15, p. 1400345, October 2014.
 115. P. Y. Gu *et al.*, “An Azaacene Derivative as Promising Electron-Transport Layer for Inverted Perovskite Solar Cells,” *Chem. - An Asian J.*, vol. 11, no. 15, pp. 2135–2138, August 2016.
 116. P. Y. Gu *et al.*, “Pushing up the efficiency of planar perovskite solar cells to 18.2% with organic small molecules as the electron transport layer,” *J. Mater. Chem. A*, vol. 5, no. 16, pp. 7339–7344, April 2017.
 117. A. Kojima, K. Teshima, Y. Shirai, and T. Miyasaka, “Organometal Halide Perovskites as Visible-Light Sensitizers for Photovoltaic Cells,” *J. Am. Chem. Soc.*, vol. 131, no. 17, pp. 6050–6051, 2009.
 118. H. Xi *et al.*, “Performance Enhancement of Planar Heterojunction Perovskite Solar Cells through Tuning the Doping Properties of Hole-Transporting Materials,” *ACS Omega*, vol. 2, no. 1, pp. 326–336, January 2017.
 119. J. Burschka *et al.*, “Tris(2-(1 H -pyrazol-1-yl)pyridine)cobalt(III) as p-type dopant for organic semiconductors and its application in highly efficient solid-state dye-sensitized solar cells,” *J. Am. Chem. Soc.*, vol. 133, no. 45, pp. 18042–18045, November 2011.
 120. J. Burschka, F. Kessler, M. K. Nazeeruddin, and M. Grätzel, “Co(III) Complexes as p-Dopants in Solid-State Dye-Sensitized Solar Cells,” *Chem. Mater.*, vol. 25, no. 15, pp. 2986–2990, August 2013.
 121. J. H. Noh, N. J. Jeon, Y. C. Choi, M. K. Nazeeruddin, M. Grätzel, and S. Il Seok,

- “Nanostructured TiO₂/CH₃NH₃PbI₃ heterojunction solar cells employing spiro-OMeTAD/Co-complex as hole-transporting material,” *J. Mater. Chem. A*, vol. 1, no. 38, p. 11842, September 2013.
122. T. M. Koh *et al.*, “Cobalt dopant with deep redox potential for organometal halide hybrid solar cells,” *ChemSusChem*, vol. 7, no. 7, pp. 1909–1914, July 2014.
 123. L. Badia, E. Mas-Marzá, R. S. Sánchez, E. M. Barea, J. Bisquert, and I. Mora-Seró, “New iridium complex as additive to the spiro-OMeTAD in perovskite solar cells with enhanced stability,” *APL Mater.*, vol. 2, no. 8, p. 081507, August 2014.
 124. C. Chen *et al.*, “Cu(II) Complexes as p-Type Dopants in Efficient Perovskite Solar Cells,” *ACS Energy Lett.*, vol. 2, no. 2, pp. 497–503, February 2017.
 125. N. J. Jeon *et al.*, “O-methoxy substituents in spiro-OMeTAD for efficient inorganic-organic hybrid perovskite solar cells,” *J. Am. Chem. Soc.*, vol. 136, no. 22, pp. 7837–7840, June 2014.
 126. N. J. Jeon, J. Lee, J. H. Noh, M. K. Nazeeruddin, M. Grätzel, and S. Il Seok, “Efficient inorganic-organic hybrid perovskite solar cells based on pyrene arylamine derivatives as hole-transporting materials,” *J. Am. Chem. Soc.*, vol. 135, no. 51, pp. 19087–19090, December 2013.
 127. A. Krishna *et al.*, “Novel hole transporting materials based on triptycene core for high efficiency mesoscopic perovskite solar cells,” *Chem. Sci.*, vol. 5, no. 7, pp. 2702–2709, May 2014.
 128. F. Di Giacomo *et al.*, “High efficiency CH₃NH₃PbI(3-x)Cl_x perovskite solar cells with poly(3-hexylthiophene) hole transport layer,” *J. Power Sources*, vol. 251, pp. 152–156, April 2014.
 129. H. Choi, S. Park, S. Paek, P. Ekanayake, M. K. Nazeeruddin, and J. Ko, “Efficient star-shaped hole transporting materials with diphenylethenyl side arms for an efficient

- perovskite solar cell,” *J. Mater. Chem. A*, vol. 2, no. 45, pp. 19136–19140, September 2014.
130. H. Choi, S. Paek, N. Lim, Y. H. Lee, M. K. Nazeeruddin, and J. Ko, “Efficient perovskite solar cells with 13.63 % efficiency based on planar triphenylamine hole conductors,” *Chem. - A Eur. J.*, vol. 20, no. 35, pp. 10894–10899, August 2014.
 131. B. Conings, L. Baeten, C. De Dobbelaere, J. D’Haen, J. Manca, and H. G. Boyen, “Perovskite-based hybrid solar cells exceeding 10% efficiency with high reproducibility using a thin film sandwich approach,” *Adv. Mater.*, vol. 26, no. 13, pp. 2041–2046, April 2014.
 132. Y. Guo, C. Liu, K. Inoue, K. Harano, H. Tanaka, and E. Nakamura, “Enhancement in the efficiency of an organic-inorganic hybrid solar cell with a doped P3HT hole-transporting layer on a void-free perovskite active layer,” *J. Mater. Chem. A*, vol. 2, no. 34, pp. 13827–13830, August 2014.
 133. J. Y. Wang, F. C. Hsu, J. Y. Huang, L. Wang, and Y. F. Chen, “Bifunctional Polymer Nanocomposites as Hole-Transport Layers for Efficient Light Harvesting: Application to Perovskite Solar Cells,” *ACS Appl. Mater. Interfaces*, vol. 7, no. 50, pp. 27676–27684, December 2015.
 134. Y. Zhang, M. Elawad, Z. Yu, X. Jiang, J. Lai, and L. Sun, “Enhanced performance of perovskite solar cells with P3HT hole-transporting materials: Via molecular p-type doping,” *RSC Adv.*, vol. 6, no. 110, pp. 108888–108895, November 2016.
 135. P. Vivo, J. Salunke, A. Priimagi, P. Vivo, J. K. Salunke, and A. Priimagi, “Hole-Transporting Materials for Printable Perovskite Solar Cells,” *Materials (Basel)*, vol. 10, no. 9, p. 1087, September 2017.
 136. J. Liu *et al.*, “Employing PEDOT as the p-type charge collection layer in regular organic-inorganic perovskite solar cells,” *J. Phys. Chem. Lett.*, vol. 6, no. 9, pp. 1666–1673, May 2015.

137. X. Jiang *et al.*, “High-Performance Regular Perovskite Solar Cells Employing Low-Cost Poly(ethylenedioxythiophene) as a Hole-Transporting Material,” *Sci. Rep.*, vol. 7, no. 1, p. 42564, December 2017.
138. Y. S. Kwon, J. Lim, H. J. Yun, Y. H. Kim, and T. Park, “A diketopyrrolopyrrole-containing hole transporting conjugated polymer for use in efficient stable organic-inorganic hybrid solar cells based on a perovskite,” *Energy Environ. Sci.*, vol. 7, no. 4, pp. 1454–1460, March 2014.
139. L. Zheng *et al.*, “A hydrophobic hole transporting oligothiophene for planar perovskite solar cells with improved stability,” *Chem. Commun.*, vol. 50, no. 76, pp. 11196–11199, August 2014.
140. Z. Zhu *et al.*, “Polyfluorene derivatives are high-performance organic hole-transporting materials for inorganic-organic hybrid perovskite solar cells,” *Adv. Funct. Mater.*, vol. 24, no. 46, pp. 7357–7365, December 2014.
141. J. Xiao *et al.*, “A thin pristine non-triarylamine hole-transporting material layer for efficient CH₃NH₃PbI₃ perovskite solar cells,” *RSC Adv.*, vol. 4, no. 62, pp. 32918–32923, July 2014.
142. G. A. Sepalage *et al.*, “Copper(I) Iodide as Hole-Conductor in Planar Perovskite Solar Cells: Probing the Origin of J-V Hysteresis,” *Adv. Funct. Mater.*, vol. 25, no. 35, pp. 5650–5661, September 2015.
143. X. Li *et al.*, “Synergistic Effect to High-Performance Perovskite Solar Cells with Reduced Hysteresis and Improved Stability by the Introduction of Na-Treated TiO₂ and Spraying-Deposited CuI as Transport Layers,” *ACS Appl. Mater. Interfaces*, vol. 9, no. 47, pp. 41354–41362, November 2017.
144. I. S. Yang *et al.*, “Formation of pristine CuSCN layer by spray deposition method for efficient perovskite solar cell with extended stability,” *Nano Energy*, vol. 32, pp. 414–

421, February 2017.

145. L. Etgar, "Hole-transport material-free perovskite-based solar cells," *MRS Bull.*, vol. 40, no. 08, pp. 674–680, August 2015.
146. L. Etgar *et al.*, "Mesoscopic CH₃NH₃PbI₃/TiO₂ Heterojunction Solar Cells," *J. Am. Chem. Soc.*, vol. 134, no. 42, pp. 17396–17399, October 2012.
147. X. Zhou *et al.*, "Hole-transport-material-free perovskite solar cells based on nanoporous gold back electrode," *RSC Adv.*, vol. 5, no. 72, pp. 58543–58548, July 2015.
148. Z. Wei, H. Chen, K. Yan, X. Zheng, and S. Yang, "Hysteresis-free multi-walled carbon nanotube-based perovskite solar cells with a high fill factor," *J. Mater. Chem. A*, vol. 3, no. 48, pp. 24226–24231, December 2015.
149. X. Zheng *et al.*, "Boron Doping of Multiwalled Carbon Nanotubes Significantly Enhances Hole Extraction in Carbon-Based Perovskite Solar Cells," *Nano Lett.*, vol. 17, no. 4, pp. 2496–2505, April 2017.
150. Y. Wang, H. Zhao, Y. Mei, H. Liu, S. Wang, and X. Li, "Carbon Nanotube Bridging Method for Hole Transport Layer-Free Paintable Carbon-Based Perovskite Solar Cells," *ACS Appl. Mater. Interfaces*, vol. 11, no. 1, pp. 916–923, January 2019.
151. P. Docampo, J. M. Ball, M. Darwich, G. E. Eperon, and H. J. Snaith, "Efficient organometal trihalide perovskite planar-heterojunction solar cells on flexible polymer substrates," *Nat. Commun.*, vol. 4, no. 1, p. 2761, December 2013.
152. J. H. Heo, H. J. Han, D. Kim, T. K. Ahn, and S. H. Im, "Hysteresis-less inverted CH₃NH₃PbI₃ planar perovskite hybrid solar cells with 18.1% power conversion efficiency," *Energy Environ. Sci.*, vol. 8, no. 5, pp. 1602–1608, May 2015.
153. K. G. Lim, H. B. Kim, J. Jeong, H. Kim, J. Y. Kim, and T. W. Lee, "Boosting the

- power conversion efficiency of perovskite solar cells using self-organized polymeric hole extraction layers with high work function,” *Adv. Mater.*, vol. 26, no. 37, pp. 6461–6466, October 2014.
154. Z. K. Wang, M. Li, D. X. Yuan, X. B. Shi, H. Ma, and L. S. Liao, “Improved hole interfacial layer for planar perovskite solar cells with efficiency exceeding 15%,” *ACS Appl. Mater. Interfaces*, vol. 7, no. 18, pp. 9645–9651, May 2015.
 155. M. Qian, M. Li, X.-B. Shi, H. Ma, Z.-K. Wang, and L.S. Liao, “Planar perovskite solar cells with 15.75% power conversion efficiency by cathode and anode interfacial modification,” *J. Mater. Chem. A*, vol. 3, no. 25, pp. 13533–13539, June 2015.
 156. J. Niu *et al.*, “Graphene-oxide doped PEDOT:PSS as a superior hole transport material for high-efficiency perovskite solar cell,” *Org. Electron. physics, Mater. Appl.*, vol. 48, pp. 165–171, September 2017.
 157. W. Yan *et al.*, “High-performance hybrid perovskite solar cells with open circuit voltage dependence on hole-transporting materials,” *Nano Energy*, vol. 16, pp. 428–437, September 2015.
 158. D. Zhao, M. Sexton, H.-Y. Park, G. Baure, J. C. Nino, and F. So, “High-Efficiency Solution-Processed Planar Perovskite Solar Cells with a Polymer Hole Transport Layer,” *Adv. Energy Mater.*, vol. 5, no. 6, p. 1401855, March 2015.
 159. Y. Ko, Y. Kim, C. Lee, Y. Kim, and Y. Jun, “Investigation of Hole-Transporting Poly(triarylamine) on Aggregation and Charge Transport for Hysteresisless Scalable Planar Perovskite Solar Cells,” *ACS Appl. Mater. Interfaces*, vol. 10, no. 14, pp. 11633–11641, April 2018.
 160. C. Xu, Z. Liu, and E.-C. Lee, “High-performance metal oxide-free inverted perovskite solar cells using poly(bis(4-phenyl)(2,4,6-trimethylphenyl)amine) as the hole transport layer,” *J. Mater. Chem. C*, vol. 6, no. 26, pp. 6975–6981, July 2018.
 161. L. Hu *et al.*, “Sequential Deposition of CH₃NH₃PbI₃ on Planar NiO Film for

- Efficient Planar Perovskite Solar Cells,” *ACS Photonics*, vol. 1, no. 7, pp. 547–553, July 2014.
162. J. H. Kim *et al.*, “High-performance and environmentally stable planar heterojunction perovskite solar cells based on a solution-processed copper-doped nickel oxide hole-transporting layer,” *Adv. Mater.*, vol. 27, no. 4, pp. 695–701, January 2015.
163. J. H. Park *et al.*, “Efficient CH₃NH₃PbI₃ Perovskite Solar Cells Employing Nanostructured p-Type NiO Electrode Formed by a Pulsed Laser Deposition,” *Adv. Mater.*, vol. 27, no. 27, pp. 4013–4019, July 2015.
164. W. Chen *et al.*, “Efficient and stable large-area perovskite solar cells with inorganic charge extraction layers,” *Science*, vol. 350, no. 6263, pp. 944–948, November 2015.
165. J. W. Jung, C.-C. Chueh, and A. K.-Y. Jen, “A Low-Temperature, Solution-Processable, Cu-Doped Nickel Oxide Hole-Transporting Layer via the Combustion Method for High-Performance Thin-Film Perovskite Solar Cells,” *Adv. Mater.*, vol. 27, no. 47, pp. 7874–7880, December 2015.
166. Y. Li *et al.*, “Hole-conductor-free planar perovskite solar cells with 16.0% efficiency,” *J. Mater. Chem. A*, vol. 3, no. 36, pp. 18389–18394, September 2015.
167. W.-Y. Chen *et al.*, “Low-cost solution-processed copper iodide as an alternative to PEDOT:PSS hole transport layer for efficient and stable inverted planar heterojunction perovskite solar cells,” *J. Mater. Chem. A*, vol. 3, no. 38, pp. 19353–19359, September 2015.
168. Z. Wu *et al.*, “Efficient planar heterojunction perovskite solar cells employing graphene oxide as hole conductor,” *Nanoscale*, vol. 6, no. 18, pp. 10505–10510, August 2014.
169. K.W. Tsai, C.-C. Chueh, S. T. Williams, T.-C. Wen, and A. K. Y. Jen, “High-performance hole-transporting layer-free conventional perovskite/fullerene

- heterojunction thin-film solar cells,” *J. Mater. Chem. A*, vol. 3, no. 17, pp. 9128–9132, April 2015.
170. F. Behrouznejad, S. Shahbazi, N. Taghavinia, H.-P. Wu, and E. Wei-Guang Diao, “A study on utilizing different metals as the back contact of $\text{CH}_3\text{NH}_3\text{PbI}_3$ perovskite solar cells,” *J. Mater. Chem. A*, vol. 4, no. 35, pp. 13488–13498, August 2016.
171. H. Zhou *et al.*, “Hole-conductor-free, metal-electrode-free $\text{TiO}_2/\text{CH}_3\text{NH}_3\text{PbI}_3$ heterojunction solar cells based on a low-temperature carbon electrode,” *J. Phys. Chem. Lett.*, vol. 5, no. 18, pp. 3241–3246, September 2014.
172. M. Hu, L. Liu, A. Mei, Y. Yang, T. Liu, and H. Han, “Efficient hole-conductor-free, fully printable mesoscopic perovskite solar cells with a broad light harvester $\text{NH}_2\text{CH}=\text{NH}_2\text{PbI}_3$,” *J. Mater. Chem. A*, vol. 2, no. 40, pp. 17115–17121, September 2014.
173. H. N. Chen, Z. H. Wei, H. X. He, X. L. Zheng, K. S. Wong, and S. H. Yang, “Solvent Engineering Boosts the Efficiency of Paintable Carbon-Based Perovskite Solar Cells to beyond 14%,” *Adv. Energy Mater.*, vol. 6, no. 8, p. 1502087, April 2016.
174. Y. Wu *et al.*, “Retarding the crystallization of PbI_2 for highly reproducible planar-structured perovskite solar cells via sequential deposition,” *Energy Environ. Sci.*, vol. 7, no. 9, pp. 2934–2938, August 2014.
175. Z. Zhang *et al.*, “High reproducibility of perovskite solar cells via a complete spin-coating sequential solution deposition process,” *Sol. Energy*, vol. 122, pp. 97–103, December 2015.
176. D. Liu *et al.*, “Highly reproducible perovskite solar cells with excellent $\text{CH}_3\text{NH}_3\text{PbI}_{3-x}\text{Cl}_x$ film morphology fabricated via high precursor concentration,” *RSC Adv.*, vol. 6, no. 56, pp. 51279–51285, May 2016.
177. S. R. Pae, S. Byun, J. Kim, M. Kim, I. Gereige, and B. Shin, “Improving Uniformity and Reproducibility of Hybrid Perovskite Solar Cells via a Low-Temperature

- Vacuum Deposition Process for NiOx/Hole Transport Layers,” *ACS Appl. Mater. Interfaces*, vol. 10, no. 1, pp. 534–540, January 2018.
178. M. Higgins *et al.*, “Enhanced reproducibility of planar perovskite solar cells by fullerene doping with silver nanoparticles,” *J. Appl. Phys.*, vol. 124, no. 6, p. 065306, August 2018.
 179. H. S. Kim and N. G. Park, “Parameters affecting I-V hysteresis of CH₃NH₃PbI₃ perovskite solar cells: Effects of perovskite crystal size and mesoporous TiO₂ layer,” *J. Phys. Chem. Lett.*, vol. 5, no. 17, pp. 2927–2934, September 2014.
 180. Y. Rong *et al.*, “Tunable hysteresis effect for perovskite solar cells,” *Energy Environ. Sci.*, vol. 10, no. 11, pp. 2383–2391, November 2017.
 181. D. Yang *et al.*, “High efficiency planar-type perovskite solar cells with negligible hysteresis using EDTA-complexed SnO₂,” *Nat. Commun.*, vol. 9, no. 1, p. 3239, December 2018.
 182. B. Chen *et al.*, “Interface band structure engineering by ferroelectric polarization in perovskite solar cells,” *Nano Energy*, vol. 13, pp. 582–591, April 2015.
 183. H. J. Snaith *et al.*, “Anomalous Hysteresis in Perovskite Solar Cells,” *J. Phys. Chem. Lett.*, vol. 5, no. 9, pp. 1511–1515, May 2014.
 184. J. P. Correa-Baena *et al.*, “The rapid evolution of highly efficient perovskite solar cells,” *Energy Environ. Sci.*, vol. 10, no. 3, pp. 710–727, March 2017.
 185. A. J. Cimaroli *et al.*, “Tracking the maximum power point of hysteretic perovskite solar cells using a predictive algorithm,” *J. Mater. Chem. C*, vol. 5, no. 39, pp. 10152–10157, October 2017.
 186. C. H. Chiang and C. G. Wu, “Film Grain-Size Related Long-Term Stability of

- Inverted Perovskite Solar Cells,” *ChemSusChem*, vol. 9, no. 18, pp. 2666–2672, September 2016.
187. D. Koushik *et al.*, “High-efficiency humidity-stable planar perovskite solar cells based on atomic layer architecture,” *Energy Environ. Sci.*, vol. 10, no. 1, pp. 91–100, January 2017.
188. N. Arora *et al.*, “Perovskite solar cells with CuSCN hole extraction layers yield stabilized efficiencies greater than 20%,” *Science (80-.)*, vol. 358, no. 6364, pp. 768–771, September 2017.
189. B. Suarez, V. Gonzalez-Pedro, T. S. Ripolles, R. S. Sanchez, L. Otero, and I. Mora-Sero, “Recombination study of combined halides (Cl, Br, I) perovskite solar cells,” *J. Phys. Chem. Lett.*, vol. 5, no. 10, pp. 1628–1635, May 2014.
190. Q. Tai *et al.*, “Efficient and stable perovskite solar cells prepared in ambient air irrespective of the humidity,” *Nat. Commun.*, vol. 7, no. 1, p. 11105, April 2016.
191. J. Yang, B. D. Siempelkamp, D. Liu, and T. L. Kelly, “Investigation of CH₃NH₃PbI₃ Degradation Rates and Mechanisms in Controlled Humidity Environments Using *in Situ* Techniques,” *ACS Nano*, vol. 9, no. 2, pp. 1955–1963, February 2015.
192. J. H. Noh, S. H. Im, J. H. Heo, T. N. Mandal, and S. Il Seok, “Chemical management for colorful, efficient, and stable inorganic-organic hybrid nanostructured solar cells,” *Nano Lett.*, vol. 13, no. 4, pp. 1764–1769, April 2013.
193. A. M. A. Leguy *et al.*, “Reversible Hydration of CH₃NH₃PbI₃ in Films, Single Crystals, and Solar Cells,” *Chem. Mater.*, vol. 27, no. 9, pp. 3397–3407, May 2015.
194. J. A. Christians, P. A. Miranda Herrera, and P. V. Kamat, “Transformation of the Excited State and Photovoltaic Efficiency of CH₃NH₃PbI₃ Perovskite upon Controlled Exposure to Humidified Air,” *J. Am. Chem. Soc.*, vol. 137, no. 4, pp. 1530–1538, February 2015.

195. N. A. Manshor *et al.*, “Humidity: Versus photo-stability of metal halide perovskite films in a polymer matrix,” *Phys. Chem. Chem. Phys.*, vol. 18, no. 31, pp. 21629–21639, August 2016.
196. M. I. Asghar, J. Zhang, H. Wang, and P. D. Lund, “Device stability of perovskite solar cells – A review,” *Renewable and Sustainable Energy Reviews*, vol. 77. Pergamon, pp. 131–146, 01-Sep-2017.
197. H. Kautsky, “Quenching of luminescence by oxygen,” *Trans. Faraday Soc.*, vol. 35, no. 0, p. 216, January 1939.
198. Mohamed S. A. Abdou, Francesco P. Orfino, and Yongkeun Son, and S. Holdcroft, “Interaction of Oxygen with Conjugated Polymers: Charge Transfer Complex Formation with Poly(3-alkylthiophenes),” May 1997.
199. R. K. Misra *et al.*, “Temperature and component-dependent degradation of perovskite photovoltaic materials under concentrated sunlight,” *J. Phys. Chem. Lett.*, vol. 6, no. 3, pp. 326–330, February 2015.
200. C. C. Stoumpos, C. D. Malliakas, and M. G. Kanatzidis, “Semiconducting Tin and Lead Iodide Perovskites with Organic Cations: Phase Transitions, High Mobilities, and Near-Infrared Photoluminescent Properties,” *Inorg. Chem.*, vol. 52, no. 15, pp. 9019–9038, August 2013.
201. B. Brunetti, C. Cavallo, A. Ciccioli, G. Gigli, and A. Latini, “On the Thermal and Thermodynamic (In)Stability of Methylammonium Lead Halide Perovskites,” *Sci. Rep.*, vol. 6, no. 1, p. 31896, October 2016.
202. I. Deretzis *et al.*, “Atomistic origins of $\text{CH}_3\text{NH}_3\text{PbI}_3$ degradation to PbI_2 in vacuum,” *Appl. Phys. Lett.*, vol. 106, no. 13, p. 131904, March 2015.
203. G. Divitini, S. Cacovich, F. Matteocci, L. Cinà, A. Di Carlo, and C. Ducati, “In situ

- observation of heat-induced degradation of perovskite solar cells,” *Nat. Energy*, vol. 1, no. 2, p. 15012, January 2016.
204. G. Abdelmageed *et al.*, “Effect of temperature on light induced degradation in methylammonium lead iodide perovskite thin films and solar cells,” *Sol. Energy Mater. Sol. Cells*, vol. 174, pp. 566–571, January 2018.
205. Y. Y. Zhang *et al.*, “Intrinsic Instability of the Hybrid Halide Perovskite Semiconductor $\text{CH}_3\text{NH}_3\text{PbI}_3$,” *Chinese Phys. Lett.*, vol. 35, no. 3, p. 036104, March 2018.
206. T. Baikie *et al.*, “Synthesis and crystal chemistry of the hybrid perovskite $(\text{CH}_3\text{NH}_3)\text{PbI}_3$ for solid-state sensitised solar cell applications,” *J. Mater. Chem. A*, vol. 1, no. 18, pp. 5628–5641, April 2013.
207. S. S. Mali, C. S. Shim, and C. K. Hong, “Highly stable and efficient solid-state solar cells based on methylammonium lead bromide $(\text{CH}_3\text{NH}_3\text{PbBr}_3)$ perovskite quantum dots,” *NPG Asia Mater.*, vol. 7, no. 8, pp. e208, August 2015.
208. F. Wang, X. Li, X. Yin, Z. Fu, and Y. Lu, “Thermal Behaviors of Methylammonium Lead Trihalide Perovskites with or without Chlorine Doping,” *J. Phys. Chem. C*, vol. 120, no. 28, pp. 15009–15016, July 2016.
209. Q. Han *et al.*, “Single Crystal Formamidinium Lead Iodide (FAPbI₃): Insight into the Structural, Optical, and Electrical Properties,” *Adv. Mater.*, vol. 28, no. 11, pp. 2253–2258, March 2016.
210. R. J. Sutton *et al.*, “Bandgap-Tunable Cesium Lead Halide Perovskites with High Thermal Stability for Efficient Solar Cells,” *Adv. Energy Mater.*, vol. 6, no. 8, p. 1502458, April 2016.
211. S. Bai, N. Cheng, Z. Yu, P. Liu, C. Wang, and X. Z. Zhao, “Cubic: Column composite structure $(\text{NH}_2\text{CH}=\text{NH}_2)_x(\text{CH}_3\text{NH}_3)_{1-x}\text{PbI}_3$ for efficient hole-transport material-

- free and insulation layer free perovskite solar cells with high stability,” *Electrochim. Acta*, vol. 190, pp. 775–779, February 2016.
212. J. Xi *et al.*, “Initiating crystal growth kinetics of α -HC(NH₂)₂PbI₃ for flexible solar cells with long-term stability,” *Nano Energy*, vol. 26, pp. 438–445, August 2016.
213. Z. Li, M. Yang, J.-S. Park, S.-H. Wei, J. J. Berry, and K. Zhu, “Stabilizing Perovskite Structures by Tuning Tolerance Factor: Formation of Formamidinium and Cesium Lead Iodide Solid-State Alloys,” *Chem. Mater.*, vol. 28, no. 1, pp. 284–292, January 2016.
214. J. H. Kim, S. T. Williams, N. Cho, C.-C. Chueh, and A. K.-Y. Jen, “Enhanced Environmental Stability of Planar Heterojunction Perovskite Solar Cells Based on Blade-Coating,” *Adv. Energy Mater.*, vol. 5, no. 4, p. 1401229, February 2015.
215. I. Mesquita, L. Andrade, and A. Mendes, “Perovskite solar cells: Materials, configurations and stability,” *Renewable and Sustainable Energy Reviews*, vol. 82. Pergamon, pp. 2471–2489, February 2018.
216. D. Yang, Z. Yang, W. Qin, Y. Zhang, S. Liu, and C. Li, “Alternating precursor layer deposition for highly stable perovskite films towards efficient solar cells using vacuum deposition,” *J. Mater. Chem. A*, vol. 3, no. 18, pp. 9401–9405, April 2015.
217. J. Wu *et al.*, “DMF as an Additive in a Two-Step Spin-Coating Method for 20% Conversion Efficiency in Perovskite Solar Cells,” *ACS Appl. Mater. Interfaces*, vol. 9, no. 32, pp. 26937–26947, August 2017.
218. Y. Deng, X. Zheng, Y. Bai, Q. Wang, J. Zhao, and J. Huang, “Surfactant-controlled ink drying enables high-speed deposition of perovskite films for efficient photovoltaic modules,” *Nat. Energy*, vol. 3, no. 7, pp. 560–566, July 2018.
219. M. R. Leyden, L. K. Ono, S. R. Raga, Y. Kato, S. Wang, and Y. Qi, “High performance perovskite solar cells by hybrid chemical vapor deposition,” *J. Mater.*

Chem. A, vol. 2, no. 44, pp. 18742–18745, October 2014.

220. D. Yang, J. Zhang, Z. Yang, and S. F. Liu, “Stable high efficiency perovskite solar cells using vacuum deposition,” in *2016 IEEE 43rd Photovoltaic Specialists Conference (PVSC)*, 2016, pp. 0086–0088.
221. S. Tombe *et al.*, “The influence of perovskite precursor composition on the morphology and photovoltaic performance of mixed halide MAPbI₃-xCl_x solar cells,” *Sol. Energy*, vol. 163, pp. 215–223, 2018.
222. F. K. Aldibaja, L. Badia, E. Mas-Marzá, R. S. Sánchez, E. M. Barea, and I. Mora-Sero, “Effect of different lead precursors on perovskite solar cell performance and stability,” *J. Mater. Chem. A*, vol. 3, no. 17, pp. 9194–9200, April 2015.
223. P. Wang *et al.*, “Solvent-controlled growth of inorganic perovskite films in dry environment for efficient and stable solar cells,” *Nat. Commun.*, vol. 9, no. 1, p. 2225, December 2018.
224. D. Liu *et al.*, “Aqueous-Containing Precursor Solutions for Efficient Perovskite Solar Cells,” *Adv. Sci. (Weinheim, Baden-Wurttemberg, Ger.)*, vol. 5, no. 1, p. 1700484, 2018.
225. W. Xiang *et al.*, “Improved air stability of perovskite hybrid solar cells via blending poly(dimethylsiloxane)–urea copolymers,” *J. Mater. Chem. A*, vol. 5, no. 11, pp. 5486–5494, March 2017.
226. Y. Zhao *et al.*, “A polymer scaffold for self-healing perovskite solar cells,” *Nat. Commun.*, vol. 7, p. 10228, January 2016.
227. Y. Guo, K. Shoyama, W. Sato, and E. Nakamura, “Polymer Stabilization of Lead(II) Perovskite Cubic Nanocrystals for Semitransparent Solar Cells,” *Adv. Energy Mater.*, vol. 6, no. 6, p. 1502317, March 2016.
228. Y. Sun *et al.*, “Long-term stability of organic–inorganic hybrid perovskite solar cells

- with high efficiency under high humidity conditions,” *J. Mater. Chem. A*, vol. 5, no. 4, pp. 1374–1379, January 2017.
229. J. Pascual *et al.*, “Electron Transport Layer-Free Solar Cells Based on Perovskite-Fullerene Blend Films with Enhanced Performance and Stability,” *ChemSusChem*, vol. 9, no. 18, pp. 2679–2685, September 2016.
230. J. Ye *et al.*, “Enhanced morphology and stability of high-performance perovskite solar cells with ultra-smooth surface and high fill factor via crystal growth engineering,” *Sustain. Energy Fuels*, vol. 1, no. 4, pp. 907–914, May 2017.
231. L. Ji *et al.*, “Realizing Full Coverage of Stable Perovskite Film by Modified Anti-Solvent Process,” *Nanoscale Res. Lett.*, vol. 12, no. 1, p. 367, December 2017.
232. Y. Wang *et al.*, “Stitching triple cation perovskite by a mixed anti-solvent process for high performance perovskite solar cells,” *Nano Energy*, vol. 39, pp. 616–625, September 2017.
233. J. Troughton, K. Hooper, and T. M. Watson, “Humidity resistant fabrication of CH₃NH₃PbI₃ perovskite solar cells and modules,” *Nano Energy*, vol. 39, pp. 60–68, September 2017.
234. M. Li *et al.*, “Enhanced Efficiency and Stability of Perovskite Solar Cells via Anti-Solvent Treatment in Two-Step Deposition Method,” *ACS Appl. Mater. Interfaces*, vol. 9, no. 8, pp. 7224–7231, March 2017.
235. P. Y. Su *et al.*, “A multifunctional poly-N-vinylcarbazole interlayer in perovskite solar cells for high stability and efficiency: a test with new triazatruxene-based hole transporting materials,” *J. Mater. Chem. A*, vol. 5, no. 5, pp. 1913–1918, January 2017.
236. N. Li *et al.*, “Enhanced efficiency and stability of inverted perovskite solar cells by interfacial engineering with alkyl bisphosphonic molecules,” *RSC Adv.*, vol. 7, no. 67,

pp. 42105–42112, August 2017.

237. A. Fakharuddin, F. Di Giacomo, I. Ahmed, Q. Wali, T. M. Brown, and R. Jose, “Role of morphology and crystallinity of nanorod and planar electron transport layers on the performance and long term durability of perovskite solar cells,” *J. Power Sources*, vol. 283, pp. 61–67, June 2015.
238. T. Leijtens, G. E. Eperon, S. Pathak, A. Abate, M. M. Lee, and H. J. Snaith, “Overcoming ultraviolet light instability of sensitized TiO₂ with meso-structured organometal tri-halide perovskite solar cells,” *Nat. Commun.*, vol. 4, no. 1, p. 2885, December 2013.
239. I. Hwang, M. Baek, and K. Yong, “Core/Shell Structured TiO₂/CdS Electrode to Enhance the Light Stability of Perovskite Solar Cells,” *ACS Appl. Mater. Interfaces*, vol. 7, no. 50, pp. 27863–27870, December 2015.
240. I. Hwang and K. Yong, “Novel CdS Hole-Blocking Layer for Photostable Perovskite Solar Cells,” *ACS Appl. Mater. Interfaces*, vol. 8, no. 6, pp. 4226–4232, February 2016.
241. W. Li, J. Li, G. Niu, and L. Wang, “Effect of cesium chloride modification on the film morphology and UV-induced stability of planar perovskite solar cells,” *J. Mater. Chem. A*, vol. 4, no. 30, pp. 11688–11695, July 2016.
242. W. Li *et al.*, “Enhanced UV-light stability of planar heterojunction perovskite solar cells with caesium bromide interface modification,” *Energy Environ. Sci.*, vol. 9, no. 2, pp. 490–498, February 2016.
243. X. Dong *et al.*, “Method for improving illumination instability of organic–inorganic halide perovskite solar cells,” *Sci. Bull.*, vol. 61, no. 3, pp. 236–244, February 2016.
244. B. Roose *et al.*, “Enhanced Efficiency and Stability of Perovskite Solar Cells Through Nd-Doping of Mesostructured TiO₂,” *Adv. Energy Mater.*, vol. 6, no. 2, p. 1501868,

January 2016.

245. F. J. Ramos, M. Oliva-Ramirez, M. K. Nazeeruddin, M. Grätzel, A. R. González-Elipe, and S. Ahmad, "Nanocolumnar 1-dimensional TiO₂ photoanodes deposited by PVD-OAD for perovskite solar cell fabrication," *J. Mater. Chem. A*, vol. 3, no. 25, pp. 13291–13298, June 2015.
246. A. Fakharuddin *et al.*, "Vertical TiO₂ Nanorods as a Medium for Stable and High-Efficiency Perovskite Solar Modules," *ACS Nano*, vol. 9, no. 8, pp. 8420–8429, August 2015.
247. P. Qin *et al.*, "Stable and Efficient Perovskite Solar Cells Based on Titania Nanotube Arrays," *Small*, vol. 11, no. 41, pp. 5533–5539, November 2015.
248. Q. Liu *et al.*, "Enhanced Stability of Perovskite Solar Cells with Low-Temperature Hydrothermally Grown SnO₂ Electron Transport Layers," *Adv. Funct. Mater.*, vol. 26, no. 33, pp. 6069–6075, September 2016.
249. L. Xiong *et al.*, "Performance enhancement of high temperature SnO₂-based planar perovskite solar cells: electrical characterization and understanding of the mechanism," *J. Mater. Chem. A*, vol. 4, no. 21, pp. 8374–8383, May 2016.
250. J. P. Correa Baena *et al.*, "Highly efficient planar perovskite solar cells through band alignment engineering," *Energy Environ. Sci.*, vol. 8, no. 10, pp. 2928–2934, October 2015.
251. J. Duan, Q. Xiong, B. Feng, Y. Xu, J. Zhang, and H. Wang, "Low-temperature processed SnO₂ compact layer for efficient mesostructure perovskite solar cells," *Appl. Surf. Sci.*, vol. 391, pp. 677–683, January 2017.
252. J. Song *et al.*, "Low-temperature SnO₂-based electron selective contact for efficient and stable perovskite solar cells," *J. Mater. Chem. A*, vol. 3, no. 20, pp. 10837–10844, May 2015.

253. Y. Dkhissi *et al.*, “Stability Comparison of Perovskite Solar Cells Based on Zinc Oxide and Titania on Polymer Substrates,” *ChemSusChem*, vol. 9, no. 7, pp. 687–695, April 2016.
254. H. Si *et al.*, “An innovative design of perovskite solar cells with Al₂O₃ inserting at ZnO/perovskite interface for improving the performance and stability,” *Nano Energy*, vol. 22, pp. 223–231, April 2016.
255. P. Zhang *et al.*, “Enhanced efficiency and environmental stability of planar perovskite solar cells by suppressing photocatalytic decomposition,” *J. Mater. Chem. A*, vol. 5, no. 33, pp. 17368–17378, August 2017.
256. X. Zhao *et al.*, “Aluminum-Doped Zinc Oxide as Highly Stable Electron Collection Layer for Perovskite Solar Cells,” *ACS Appl. Mater. Interfaces*, vol. 8, no. 12, pp. 7826–7833, March 2016.
257. J. Song, L. Liu, X. F. Wang, G. Chen, W. Tian, and T. Miyasaka, “Highly efficient and stable low-temperature processed ZnO solar cells with triple cation perovskite absorber,” *J. Mater. Chem. A*, vol. 5, no. 26, pp. 13439–13447, July 2017.
258. J. H. Heo, S. C. Lee, S. K. Jung, O. P. Kwon, and S. H. Im, “Efficient and thermally stable inverted perovskite solar cells by introduction of non-fullerene electron transporting materials,” *J. Mater. Chem. A*, vol. 5, no. 39, pp. 20615–20622, October 2017.
259. G.-H. Kim *et al.*, “Fluorine Functionalized Graphene Nano Platelets for Highly Stable Inverted Perovskite Solar Cells,” *Nano Lett.*, vol. 17, no. 10, pp. 6385–6390, October 2017.
260. C. Y. Chang, W. K. Huang, Y. C. Chang, K. T. Lee, and C. T. Chen, “A solution-processed n-doped fullerene cathode interfacial layer for efficient and stable large-area perovskite solar cells,” *J. Mater. Chem. A*, vol. 4, no. 2, pp. 640–648, December

- 2015.
261. S. Bai *et al.*, “High-performance planar heterojunction perovskite solar cells: Preserving long charge carrier diffusion lengths and interfacial engineering,” *Nano Res.*, vol. 7, no. 12, pp. 1749–1758, December 2014.
 262. C. Y. Chang, W. K. Huang, J. L. Wu, Y. C. Chang, K. T. Lee, and C. T. Chen, “Room-Temperature Solution-Processed n-Doped Zirconium Oxide Cathode Buffer Layer for Efficient and Stable Organic and Hybrid Perovskite Solar Cells,” *Chem. Mater.*, vol. 28, no. 1, pp. 242–251, January 2016.
 263. M. Kaltenbrunner *et al.*, “Flexible high power-per-weight perovskite solar cells with chromium oxide-metal contacts for improved stability in air,” *Nat. Mater.*, vol. 14, no. 10, pp. 1032–1039, October 2015.
 264. Z. Zhu, Y. Bai, X. Liu, C. C. Chueh, S. Yang, and A. K.-Y. Jen, “Enhanced Efficiency and Stability of Inverted Perovskite Solar Cells Using Highly Crystalline SnO₂ Nanocrystals as the Robust Electron-Transporting Layer,” *Adv. Mater.*, vol. 28, no. 30, pp. 6478–6484, August 2016.
 265. R. S. Sanchez and E. Mas-Marza, “Light-induced effects on Spiro-OMeTAD films and hybrid lead halide perovskite solar cells,” *Sol. Energy Mater. Sol. Cells*, vol. 158, pp. 189–194, December 2016.
 266. J. Chen *et al.*, “Recent progress in stabilizing hybrid perovskites for solar cell applications,” *J. Power Sources*, vol. 355, pp. 98–133, July 2017.
 267. B. Xu, J. Huang, H. Ågren, L. Kloo, A. Hagfeldt, and L. Sun, “AgTFSI as p-Type Dopant for Efficient and Stable Solid-State Dye-Sensitized and Perovskite Solar Cells,” *ChemSusChem*, vol. 7, no. 12, pp. 3252–3256, December 2014.
 268. L. Huang *et al.*, “Efficient and stable planar perovskite solar cells with a non-hygroscopic small molecule oxidant doped hole transport layer,” *Electrochim. Acta*,

- vol. 196, pp. 328–336, April 2016.
269. J. Liu *et al.*, “A dopant-free hole-transporting material for efficient and stable perovskite solar cells,” *Energy Environ. Sci.*, vol. 7, no. 9, pp. 2963–2967, August 2014.
270. F. Zhang *et al.*, “A Novel Dopant-Free Triphenylamine Based Molecular ‘Butterfly’ Hole-Transport Material for Highly Efficient and Stable Perovskite Solar Cells,” *Adv. Energy Mater.*, vol. 6, no. 14, p. 1600401, July 2016.
271. Y.-K. Wang *et al.*, “Dopant-Free Spiro-Triphenylamine/Fluorene as Hole-Transporting Material for Perovskite Solar Cells with Enhanced Efficiency and Stability,” *Adv. Funct. Mater.*, vol. 26, no. 9, pp. 1375–1381, March 2016.
272. J. Ye, X. Li, J. Zhao, X. Mei, and Q. Li, “Efficient and stable perovskite solar cells based on functional graphene-modified P3HT hole-transporting layer,” *RSC Adv.*, vol. 6, no. 43, pp. 36356–36361, April 2016.
273. Y. Zhang, W. Liu, F. Tan, and Y. Gu, “The essential role of the poly(3-hexylthiophene) hole transport layer in perovskite solar cells,” *J. Power Sources*, vol. 274, pp. 1224–1230, January 2015.
274. B. A. de Carvalho, S. Kavadiya, S. Huang, D. M. Niedzwiedzki, and P. Biswas, “Highly Stable Perovskite Solar Cells Fabricated Under Humid Ambient Conditions,” *IEEE J. Photovoltaics*, vol. 7, no. 2, pp. 532–538, March 2017.
275. G.-W. Kim, G. Kang, M. Malekshahi Byranvand, G.-Y. Lee, and T. Park, “Gradated Mixed Hole Transport Layer in a Perovskite Solar Cell: Improving Moisture Stability and Efficiency,” *ACS Appl. Mater. Interfaces*, vol. 9, no. 33, pp. 27720–27726, August 2017.
276. J. Kim, N. Park, J. S. Yun, S. Huang, M. A. Green, and A. W. Y. Ho-Baillie, “An effective method of predicting perovskite solar cell lifetime—Case study on planar

- CH₃NH₃PbI₃ and HC(NH₂)₂PbI₃ perovskite solar cells and hole transfer materials of spiro-OMeTAD and PTAA,” *Sol. Energy Mater. Sol. Cells*, vol. 162, pp. 41–46, April 2017.
277. S. N. Habisreutinger, T. Leijtens, G. E. Eperon, S. D. Stranks, R. J. Nicholas, and H. J. Snaith, “Carbon Nanotube/Polymer Composites as a Highly Stable Hole Collection Layer in Perovskite Solar Cells,” *Nano Lett.*, vol. 14, no. 10, pp. 5561–5568, October 2014.
278. S. S. Reddy *et al.*, “Highly Efficient Organic Hole Transporting Materials for Perovskite and Organic Solar Cells with Long-Term Stability,” *Adv. Mater.*, vol. 28, no. 4, pp. 686–693, January 2016.
279. X. Liu *et al.*, “Diketopyrrolopyrrole or benzodithiophene-arylamine small-molecule hole transporting materials for stable perovskite solar cells,” *RSC Adv.*, vol. 6, no. 90, pp. 87454–87460, September 2016.
280. J. A. Christians, R. C. M. Fung, and P. V. Kamat, “An inorganic hole conductor for Organo-lead halide perovskite solar cells. improved hole conductivity with copper iodide,” *J. Am. Chem. Soc.*, vol. 136, no. 2, pp. 758–764, January 2014.
281. M. Jørgensen, K. Norrman, and F. C. Krebs, “Stability/degradation of polymer solar cells,” *Sol. Energy Mater. Sol. Cells*, vol. 92, no. 7, pp. 686–714, July 2008.
282. J. Huang, K.-X. Wang, J.-J. Chang, Y.-Y. Jiang, Q.-S. Xiao, and Y. Li, “Improving the efficiency and stability of inverted perovskite solar cells with dopamine-copolymerized PEDOT:PSS as a hole extraction layer,” *J. Mater. Chem. A*, vol. 5, no. 26, pp. 13817–13822, July 2017.
283. M. M. de Kok *et al.*, “Modification of PEDOT:PSS as hole injection layer in polymer LEDs,” *Phys. status solidi*, vol. 201, no. 6, pp. 1342–1359, May 2004.
284. J. P. Thomas, L. Zhao, D. McGillivray, and K. T. Leung, “High-efficiency hybrid

- solar cells by nanostructural modification in PEDOT:PSS with co-solvent addition,” *J. Mater. Chem. A*, vol. 2, no. 7, p. 2383, January 2014.
285. Z. Zhu *et al.*, “High-Performance Hole-Extraction Layer of Sol-Gel-Processed NiO Nanocrystals for Inverted Planar Perovskite Solar Cells,” *Angew. Chemie Int. Ed.*, vol. 53, no. 46, July 2014.
286. J. You *et al.*, “Improved air stability of perovskite solar cells via solution-processed metal oxide transport layers,” *Nat. Nanotechnol.*, vol. 11, no. 1, pp. 75–81, January 2016.
287. S. Ye *et al.*, “CuSCN-Based Inverted Planar Perovskite Solar Cell with an Average PCE of 15.6%,” *Nano Lett.*, vol. 15, no. 6, pp. 3723–3728, June 2015.
288. Q.-D. Yang *et al.*, “Graphene oxide as an efficient hole-transporting material for high-performance perovskite solar cells with enhanced stability,” *J. Mater. Chem. A*, vol. 5, no. 20, pp. 9852–9858, May 2017.
289. J. Zhao *et al.*, “Is Cu a stable electrode material in hybrid perovskite solar cells for a 30-year lifetime?,” *Energy Environ. Sci.*, vol. 9, no. 12, pp. 3650–3656, November 2016.
290. A. Mei *et al.*, “A hole-conductor-free, fully printable mesoscopic perovskite solar cell with high stability,” *Science*, vol. 345, no. 6194, pp. 295–8, July 2014.
291. K. Aitola *et al.*, “High Temperature-Stable Perovskite Solar Cell Based on Low-Cost Carbon Nanotube Hole Contact,” *Adv. Mater.*, vol. 29, no. 17, p. 1606398, May 2017.
292. A. Priyadarshi *et al.*, “A large area (70 cm²) monolithic perovskite solar module with a high efficiency and stability,” *Energy Environ. Sci.*, vol. 9, no. 12, pp. 3687–3692, November 2016.
293. D. Hand, H. Mannila, and P. Smyth, *Principles of Data Mining*. Cambridge: The MIT

Press, 2001.

294. P. Cabena, P. Hadjinian, R. Stadler, J. Verhees, and A. Zanasi, *Discovering data mining: from concept to implementation*. Prentice Hall, 1998.
295. M. E. Günay and R. Yildirim, "Analysis of selective CO oxidation over promoted Pt/Al₂O₃ catalysts using modular neural networks: Combining preparation and operational variables," *Appl. Catal. A Gen.*, vol. 377, no. 1–2, pp. 174–180, April 2010.
296. D. T. Larose, "Discovering Knowledge in Data: an Introduction to Data Mining. John & Wiley & Sons," *Inc., Publ.*, p. 316, 2005.
297. M. Benghanem, A. Mellit, and S. N. Alamri, "ANN-based modelling and estimation of daily global solar radiation data: A case study," *Energy Convers. Manag.*, vol. 50, no. 7, pp. 1644–1655, July 2009.
298. T. R. Ayodele, A. S. O. Ogunjuyigbe, and C. G. Monyei, "On the global solar radiation prediction methods," *J. Renew. Sustain. Energy*, vol. 8, no. 2, p. 023702, March 2016.
299. H. A. N. Hejase and A. H. Assi, "Time-Series Regression Model for Prediction of Mean Daily Global Solar Radiation in Al-Ain, UAE," *ISRN Renew. Energy*, vol. 2012, pp. 1–11, April 2012.
300. J. Zeng and W. Qiao, "Short-term solar power prediction using a support vector machine," *Renew. Energy*, vol. 52, pp. 118–127, April 2013.
301. F. Almonacid, C. Rus, L. Hontoria, M. Fuentes, and G. Nofuentes, "Characterisation of Si-crystalline PV modules by artificial neural networks," *Renewable Energy*, vol. 34, no. 4. Pergamon, pp. 941–949, April 2009.
302. R. Evans, J. Dore, E. Van Voorthuysen, J. Zhu, and M. A. Green, "Data mining

- photovoltaic cell manufacturing data,” in *2014 IEEE 40th Photovoltaic Specialist Conference (PVSC)*, 2014, pp. 2699–2704.
303. M. K. Riede *et al.*, “Datamining and analysis of the key parameters in organic solar cells,” vol. 6197, p. 61970, 2006.
304. H. Sahu, W. Rao, A. Troisi, and H. Ma, “Toward Predicting Efficiency of Organic Solar Cells via Machine Learning and Improved Descriptors,” *Adv. Energy Mater.*, vol. 8, no. 24, p. 1801032, August 2018.
305. X. Li, Q. Xie, J. Jiang, Y. Zhou, and L. Huang, “Identifying and monitoring the development trends of emerging technologies using patent analysis and Twitter data mining: The case of perovskite solar cell technology,” *Technol. Forecast. Soc. Change*, June 2018.
306. J. M. Cole *et al.*, “Data mining with molecular design rules identifies new class of dyes for dye-sensitised solar cells,” *Phys. Chem. Chem. Phys.*, vol. 16, no. 48, pp. 26684–26690, November 2014.
307. C. Kim, T. D. Huan, S. Krishnan, and R. Ramprasad, “A hybrid organic-inorganic perovskite dataset,” *Sci. Data*, vol. 4, p. 170057, May 2017.
308. Ç. Odabaşı and R. Yıldırım, “Performance analysis of perovskite solar cells in 2013–2018 using machine-learning tools,” *Nano Energy*, vol. 56, pp. 770–791, February 2019.
309. “Digitizelt Digitizer Software.” .
310. Y. H. Chiang, H. M. Cheng, M. H. Li, T. F. Guo, and P. Chen, “Low-Pressure Vapor-Assisted Solution Process for Thiocyanate-Based Pseudohalide Perovskite Solar Cells,” *ChemSusChem*, vol. 9, no. 18, pp. 2620–2627, September 2016.
311. M. K. Kim, T. Jeon, H. Il Park, J. M. Lee, S. A. Nam, and S. O. Kim, “Effective

- control of crystal grain size in CH₃NH₃PbI₃ perovskite solar cells with a pseudohalide Pb(SCN)₂ additive,” *CrystEngComm*, vol. 18, no. 32, pp. 6090–6095, August 2016.
312. RStudio Team, “RStudio: Integrated Development Environment for R.” Boston, MA, 2016.
313. A. Liaw and M. Wiener, “Classification and Regression by randomForest,” *R News*, vol. 2, no. 3, 2002.
314. M. Hahsler, B. Gruen, and K. Hornik, “arules -- {A} Computational Environment for Mining Association Rules and Frequent Item Sets,” *J. Stat. Softw.*, vol. 14, no. 15, pp. 1–25, 2005.
315. T. Therneau and B. Atkinson, “rpart: Recursive Partitioning and Regression Trees.” 2018.
316. H. Wickham, R. François, L. Henry, and K. Müller, “dplyr: A Grammar of Data Manipulation.” 2018.
317. O. Grånäs, D. Vinichenko, and E. Kaxiras, “Establishing the limits of efficiency of perovskite solar cells from first principles modeling,” *Sci. Rep.*, vol. 6, no. 1, p. 36108, December 2016.
318. W. E. I. Sha, X. Ren, L. Chen, and W. C. H. Choy, “The efficiency limit of CH₃NH₃PbI₃ perovskite solar cells,” *Appl. Phys. Lett.*, vol. 106, no. 22, p. 221104, June 2015.
319. D. Montgomery and G. Runger, *Applied Statistics and Probability for Engineers*. New York: John Wiley & Sons, Inc., 2003.
320. Q. Jiang *et al.*, “Planar-Structure Perovskite Solar Cells with Efficiency beyond 21%,” *Adv. Mater.*, vol. 29, no. 46, p. 1703852, December 2017.

321. Y. Shi *et al.*, “CH₃NH₃PbI₃ and CH₃NH₃PbI_{3-x}Cl_x in Planar or Mesoporous Perovskite Solar Cells: Comprehensive Insight into the Dependence of Performance on Architecture,” *J. Phys. Chem. C*, vol. 119, no. 28, pp. 15868–15873, July 2015.
322. W. Li, J. Fan, J. Li, Y. Mai, and L. Wang, “Controllable grain morphology of perovskite absorber film by molecular self-assembly toward efficient solar cell exceeding 17%,” *J. Am. Chem. Soc.*, vol. 137, no. 32, pp. 10399–10405, August 2015.
323. M. R. Ahmadian-Yazdi, F. Zabihi, M. Habibi, and M. Eslamian, “Effects of Process Parameters on the Characteristics of Mixed-Halide Perovskite Solar Cells Fabricated by One-Step and Two-Step Sequential Coating,” *Nanoscale Res. Lett.*, vol. 11, no. 1, p. 408, December 2016.
324. H. L. Hsu, C. P. Chen, J. Y. Chang, Y. Y. Yu, and Y. K. Shen, “Two-step thermal annealing improves the morphology of spin-coated films for highly efficient perovskite hybrid photovoltaics,” *Nanoscale*, vol. 6, no. 17, pp. 10281–10288, June 2014.
325. L. Huang, Z. Hu, J. Xu, K. Zhang, J. Zhang, and Y. Zhu, “Multi-step slow annealing perovskite films for high performance planar perovskite solar cells,” *Sol. Energy Mater. Sol. Cells*, vol. 141, pp. 377–382, October 2015.
326. R. Rajeswari, M. Mrinalini, S. Prasanthkumar, and L. Giribabu, “Emerging of Inorganic Hole Transporting Materials For Perovskite Solar Cells,” *Chem. Rec.*, vol. 17, no. 7, pp. 681–699, July 2017.
327. G. Han *et al.*, “Nitrogen doped cuprous oxide as low cost hole-transporting material for perovskite solar cells,” *Scr. Mater.*, vol. 153, pp. 104–108, August 2018.
328. H. Zhang, H. Wang, W. Chen, and A. K.-Y. Jen, “CuGaO₂: A Promising Inorganic Hole-Transporting Material for Highly Efficient and Stable Perovskite Solar Cells,” *Adv. Mater.*, vol. 29, no. 8, p. 1604984, February 2017.

329. M. I. Hossain, F. H. Alharbi, and N. Tabet, "Copper oxide as inorganic hole transport material for lead halide perovskite based solar cells," *Sol. Energy*, vol. 120, pp. 370–380, October 2015.
330. Z. Yu and L. Sun, "Inorganic Hole-Transporting Materials for Perovskite Solar Cells," *Small Methods*, vol. 2, no. 2, p. 1700280, February 2018.
331. Q. Wang, C. Bi, and J. Huang, "Doped hole transport layer for efficiency enhancement in planar heterojunction organolead trihalide perovskite solar cells," *Nano Energy*, vol. 15, pp. 275–280, July 2015.
332. T. Liu, W. Liu, Y. Zhu, S. Wang, G. Wu, and H. Chen, "All solution processed perovskite solar cells with Ag@Au nanowires as top electrode," *Sol. Energy Mater. Sol. Cells*, vol. 171, pp. 43–49, November 2017.
333. M. Ye, X. Hong, F. Zhang, and X. Liu, "Recent advancements in perovskite solar cells: Flexibility, stability and large scale," *Journal of Materials Chemistry A*, vol. 4, no. 18. The Royal Society of Chemistry, pp. 6755–6771, 03-May-2016.
334. M. Saliba *et al.*, "How to Make over 20% Efficient Perovskite Solar Cells in Regular ($n-i-p$) and Inverted ($p-i-n$) Architectures," *Chem. Mater.*, vol. 30, no. 13, pp. 4193–4201, July 2018.
335. N. V. Chawla, "Data Mining for Imbalanced Datasets: An Overview," in *Data Mining and Knowledge Discovery Handbook*, 2009, pp. 875–886.
336. Y. Tu *et al.*, "Modulated CH₃NH₃PbI₃-xBr_xfilm for efficient perovskite solar cells exceeding 18%," *Sci. Rep.*, vol. 7, p. 44603, 2017.
337. J. Lee and S. Baik, "Enhanced crystallinity of CH₃NH₃PbI₃ by the pre-coordination of PbI₂-DMSO powders for highly reproducible and efficient planar heterojunction perovskite solar cells," *RSC Adv.*, vol. 8, no. 2, pp. 1005–1013, January 2018.

338. Y. Wu *et al.*, “Retarding the crystallization of PbI₂ for highly reproducible planar-structured perovskite solar cells via sequential deposition,” *Energy Environ. Sci.*, vol. 7, no. 9, pp. 2934–2938, August 2014.
339. Q. Dong *et al.*, “Insight into perovskite solar cells based on SnO₂ compact electron-selective layer,” *J. Phys. Chem. C*, vol. 119, no. 19, pp. 10212–10217, May 2015.
340. Z. Chen *et al.*, “Bulk heterojunction perovskite solar cells based on room temperature deposited hole-blocking layer: Suppressed hysteresis and flexible photovoltaic application,” *J. Power Sources*, vol. 351, pp. 123–129, May 2017.
341. T. Ye, J. Wang, W. Chen, Y. Yang, and D. He, “Improved Performance and Reproducibility of Perovskite Solar Cells by Well-Soluble Tris(pentafluorophenyl)borane as a p-Type Dopant,” *ACS Appl. Mater. Interfaces*, vol. 9, no. 21, pp. 17923–17931, May 2017.
342. S. G. Hashmi *et al.*, “High performance carbon-based printed perovskite solar cells with humidity assisted thermal treatment,” *J. Mater. Chem. A*, vol. 5, no. 24, pp. 12060–12067, 2017.
343. Y. Xu *et al.*, “Efficient hybrid mesoscopic solar cells with morphology-controlled CH₃NH₃PbI₃-xCl_x derived from two-step spin coating method,” *ACS Appl. Mater. Interfaces*, vol. 7, no. 4, pp. 2242–2248, February 2015.
344. D. Liu *et al.*, “Improved performance of inverted planar perovskite solar cells with F4-TCNQ doped PEDOT:PSS hole transport layers,” *J. Mater. Chem. A*, vol. 5, no. 12, pp. 5701–5708, March 2017.
345. T. Singh and T. Miyasaka, “Stabilizing the Efficiency Beyond 20% with a Mixed Cation Perovskite Solar Cell Fabricated in Ambient Air under Controlled Humidity,” *Adv. Energy Mater.*, vol. 8, no. 3, p. 1700677, January 2018.

346. T. Jesper Jacobsson *et al.*, “Exploration of the compositional space for mixed lead halogen perovskites for high efficiency solar cells,” *Energy Environ. Sci.*, vol. 9, no. 5, pp. 1706–1724, May 2016.
347. Y. H. Seo, E. C. Kim, S. P. Cho, S. S. Kim, and S. I. Na, “High-performance planar perovskite solar cells: Influence of solvent upon performance,” *Appl. Mater. Today*, vol. 9, pp. 598–604, December 2017.
348. S. Paek *et al.*, “From Nano- to Micrometer Scale: The Role of Antisolvent Treatment on High Performance Perovskite Solar Cells,” *Chem. Mater.*, vol. 29, no. 8, pp. 3490–3498, April 2017.
349. B. El Cohen, S. Aharon, A. Dymshits, and L. Etgar, “Impact of Antisolvent Treatment on Carrier Density in Efficient Hole-Conductor-Free Perovskite-Based Solar Cells,” *J. Phys. Chem. C*, vol. 120, no. 1, pp. 142–147, January 2016.
350. Q. Cai *et al.*, “Enhancing efficiency of planar structure perovskite solar cells using Sn-doped TiO₂ as electron transport layer at low temperature,” *Electrochim. Acta*, vol. 261, pp. 227–235, January 2018.
351. J. K. Kim *et al.*, “Resolving Hysteresis in Perovskite Solar Cells with Rapid Flame-Processed Cobalt-Doped TiO₂,” *Advanced Energy Materials*, vol. 8, no. 29, Wiley-Blackwell, p. 1801717, October 2018.
352. J. H. Heo, M. H. Lee, H. J. Han, B. R. Patil, J. S. Yu, and S. H. Im, “Highly efficient low temperature solution processable planar type CH₃NH₃PbI₃ perovskite flexible solar cells,” *J. Mater. Chem. A*, vol. 4, no. 5, pp. 1572–1578, January 2016.
353. J. Cao *et al.*, “Efficient, Hysteresis-Free, and Stable Perovskite Solar Cells with ZnO as Electron-Transport Layer: Effect of Surface Passivation,” *Adv. Mater.*, vol. 30, no. 11, p. 1705596, March 2018.
354. F. Giordano *et al.*, “Enhanced electronic properties in mesoporous TiO₂ via lithium

- doping for high-efficiency perovskite solar cells,” *Nat. Commun.*, vol. 7, p. 10379, January 2016.
355. S. Sidhik, A. Cerdan Pasarán, D. Esparza, T. López Luke, R. Carriles, and E. De La Rosa, “Improving the Optoelectronic Properties of Mesoporous TiO₂ by Cobalt Doping for High-Performance Hysteresis-free Perovskite Solar Cells,” *ACS Appl. Mater. Interfaces*, vol. 10, no. 4, pp. 3571–3580, January 2018.
356. A. Magomedov *et al.*, “Diphenylamine-Substituted Carbazole-Based Hole Transporting Materials for Perovskite Solar Cells: Influence of Isomeric Derivatives,” *Adv. Funct. Mater.*, vol. 28, no. 9, p. 1704351, February 2018.
357. M. Salado *et al.*, “Interface Play between Perovskite and Hole Selective Layer on the Performance and Stability of Perovskite Solar Cells,” *ACS Appl. Mater. Interfaces*, vol. 8, no. 50, pp. 34414–34421, December 2016.
358. Z. Li *et al.*, “Extrinsic ion migration in perovskite solar cells,” *Energy Environ. Sci.*, vol. 10, no. 5, pp. 1234–1242, May 2017.
359. J. Luo *et al.*, “Toward high-efficiency, hysteresis-less, stable perovskite solar cells: Unusual doping of a hole-transporting material using a fluorine-containing hydrophobic Lewis acid,” *Energy Environ. Sci.*, vol. 11, no. 8, pp. 2035–2045, August 2018.
360. J. Xu *et al.*, “Perovskite-fullerene hybrid materials suppress hysteresis in planar diodes,” *Nat. Commun.*, vol. 6, p. 7081, May 2015.
361. X. Yin, M. Que, Y. Xing, and W. Que, “High efficiency hysteresis-less inverted planar heterojunction perovskite solar cells with a solution-derived NiO_x hole contact layer,” *J. Mater. Chem. A*, vol. 3, no. 48, pp. 24495–24503, December 2015.
362. I. J. Park *et al.*, “New Hybrid Hole Extraction Layer of Perovskite Solar Cells with a Planar p-i-n Geometry,” *J. Phys. Chem. C*, vol. 119, no. 49, pp. 27285–27290,

December 2015.

363. Y. Bai *et al.*, “A pure and stable intermediate phase is key to growing aligned and vertically monolithic perovskite crystals for efficient PIN planar perovskite solar cells with high processibility and stability,” *Nano Energy*, vol. 34, pp. 58–68, April 2017.
364. Q. Chen *et al.*, “Ag-Incorporated Organic-Inorganic Perovskite Films and Planar Heterojunction Solar Cells,” *Nano Lett.*, vol. 17, no. 5, pp. 3231–3237, May 2017.
365. F. Xu, T. Zhang, G. Li, and Y. Zhao, “Mixed cation hybrid lead halide perovskites with enhanced performance and stability,” *Journal of Materials Chemistry A*, vol. 5, no. 23. The Royal Society of Chemistry, pp. 11450–11461, June 2017.
366. Q. Fu *et al.*, “Recent Progress on the Long-Term Stability of Perovskite Solar Cells,” *Advanced Science*, vol. 5, no. 5. Wiley-Blackwell, p. 1700387, May 2018.
367. P. H. Huang, Y. H. Wang, J. C. Ke, and C. J. Huang, “The effect of solvents on the performance of CH₃NH₃PbI₃perovskite solar cells,” *Energies*, vol. 10, no. 5, p. 599, April 2017.
368. W. Yu *et al.*, “Two-in-one additive-engineering strategy for improved air stability of planar perovskite solar cells,” *Nano Energy*, vol. 45, pp. 229–235, March 2018.
369. F. Li *et al.*, “A Universal Strategy to Utilize Polymeric Semiconductors for Perovskite Solar Cells with Enhanced Efficiency and Longevity,” *Adv. Funct. Mater.*, vol. 28, no. 15, p. 1706377, April 2018.
370. M. Xiao *et al.*, “Selection of an anti-solvent for efficient and stable cesium-containing triple cation planar perovskite solar cells,” *Nanoscale*, vol. 10, no. 25, pp. 12141–12148, July 2018.
371. Q. Jiang, X. Zhang, and J. You, “SnO₂ : A Wonderful Electron Transport Layer for Perovskite Solar Cells,” *Small*, vol. 14, no. 31, p. 1801154, August 2018.

372. H. Li *et al.*, “Synergistic effect of caprolactam as lewis base and interface engineering for efficient and stable planar perovskite solar cells,” *Nano Energy*, vol. 42, pp. 222–231, December 2017.
373. Y. Lee *et al.*, “Efficient Planar Perovskite Solar Cells Using Passivated Tin Oxide as an Electron Transport Layer,” *Adv. Sci.*, vol. 5, no. 6, p. 1800130, June 2018.
374. Y. Lei *et al.*, “Intrinsic charge carrier dynamics and device stability of perovskite/ZnO mesostructured solar cells in moisture,” vol. 4, no. 15, pp. 5474–5481, April 2016.
375. A. K. Jena, Y. Numata, M. Ikegami, and T. Miyasaka, “Role of spiro-OMeTAD in performance deterioration of perovskite solar cells at high temperature and reuse of the perovskite films to avoid Pb-waste,” *J. Mater. Chem. A*, vol. 6, no. 5, pp. 2219–2230, January 2018.
376. Z. Hawash, L. K. Ono, S. R. Raga, M. V. Lee, and Y. Qi, “Air-exposure induced dopant redistribution and energy level shifts in spin-coated Spiro-Meotad films,” *Chem. Mater.*, vol. 27, no. 2, pp. 562–569, January 2015.
377. I. Lee, J. H. Yun, H. J. Son, and T. S. Kim, “Accelerated Degradation Due to Weakened Adhesion from Li-TFSI Additives in Perovskite Solar Cells,” *ACS Appl. Mater. Interfaces*, vol. 9, no. 8, pp. 7029–7035, March 2017.
378. A. Magomedov *et al.*, “Pyridination of hole transporting material in perovskite solar cells questions the long-term stability,” *J. Mater. Chem. C*, vol. 6, no. 33, pp. 8874–8878, August 2018.
379. Y. Kato, L. K. Ono, M. V. Lee, S. Wang, S. R. Raga, and Y. Qi, “Silver Iodide Formation in Methyl Ammonium Lead Iodide Perovskite Solar Cells with Silver Top Electrodes,” *Adv. Mater. Interfaces*, vol. 2, no. 13, p. 1500195, September 2015.
380. D. Bryant *et al.*, “Light and oxygen induced degradation limits the operational

- stability of methylammonium lead triiodide perovskite solar cells,” *Energy Environ. Sci.*, vol. 9, no. 5, pp. 1655–1660, May 2016.
381. L. L. Gao *et al.*, “Small molecule-driven directional movement enabling pin-hole free perovskite film: Via fast solution engineering,” *Nanoscale*, vol. 9, no. 41, pp. 15778–15785, October 2017.
382. C. Chen *et al.*, “Carrier Interfacial Engineering by Bismuth Modification for Efficient and Thermoresistant Perovskite Solar Cells,” *Adv. Energy Mater.*, vol. 8, no. 20, p. 1703659, July 2018.
383. J. Ye *et al.*, “High-temperature shaping perovskite film crystallization for solar cell fast preparation,” *Sol. Energy Mater. Sol. Cells*, vol. 160, pp. 60–66, February 2017.
384. L. K. Ono, E. J. Juarez-Perez, and Y. Qi, “Progress on Perovskite Materials and Solar Cells with Mixed Cations and Halide Anions,” *ACS Applied Materials and Interfaces*, vol. 9, no. 36. American Chemical Society, pp. 30197–30246, September 2017.
385. S. Luo and W. A. Daoud, “Crystal structure formation of $\text{CH}_3\text{NH}_3\text{Pb}_{1-x}\text{Cl}_x$ perovskite,” *Materials*, vol. 9, no. 3. Multidisciplinary Digital Publishing Institute, p. 123, February 2016.
386. C. Chen *et al.*, “Effect of BCP buffer layer on eliminating charge accumulation for high performance of inverted perovskite solar cells,” *RSC Adv.*, vol. 7, no. 57, pp. 35819–35826, July 2017.
387. Z. Jiang *et al.*, “Amazing stable open-circuit voltage in perovskite solar cells using AgAl alloy electrode,” *Sol. Energy Mater. Sol. Cells*, vol. 146, pp. 35–43, March 2016.
388. C.-C. Chung, S. Narra, E. Jokar, H.-P. Wu, and E. Wei-Guang Diau, “Inverted planar solar cells based on perovskite/graphene oxide hybrid composites,” *J. Mater. Chem. A*, vol. 5, no. 27, pp. 13957–13965, July 2017.

389. R. Kang *et al.*, “Exploration of fabrication methods for planar CH₃NH₃PbI₃ perovskite solar cells,” *Nano Energy*, vol. 27, pp. 175–184, September 2016.

APPENDIX A: ADDITIONAL INFORMATION ON ANALYSIS OF PCE

Table A.1. Explanation for the Term of “others” in Figure 4.21.

	Article name	Instance	Article name	Instance	Article name	Instance
Others1	Bashir, A. <i>et al.</i> , Nanoscale 10, 2341– 2350 (2018)	Co ₃ O ₄	Liu, J. <i>et al.</i> , J. Phys. Chem. Lett. 6, 1666–1673 (2015)	PEDOT	Magomedov, A. <i>et al.</i> , Adv. Funct. Mater. 28, 1704351 (2018)	V885
	Cheng, N. <i>et al.</i> , Electrochim. Acta 246, 990–996 (2017)	CuPc	Liu, Z. <i>et al.</i> , J. Mater. Chem. A 5, 6597–6605 (2017)	NiO _x	Mahmud, M. A. <i>et al.</i> , Phys. Chem. Chem. Phys. 19, 21033–21045 (2017)	FDT
	Christians, J. A. <i>et al.</i> , Nat. Energy 3, 68–74 (2018)	EH44	Luo, Q. <i>et al.</i> , J. Mater. Chem. A 3, 15996–16004 (2015)	RGO-1	Sepalage, G. A. <i>et al.</i> , Adv. Funct. Mater. 25, 5650–5661 (2015)	CuI
	Hou, Y. <i>et al.</i> , Adv. Energy Mater. 5, 1500543 (2015)	PEDOT	Luo, Q. <i>et al.</i> , J. Mater. Chem. A 3, 15996–16004 (2015)	RGO-2	Zhang, F. <i>et al.</i> , Nano Energy 41, 469–475 (2017)	Z26
	Huckaba, A. J. <i>et al.</i> , Small Methods 1, 1700250 (2017)	TiS ₂	Luo, Q. <i>et al.</i> , J. Mater. Chem. A 3, 15996–16004 (2015)	RGO-3	Zhang, F. <i>et al.</i> , Nano Energy 41, 469–475 (2017)	Z25
	Jiang, X. <i>et al.</i> , Sci. Rep. 7, 42564 (2017)	PEDOT	Luo, Q. <i>et al.</i> , J. Mater. Chem. A 3, 15996–16004 (2015)	GO		
	Article name	Instance	Article name	Instance	Article name	Instance
Others2	Cimaroli, A. J. <i>et al.</i> , J. Mater. Chem. C 5, 10152–10157 (2017)	Pb(SCN) ₂	Lee, S. J. <i>et al.</i> , J. Am. Chem. Soc. 138, 3974– 3977 (2016)	SnF ₂ +pyrazine	Wu, T. <i>et al.</i> , J. Power Sources 365, 1–6 (2017)	NMP
	Ke, W. <i>et al.</i> , Adv. Mater. 28, 5214–5221 (2016)	Pb(SCN) ₂	Li, B. <i>et al.</i> , Nat. Commun. 9, 1076 (2018)	PVP	Yang, G. <i>et al.</i> , J. Mater. Chem. A 5, 1658–1666 (2017)	Pb(SCN) ₂
	Lee, J. W. <i>et al.</i> , Acc. Chem. Res. 49, 311– 319 (2016)	thiourea	Sun, M. <i>et al.</i> , J. Mater. Chem. A 5, 13448–13456 (2017)	2-pyridylthiourea	Yu, Y. <i>et al.</i> , ChemSusChem 9, 3288–3297 (2016)	Pb(SCN) ₂
	Article name	HTL	Article name	HTL	Article name	HTL
Others3	Chen, H. N. <i>et al.</i> , Adv. Energy Mater. 6, 1502087 (2016)	CYHEX	Kim, J. <i>et al.</i> , J. Phys. Chem. C 120, 11262–11267 (2016)	HI	Wei, J. <i>et al.</i> , Nano Energy 26, 139–147 (2016)	PCBM+PEG
	Fei, C. <i>et al.</i> , Adv. Energy Mater. 7, 1602017 (2017)	thiourea	Wang, F. <i>et al.</i> , Adv. Funct. Mater. 25, 1120– 1126 (2015)	HCl	Zhang, T. <i>et al.</i> , Sci. Adv. 3, e1700841 (2017)	EDAI2

Table A.1. Explanation for the Term of “others” in Figure 4.21 (cont.).

	Article name	Instance	Article name	Instance	Article name	Instance
Others3	Han, F. <i>et al.</i> , J. Power Sources 359, 577–584 (2017)	4MSA	Wang, Z. <i>et al.</i> , Chem. Mater. 27, 7149–7155 (2015)	FACl	Zhang, Y. <i>et al.</i> , Chem. Commun. 52, 5674–5677 (2016)	s-CNT
	Heo, J. H. and Im, S. H., Nanoscale 8, 2554–2560 (2016)	HI	Wang, Z. <i>et al.</i> , Nat. Energy 2, 17135 (2017)	HI+HBr	Zuo, L. <i>et al.</i> , Sci. Adv. 3, e1700106 (2017)	PVP
	Habisreutinger, S. N. <i>et al.</i> , Adv. Energy Mater. 7, 1601079 (2017)	H3P	Wang, F. <i>et al.</i> , Adv. Funct. Mater. 25, 1120–1126 (2015)	HI	Zhang, X. <i>et al.</i> , Sol. Energy 148, 70–77 (2017)	Al
	Article name	Instance	Article name	Instance	Article name	Instance
Others4	Jiang, H. <i>et al.</i> , ACS Appl. Energy Mater. 1, 900–909 (2018)	HaHc				
	Article name	Instance	Article name	Instance	Article name	Instance
Others5	Eze, V. O. <i>et al.</i> , Org. Electron. physics, Mater. Appl. 46, 253–262 (2017)	NMP				

Table A.2 Explanation for the Term of “others” in Figure 4.22.

	Article name	Instance	Article name	Instance	Article name	Instance
Others1	Lee, J. W. <i>et al.</i> , Acc. Chem. Res. 49, 311–319 (2016)	thiourea	Li, B. <i>et al.</i> , Nat. Commun. 9, 1076 (2018)	PVP	Sun, M. <i>et al.</i> , J. Mater. Chem. A 5, 13448–13456 (2017)	2-pyridylthiourea
	Lee, S. J. <i>et al.</i> , J. Am. Chem. Soc. 138, 3974–3977 (2016)	SnF2+pyrazine	Luo, H. <i>et al.</i> , Energy Technol. 5, 1814–1819 (2017)	LiI	Wu, T. <i>et al.</i> , J. Power Sources 365, 1–6 (2017)	NMP
	Lee, S. J. <i>et al.</i> , J. Am. Chem. Soc. 138, 3974–3977 (2016)	SnF2	Son, D.-Y. <i>et al.</i> , J. Am. Chem. Soc. 140, jacs.7b10430 (2018)	KI		
	Article name	Instance	Article name	Instance	Article name	Instance
Others2	Yang, Y. <i>et al.</i> , J. Alloys Compd. 684, 84–90 (2016)	BAI	Chen, H. N. <i>et al.</i> , Adv. Energy Mater. 6, 1502087 (2016)	CYHEX	Wang, Z. <i>et al.</i> , Chem. Mater. 27, 7149–7155 (2015)	MACl
	Mabrouk, S. <i>et al.</i> , Sustain. Energy Fuels 1, 2162–2171 (2017)	BMImI	Wei, W. <i>et al.</i> , Ind. Eng. Chem. Res. 56, 1803–1809 (2017)	graphene	Wei, W. <i>et al.</i> , Ind. Eng. Chem. Res. 56, 1803–1809 (2017)	MCN

Table A.2 Explanation for the Term of “others” in Figure 4.22 (cont.).

	Article name	Instance	Article name	Instance	Article name	Instance
Others2	Adhikari, N. <i>et al.</i> , <i>Nanoscale</i> 8, 2693–2703 (2016)	H ₂ O	Huang, J. <i>et al.</i> , <i>RSC Adv.</i> 6, 55720–55725 (2016)	H ₂ O	Yang, S. <i>et al.</i> , <i>J. Mater. Chem. A</i> 4, 9430–9436 (2016)	NH ₄ SCN
	Zhang, Y. <i>et al.</i> , <i>Chem. Commun.</i> 52, 5674–5677 (2016)	CNT	Wu, F. and Zhu, L., <i>Sol. Energy Mater. Sol. Cells</i> 167, 1–6 (2017)	H ₂ O	Wang, Z. <i>et al.</i> , <i>Chem. Mater.</i> 27, 7149–7155 (2015)	NH ₄ Cl
	Wang, F. <i>et al.</i> , <i>Adv. Funct. Mater.</i> 25, 1120–1126 (2015)	HCl	Wang, W. <i>et al.</i> , <i>J. Mater. Sci. Mater. Electron.</i> 27, 9384–9390 (2016)	H ₃ PO ₂	Zuo, L. <i>et al.</i> , <i>Sci. Adv.</i> 3, e1700106 (2017)	PAA
	Kim, J. <i>et al.</i> , <i>J. Phys. Chem. C</i> 120, 11262–11267 (2016)	HI	Zhao, Q. <i>et al.</i> , <i>Sci. Rep.</i> 6, 38670 (2016)	HAc	Wei, J. <i>et al.</i> , <i>Nano Energy</i> 26, 139–147 (2016)	PCBM
	Wang, F. <i>et al.</i> , <i>Adv. Funct. Mater.</i> 25, 1120–1126 (2015)	HI	Huang, J. <i>et al.</i> , <i>RSC Adv.</i> 6, 55720–55725 (2016)	HBr	Wei, J. <i>et al.</i> , <i>Nano Energy</i> 26, 139–147 (2016)	PCBM+PEG
	Mabrouk, S. <i>et al.</i> , <i>Sustain. Energy Fuels</i> 1, 2162–2171 (2017)	Li	Dar, M. I. <i>et al.</i> , <i>Adv. Funct. Mater.</i> 27, 1701433 (2017)	HBr	Xiang, W. <i>et al.</i> , <i>J. Mater. Chem. A</i> 5, 5486–5494 (2017)	PDMSurea
	Mabrouk, S. <i>et al.</i> , <i>Sustain. Energy Fuels</i> 1, 2162–2171 (2017)	LiI	Yang, L. <i>et al.</i> , <i>ACS Appl. Mater. Interfaces</i> 7, 14614–14619 (2015)	HCl	Wei, J. <i>et al.</i> , <i>Nano Energy</i> 26, 139–147 (2016)	PEG
	Yang, Y. <i>et al.</i> , <i>J. Alloys Compd.</i> 684, 84–90 (2016)	NH ₄ I	Huang, J. <i>et al.</i> , <i>RSC Adv.</i> 6, 55720–55725 (2016)	HCl	Zuo, L. <i>et al.</i> , <i>Sci. Adv.</i> 3, e1700106 (2017)	PEI
	Chang, C. Y. <i>et al.</i> , <i>ACS Appl. Mater. Interfaces</i> 7, 4955–4961 (2015)	PEG	Heo, J. H. and Im, S. H., <i>Nanoscale</i> 8, 2554–2560 (2016)	HI	Zuo, L. <i>et al.</i> , <i>Sci. Adv.</i> 3, e1700106 (2017)	PVP
	Zhang, Y. <i>et al.</i> , <i>Chem. Commun.</i> 52, 5674–5677 (2016)	s-CNT	Huang, J. <i>et al.</i> , <i>RSC Adv.</i> 6, 55720–55725 (2016)	HI	Ding, Y. <i>et al.</i> , <i>J. Power Sources</i> 272, Ahead of Print (2014)	PVP

Table A.2 Explanation for the Term of “others” in Figure 4.22 (cont.).

	Article name	Instance	Article name	Instance	Article name	Instance
Others2	Zhang, X. <i>et al.</i> , Sol. Energy 148, 70–77 (2017)	Al	Wang, Z. <i>et al.</i> , Nat. Energy 2, 17135 (2017)	HI+HBr	Mahmud, M. A. <i>et al.</i> , Sol. Energy Mater. Sol. Cells 159, 251–264 (2017)	TBP
	Han, F. <i>et al.</i> , J. Power Sources 359, 577–584 (2017)	4MSA	Yang, L. <i>et al.</i> , ACS Appl. Mater. Interfaces 7, 14614–14619 (2015)	HI	Liu, C. <i>et al.</i> , J. Phys. Chem. C 121, 6546–6553 (2017)	TBP
	Wu, S. <i>et al.</i> , J. Power Sources 359, 303–310 (2017)	CuPc(tBu) ₄	Zhang, Z. <i>et al.</i> , Sol. Energy 122, 97–103 (2015)	IPA	Fei, C. <i>et al.</i> , Adv. Energy Mater. 7, 1602017 (2017)	thiourea
	Article name	Instance	Article name	Instance		
Others3	Jiang, H. <i>et al.</i> , ACS Appl. Energy Mater. 1, 900–909 (2018)	HaHc	Wei, Q. <i>et al.</i> , RSC Adv. 6, 56807–56811 (2016)	CN		
	Article name	Instance	Article name	Instance	Article name	Instance
Others4	Chen, R. <i>et al.</i> , Energy Fuels 2, 1093–1100 (2018)	MAPb _{1-x} Zn _x I _{3-y} Cl _y	Jin, J. <i>et al.</i> , ACS Appl. Mater. Interfaces 9, acsami.7b15310 (2017)	MAI(Pb ₂) _{0.97} (ZnCl ₂) _{0.03}	Suarez, B. <i>et al.</i> , J. Phys. Chem. Lett. 5, 1628–1635 (2014)	MAPb(I _{1-x} Br _x) _{3-y} Cl _y
	Article name	Instance	Article name	Instance	Article name	Instance
Others5	Wang, F. <i>et al.</i> , Nanoscale 8, 11882–11888 (2016)	GO	Habisreutinger, S. N. <i>et al.</i> , Adv. Energy Mater. 7, 1601079 (2017)	PMMA	Habisreutinger, S. N. <i>et al.</i> , Adv. Energy Mater. 7, 1601079 (2017)	polycarbonate
	Article name	Instance	Article name	Instance	Article name	Instance
Others6	Wang, J. <i>et al.</i> , Chem. Commun. 50, 5829 (2014)	2TPA-2-DP	Mahmud, M. A. <i>et al.</i> , Phys. Chem. Chem. Phys. 19, 21033–21045 (2017)	FDT	Pratyusha, T. <i>et al.</i> , Mater. Today Proc. 4, 6820–6826 (2017)	PCDTBT:PCPDTBT
	Cho, A.-N. <i>et al.</i> , J. Mater. Chem. A 5, 7603–7611 (2017)	ACR-TPA	Qin, P. <i>et al.</i> , J. Am. Chem. Soc. 136, 8516–8519 (2014)	Fused-F	Heo, J. H. <i>et al.</i> , Nat. Photonics 7, 486–491 (2013)	PCPDTBT
	Dao, Q. D. <i>et al.</i> , Org. Electron. physics, Mater. Appl. 43, 156–161 (2017)	C5PcH2	Luo, Q. <i>et al.</i> , J. Mater. Chem. A 3, 15996–16004 (2015)	GO	Abrusci, A. <i>et al.</i> , Nano Lett. 13, 3124–3128 (2013)	PCPDTBT

Table A.2 Explanation for the Term of “others” in Figure 4.22 (cont.).

	Article name	Instance	Article name	Instance	Article name	Instance
Others6	Edri, E. <i>et al.</i> , J. Phys. Chem. Lett. 5, 429–433 (2014)	CBP	Wang, J. <i>et al.</i> , Electrochim. Acta 210, 673–680 (2016)	HBZ-70	Dubey, A. <i>et al.</i> , Sol. Energy Mater. Sol. Cells 145, 193–199 (2016)	PDPP3T
	Mali, S. S. <i>et al.</i> , Mater. Today Chem. 4, 53–63 (2017).	carbon+M Al	Li, H. <i>et al.</i> , Angew. Chemie - Int. Ed. 53, 4085–4088 (2014)	H101	Edri, E. <i>et al.</i> , J. Phys. Chem. Lett. 4, 897–902 (2013)	PDI
	Kulbak, M. <i>et al.</i> , J. Phys. Chem. Lett. 6, 2452–2456 (2015)	CBP	Lv, S. <i>et al.</i> , Chem. Commun. 50, 6931 (2014)	HTL1	Kwon, Y. S. <i>et al.</i> , Energy Environ. Sci. 7, 1454 (2014)	PDPPDBTE
	Li, M. <i>et al.</i> , ChemSusChem 9, 2862–2869 (2016)	Chl-1	Lv, S. <i>et al.</i> , Chem. Commun. 50, 6931 (2014)	HTL2	Wang, Z. <i>et al.</i> , Org. Electron. physics, Mater. Appl. 33, 142–149 (2016)	PDTSTTz
	Li, M. <i>et al.</i> , ChemSusChem 9, 2862–2869 (2016)	Chl-2	Wu, F. <i>et al.</i> , Dye. Pigment. 143, 356–360 (2017)	JY5	Wang, Z. <i>et al.</i> , Org. Electron. physics, Mater. Appl. 33, 142–149 (2016)	PDTSTTz-4
	Bashir, A. <i>et al.</i> , Nanoscale 10, 2341–2350 (2018)	Co ₃ O ₄	Rakstys, K. <i>et al.</i> , J. Am. Chem. Soc. 137, 16172–16178 (2015)	KR122	Ryu, S. <i>et al.</i> , Energy Environ. Sci. 7, 2614–2618 (2014)	PF8-TAA
	Guo, J. J. <i>et al.</i> , Synth. Met. 220, 462–468 (2016)	CoPcNO ₂ -Oph	Rakstys, K. <i>et al.</i> , J. Am. Chem. Soc. 137, 16172–16178 (2015)	KR131	Zhu, Z. <i>et al.</i> , Adv. Funct. Mater. 24, 7357–7365 (2014)	PFB
	Nagarjuna, P. <i>et al.</i> , Electrochim. Acta 151, 21–26 (2014)	Copolymer P	Rakstys, K. <i>et al.</i> , J. Am. Chem. Soc. 137, 16172–16178 (2015)	KR133	Zhu, Z. <i>et al.</i> , Adv. Funct. Mater. 24, 7357–7365 (2014)	PFO
	Nejand, B. A. <i>et al.</i> , ChemSusChem 9, 302–313 (2016)	Cu ₂ O	Rakstys, K. <i>et al.</i> , J. Am. Chem. Soc. 137, 16172–16178 (2015)	KR145	Liu, X. <i>et al.</i> , ChemSusChem 10, 968–975 (2017)	Ph-TPM

Table A.2 Explanation for the Term of “others” in Figure 4.22 (cont.).

	Article name	Instance	Article name	Instance	Article name	Instance
Others6	Huangfu, M. <i>et al.</i> , Appl. Surf. Sci. 357, 2234–2240 (2015)	CuI	Sun, M. <i>et al.</i> , Appl. Surf. Sci. 416, 124–132 (2017)	Me-BPZTPA	Xiao, J. <i>et al.</i> , RSC Adv. 4, 32918 (2014)	PNBA
	Sepalage, G. A. <i>et al.</i> , Adv. Funct. Mater. 25, 5650–5661 (2015)	CuI	Krishnamoorthy, T. <i>et al.</i> , J. Mater. Chem. A 2, 6305–6309 (2014)	KTM3	Ryu, S. <i>et al.</i> , Energy Environ. Sci. 7, 2614–2618 (2014)	PIF8-TAA
	Lv, M. <i>et al.</i> , ACS Appl. Mater. Interfaces 7, 17482–17488 (2015)	CuInS ₂	Chen, H. W. <i>et al.</i> , Sci. Rep. 6, 34319 (2016)	MEH-PPV	Cheng, M. <i>et al.</i> , Chem. Mater. 27, 1808–1814 (2015)	POZ2
	Lv, M. <i>et al.</i> , ACS Appl. Mater. Interfaces 7, 17482–17488 (2015)	CuInS ₂ /ZnS	Sun, M. <i>et al.</i> , Appl. Surf. Sci. 416, 124–132 (2017)	Me-QTPA	Cheng, M. <i>et al.</i> , Chem. Mater. 27, 1808–1814 (2015)	POZ3
	Sfyri, G. <i>et al.</i> , Appl. Surf. Sci. 360, 767–771 (2016)	CuMePc	Liu, Z. <i>et al.</i> , Dalt. Trans. 44, 3967–3973 (2015)	mNiO	Lee, J.-W. <i>et al.</i> , ChemPhysChem 15, 2595–2603 (2014)	PTB-BO
	Cheng, N. <i>et al.</i> , Electrochim. Acta 246, 990–996 (2017)	CuPc	Liu, Z. <i>et al.</i> , J. Mater. Chem. A 5, 6597–6605 (2017)	NiO _x	Lee, J.-W. <i>et al.</i> , ChemPhysChem 15, 2595–2603 (2014)	PTB-DCB21
	Torabi, N. <i>et al.</i> , Org. Electron. 48, 211–216 (2017)	CuPC	Nejand, B. A. <i>et al.</i> , ACS Appl. Mater. Interfaces 7, 21807–21818 (2015)	NiO _x	Grisorio, R. <i>et al.</i> ACS Energy Lett. 2, 1029–1034 (2017)	PTZ1
	Guo, J. J. <i>et al.</i> , Sol. Energy 155, 121–129 (2017)	CuPcNO ₂ -Oph	Choi, H. <i>et al.</i> , Chem. - A Eur. J. 20, 10894–10899 (2014)	OMeTPA-FA	Grisorio, R. <i>et al.</i> ACS Energy Lett. 2, 1029–1034 (2017)	PTZ2
	Yuan, M. <i>et al.</i> , Electrochim. Acta 215, 374–379 (2016)	CZTSe-QD	Choi, H. <i>et al.</i> , Chem. - A Eur. J. 20, 10894–10899 (2014)	OMeTPA-TPA	Cheng, H. <i>et al.</i> , Journal of Energy Chemistry (2017), doi:10.1016/j.jchem.2017.08.007	PTZDPP-2

Table A.2 Explanation for the Term of “others” in Figure 4.22 (cont.).

	Article name	Instance	Article name	Instance	Article name	Instance
Others6	Gong, G. <i>et al.</i> , Org. Electron. physics, Mater. Appl. 35, 171–175 (2016)	DEPT-SC	Xiao, M. <i>et al.</i> , J. Am. Chem. Soc. 139, 3378–3386 (2017)	P3DT	Zong, X. <i>et al.</i> , Tetrahedron 73, 3398–3405 (2017)	Q221
	Gong, G. <i>et al.</i> , J. Mater. Chem. A 4, 3661–3666 (2016)	DHPT-SC	Xiao, M. <i>et al.</i> , J. Am. Chem. Soc. 139, 3378–3386 (2017)	P3OT	Zong, X. <i>et al.</i> , Tetrahedron 73, 3398–3405 (2017)	Q222
	Bi, D. <i>et al.</i> , J. Phys. Chem. Lett. 4, 1532–1536 (2013)	DEH	Xiao, M. <i>et al.</i> , J. Am. Chem. Soc. 139, 3378–3386 (2017)	P3DDT	Jeon, N. J. <i>et al.</i> , J. Am. Chem. Soc. 135, 19087–19090 (2013)	Py-C
	Gong, G. <i>et al.</i> , J. Mater. Chem. A 4, 3661–3666 (2016)	DOPT-SC	Zhang, M.-D. <i>et al.</i> , Dye. Pigment. 146, 589–595 (2017)	PARA1	Wang, H. <i>et al.</i> , ACS Photonics 2, 849–855 (2015)	R01
	Liu, X. <i>et al.</i> , ChemSusChem 10, 968–975 (2017)	DPA-TPM	Gaml, E. A. <i>et al.</i> , Sol. Energy Mater. Sol. Cells 168, 8–13 (2017)	PBDTT-FTTE	Luo, Q. <i>et al.</i> , J. Mater. Chem. A 3, 15996–16004 (2015)	RGO-1
	Jeon, S. <i>et al.</i> , Org. Electron. physics, Mater. Appl. 37, 134–140 (2016)	DPIE	Etgar, L. <i>et al.</i> , J. Mater. Chem. A 2, 11586–11590 (2014)	PbS QDs	Luo, Q. <i>et al.</i> , J. Mater. Chem. A 3, 15996–16004 (2015)	RGO-2
	Jeon, S. <i>et al.</i> , Org. Electron. physics, Mater. Appl. 37, 134–140 (2016)	DPIO	Edri, E. <i>et al.</i> , J. Phys. Chem. Lett. 4, 897–902 (2013)	PCBM	Luo, Q. <i>et al.</i> , J. Mater. Chem. A 3, 15996–16004 (2015)	RGO-3
	Zheng, L. <i>et al.</i> , Chem. Commun. 50, 11196–11199 (2014)	DR3TBDT T	Bi, H. and Zhang, Y., Mater. Lett. 161, 767–769 (2015)	PCBM	Kang, M. S. <i>et al.</i> , ACS Appl. Mater. Interfaces 7, 22213–22217 (2015)	SGT-409
	Zheng, L. <i>et al.</i> , Chem. Commun. 50, 11196–11199 (2014)	DR3TBDT T-PDMS	Cai, B. <i>et al.</i> , Energy Environ. Sci. 6, 1480 (2013)	PCBTD PP	Kang, M. S. <i>et al.</i> , ACS Appl. Mater. Interfaces 7, 22213–22217 (2015)	SGT-410

Table A.2 Explanation for the Term of “others” in Figure 4.22 (cont.).

	Article name	Instance	Article name	Instance	Article name	Instance
Others6	Paek, S. <i>et al.</i> , <i>Adv. Mater.</i> 29, 1606555 (2017)	FA-CN	Heo, J. H. <i>et al.</i> , <i>Nat. Photonics</i> 7, 486–491 (2013)	PCDTBT	Su, P. Y. <i>et al.</i> , <i>Electrochim. Acta</i> 209, 529–540 (2016)	SP-01
	Christians, J. A. <i>et al.</i> , <i>Nat. Energy</i> 3, 68–74 (2018)	EH44	Pratyusha, T. <i>et al.</i> , <i>Mater. Today Proc.</i> 4, 6820–6826 (2017)	PCDTBT	Kang, M. S. <i>et al.</i> , <i>ACS Appl. Mater. Interfaces</i> 7, 22213–22217 (2015)	SGT-411
	Su, P. Y. <i>et al.</i> , <i>Electrochim. Acta</i> 209, 529–540 (2016)	SP-01-Co	Cheng, H. <i>et al.</i> , <i>Journal of Energy Chemistry</i> (2017), doi:10.1016/j.jechem.2017.08.007	TPADPP-2	Magomedov, A. <i>et al.</i> , <i>Adv. Funct. Mater.</i> 28, 1704351 (2018)	V911
	Su, P. Y. <i>et al.</i> , <i>Electrochim. Acta</i> 209, 529–540 (2016)	SP-02	Edri, E. <i>et al.</i> , <i>J. Phys. Chem. Lett.</i> 4, 897–902 (2013)	TPD	Magomedov, A. <i>et al.</i> , <i>Adv. Funct. Mater.</i> 28, 1704351 (2018)	V928
	Zhang, M.-D. <i>et al.</i> , <i>Dye. Pigment.</i> 146, 589–595 (2017)	SYN1	Do, K. <i>et al.</i> , <i>Chem. Commun.</i> 50, 10971–10974 (2014)	Triazine-Ph-OMeTPA	Magomedov, A. <i>et al.</i> , <i>Adv. Funct. Mater.</i> 28, 1704351 (2018)	V931
	Krishna, A. <i>et al.</i> , <i>Chem. Sci.</i> 5, 2702–2709 (2014)	T101	Do, K. <i>et al.</i> , <i>Chem. Commun.</i> 50, 10971–10974 (2014)	Triazine-Th-OMeTPA	Magomedov, A. <i>et al.</i> , <i>Adv. Funct. Mater.</i> 28, 1704351 (2018)	V946
	Krishna, A. <i>et al.</i> , <i>Chem. Sci.</i> 5, 2702–2709 (2014)	T102	Cao, J. <i>et al.</i> , <i>J. Am. Chem. Soc.</i> 137, 10914–10917 (2015)	TSHBC	Magomedov, A. <i>et al.</i> , <i>Adv. Funct. Mater.</i> 28, 1704351 (2018)	V957
	Krishna, A. <i>et al.</i> , <i>Chem. Sci.</i> 5, 2702–2709 (2014)	T103	Liu, J. <i>et al.</i> , <i>Energy Environ. Sci.</i> 7, 2963–2967 (2014)	TTF-1	Wu, F. <i>et al.</i> , <i>Dye. Pigment.</i> 143, 356–360 (2017)	X51
	Zhu, Z. <i>et al.</i> , <i>Adv. Funct. Mater.</i> 24, 7357–7365 (2014)	TFB	Magomedov, A. <i>et al.</i> , <i>Adv. Funct. Mater.</i> 28, 1704351 (2018)	V1039	Zhang, F. <i>et al.</i> , <i>Nano Energy</i> 41, 469–475 (2017)	Z25
	Huckaba, A. J. <i>et al.</i> , <i>Small Methods</i> 1, 1700250 (2017)	TiS ₂	Magomedov, A. <i>et al.</i> , <i>Adv. Funct. Mater.</i> 28, 1704351 (2018)	V885	Zhang, F. <i>et al.</i> , <i>Nano Energy</i> 41, 469–475 (2017)	Z26

Table A.2 Explanation for the Term of “others” in Figure 4.22 (cont.).

	Article name	Instance	Article name	Instance	Article name	Instance
Others6	Paek, S. <i>et al.</i> , Adv. Mater. 29, 1606555 (2017)	TPA-CN	Magomedov, A. <i>et al.</i> , Adv. Funct. Mater. 28, 1704351 (2018)	V908	Liu, Z. <i>et al.</i> , Dalt. Trans. 44, 3967–3973 (2015)	ZrO ₂
	Liu, X. <i>et al.</i> , ChemSusChem 10, 968–975 (2017)	TPA-TPM	Magomedov, A. <i>et al.</i> , Adv. Funct. Mater. 28, 1704351 (2018)	V886	Guo, J. J. <i>et al.</i> , Sol. Energy 155, 121–129 (2017)	ZnPcNO ₂ -Oph
	Cheng, H. <i>et al.</i> , Journal of Energy Chemistry (2017), doi:10.1016/j.jechem.2017.08.007	TPADPP-1				
	Article name	Instance	Article name	Instance	Article name	Instance
Others7	Badia, L. <i>et al.</i> , APL Mater. 2, 081507 (2014)	Ir	Koh, T. M. <i>et al.</i> , ChemSusChem 7, 1909–1914 (2014)	MY11	Wang, H. <i>et al.</i> , ACS Photonics 2, 849–855 (2015)	MY11
	Chen, C. <i>et al.</i> , ACS Energy Letters 2, 497–503 (2017)	Cu(bpcm)	Liu, Q. <i>et al.</i> , ChemSusChem 10, 3098–3104 (2017)	BPO		
	Article name	Instance	Article name	Instance	Article name	Instance
Others8	Zhang, H. <i>et al.</i> , Chem. Commun. 50, 5020 (2014)	BuPyIm-TFSI	Gong, G. <i>et al.</i> , Org. Electron. physics, Mater. Appl. 35, 171–175 (2016)	F4TCNQ	Lee, S. J. <i>et al.</i> , J. Am. Chem. Soc. 138, 3974–3977 (2016)	lutidiene+TBP
	Li, M. <i>et al.</i> , Adv. Energy Mater. 6, 1601156 (2016)	CuI	Mahmud, M. A. <i>et al.</i> , Phys. Chem. Chem. Phys. 19, 21033–21045 (2017)	F4TCNQ	Nguyen, W. H. <i>et al.</i> , J. Am. Chem. Soc. 136, 10996–11001 (2014)	spiro(TFSI) ₂ +TBP
	Li, M. <i>et al.</i> , Adv. Energy Mater. 6, 1601156 (2016)	CuSCN	Cao, J. <i>et al.</i> , J. Am. Chem. Soc. 137, 10914–10917 (2015)	graphene	Edri, E. <i>et al.</i> , J. Phys. Chem. Lett. 5, 429–433 (2014)	TBP
	Gaml, E. A. <i>et al.</i> , Sol. Energy Mater. Sol. Cells 168, 8–13 (2017)	DIO	Noel, N. K. <i>et al.</i> , Energy Environ. Sci. 7, 3061–3068 (2014)	H:TBP	Habisreutinger, S. N. <i>et al.</i> , Adv. Energy Mater. 7, 1601079 (2017)	TBP
	Guo, Y. <i>et al.</i> , J. Mater. Chem. A 2, 13827–13830 (2014)	D-TBP	Guarnera, S. <i>et al.</i> , J. Phys. Chem. Lett. 6, 432–437 (2015)	H-TFSI:Et ₄ N-TFSI	Huang, J. <i>et al.</i> , RSC Adv. 6, 55720–55725 (2016)	TFSI+TBP
	Christians, J. A. <i>et al.</i> , Nat. Energy 3, 68–74 (2018)	EH44-ox:TBP	Guarnera, S. <i>et al.</i> , J. Phys. Chem. Lett. 6, 432–437 (2015)	H-TFSI:Et ₄ N-TFSI+Al ₂ O ₃		

Table A.2 Explanation for the Term of “others” in Figure 4.22 (cont.).

	Article name	Instance	Article name	Instance	Article name	Instance
Others9	Amini, M. <i>et al.</i> , J. Mater. Chem. A 6, 2632–2642 (2018)	P123-ib	Hu, Q. <i>et al.</i> , ACS Nano 8, 10161–10167 (2014)	CS ₂ CO ₃	Liu, J. <i>et al.</i> , J. Mater. Chem. A 3, 11750–11755 (2015)	CdS
	Bera, A. <i>et al.</i> , ACS Appl. Mater. Interfaces 7, 12404–12411 (2015)	Zn ₂ SnO ₄	Hu, W. <i>et al.</i> , J. Mater. Chem. A 5, 1434–1441 (2017)	α-Fe ₂ O ₃	Liu, J. <i>et al.</i> , J. Mater. Chem. A 3, 11750–11755 (2015)	ZnS
	Chang, S. <i>et al.</i> , ACS Appl. Mater. Interfaces 8, 8511–8519 (2016)	IBF-Ep	Hu, W. <i>et al.</i> , J. Mater. Chem. A 5, 1434–1441 (2017)	In ₂ S ₃	Shin, S. S. <i>et al.</i> , J. Phys. Chem. Lett. 7, 1845–1851 (2016)	Zn ₂ SnO ₄
	Chen, T.-P. <i>et al.</i> , Adv. Energy Mater. 8, 1701722 (2018)	2D titania	Huang, J. <i>et al.</i> , Sol. Energy 133, 331–338 (2016)	FPDI	Song, J. <i>et al.</i> , Sol. Energy Mater. Sol. Cells 144, 623–630 (2016)	ZnO-SnO ₂
	Duan, J. <i>et al.</i> , Int. J. Energy Res. 40, 806–813 (2016)	TiO ₂ /ZnO/ TiO ₂	Huang, Y. T. <i>et al.</i> , Electrochim. Acta 236, 131–139 (2017)	Nb ₂ O ₅	Song, S. <i>et al.</i> , Nano Energy 28, 269–276 (2016)	PEIE
	Eze, V. O. <i>et al.</i> , Org. Electron. physics, Mater. Appl. 46, 253–262 (2017)	Wox	Jiang, J. <i>et al.</i> , J. Mater. Chem. A 5, 9514–9522 (2017)	ITIC	Sun, C. <i>et al.</i> , J. Alloys Compd. 722, 196–206 (2017)	BaSnO ₃
	Fernandes, S. L. <i>et al.</i> , Mater. Lett. 181, 103–107 (2016)	Nb ₂ O ₅	Juarez-Perez, E. J. <i>et al.</i> , J. Phys. Chem. Lett. 5, 680–685 (2014)	CdS	Tong, G. <i>et al.</i> , RSC Adv. 7, 19457–19463 (2017)	CdS
	Guerrero, A. <i>et al.</i> , J. Phys. Chem. C 120, 8023–8032 (2016)	Nb ₂ O ₅	Lee, W. <i>et al.</i> , Org. Electron. 51, 404–409 (2017)	PEIE-LiQ	Wang, K. <i>et al.</i> , J. Phys. Chem. Lett. 6, 755–759 (2015)	Wox
	Guo, Y. <i>et al.</i> , ACS Appl. Energy Mater. aesaem.8b00094 (2018). doi:10.1021/aesaem.8b00094	IL	Lee, Y. <i>et al.</i> , J. Mater. Chem. A 5, 12729–12734 (2017)	TiO ₂ -SnO ₂	Xie, X. <i>et al.</i> , Org. Electron. 44, 120–125 (2017)	PFN

Table A.2 Explanation for the Term of “others” in Figure 4.22 (cont.).

	Article name	Instance	Article name	Instance	Article name	Instance
Others9	Guo, Y. <i>et al.</i> , ACS Appl. Energy Mater. acsaem.8b00094 (2018). doi:10.1021/acsaem.8b00094	IL/PCBM	Li, D. <i>et al.</i> , Chem. Sci. 8, 4587–4594 (2017)	PFN-2TNDI	Yin, X. <i>et al.</i> , ACS Appl. Mater. Interfaces 8, 29580–29587 (2016)	TiZn ₂ O ₄
	Ha, S.-J. <i>et al.</i> , J. Mater. Chem. A 5, 1972–1977 (2017)	PS	Zheng, L. <i>et al.</i> , ACS Appl. Mater. Interfaces 9, 14129–14135 (2017)	PTEBS	Yoon, H. <i>et al.</i> , Energy Environ. Sci. 9, 2262–2266 (2016)	BCP
	Hou, Y. <i>et al.</i> , Adv. Funct. Mater. 27, 1700878 (2017)	TiO ₂ -SnO ₂	Liu, D. <i>et al.</i> , RSC Adv. 7, 8295–8302 (2017)	Cd ₂ SnO ₄	Zhang, H. <i>et al.</i> , J. Mater. Chem. A 4, 8724–8733 (2016)	PDI
	Article name	Instance	Article name	Instance	Article name	Instance
Others10	Ye, J. <i>et al.</i> , Sol. Energy 136, 505–514 (2016)	acetonitrile	Li, F. <i>et al.</i> , Adv. Funct. Mater. 28, 1706377 (2018)	N2200	Li, F. <i>et al.</i> , Adv. Funct. Mater. 28, 1706377 (2018)	PF1
	Han, F. <i>et al.</i> , Appl. Surf. Sci. 408, 34–37 (2017)	DMSO	Li, F. <i>et al.</i> , Adv. Funct. Mater. 28, 1706377 (2018)	PF0	Guo, J. J. <i>et al.</i> , Sol. Energy 155, 121–129 (2017)	toluene
	Li, F. <i>et al.</i> , Adv. Funct. Mater. 28, 1706377 (2018)	F-N2200				
	Article name	Instance	Article name	Instance	Article name	Instance
Others11	Cheng, N. <i>et al.</i> , J. Power Sources 319, 111–115 (2016)	IPA	Yu, Y. <i>et al.</i> , ACS Appl. Mater. Interfaces 9, 23624–23634 (2017)	n-hexane	Zhang, M. <i>et al.</i> , Sol. RRL 2, 1700213 (2018)	methoxybenzene
	Wang, L.-Y. <i>et al.</i> , Nanoscale 9, 17893–17901 (2017)	di-isopropyl ether	Sidhik, S. <i>et al.</i> , J. Phys. Chem. C 121, 4239–4245 (2017)	anhydrous ethoxyethane		
	Article name	Instance	Article name	Instance	Article name	Instance
Others12	Cao, K. <i>et al.</i> , Nano Energy 17, 171–179 (2015)	infiltration-dip	Gao, L.-L. <i>et al.</i> , J. Mater. Chem. A 5, 1548–1557 (2017)	spin-MAK	Nejand, B. A. <i>et al.</i> , J. Phys. Chem. C 120, 2520–2528 (2016)	sprayroll

Table A.2 Explanation for the Term of “others” in Figure 4.22 (cont.).

	Article name	Instance	Article name	Instance	Article name	Instance
Others12	Chen, H. <i>et al.</i> , Nano Energy 15, 216–226 (2015)	electrodeposition-dip	Razza, S. <i>et al.</i> , J. Power Sources 277, 286–291 (2015)	blade-dip	Kim, W. <i>et al.</i> , Electrochim. Acta 245, 734–741 (2017)	dip-spin
	Raminafshar, C. <i>et al.</i> , Electrochim. Acta 276, 261–267 (2018)	dripping	Kavadiya, S. <i>et al.</i> , Adv. Energy Mater. 7, 1700210 (2017)	spin-electrospay	Bansode, U. <i>et al.</i> , J. Phys. Chem. C 119, 9177–9185 (2015)	pulsed laser deposition
	Zhang, M. <i>et al.</i> , Chem. Commun. 51, 10038–10041 (2015)	blowdry	Matteocci, F. <i>et al.</i> , ACS Appl. Mater. Interfaces 7, 26176–26183 (2015)	blade-dip	Mathies, F. <i>et al.</i> , ACS Appl. Energy Mater. acaem.8b00222 (2018). doi:10.1021/acsaem.8b00222	printed
	Hwang, K. <i>et al.</i> , Adv. Mater. 27, 1241–1247 (2015)	slot-die	Kosta, I. <i>et al.</i> , Electrochim. Acta 246, 1193–1199 (2017)	electrodeposition-dip	Zheng, J. <i>et al.</i> , Sol. Energy Mater. Sol. Cells 168, 165–171 (2017)	blowdry
	He, M. <i>et al.</i> , Nat. Commun. 8, 16045 (2017)	meniscus assisted spin				
	Article name	Instance	Article name	Instance	Article name	Instance
Others13	Tavakoli, M. M. <i>et al.</i> , J. Phys. Chem. C 120, 19531–19536 (2016)	2D-graphene	Yu, X. <i>et al.</i> , J. Power Sources 325, 534–540 (2016)	mSiO ₂	Zuo, L. <i>et al.</i> , Nano Lett. 17, 269–275 (2017)	PA-SAM
	Zhang, W. <i>et al.</i> , Nano Lett. 13, 4505–4510 (2013)	Au@SiO ₂	Li, Y. <i>et al.</i> , RSC Adv. 5, 28424–28429 (2015)	mSnO ₂	An, Q. <i>et al.</i> , Nano Energy 39, 400–408 (2017)	PCBA
	Ye, Q.-Q. <i>et al.</i> , ACS Energy Lett. 3, 875–882 (2018)	bis-PCBM	Bera, A. <i>et al.</i> , J. Phys. Chem. C 118, 28494–28501 (2014)	mSrTiO ₃	Li, Y. <i>et al.</i> , J. Am. Chem. Soc. 137, 15540–15547 (2015)	PCBB-2CN-2C8
	Ye, Q.-Q. <i>et al.</i> , ACS Energy Lett. 3, 875–882 (2018)	bis-PCBM-DMC	Aeineh, N. <i>et al.</i> , ACS Appl. Mater. Interfaces 9, 13181–13187 (2017)	mTiO ₂	Cheng, Y. <i>et al.</i> , ACS Appl. Mater. Interfaces 7, 19986–19993 (2015)	PEI
	Zuo, L. <i>et al.</i> , J. Am. Chem. Soc. 137, 2674–2679 (2015)	C3-SAM	Bera, A. <i>et al.</i> , ACS Appl. Mater. Interfaces 7, 12404–12411 (2015)	mZn ₂ SnO ₄	Chen, B.X. <i>et al.</i> , J. Mater. Chem. A 4, 15662–15669 (2016)	polystyrene
	Guo, Y. <i>et al.</i> , Sol. Energy Mater. Sol. Cells 178, 186–192 (2018)	CdS	Mahmood, K. <i>et al.</i> , Nanoscale 6, 9127 (2014)	mZnO	Tavakoli, M. M. <i>et al.</i> , J. Phys. Chem. C 120, 19531–19536 (2016)	reduced graphene scaffolds
	Gu, Z. <i>et al.</i> , Sol. Energy Mater. Sol. Cells 140, 396–404 (2015)	CdS-nr	Lei, Y. <i>et al.</i> , J. Mater. Chem. A 4, 5474–5481 (2016)	mZnO	Kırbıyık, Ç. <i>et al.</i> , Appl. Surf. Sci. 423, 521–527 (2017)	SAM

Table A.2 Explanation for the Term of “others” in Figure 4.22 (cont.).

	Article name	Instance	Article name	Instance	Article name	Instance
Others13	Jiang, J. <i>et al.</i> , J. Mater. Chem. A 5, 9514–9522 (2017)	ITIC	Raminafshar, C. <i>et al.</i> , Electrochim. Acta 276, 261–267 (2018)	mZrO ₂	Zhou, P. <i>et al.</i> , Sol. Energy 137, 579–584 (2016)	SnO ₂ -ns
	Luo, Q. <i>et al.</i> , Adv. Funct. Mater. 27, 1702090 (2017)	m- α - Fe ₂ O ₃	Bi, D. <i>et al.</i> , RSC Adv. 3, 18762 (2013)	mZrO ₂	Hou, X. <i>et al.</i> , Sol. Energy Mater. Sol. Cells 149, 121–127 (2016)	ZnGa ₂ O ₄
	Mahmood, K. <i>et al.</i> , Nanoscale 6, 9127 (2014)	m-Al- ZnO	Guo, Y. <i>et al.</i> , ACS Appl. Energy Mater. 1, 2000 (2018).	Nb ₂ O ₅	Gao, C. <i>et al.</i> , Chem. Eng. J. 325, 378–385 (2017)	ZnO-SnO ₂ -ndt

Table A.3 Explanation for the Term of “others” in Figure 4.23.

	Article name	Instance	Article name	Instance	Article name	Instance
Others1	Liu, D. <i>et al.</i> , Adv. Sci., 5, 1700484 (2018)	H ₂ O	Zhang, J. <i>et al.</i> , Adv. Energy Mater., 8, 1701981 (2017)	LiI	Qing, J. <i>et al.</i> , Org. Electron. physics, Mater. Appl. 38, 144–149 (2016)	MACl
	Liu, C. <i>et al.</i> , Nanoscale, 9, 13967–13975 (2017)	C60				
Others2	Wu, W.-Q. <i>et al.</i> , Nat. Commun., 9, 1625 (2018)	F4TCNQ	Chung, C.-C. <i>et al.</i> , J. Mater. Chem. A 5, 13957–13965 (2017)	GO	Ran, C. <i>et al.</i> , J. Mater. Chem. A, 4, 8566–8572 (2016).	PCBM
	Wu, C.-G. <i>et al.</i> , Energy Environ. Sci. 8, 2725– 2733 (2015)	H ₂ O	Chang, C.-Y. <i>et al.</i> , J. Mater. Chem. A, 6, 4179–4188 (2018)	5F- PC61BM	Zuo, C. and Ding, L., Adv. Energy Mater. 7, 1601193 (2017)	NH ₄ Cl
	Jošt, M. <i>et al.</i> , ACS Photonics 4, 1232–1239 (2017)	HPA	Xia, Y. <i>et al.</i> , J. Mater. Chem. A 5, 3193–3202 (2017)	PbAc ₂ +H ₂ O	Gong, X. <i>et al.</i> , Adv. Funct. Mater. 25, 6671–6678 (2015)	H ₂ O
	Chang, C.-Y. <i>et al.</i> , J. Mater. Chem. A, 6, 4179–4188 (2018)	3F-PC61BM	Chen, Y. <i>et al.</i> , Chem. Mater. 27, 1448–1451 (2015)	NH ₄ Cl	Sun, C. <i>et al.</i> , Small 11, 3344–3350 (2015)	TPPI
	Alsari, M. <i>et al.</i> , Sci. Rep., 8, 5977 (2018)	HPA	Ling, L. <i>et al.</i> , Adv. Funct. Mater. 26, 5028– 5034 (2016)	PbAc ₂ +H ₂ O		
Others3	Bao, X. <i>et al.</i> , J. Power Sources 297, 53–58 (2015)	NMP	Chen, Q. <i>et al.</i> , Nano Lett. 17, 3231–3237 (2017)	Ag	Han, C. <i>et al.</i> , J. Mater. Chem. C (2018). doi:10.1039/C8TC01033A	ITIC
	Chen, Q. <i>et al.</i> , Nano Lett. 17, 3231–3237 (2017)	Ag	Chen, W. <i>et al.</i> , Org. Electron., 58, 283–289 (2018)	ASCl	Liu, X. <i>et al.</i> , Nano Energy 30, 417–425 (2016)	DFC60

Table A.3 Explanation for the Term of “others” in Figure 4.23(cont.).

	Article name	Instance	Article name	Instance	Article name	Instance
Others4	Chen, Q. <i>et al.</i> , Dye. Pigment., 147, 113–119 (2017)	TTA	Lou, Y.-H. and Wang, Z.-K., Nanoscale, 9, 13506–13514 (2017)	V ₂ O ₅	Wang, C. <i>et al.</i> , RSC Adv. 7, 29944–29952 (2017)	rub
	Chen, W.-Y. <i>et al.</i> , J. Mater. Chem. A 3, 19353–19359 (2015)	CuI	Lou, Y.-H. and Wang, Z.-K., Nanoscale, 9, 13506–13514 (2017)	MoO ₃	Wang, J. M. <i>et al.</i> , ACS Appl. Mater. Interfaces, 9, 13240–13246 (2017)	TS–CuPc
	Ge, J. <i>et al.</i> , J. Mater. Chem. A 5, 2920–2928 (2017)	Cu ₂ BaSnS ₄	Lou, Y.-H. and Wang, Z.-K., Nanoscale, 9, 13506–13514 (2017)	GeO ₂	Xu, X. <i>et al.</i> , J. Power Sources 360, 157–165 (2017)	polyTPD
	Igbari, F. <i>et al.</i> , J. Mater. Chem. A 4, 1326–1335 (2016)	CuAlO ₂	Lou, Y.-H. and Wang, Z.-K., Nanoscale, 9, 13506–13514 (2017)	CrO ₃	Yan, W. <i>et al.</i> , RSC Adv. 4, 33039 (2014)	polythiophene
	Kang, J. S. <i>et al.</i> , Advanced Energy Materials 8, 1703114 (2018)	CoN	Niu, G. <i>et al.</i> , J. Mater. Chem. A, 6, 4721–4728 (2018)	NiMgLiO	Yao, X. <i>et al.</i> , Org. Electron. physics, Mater. Appl. 47, 85–93 (2017)	Vox
	Kim, B. S. <i>et al.</i> , Org. Electron. physics, Mater. Appl. 17, 102–106 (2015)	MoO ₃	Niu, G. <i>et al.</i> , J. Mater. Chem. A, 6, 4721–4728 (2018)	NiMgLiO	Yeo, J.-S. <i>et al.</i> , Nano Energy 12, 96–104 (2015)	RGO
	Kim, J. <i>et al.</i> , Sci. Rep. 6, 27773 (2016)	NGO-NR	Rao, H. <i>et al.</i> , Nano Energy 27, 51–57 (2016)	CuO _x	Yu, J. C. <i>et al.</i> , Sci. Rep. 8, 1070 (2018)	PEDOT:GO
	Li, J. <i>et al.</i> , Nano Energy, 46, 331–337 (2018)	P3CT-K	Sun, W. <i>et al.</i> , Nanoscale 8, 10806–10813 (2016)	CuO _x	Yu, W. <i>et al.</i> , J. Power Sources 358, 29–38 (2017)	PEDOT:SAF
	Lin, Q. <i>et al.</i> , Adv. Opt. Mater., 5, 1600819 (2017)	PCDTBT	Sun, W. <i>et al.</i> , Nanoscale 8, 15954–15960 (2016)	CuI	Yu, W. <i>et al.</i> , Nanoscale 8, 6173–6179 (2016)	Cu ₂ O
	Lin, Q. <i>et al.</i> , Interfaces, 9, 9096–9101 (2017)	1	Tseng, Z. L. <i>et al.</i> , Sol. Energy 139, 484–488 (2016)	MoO _x	Yusoff, A. R. bin M. <i>et al.</i> , ChemSusChem, 9, 1736–1742 (2016)	DNA-CTMA
Liu, Z. <i>et al.</i> , Nano Energy, 28, 151–157 (2016)	P3HT	Tseng, Z. L. <i>et al.</i> , Sol. Energy 139, 484–488 (2016)	WO _x			
	Article name	Instance	Article name	Instance	Article name	Instance
Others5	Malinkiewicz, O. <i>et al.</i> , Adv. Energy Mater. 4, 1400345 (2014)	3TPYMB	Wang, N. <i>et al.</i> , Adv. Energy Mater. 7, 1700522 (2017)	HATNT	Karuppuswamy, P. <i>et al.</i> , Sol. Energy Mater. Sol. Cells 169, 78–85 (2017)	PDI-C60
	Erten-Ela, S. <i>et al.</i> , New J. Chem. 40, 2829–2834 (2016)	BAFB	Jeng, J. Y. <i>et al.</i> , Adv. Mater. 25, 3727–3732 (2013)	ICBA	Akbulatov, A. F. <i>et al.</i> , Adv. Energy Mater., 7, 1700476 (2017)	PDI-EH
	Qing, J. <i>et al.</i> , ACS Appl. Mater. Interfaces 7, 23110–23116 (2015)	BCP	Wang, Q. <i>et al.</i> , Energy Environ. Sci. 7, 2359–2365 (2014)	ICBA-C60	Wang, W. <i>et al.</i> , ACS Appl. Mater. Interfaces 7, 3994–3999 (2015)	PNDI2OD-TT

Table A.3 Explanation for the Term of “others” in Figure 4.23(cont.).

	Article name	Instance	Article name	Instance	Article name	Instance
Others5	Liu, J. <i>et al.</i> , ChemPhysChem 18, 617–625 (2017)	BCP	Lin, Y. <i>et al.</i> , Adv. Mater., 29, 1700607 (2017)	ICBA-tran3-C60	Wang, W. <i>et al.</i> , ACS Appl. Mater. Interfaces 7, 3994–3999 (2015)	PNVT-8
	Dai, S.-M. <i>et al.</i> , Inorganica Chim. Acta 468, 146–151 (2017)	BDNC	Gil-Escrig, L. <i>et al.</i> , Org. Electron. 37, 396–401 (2016)	IPH (fullerene)	Kaltenbrunner, M. <i>et al.</i> , Nat. Mater. 14, 1032–1039 (2015)	PTCDI
	Xue, Q. <i>et al.</i> , Adv. Energy Mater. 7, 1602333 (2017)	C60(CH2)	Chiang, Y.-H. <i>et al.</i> , J. Mater. Chem. A, 5, 25485–25493 (2017)	IZO	Mohd Yusoff, A. R. bin <i>et al.</i> , Nanoscale 8, 6328–6334 (2016)	Ru(acac)
	Zheng, X. <i>et al.</i> , Nat. Energy, 2, 17102 (2017)	choline chloride-C60	Wang, W. <i>et al.</i> , ACS Appl. Mater. Interfaces 7, 3994–3999 (2015)	N2200	Liu, C. <i>et al.</i> , J. Am. Chem. Soc., 140, 3825–3828 (2018)	ZnO+C60
	Chen, S. <i>et al.</i> , J. Power Sources 353, 123–130 (2017)	CoSe+PCBM	Heo, J. H. <i>et al.</i> , J. Mater. Chem. A, 5, 20615–20622 (2017)	NDI-PM	Mohd Yusoff, A. R. bin <i>et al.</i> , Nanoscale 8, 6328–6334 (2016)	Zr(acac)
	Dai, S.-M. <i>et al.</i> , Inorganica Chim. Acta 468, 146–151 (2017)	EDNC	Karuppuswamy, P. <i>et al.</i> , Sol. Energy Mater. Sol. Cells 169, 78–85 (2017)	PDI-C60		
	Article name	Instance	Article name	Instance	Article name	Instance
Others6	Xie, J. <i>et al.</i> , Nano Energy 28, 330–337 (2016)	PCBDAN	Kakavelakis, G. <i>et al.</i> , Adv. Energy Mater. 7, 1602120 (2017)	PFN	Sun, C. <i>et al.</i> , Small 11, 3344–3350 (2015)	TPPI
	Xia, Y. <i>et al.</i> , J. Mater. Chem. A 5, 3193–3202 (2017)	FPI-PEIE	Sun, C. <i>et al.</i> , Small 11, 3344–3350 (2015)	TPPI	Khatiwada, D. <i>et al.</i> , J. Phys. Chem. C 119, 25747–25753 (2015)	rhodamine
	Kim, G. H. <i>et al.</i> , Nano Lett., 17, 6385–6390 (2017)	EFGnPs-F	Fu, G. <i>et al.</i> , Sol. Energy Mater. Sol. Cells 165, 36–44 (2017)	TIPD	Sun, K. <i>et al.</i> , ACS Appl. Mater. Interfaces 7, 15314–15320 (2015)	rhodamine/C60/BCP/rhodamine/LiF
	Mamun, A. <i>et al.</i> , Phys. Chem. Chem. Phys. 19, 17960–17966 (2017)	carbon	Chen, W. <i>et al.</i> , J. Phys. Chem. Lett. 8, 591–598 (2017)	ZrAcAc	Kakavelakis, G. <i>et al.</i> , Adv. Energy Mater. 7, 1602120 (2017)	PFN
	Min, J. <i>et al.</i> , Chem. Mater. 27, 227–234 (2015)	PDINO	Xia, Y. <i>et al.</i> , J. Mater. Chem. A 5, 3193–3202 (2017)	FPI-PEIE		
	Article name	Instance	Article name	Instance	Article name	Instance
Others7	Yao, X. <i>et al.</i> , Org. Electron. physics, Mater. Appl. 47, 85–93 (2017)	APPA	Xue, Q. <i>et al.</i> , Adv. Energy Mater. 6, 1502021 (2016)	HSL2	Park, I. J. <i>et al.</i> , J. Phys. Chem. C 119, 27285–27290 (2015)	PEDOT:PSS
	Chen, W. <i>et al.</i> , J. Phys. Chem. Lett. 8, 591–598 (2017)	BPQDs	Xue, Q. <i>et al.</i> , Adv. Energy Mater. 6, 1502021 (2016)	HSL2	Igbari, F. <i>et al.</i> , J. Mater. Chem. A 4, 1326–1335 (2016)	PEDOT:PSS
	Bai, Y. <i>et al.</i> , Adv. Funct. Mater. 26, 2950–2958 (2016)	DEA	Chen, W. <i>et al.</i> , Energy Environ. Sci. 8, 629–640 (2015)	mAl ₂ O ₃	Lee, D.-Y. <i>et al.</i> , Nanoscale 8, 1513–1522 (2016)	PEDOT:PSS

Table A.3 Explanation for the Term of “others” in Figure 4.23(cont.).

	Article name	Instance	Article name	Instance	Article name	Instance
Others7	Li, D. <i>et al.</i> , Sol. Energy 131, 176–182 (2016)	GO	Chen, Y. <i>et al.</i> , ACS Appl. Mater. Interfaces 7, 4471–4475 (2015)	mTiO ₂	Liu, H. <i>et al.</i> , Org. Electron. physics, Mater. Appl. 47, 220–227 (2017)	PSSNa
	Xue, Q. <i>et al.</i> , Adv. Energy Mater. 6, 1502021 (2016)	HSL1	Kim, B. S. <i>et al.</i> , Org. Electron. physics, Mater. Appl. 17, 102– 106 (2015)	NPB	Wang, C. <i>et al.</i> , RSC Adv. 7, 29944–29952 (2017)	rub

Table B.1. F-test of Pooled Standard Deviations of Perovskite Layer Related Factors in Regular (n-i-p) Cells (cont.).

Anti-solvent	toluene		chlorobenzene		w/o anti-solvent	
	F	F _{critical}	F	F _{critical}	F	F _{critical}
diethyl ether	1.17	1.13	1.20	1.10	1.99	1.09
toluene			1.02	1.11	1.70	1.10
chlorobenzene					1.66	1.06

Table B.2. F-test of Pooled Standard Deviations of Other Layers in Regular Cells.

ETL	w/o ETL		doped-TiO ₂		ZnO		TiO ₂	
	F	F _{critical}	F	F _{critical}	F	F _{critical}	F	F _{critical}
SnO ₂	1.04	1.24	1.36	1.12	2.15	1.12	2.20	1.07
w/o ETL			1.31	1.28	2.06	1.28	2.12	1.26
doped-TiO ₂					1.58	1.14	1.62	1.11
ZnO							1.03	1.10
ETL-2	TiO ₂ -ns		doped-mTiO ₂		mTiO ₂		ETL-2=0	
	F	F _{critical}	F	F _{critical}	F	F _{critical}	F	F _{critical}
PCBM	1.06	1.13	1.11	1.14	1.26	1.11	1.38	1.11
TiO ₂ -ns			1.05	1.13	1.18	1.09	1.30	1.09
doped-mTiO ₂					1.13	1.10	1.24	1.10
mTiO ₂							1.10	1.04
HTL	PTAA		w/o HTL		spiro-MeOTAD		inorganic	
	F	F _{critical}	F	F _{critical}	F	F _{critical}	F	F _{critical}
P3HT	1.22	1.21	1.51	1.22	1.78	1.20	1.85	1.24
PTAA			1.24	1.13	1.46	1.09	1.52	1.15
w/o HTL					1.18	1.10	1.23	1.16
spiro-MeOTAD							1.04	1.12
HTL additive	LiTFSI+TBP+FK209		LiTFSI+TBP		w/o additive			
	F	F _{critical}	F	F _{critical}	F	F _{critical}		
LiTFSI+TBP+FK102	2.09	1.17	4.42	1.15	5.27	1.16		
LiTFSI+TBP+FK209			2.11	1.07	2.52	1.08		
LiTFSI+TBP					1.19	1.05		

Table B.2. F-test of Pooled Standard Deviations of Other Layers in Regular Cells
(cont.).

Back contact	Au		Ag	
	F	F _{critical}	F	F _{critical}
carbon	1.13	1.09	1.99	1.10
Au			1.77	1.04

Table B.3. F-test of Pooled Standard Deviations of Perovskite Related Factors in Inverted Cells

Perovskite	MAPbI _{3-x} Br _x		mixed cation		MAPbI ₃			
	F	F _{critical}	F	F _{critical}	F	F _{critical}		
MAPbI _{3-x} Cl _x	1.02	1.14	1.07	1.11	1.23	1.06		
MAPbI _{3-x} Br _x			1.05	1.17	1.21	1.15		
mixed cation					1.15	1.11		
Deposition procedure	two-step							
	F	F _{critical}						
one-step	1.53	1.07						
Deposition method	spin 2-3		spin		spin-dip			
	F	F _{critical}	F	F _{critical}	F	F _{critical}		
spin-spin	1.08	1.10	1.47	1.90	5.78	1.17		
spin 2-3			1.36	1.06	5.35	1.15		
spin					3.93	1.15		
Precursor solution	DMSO		DMSO+GBL		DMF		DMF+others	
	F	F _{critical}	F	F _{critical}	F	F _{critical}	F	F _{critical}
DMF+DMSO	1.04	1.14	1.13	1.09	1.42	1.08	1.65	1.11
DMSO			1.08	1.15	1.36	1.14	1.58	1.16
DMSO+GBL					1.26	1.08	1.47	1.11
DMF							1.17	1.10
Anti-solvent	chlorobenzene		w/o anti-solvent treatment		diethyl ether			
	F	F _{critical}	F	F _{critical}	F	F _{critical}		
toluene	1.54	1.09	2.07	1.08	2.52	1.15		
chlorobenzene			1.35	1.07	1.64	1.14		
w/o anti-solvent treatment					1.22	1.13		

Table B.4. F-test of Pooled Standard Deviations of Other Layers in Inverted Cells.

ETL	C60		PCBM							
	F	F _{critical}	F	F _{critical}						
PCBM+C60	1.26	1.14	1.52	1.13						
C60			1.21	1.08						
ETL-2	PEI		BCP		ETL-2=0					
	F	F _{critical}	F	F _{critical}	F	F _{critical}				
ZnO	1.81	1.18	2.18	1.14	2.35	1.13				
PEI			1.21	1.14	1.30	1.14				
BCP					1.07	1.07				
HTL	w/o HTL		PEDOT:PSS		NiO _x		PTAA		inorganic (NiO _x is included)	
	F	F _{critical}	F	F _{critical}	F	F _{critical}	F	F _{critical}	F	F _{critical}
doped- PEDOT:PS S	1.21	1.23	1.55	1.14	1.58	1.16	2.24	1.19	2.69	1.15
w/o HTL			1.28	1.20	1.31	1.21	1.85	1.24	2.22	1.20
PEDOT:PS S					1.02	1.08	1.44	1.13	1.73	1.06
NiO _x							1.42	1.15	1.70	1.09
PTAA									1.20	1.15
HTL-2	present									
	F	F _{critical}								
absent	1.53	1.10								
Back contact	Al		Cu		Au					
	F	F _{critical}	F	F _{critical}	F	F _{critical}				
Ag	1.11	1.05	1.21	1.13	4.01	1.24				
Al			1.10	1.13	3.63	1.24				
Cu					3.31	1.28				

APPENDIX C: ADDITIONAL INFORMATION ON ANALYSIS OF HYSTERESIS

Table C.1. Association Rule Mining for $HI \leq 0.01$ and $PCE \geq 10\%$ for Regular (n-i-p) Cells with Scan Rate ≤ 0.05 V/s.

Antecedent	Consequent	Support	Confidence	Lift	Data count
$HI \leq 0.01$ $PCE \geq 10\%$ $Scan\ rate \leq 0.05\ V/s$	Back contact=others (IZO*)	0.01	0.06	6.11	1
	HTL=no	0.02	0.11	6.11	2
	ETL=ZnO	0.04	0.22	4.07	4
	Precursor solution=GBL	0.01	0.06	3.06	1
	ETL=0	0.01	0.06	3.06	1
	Precursor solution=DMF+others (HI)	0.01	0.06	3.06	1
	ETL=others (Nb ₂ O ₅ , PCBM)	0.02	0.11	3.06	2
	ETL-2=others (ZnO-nanorod, ZnO-N-nanorod)	0.02	0.11	3.06	2
	ETL-2=doped-mTiO ₂	0.06	0.39	2.52	7
	Back contact=carbon	0.02	0.11	2.44	2
	Deposition method=spin-spin	0.05	0.28	2.35	5
	Anti-solvent treatment=trifluorotoluene	0.05	0.28	2.35	5
	HTL additive=no	0.03	0.17	1.83	3
	Deposition procedure=two-step	0.06	0.39	1.58	7
	HTL additive=LiTFSI+TBP+FK209	0.06	0.39	1.53	7
	HTL=others **	0.05	0.28	1.39	5
	Precursor solution=DMF	0.07	0.44	1.29	8
	Perovskite=mixed cation	0.07	0.44	1.25	8
	Back contact=Ag	0.05	0.33	1.22	6
	Anti-solvent treatment=no	0.09	0.56	1.18	10
	HTL=PTAA	0.01	0.06	1.02	1
	Deposition method=spin-dip	0.02	0.11	1.02	2
	Perovskite=MAPbI ₃	0.08	0.50	0.95	9
	Deposition method=spin	0.07	0.44	0.94	8
	Precursor solution=DMF+DMSO	0.06	0.39	0.86	7
	Deposition procedure=one-step	0.10	0.61	0.81	11
	ETL=TiO ₂	0.10	0.61	0.77	11
	HTL=spiro-OMeTAD	0.09	0.56	0.76	10
	Anti-solvent treatment=toluene	0.01	0.06	0.76	1
	Precursor solution=DMSO+GBL	0.01	0.06	0.76	1
	Back contact=Au	0.08	0.50	0.75	9
	HTL additive=LiTFSI+TBP	0.07	0.44	0.73	8
	ETL-2=mTiO ₂	0.05	0.28	0.66	5
	Deposition method=spin 2-3	0.03	0.17	0.63	3
ETL-2=0	0.04	0.22	0.58	4	
Perovskite=MAPbI _{3-x} Cl _x	0.01	0.06	0.56	1	
Anti-solvent treatment=chlorobenzene	0.02	0.11	0.45	2	

*IZO: sputtered amorphous indium zinc oxide
**others: Diphenylamine-substituted carbazole-based derivatives(V885, V886, V908, V911, V946)

Table C.2. Association Rule Mining for $HI \leq 0.05$ and $PCE \geq 10\%$ for Regular (n-i-p) Cells with Scan Rate ≤ 0.05 V/s.

Antecedent	Consequent	Support	Confidence	Lift	Data count
$HI \leq 0.05$ $PCE \geq 10\%$ Scan rate \leq 0.05 V/s	Deposition method=spin-meniscus asissted	0.01	0.02	2.68	1
	Precursor solution=DMSO+GBL+HaHc*	0.01	0.02	2.68	1
	Anti-solvent treatment=ethylacetate	0.01	0.02	2.68	1
	Back contact=others (IZO**)	0.01	0.02	2.68	1
	Precursor solution=GBL	0.02	0.05	2.68	2
	HTL=no	0.02	0.05	2.68	2
	ETL-2=doped-mTiO ₂	0.13	0.34	2.21	14
	Anti-solvent treatment=trifluorotoluene	0.09	0.24	2.06	10
	HTL=PTAA	0.04	0.10	1.79	4
	ETL=ZnO	0.04	0.10	1.79	4
	Deposition method=spin-spin	0.07	0.20	1.65	8
	HTL=others***	0.11	0.29	1.46	12
	HTL additive=LiTFSI+TBP+FK209	0.14	0.37	1.44	15
	ETL=0	0.01	0.02	1.34	1
	Precursor solution=DMF+others (HI)	0.01	0.02	1.34	1
	ETL=others (Nb ₂ O ₅ , PCBM)	0.02	0.05	1.34	2
	ETL-2=others (ZnO-nanorod, ZnO-N-nanorod)	0.02	0.05	1.34	2
	HTL additive=no	0.05	0.12	1.34	5
	Perovskite=mixed cation	0.16	0.44	1.24	18
	Anti-solvent treatment=no	0.21	0.56	1.19	23
	Deposition procedure=two-step	0.10	0.27	1.09	11
	Back contact=carbon	0.02	0.05	1.07	2
	Precursor solution=DMF	0.14	0.37	1.06	15
	Back contact=Au	0.25	0.68	1.03	28
	ETL=TiO ₂	0.30	0.80	1.02	33
	Precursor solution=DMSO	0.03	0.07	1.01	3
	Deposition method=spin	0.17	0.46	0.98	19
	Perovskite=MAPbI _{3-x} Cl _x	0.04	0.10	0.98	4
	Deposition procedure=one-step	0.27	0.73	0.97	30
	Deposition method=spin 2-3	0.09	0.24	0.93	10
	Precursor solution=DMF+DMSO	0.15	0.41	0.91	17
	ETL=SnO ₂	0.01	0.02	0.89	1
	HTL additive=others (BCF****)	0.01	0.02	0.89	1
	Back contact=Ag	0.09	0.24	0.89	10
	Perovskite=MAPbI ₃	0.17	0.46	0.88	19
	HTL additive=LiTFSI+TBP	0.18	0.49	0.80	20
	HTL=spiro-OMeTAD	0.21	0.56	0.77	23
	ETL-2=0	0.11	0.29	0.77	12
	ETL-2=mTiO ₂	0.12	0.32	0.76	13
	Anti-solvent treatment=toluene	0.02	0.05	0.67	2
	Precursor solution=DMSO+GBL	0.02	0.05	0.67	2
	Deposition method=spin-dip	0.03	0.07	0.67	3
Anti-solvent treatment=chlorobenzene	0.04	0.10	0.40	4	
Anti-solvent treatment=diethyl ether	0.01	0.02	0.38	1	

Table C.2. Association Rule Mining for $HI \leq 0.05$ and $PCE \geq 10\%$ for Regular (n-i-p) Cells with Scan Rate ≤ 0.05 V/s (cont.).

<p>*HaHc: hydroxylamine hydrochloride **IZO: sputtered amorphous indium zinc oxide ***others: poly[(2,5-bis(2-hexyldecyloxy)phenylene)-alt-(5,6-difluoro-4,7-di(thiophen-2-yl)benzo[c][1,2,5]-thiadiazole) (PPDT2FBT), a novel N-phenylindole-diketopyrrolopyrrole-containing narrow band-gap material (DPIO), Dimethoxydiphenylamine-substituted dispiro-oxepine derivative 2,2',7,7'-tetrakis-(N,N'-di-4-methoxyphenylamine)dispiro-[fluorene-9,4'-dithieno[3,2-c:2',3'-e]oxepine-6',9''-fluorene] (DDOF), Diphenylamine-substituted carbazole-based derivatives (V885, V886, V908, V911, V928, V931, V946, V957, V1039) ****BCF: tris(pentafluorophenyl)borane</p>
--

Table C.3. Association Rule Mining for $HI \leq 0.01$ for Regular (n-i-p) Cells with Scan Rate ≤ 0.05 V/s (without PCE restriction)

Antecedent	Consequent	Support	Confidence	Lift	Data count
$HI \leq 0.01$ Scan rate ≤ 0.05 V/s	ETL=ZnO	0.03	0.20	4.30	4
	HTL=no	0.02	0.15	3.87	3
	ETL=0	0.01	0.05	3.23	1
	Back contact=others (IZO*)	0.01	0.05	3.23	1
	ETL=others (Nb ₂ O ₅ , PCBM)	0.02	0.10	3.23	2
	ETL-2=others (ZnO-nanorod, ZnO-N-nanorod)	0.02	0.10	3.23	2
	ETL-2=doped-mTiO ₂	0.05	0.35	2.66	7
	Anti-solvent treatment=trifluorotoluene	0.04	0.25	2.30	5
	Precursor solution=GBL	0.01	0.05	2.15	1
	Precursor solution=DMF+others (HI)	0.01	0.05	2.15	1
	Back contact=carbon	0.02	0.10	2.15	2
	Deposition method=spin-spin	0.05	0.30	2.15	6
	HTL additive=no	0.04	0.25	2.02	5
	Deposition procedure=two-step	0.06	0.40	1.47	8
	HTL=others**	0.05	0.30	1.43	6
	HTL additive=LiTFSI+TBP+FK209	0.05	0.35	1.37	7
	Perovskite=mixed cation	0.06	0.40	1.29	8
	Precursor solution=DMF	0.07	0.45	1.24	9
	Back contact=Ag	0.05	0.30	1.21	6
	Anti-solvent treatment=no	0.09	0.55	1.09	11
	HTL=PTAA	0.01	0.05	1.08	1
	Deposition method=spin	0.07	0.45	1.02	9
	Perovskite=MAPb _{1-x} Cl _x	0.02	0.10	0.99	2
	Precursor solution=DMF+DMSO	0.06	0.40	0.94	8
	Perovskite=MAPbI ₃	0.08	0.50	0.93	10
	Deposition method=spin-dip	0.02	0.10	0.86	2
	Deposition procedure=one-step	0.09	0.60	0.82	12
	Anti-solvent treatment=diethyl ether	0.01	0.05	0.81	1
	Anti-solvent treatment=toluene	0.01	0.05	0.81	1
	Back contact=Au	0.09	0.55	0.81	11
	ETL=TiO ₂	0.10	0.65	0.79	13
	Precursor solution=DMSO+GBL	0.01	0.05	0.72	1
	ETL-2=mTiO ₂	0.05	0.35	0.72	7
HTL=spiro-OMeTAD	0.08	0.50	0.71	10	
HTL additive=LiTFSI+TBP	0.06	0.40	0.69	8	

Table C.3. Association Rule Mining for $HI \leq 0.01$ for Regular (n-i-p) Cells with Scan Rate ≤ 0.05 V/s (without PCE restriction)

Antecedent	Consequent	Support	Confidence	Lift	Data count
$HI \leq 0.01$ Scan rate ≤ 0.05 V/s	ETL-2=0	0.03	0.20	0.59	4
	Deposition method=spin 2-3	0.02	0.15	0.55	3
	Anti-solvent treatment=chlorobenzene	0.02	0.10	0.42	2
*IZO: sputtered amorphous indium zinc oxide **others: Diphenylamine-substituted carbazole-based derivatives (V885, V886, V908, V911, V946), a novel N-phenylindole-diketopyrrolopyrrole-containing narrow band-gap material (DPIE)					

Table C.4. Association Rule Mining for $HI \leq 0.05$ for Regular (n-i-p) Cells with Scan Rate ≤ 0.05 V/s (without PCE restriction)

Antecedent	Consequent	Support	Confidence	Lift	Data count
$HI \leq 0.05$ Scan rate ≤ 0.05 V/s	Deposition method=spin-meniscus assisted	0.01	0.02	2.69	1
	Precursor solution=DMSO+GBL+HaHe*	0.01	0.02	2.69	1
	Anti-solvent treatment=ethylacetate	0.01	0.02	2.69	1
	Back contact=others (IZO**, NbS ₂)	0.02	0.04	2.69	2
	ETL-2=doped-mTiO ₂	0.11	0.29	2.21	14
	HTL=no	0.03	0.08	2.15	4
	Anti-solvent treatment=trifluorotoluene	0.09	0.23	2.11	11
	Precursor solution=GBL	0.02	0.04	1.79	2
	HTL=PTAA	0.03	0.08	1.79	4
	ETL=ZnO	0.03	0.08	1.79	4
	HTL additive=no	0.07	0.19	1.51	9
	Deposition method=spin-spin	0.08	0.21	1.49	10
	HTL additive=LiTFSI+TBP+FK209	0.14	0.38	1.47	18
	HTL=others***	0.11	0.29	1.39	14
	Perovskite=FA based	0.01	0.02	1.34	1
	ETL=0	0.01	0.02	1.34	1
	ETL=others (Nb ₂ O ₅ , PCBM)	0.02	0.04	1.34	2
	ETL-2=others (ZnO-nanorod, ZnO-N-nanorod)	0.02	0.04	1.34	2
	Back contact=carbon	0.02	0.06	1.34	3
	Perovskite=mixed cation	0.15	0.40	1.28	19
	Deposition procedure=two-step	0.12	0.31	1.15	15
	Anti-solvent treatment=no	0.21	0.56	1.12	27
	Precursor solution=DMSO	0.03	0.08	1.08	4
	Perovskite=MAPbI _{3-x} Cl _x	0.04	0.10	1.03	5
	Precursor solution=DMF	0.14	0.38	1.03	18
	ETL=TiO ₂	0.31	0.83	1.01	40
	Back contact=Au	0.26	0.69	1.01	33
	Precursor solution=DMF+DMSO	0.16	0.42	0.98	20
	Deposition procedure=one-step	0.26	0.69	0.94	33
	Deposition method=spin	0.16	0.42	0.94	20
	Deposition method=spin 2-3	0.09	0.25	0.92	12
	HTL additive=others (BCF****)	0.01	0.02	0.90	1
Precursor solution=DMF+others (HI)	0.01	0.02	0.90	1	
ETL=SnO ₂	0.01	0.02	0.90	1	

Table C.4. Association Rule Mining for $HI \leq 0.05$ for Regular (n-i-p) Cells with Scan Rate ≤ 0.05 V/s (without PCE restriction) (cont.).

Antecedent	Consequent	Support	Confidence	Lift	Data count
$HI \leq 0.05$ Scan rate ≤ 0.05 V/s	Deposition method=spin-dip	0.04	0.10	0.90	5
	Perovskite=MAPbI ₃	0.18	0.48	0.90	23
	ETL-2=mTiO ₂	0.16	0.42	0.85	20
	Back contact=Ag	0.08	0.21	0.84	10
	HTL=spiro-OMeTAD	0.20	0.54	0.77	26
	ETL-2=0	0.09	0.25	0.73	12
	HTL additive=LiTFSI+TBP	0.16	0.42	0.72	20
	Anti-solvent treatment=diethyl ether	0.02	0.04	0.67	2
	Anti-solvent treatment=toluene	0.02	0.04	0.67	2
	Precursor solution=DMSO+GBL	0.02	0.04	0.60	2
Anti-solvent treatment=chlorobenzene	0.04	0.10	0.43	5	
<p>*HaHc: hydroxylamine hydrochloride **IZO: sputtered amorphous indium zinc oxide ***others: poly[(2,5-bis(2-hexyldecyloxy)phenylene)-alt-(5,6-difluoro-4,7-di(thiophen-2-yl)benzo[c][1,2,5]-thiadiazole) (PPDT2FBT), novel N-phenylindole-diketopyrrolopyrrole-containing narrow band-gap materials (DPIE, DPIO), Dimethoxydiphenylamine-substituted dispiro-oxepine derivative 2,2',7,7'-tetrakis-(N,N'-di-4-methoxyphenylamine)dispiro-[fluorene-9,4'-dithieno[3,2-c:2',3'-e]oxepine-6',9''-fluorene] (DDOF), 5,10,15-trihexyl-3,8,13-trimethoxy-10,15-dihydro-5H-diindolo[3,2-a:3',2'-c]carbazole (KR122), diphenylamine-substituted carbazole-based derivatives (V885, V886, V908, V911, V928, V931, V946, V957, V1039) ****BCF: tris(pentafluorophenyl)borane</p>					

Table C.5. Association Rule Mining for $HI \leq 0.01$ and $PCE \geq 10\%$ for Regular (n-i-p) Cells with Various Scan Rates.

Antecedent	Consequent	Support	Confidence	Lift	Data count
$HI \leq 0.01$ $PCE \geq 10\%$	Back contact=others (IZO*)	0.00	0.05	5.57	1
	HTL=no	0.01	0.09	4.45	2
	Anti-solvent treatment=trifluorotoluene	0.02	0.23	4.28	5
	ETL=ZnO	0.02	0.18	4.05	4
	ETL=0	0.00	0.05	3.71	1
	ETL=others (PCBM, PTEBS**, Nb ₂ O ₅)	0.01	0.14	3.34	3
	ETL-2=doped-mTiO ₂	0.03	0.32	3.00	7
	Precursor solution=GBL	0.00	0.05	2.78	1
	Back contact=carbon	0.01	0.09	2.78	2
	Deposition method=spin-spin	0.02	0.27	2.39	6
	ETL-2=TiO ₂ -ns	0.00	0.05	2.23	1
	HTL=others***	0.02	0.23	1.99	5
	HTL additive=LiTFSI+TBP+FK209	0.03	0.36	1.98	8
	Perovskite=mixed cation	0.04	0.45	1.95	10
	Scan rate=1-20V/s	0.00	0.05	1.86	1
	Precursor solution=DMF+DMSO+others (KI)	0.00	0.05	1.86	1
	HTL=PTAA	0.00	0.05	1.86	1
	Scan rate=0.005-0.05V/s	0.07	0.82	1.82	18
	ETL-2=others (ZnO-nanorod, ZnO-N-nanorod)	0.01	0.09	1.71	2
	HTL additive=no	0.01	0.14	1.67	3
Back contact=Ag	0.03	0.32	1.34	7	

Table C.5. Association Rule Mining for $HI \leq 0.01$ and $PCE \geq 10\%$ for Regular (n-i-p) Cells with Various Scan Rates (cont.).

Antecedent	Consequent	Support	Confidence	Lift	Data count
HI < 0.01 PCE ≥ 10%	Deposition procedure=two-step	0.04	0.41	1.27	9
	Precursor solution=DMF	0.04	0.45	1.11	10
	Precursor solution=DMF+DMSO	0.03	0.36	1.02	8
	ETL-2=mTiO ₂	0.03	0.32	0.94	7
	Anti-solvent treatment=no	0.05	0.55	0.93	12
	Deposition method=spin 2-3	0.02	0.18	0.91	4
	Deposition method=spin	0.04	0.41	0.88	9
	Deposition procedure=one-step	0.05	0.59	0.87	13
	Perovskite= MAPbI ₃	0.04	0.50	0.86	11
	Precursor solution=DMF+others (HI)	0.00	0.05	0.86	1
	Deposition method=spin-dip	0.01	0.14	0.84	3
	ETL=TiO ₂	0.06	0.64	0.81	14
	Back contact=Au	0.05	0.55	0.78	12
	HTL=spiro-OMeTAD	0.06	0.64	0.76	14
	Anti-solvent treatment=toluene	0.00	0.05	0.74	1
	HTL additive=LiTFSI+TBP	0.04	0.50	0.74	11
	Anti-solvent treatment=chlorobenzene	0.01	0.14	0.71	3
	Precursor solution=DMSO+GBL	0.00	0.05	0.66	1
	ETL-2=0	0.02	0.23	0.52	5
	Anti-solvent treatment=diethylether	0.00	0.05	0.48	1
	Scan rate=0.05-0.1V/s	0.01	0.09	0.37	2
	Perovskite=MAPbI _{3-x} Cl _x	0.00	0.05	0.30	1
	Scan rate=0.1-0.5V/s	0.00	0.05	0.19	1

*IZO: sputtered amorphous indium zinc oxide
**PTEBS: polythiophene derivative sodium poly[2-(3-thienyl)ethoxy-4-butylsulfonate]
***others: diphenylamine-substituted carbazole-based derivatives (V885, V886, V908, V911, V946)

Table C.6. Association Rule Mining for $HI \leq 0.05$ and $PCE \geq 10\%$ for Regular (n-i-p) Cells with Various Scan Rates.

Antecedent	Consequent	Support	Confidence	Lift	Data count
HI < 0.05 PCE ≥ 10%	Anti-solvent treatment=ethylacetate	0.00	0.01	3.36	1
	Anti-solvent treatment=ethoxyethane	0.00	0.01	3.36	1
	Precursor solution=DMSO+GBL+HaHc*	0.00	0.01	3.36	1
	Deposition method=spin-meniscus asissted	0.00	0.01	3.36	1
	Precursor solution=GBL	0.02	0.05	3.36	4
	Anti-solvent treatment=trifluorotoluene	0.04	0.14	2.58	10
	HTL=PTAA	0.02	0.05	2.24	4
	ETL-2=doped-mTiO ₂	0.07	0.23	2.19	17
	HTL=no	0.01	0.04	2.01	3
	ETL-2=TiO ₂ -ns	0.01	0.04	2.01	3
	ETL-2=others (ZnO-nanorod, ZnO-N-nanorod, mZn ₂ SnO ₄ , Rgs**, SiO ₂ , C60)	0.03	0.10	1.81	7
	Precursor solution=DMF+DMSO+others (KL ₂ Pb(SCN) ₂)	0.01	0.04	1.68	3
	HTL=others*****	0.06	0.19	1.68	14

Table C.6. Association Rule Mining for $HI \leq 0.05$ and $PCE \geq 10\%$ for Regular (n-i-p) Cells with Various Scan Rates (cont.).

Antecedent	Consequent	Support	Confidence	Lift	Data count
$HI \leq 0.05$ $PCE \geq 10\%$	Back contact=others (IZO***)	0.00	0.01	1.68	1
	ETL= doped-SnO ₂	0.00	0.01	1.68	1
	HTL additive=others (BCF****, LiTFSI+TBP+Co(II)TFSI)	0.01	0.03	1.68	2
	Deposition method=spin-spin	0.05	0.16	1.44	12
	Perovskite=mixed cation	0.10	0.33	1.41	24
	ETL=others (PCBM, PTEBS*****, Nb ₂ O ₅ , Zn ₂ SnO ₄)	0.02	0.05	1.34	4
	HTL additive=no	0.03	0.11	1.34	8
	HTL additive=LiTFSI+TBP+FK209	0.07	0.25	1.34	18
	Back contact=carbon	0.01	0.04	1.26	3
	Scan rate=0.005-0.05 V/s	0.17	0.56	1.25	41
	Deposition method=spin 2-3	0.07	0.25	1.23	18
	ETL= ZnO	0.02	0.05	1.22	4
	ETL=0	0.00	0.01	1.12	1
	ETL-2= PCBM	0.01	0.03	1.12	2
	Anti-solvent treatment=toluene	0.02	0.07	1.12	5
	Back contact=Ag	0.08	0.26	1.10	19
	Deposition procedure=one-step	0.21	0.71	1.05	52
	Precursor solution=DMF+DMSO	0.11	0.37	1.04	27
	ETL=TiO ₂	0.24	0.81	1.03	59
	Anti-solvent treatment=diethyl ether	0.03	0.10	1.02	7
	Scan rate=0.05-0.1 V/s	0.07	0.25	0.99	18
	Precursor solution=DMSO+GBL	0.02	0.07	0.99	5
	Deposition method=spin	0.13	0.45	0.97	33
	Anti-solvent treatment=no	0.17	0.56	0.96	41
	Back contact=Au	0.20	0.67	0.96	49
	Perovskite=MAPbI ₃	0.16	0.55	0.95	40
	ETL=SnO ₂	0.01	0.04	0.92	3
	Precursor solution=DMSO	0.01	0.04	0.92	3
	HTL additive=LiTFSI+TBP	0.18	0.62	0.91	45
	Precursor solution=DMF	0.11	0.37	0.91	27
	Deposition procedure=two-step	0.09	0.29	0.89	21
	ETL-2=mTiO ₂	0.09	0.29	0.85	21
	HTL=spiro-OMeTAD	0.21	0.71	0.85	52
	Back contact=Ag-Al	0.00	0.01	0.84	1
	Precursor solution=DMF+others (HI, Al, 4MSA*****)	0.01	0.04	0.77	3
	Scan rate=0.5-1 V/s	0.01	0.03	0.75	2
	Perovskite=MAPbI _{3-x} Cl _x	0.03	0.11	0.73	8
	ETL-2=0	0.09	0.32	0.72	23
	Deposition method=spin-dip	0.03	0.11	0.67	8
	Scan rate=0.1-0.5 V/s	0.04	0.15	0.63	11
	Anti-solvent treatment=chlorobenzene	0.03	0.11	0.57	8
	Scan rate=1-20 V/s	0.00	0.01	0.56	1
Deposition method=vasp	0.00	0.01	0.56	1	
Perovskite=FA based	0.00	0.01	0.48	1	
ETL= doped-TiO ₂	0.00	0.01	0.42	1	

Table C.6. Association Rule Mining for $HI \leq 0.05$ and $PCE \geq 10\%$ for Regular (n-i-p) Cells with Various Scan Rates (cont.).

*HaHc: hydroxylamine hydrochloride
**Rgs: Reduced graphene scaffold
***IZO: sputtered amorphous indium zinc oxide
****BCF: tris(pentafluorophenyl)borane
*****others: poly[(2,5-bis(2-hexyldecyloxy)phenylene)-alt-(5,6-difluoro-4,7-di(thiophen-2-yl)benzo[c][1,2,5]-thiadiazole) (PPDT2FBT), a novel N-phenylindole-diketopyrrolopyrrole-containing narrow band-gap material (DPIO), Dimethoxydiphenylamine-substituted dispiro-oxepine derivative 2,2',7,7'-tetrakis-(N,N'-di-4-methoxyphenylamine)dispiro-[fluorene-9,4'-dithieno[3,2-c:2',3'-e]oxepine-6',9''-fluorene] (DDOF), diphenylamine-substituted carbazole-based derivatives (V885, V886, V908,V911, V928, V931, V946, V957, V1039), 4,4'-(10-(4-methoxyphenyl)-9,9-dimethyl-9,10-dihydroacridine-2,7-diyl)bis(N,Nbis(4-methoxyphenyl)aniline) (ACR-TPA), a novel carbazole-based HTL including extended π -conjugated central core+hexyloxy flexible group (SGT-410)
*****PTEBS: polythiophene derivative sodium poly[2-(3-thienyl)ethyloxy-4-butylsulfonate]
*****4MSA: 4-methylbenzenesulfonic acid

Table C.7. Association Rule Mining for $HI \leq 0.01$ for Regular (n-i-p) Cells with Various Scan Rates (without PCE restriction).

Antecedent	Consequent	Support	Confidence	Lift	Data count
HI \leq 0.01	Anti-solvent treatment=trifluorotoluene	0.02	0.20	4.20	5
	ETL=0	0.00	0.04	3.92	1
	Back contacy=others (IZO*)	0.00	0.04	3.92	1
	ETL= ZnO	0.01	0.16	3.62	4
	ETL=others (PCBM, PTEBS**, Nb ₂ O ₅)	0.01	0.12	3.53	3
	Back contact=carbon	0.01	0.12	3.21	3
	ETL-2= doped-mTiO ₂	0.02	0.28	3.05	7
	HTL=no	0.01	0.12	2.94	3
	ETL-2=TiO ₂ -ns	0.00	0.04	2.35	1
	Precursor solution=GBL	0.00	0.04	2.35	1
	Deposition method=spin-spin	0.02	0.28	2.29	7
	HTL=others***	0.02	0.28	2.22	7
	Perovskite=mixed cation	0.03	0.40	1.99	10
	Precursor solution=DMF+DMSO+others (KI)	0.00	0.04	1.96	1
	HTL additive=no	0.02	0.24	1.91	6
	HTL additive=LiTFSI+TBP+FK209	0.03	0.32	1.88	8
	Scan rate=0.005-0.05 V/s	0.07	0.80	1.82	20
	ETL-2=others (ZnO-nanorod, ZnO-N-nanorod)	0.01	0.08	1.81	2
	Scan rate=1-20V/s	0.00	0.04	1.68	1
	HTL=PTAA	0.00	0.04	1.31	1
	Back contact=Ag	0.02	0.28	1.19	7
	Precursor solution=DMF+DMSO	0.03	0.36	1.13	9
	Deposition procedure=two-step	0.03	0.40	1.12	10
	Precursor solution=DMF	0.04	0.48	1.06	12
	Deposition method=spin	0.04	0.44	1.01	11
	Anti-solvent treatment=diethyl ether	0.01	0.08	0.98	2
	ETL-2=mTiO ₂	0.03	0.36	0.94	9
	Deposition procedure=one-step	0.05	0.60	0.93	15
	Perovskite=MAPbI ₃	0.04	0.52	0.92	13
	Anti-solvent treatment=no	0.05	0.56	0.91	14
ETL=TiO ₂	0.06	0.68	0.84	17	

Table C.7. Association Rule Mining for $HI \leq 0.01$ for Regular (n-i-p) Cells with Various Scan Rates (without PCE restriction) (cont.).

Antecedent	Consequent	Support	Confidence	Lift	Data count
HI \leq 0.01	Deposition method=spin 2-3	0.01	0.16	0.81	4
	Back contact=Au	0.05	0.56	0.80	14
	Precursor solution=DMF+others (HI)	0.00	0.04	0.78	1
	Anti-solvent treatment=toluene	0.00	0.04	0.78	1
	HTL=spiro-OMeTAD	0.05	0.56	0.70	14
	HTL additive=LiTFSI+TBP	0.04	0.44	0.67	11
	Anti-solvent treatment=chlorobenzene	0.01	0.12	0.63	3
	Deposition method=spin-dip	0.01	0.12	0.61	3
	Precursor solution=DMSO+GBL	0.00	0.04	0.59	1
	ETL-2=0	0.02	0.24	0.59	6
	Perovskite=MAPbI _{3-x} Cl _x	0.01	0.08	0.51	2
	Scan rate=0.05-0.1 V/s	0.01	0.12	0.44	3
	Scan rate=0.1-0.5V/s	0.00	0.04	0.17	1

*IZO: sputtered amorphous indium zinc oxide
**PTEBS: polythiophene derivative sodium poly[2-(3-thienyl)ethoxy-4-butylsulfonate]
***others: Diphenylamine-substituted carbazole-based derivatives (V885, V886, V908, V911, V946), a novel N-phenylindole-diketopyrrolopyrrole-containing narrow band-gap material (DPIE), CuI

Table C.8. Association Rule Mining for $HI \leq 0.05$ for Regular (n-i-p) Cells with Various Scan Rates (without PCE restriction).

Antecedent	Consequent	Support	Confidence	Lift	Data count
HI \leq 0.05	Anti-solvent treatment=ethylacetate	0.00	0.01	3.34	1
	Precursor solution=DMSO+GBL+HaHc*	0.00	0.01	3.34	1
	Anti-solvent treatment=ethoxyethane	0.00	0.01	3.34	1
	Deposition method=spin-meniscus assisted	0.00	0.01	3.34	1
	Precursor solution=GBL	0.01	0.05	2.67	4
	Anti-solvent treatment=trifluorotoluene	0.04	0.13	2.63	11
	HTL=PTAA	0.02	0.08	2.60	7
	Perovskite=Cs based	0.02	0.06	2.39	5
	Back contact=others (IZO**, NbS ₂)	0.01	0.02	2.23	2
	ETL-2= doped-mTiO ₂	0.06	0.19	2.10	17
	ETL-2=TiO ₂ -ns	0.01	0.03	2.00	3
	ETL-2=other (ZnO-nanorod, ZnO-N-nanorod, mZn ₂ SnO ₄ , Rgs***, SiO ₂ , C60)	0.02	0.08	1.80	7
	Perovskite=MAPbBr ₃	0.00	0.01	1.67	1
	ETL=doped-SnO ₂	0.00	0.01	1.67	1
	HTL additive=others (BCF****, LiTFSI+TBP+Co(II)TFSI)	0.01	0.02	1.67	2
	Precursor solution=DMF+DMSO+other (KL,Pb(SCN) ₂)	0.01	0.03	1.67	3
	HTL=no	0.02	0.07	1.67	6
	HTL additive=no	0.06	0.19	1.54	17
	HTL=others*****	0.06	0.19	1.54	17
	Back contact=carbon	0.02	0.06	1.52	5
Perovskite=mixed cation	0.09	0.28	1.42	25	

Table C.8. Association Rule Mining for $HI \leq 0.05$ for Regular (n-i-p) Cells with Various Scan Rates (without PCE restriction) (cont.).

Antecedent	Consequent	Support	Confidence	Lift	Data count
HI \leq 0.05	HTL additive=LiTFSI+TBP+FK209	0.07	0.24	1.40	21
	ETL=others (PCBM, PTEBS*****, Nb2O5, Zn2SnO4)	0.01	0.05	1.34	4
	Deposition method=spin-spin	0.05	0.16	1.30	14
	Scan rate=0.005-0.05V/s	0.16	0.55	1.24	48
	Deposition method=spin 2-3	0.07	0.23	1.15	20
	ETL=0	0.00	0.01	1.11	1
	ETL-2=PCBM	0.01	0.02	1.11	2
	Anti-solvent treatment=toluene	0.02	0.06	1.11	5
	Anti-solvent treatment=diethyl ether	0.03	0.09	1.11	8
	Precursor solution=DMF+DMSO	0.10	0.34	1.07	30
	Scan rate=0.05-0.1V/s	0.09	0.28	1.04	25
	ETL=TiO ₂	0.25	0.84	1.04	74
	ETL=ZnO	0.01	0.05	1.03	4
	Precursor solution=DMSO	0.01	0.05	1.03	4
	Deposition procedure=two-step	0.11	0.36	1.02	32
	ETL-2=mTiO ₂	0.12	0.39	1.01	34
	Deposition procedure=one-step	0.19	0.64	0.99	56
	Deposition method=spin-dip	0.06	0.19	0.98	17
	Anti-solvent treatment=no	0.18	0.60	0.98	53
	Back contact=Au	0.20	0.68	0.98	60
	Back contact=Ag	0.07	0.23	0.97	20
	Precursor solution=DMF	0.13	0.43	0.95	38
	Perovskite=MAPbI ₃	0.16	0.52	0.92	46
	Deposition method=spin	0.12	0.40	0.91	35
	Precursor solution=DMSO+GBL	0.02	0.06	0.84	5
	ETL=SnO ₂	0.01	0.03	0.84	3
	HTL additive=LiTFSI+TBP	0.16	0.55	0.83	48
	HTL=spiro-OMeTAD	0.20	0.66	0.82	58
	Scan rate=0.5-1 V/s	0.01	0.02	0.74	2
	Perovskite=FA based	0.01	0.02	0.74	2
	Back contact=Ag-Al	0.00	0.01	0.67	1
	Precursor solution=DMF+others (HI, Al, 4MSA*****)	0.01	0.03	0.67	3
	ETL-2=0	0.08	0.27	0.67	24
	Perovskite=MAPbI _{3-x} Cl _x	0.03	0.10	0.65	9
	Scanrate=0.1-0.5 V/s	0.04	0.14	0.58	12
	Deposition methods=vasp	0.00	0.01	0.56	1
	Anti-solvent treatment=chlorobenzene	0.03	0.10	0.54	9
	ETL-2=mAl ₂ O ₃	0.00	0.01	0.48	1
	Scan rate=1-20 V/s	0.00	0.01	0.48	1
	ETL= doped TiO ₂	0.00	0.01	0.42	1

Table C.8. Association Rule Mining for $HI \leq 0.05$ for Regular (n-i-p) Cells with Various Scan Rates (without PCE restriction) (cont.).

*HaHc: hydroxylamine hydrochloride
**IZO: sputtered amorphous indium zinc oxide
***Rgs: Reduced graphene scaffold
****BCF: tris(pentafluorophenyl)borane
*****others: poly[(2,5-bis(2-hexyldecyloxy)phenylene)-alt-(5,6-difluoro-4,7-di(thiophen-2-yl)benzo[c][1,2,5]-thiadiazole) (PPDT2FBT), a novel N-phenylindole-diketopyrrolopyrrole-containing narrow band-gap material (DPIO), Dimethoxydiphenylamine-substituted dispiro-oxepine derivative 2,2',7,7'-tetrakis-(N,N'-di-4-methoxyphenylamine)dispiro-[fluorene-9,4'-dithieno[3,2-c:2',3'-e]oxepine-6',9''-fluorene] (DDOF), diphenylamine-substituted carbazole-based derivatives (V885, V886, V908, V911, V928, V931, V946, V957, V1039), 4,40
-(10-(4-methoxyphenyl)-9,9-dimethyl-9,10-dihydroacridine-2,7-diyl)bis(N,Nbis(4-methoxyphenyl)aniline) (ACR-TPA), a novel carbazole-based HTL including extended π -conjugated central core+hexyloxy flexible group (SGT-410), 5,10,15-trihexyl-3,8,13-trimethoxy-10,15-dihydro-5H-diindolo[3,2-a:3',2'-c]carbazole (KR122), CuI
*****PTEBS: polythiophene derivative sodium poly[2-(3-thienyl)ethyloxy-4-butylsulfonate]
*****4MSA: 4-methylbenzenesulfonic acid

Table C.9. Association Rule Mining for $HI \leq 0.01$ and $PCE \geq 10\%$ for Inverted (p-i-n) Cells with Scan Rate ≤ 0.05 V/s ($PCE \geq 10\%$ for All Cells)

Antecedent	Consequent	Support	Confidence	Lift	Data count	
$HI \leq 0.01$	Precursor solution=DMSO+GBL+others (Ag)	0.03	0.06	2.06	1	
	Deposition method=masp*	0.03	0.06	2.06	1	
	HTL=doped-NiO _x	0.03	0.06	2.06	1	
	Deposition method=spin2-3	0.23	0.47	1.65	8	
	Anti-solventtreatment=toluene	0.26	0.53	1.43	9	
	ETL=PCBM+C60	0.06	0.12	1.37	2	
	Precursor solution=DMSO+GBL	0.11	0.24	1.37	4	
	HTL-2=others (mNiO _x -Cu, PEDOT:PSS, DEA**)	0.11	0.24	1.37	4	
	ETL-2=others (TiO _x , PN4N***, LiF)	0.11	0.24	1.37	4	
	HTL=NiO _x	0.17	0.35	1.24	6	
	Perovskite=MAPbI ₃	0.34	0.71	1.18	12	
	ETL=PCBM	0.40	0.82	1.15	14	
	Deposition procedure=one-step	0.46	0.94	1.14	16	
	$PCE \geq 10\%$	ETL-2=BCP	0.17	0.35	1.12	6
		Scan rate ≤ 0.05 V/s	BC=Ag	0.31	0.65	1.08
	Precursor solution=DMF		0.09	0.18	1.03	3
HTL=PTAA	0.03		0.06	1.03	1	
HTL=others (P3HT)	0.03		0.06	1.03	1	
Anti-solventtreatment=chlorobenzene	0.06		0.12	1.03	2	
Perovskite=mixed cation	0.06		0.12	1.03	2	
Scan rate=0-0.05 V/s	0.49		1.00	1.00	17	
Back contact=Al	0.17		0.35	0.95	6	
Precursor solution=DMF+DMSO	0.17		0.35	0.95	6	
HTL-2=0	0.37		0.76	0.92	13	
Perovskite=MAPbI _{3-x} Cl _x	0.09		0.18	0.88	3	
HTL=PEDOT:PSS	0.20		0.41	0.85	7	
Precursor solution=DMF+others (HI, DIO****)	0.06		0.12	0.82	2	
ETL-2=0	0.20		0.41	0.80	7	
Deposition method=spin	0.20		0.41	0.80	7	

Table C.9. Association Rule Mining for $HI \leq 0.01$ and $PCE \geq 10\%$ for Inverted (p-i-n) Cells with Scan Rate ≤ 0.05 V/s ($PCE \geq 10\%$ for All Cells) (cont.).

Antecedent	Consequent	Support	Confidence	Lift	Data count
$HI \leq 0.01$	Anti-solvent treatment=no	0.17	0.35	0.69	6
$PCE \geq 10\%$	HTL=doped-PEDOT:PSS	0.03	0.06	0.69	1
	Precursor solution=DMSO	0.03	0.06	0.69	1
Scan rate ≤ 0.05 V/s	ETL=C60	0.03	0.06	0.51	1
	Deposition method=spin-spin	0.03	0.06	0.34	1
	Deposition procedure=two-step	0.03	0.06	0.34	1
*masp: meniscus asisted spin coating					
**DEA: diethanolamine					
***PN4N: polymeric interfacial modification layer to improve the cathode interface					
****DIO: 1,8-diiodooctane					

Table C.10. Association Rule Mining for $HI \leq 0.01$ for Inverted (p-i-n) Cells with Various Scan Rates (all cells except two have $PCE \geq 10\%$).

Antecedent	Consequent	Support	Confidence	Lift	Data count
$HI \leq 0.01$	Deposition method=masp*	0.01	0.04	3.44	1
	Anti-solvent treatment=diethyl ether	0.02	0.07	2.30	2
	Anti-solvent treatment=toluene	0.14	0.48	1.95	13
	ETL-2=BCP	0.10	0.33	1.72	9
	Precursor solution=na	0.01	0.04	1.72	1
	Anti-solvent treatment=chlorobenzene+others (ITIC)	0.01	0.04	1.72	1
	Precursor solution=DMSO+GBL+others**	0.02	0.07	1.72	2
	Perovskite=mixed cation	0.04	0.15	1.72	4
	Deposition method=spin 2-3	0.11	0.37	1.72	10
	Scan rate=0-0.05 V/s	0.18	0.63	1.67	17
	Precursor solution=DMSO+GBL	0.09	0.30	1.62	8
	HTL-2=others (mNiO _x -Cu, PEDOT:PSS, DEA***)	0.08	0.26	1.61	7
	ETL-2=others****	0.08	0.26	1.42	7
	ETL=PCBM	0.23	0.78	1.29	21
	Back contact=Ag	0.23	0.78	1.17	21
	Precursor solution=DMSO	0.01	0.04	1.15	1
	Precursor solution=DMF+others (HI, DIO)	0.02	0.07	1.15	2
	HTL=NiO _x	0.09	0.30	1.15	8
	HTL=doped-NiO _x	0.03	0.11	1.15	3
	Deposition procedure=one-step	0.28	0.96	1.12	26
	Scan rate=0.05-0.1 V/s	0.06	0.22	1.09	6
	Perovskite=MAPbI ₃	0.19	0.67	1.02	18
	Precursor solution=DMF+DMSO	0.11	0.37	1.01	10
	HTL=PEDOT:PSS	0.14	0.48	1.00	13
	HTL-2=0	0.22	0.74	0.88	20
	Deposition method=spin	0.16	0.56	0.88	15
	HTL=doped-PEDOT:PSS	0.01	0.04	0.86	1
	Perovskite=MAPbI _{3-x} Cl _x	0.05	0.19	0.82	5
	ETL=C60	0.02	0.07	0.77	2
	Back contact=Al	0.06	0.22	0.74	6
	HTL=PTAA	0.01	0.04	0.69	1

Table C.10. Association Rule Mining for $HI \leq 0.01$ for Inverted (p-i-n) Cells with Various Scan Rates (all cells except two have PCE $\geq 10\%$) (cont.).

Antecedent	Consequent	Support	Confidence	Lift	Data count
	Anti-solvent treatment=no	0.08	0.26	0.69	7
	ETL-2=0	0.12	0.41	0.65	11
	ETL=PCBM+C60	0.04	0.15	0.63	4
	Scan rate=1-10 V/s	0.01	0.04	0.57	1
	HTL=others (P3HT)	0.01	0.04	0.57	1
	Anti-solvent treatment=chlorobenzene	0.04	0.15	0.48	4
	Precursor solution=DMF	0.03	0.11	0.43	3
	Scan rate=0.1-0.5 V/s	0.03	0.11	0.40	3
	Deposition method=spin-spin	0.01	0.04	0.31	1
	Deposition procedure=two-step	0.01	0.04	0.26	1

*masp: meniscus asisted spin coating
 **others: 2-aminoethanesulfonamide hydrochloride (ASCI), Ag
 ***DEA: diethanolamine
 ****others: polymeric interfacial modification layer to improve the cathode interface (PN4N), TiO_x, LiF, rhodamine 101/LiF, aluminium-doped ZnO (AZO)/SnO_x, PEI

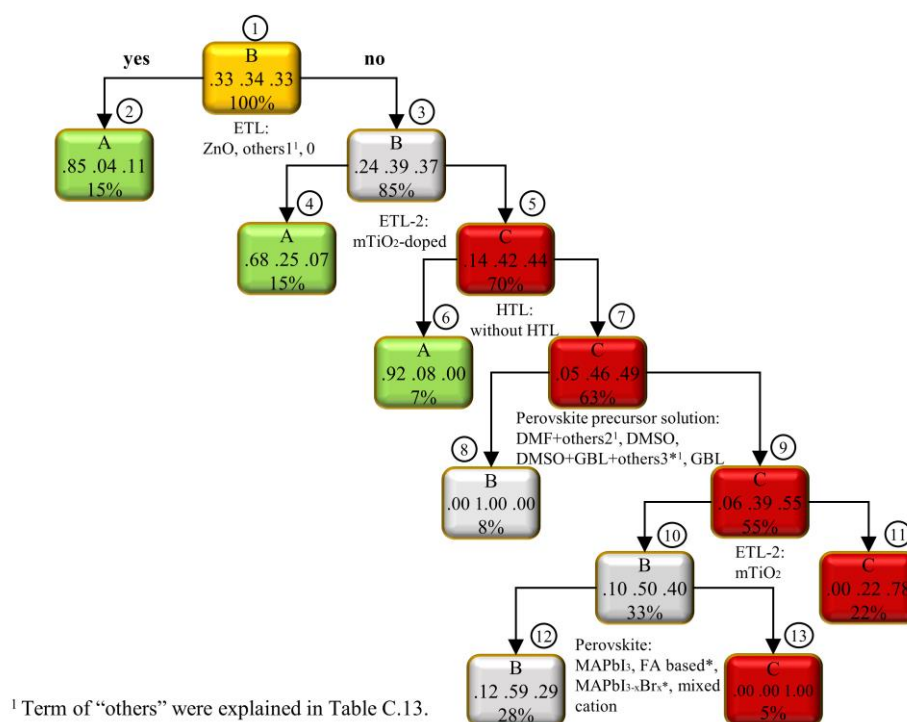


Figure C.1. Decision tree model for regular (n-i-p) cells in hysteresis analysis without PCE restriction (minimum split number=5, maximum depth=6, complexity parameter=0).

Table C.11. Confusion Matrix of Hysteresis Analysis of Regular Cells without PCE Restriction

		Actual Class			
		Class A	Class B	Class C	Precision
Predicted Class	Class A	54	9	5	79%
	Class B	6	44	15	68%
	Class C	0	9	41	82%
	Accuracy	90%	71%	67%	
Overall accuracy		76%			

Table C.12. Explanation for the Term of “others” in Figure 4.25.

	Article name	Instance	Article name	Instance	Article name	Instance
Others1	Li, M. <i>et al.</i> , ChemSusChem 9, 2862–2869 (2016)	Chl-1	Rakstys, K. <i>et al.</i> , J. Am. Chem. Soc. 137, 16172–16178 (2015)	KR145	Magomedov, A. <i>et al.</i> , Adv. Funct. Mater. 28, 1704351 (2018)	V908
	Cheng, N. <i>et al.</i> , Electrochim. Acta 246, 990–996 (2017)	CuPc	Koh, C. W. <i>et al.</i> , ACS Appl. Mater. Interfaces 9, 43846– 43854 (2017)	PPDT2FBT-BCF	Magomedov, A. <i>et al.</i> , Adv. Funct. Mater. 28, 1704351 (2018)	V911
	Rakstys, K. <i>et al.</i> , J. Mater. Chem. A 4, 18259–18264 (2016)	DDOF	Paek, S. <i>et al.</i> , Adv. Mater. 29, 1606555 (2017)	TPA-CN	Magomedov, A. <i>et al.</i> , Adv. Funct. Mater. 28, 1704351 (2018)	V928
	Jeon, S. <i>et al.</i> , Org. Electron. physics, Mater. Appl. 37, 134–140 (2016)	DPIO	Liu, X. <i>et al.</i> , ChemSusChem 10, 968–975 (2017)	TPA-TPM	Magomedov, A. <i>et al.</i> , Adv. Funct. Mater. 28, 1704351 (2018)	V931
	Paek, S. <i>et al.</i> , Adv. Mater. 29, 1606555 (2017)	FA-CN	Liu, X. <i>et al.</i> , ChemSusChem 10, 968–975 (2017)	TPA-TPM	Magomedov, A. <i>et al.</i> , Adv. Funct. Mater. 28, 1704351 (2018)	V946
	Mahmud, M. A. <i>et al.</i> , 19, 21033–21045 (2017)	FDT	Magomedov, A. <i>et al.</i> , Adv. Funct. Mater. 28, 1704351 (2018)	V1039	Magomedov, A. <i>et al.</i> , Adv. Funct. Mater. 28, 1704351 (2018)	V957

Table C.12. Explanation for the Term of “others” in Figure 4.25 (cont.).

	Article name	Instance	Article name	Instance	Article name	Instance
Others1	Rakstys, K. <i>et al.</i> , J. Am. Chem. Soc. 137, 16172–16178 (2015)	KR131	Magomedov, A. <i>et al.</i> , Adv. Funct. Mater. 28, 1704351 (2018)	V885		
	Rakstys, K. <i>et al.</i> , J. Am. Chem. Soc. 137, 16172–16178 (2015)	KR133	Magomedov, A. <i>et al.</i> , Adv. Funct. Mater. 28, 1704351 (2018)	V886		
	Article name	Instance	Article name	Instance	Article name	Instance
Others2	Fernandes, S. L. <i>et al.</i> , Mater. Lett. 181, 103–107 (2016)	Nb ₂ O ₅	Upama, M. B. <i>et al.</i> , Org. Electron. 50, 279–289 (2017)	PCBM	Luo, Q. <i>et al.</i> , Adv. Funct. Mater. 27, 1702090 (2017)	α -Fe ₂ O ₃
	Hu, W. <i>et al.</i> , J. Mater. Chem. A 5, 1434–1441 (2017)	In ₂ S ₃				

Table C.13. Explanation for the Term of “others” in Figure C.1.

	Article name	Instance	Article name	Instance	Article name	Instance
Others1	Fernandes, S. L. <i>et al.</i> , Mater. Lett. 181, 103–107 (2016)	Nb ₂ O ₅	Upama, M. B. <i>et al.</i> , Org. Electron. 50, 279–289 (2017)	PCBM	Luo, Q. <i>et al.</i> , Adv. Funct. Mater. 27, 1702090 (2017)	α -Fe ₂ O ₃
	Hu, W. <i>et al.</i> , J. Mater. Chem. A 5, 1434–1441 (2017)	In ₂ S ₃				
Others2	Heo, J. H. and Im, S. H., Nanoscale 8, 2554–2560 (2016)	HI	Dar, M. I. <i>et al.</i> , Adv. Funct. Mater. 27, 1701433 (2017)	HBr	Chen, H. Bin <i>et al.</i> , ACS Appl. Mater. Interfaces 10, 2603–2611 (2018)	C60/o-DCB
Others3	Jiang, H. <i>et al.</i> , ACS Appl. Energy Mater. 1, 900–909 (2018)	HaHc				

APPENDIX D: ADDITIONAL INFORMATION ON ANALYSIS OF LONG-TERM STABILITY

Table D.1. Association Rule Mining for Regular (n-i-p) Cells with PCE \geq 10% Stable
More Than 15 Days .

Antecedent	Consequent	Support	Confidence	Lift	Data count
Stable more than 15 days	ETL-2=PCBM	0.02	0.04	2.18	5
	Anti-solvent treatment=ethylacetate	0.00	0.01	2.18	1
	Anti-solvent treatment=IPA	0.00	0.01	2.18	1
	ETL=doped-ZnO	0.00	0.01	2.18	1
	HTL=doped-P3HT	0.00	0.01	2.18	1
	Deposition method=dip-spin	0.00	0.01	2.18	1
	ETL=others (Ti _{0.94} Li _{0.03} Mg _{0.03} O ₂ , Cd ₂ SnO ₄)	0.01	0.02	2.18	2
	ETL= doped-TiO ₂	0.01	0.02	2.18	2
	ETL= α -Fe ₂ O ₃	0.01	0.03	2.18	4
	Anti-solvent treatment=chlorobenzene+others*	0.03	0.06	2.18	8
	HTL=inorganic	0.03	0.07	1.96	9
	HTL=no	0.04	0.08	1.85	11
	Precursor solution=DMF+DMSO+others**	0.04	0.09	1.75	12
	Deposition method=spin-drip	0.01	0.02	1.64	3
	HTL=PTAA	0.01	0.02	1.64	3
	ETL-2=others***	0.02	0.05	1.53	7
	ETL-2=doped-mTiO ₂	0.03	0.08	1.45	10
	Back contact=carbon	0.03	0.08	1.45	10
	Perovskite=mixed cation	0.16	0.36	1.42	47
	HTL additive=F4TCNQ	0.02	0.04	1.36	5
	Stored humidity=0-30% RH	0.30	0.66	1.36	87
	Precursor solution=DMF+others****	0.04	0.09	1.31	12
	Precursor solution=DMSO+GBL	0.02	0.05	1.27	7
	ETL=SnO ₂	0.03	0.06	1.25	8
	HTL additive=no	0.15	0.33	1.25	44
	Anti-solvent treatment=diethyl ether	0.03	0.07	1.23	9
	Deposition method=spin 2-3	0.15	0.33	1.20	44
	Precursor solution=DMF+DMSO	0.17	0.37	1.17	49
	Anti-solvent treatment=chlorobenzene	0.13	0.28	1.15	37
	Back contact=Au	0.36	0.78	1.10	103
	Deposition method=vasp	0.02	0.05	1.09	6
	HTL additive=LiTFSI+TBP+FK209	0.06	0.13	1.09	17
	Perovskite=C _s ₂ AgBiBr ₆	0.00	0.01	1.09	1
	Anti-solvent treatment=polystyrene	0.00	0.01	1.09	1
	Perovskite=Cs based	0.00	0.01	1.09	1
	Perovskite=MAPbI _{3-x} Br _x	0.00	0.01	1.09	1
	Precursor solution=na	0.00	0.01	1.09	1
	Deposition procedure=one-step	0.33	0.71	1.07	94
	O ₂ =no	0.05	0.11	1.06	15
	Stored condition=dark	0.21	0.45	1.04	60

Table D.1. Association Rule Mining for Regular (n-i-p) Cells with PCE \geq 10%
Stable More Than 15 Days (cont.).

Antecedent	Consequent	Support	Confidence	Lift	Data count
Stable more than 15 days	ETL=ZnO	0.02	0.05	1.02	7
	ETL-2=0	0.18	0.39	1.00	51
	O ₂ =yes	0.41	0.89	0.99	117
	Deposition method=spin	0.17	0.38	0.97	50
	Perovskite=FA based	0.01	0.03	0.97	4
	Stored condition=room-light	0.25	0.55	0.97	72
	HTL=spiro-OMeTAD	0.32	0.69	0.96	91
	ETL-2=mTiO ₂	0.20	0.43	0.95	57
	ETL=TiO ₂	0.38	0.82	0.95	108
	Perovskite=MAPbI ₃	0.24	0.53	0.91	70
	HTL additive=LiTFSI+TBP	0.22	0.48	0.90	64
	Anti-solvent treatment=no	0.24	0.53	0.88	70
	HTL=others*****	0.05	0.11	0.87	14
	Deposition procedure=two-step	0.13	0.29	0.86	38
	Deposition method=spin-spin	0.05	0.11	0.82	15
	Precursor solution=DMF	0.15	0.33	0.77	44
	Stored humidity=30-60% RH	0.14	0.30	0.75	39
	Deposition method=spin-dip	0.05	0.10	0.75	13
	Precursor solution=GBL	0.00	0.01	0.73	1
	Precursor solution=DMSO+others (Pb(SCN) ₂)	0.00	0.01	0.73	1
	HTL additive=other (LiTFSI+2- amylpyridine+FK102, Cu(bpcm))	0.01	0.02	0.73	2
	Anti-solvent treatment=toluene	0.02	0.04	0.68	5
	Precursor solution=DMSO	0.02	0.04	0.68	5
	Back contact=Ag	0.06	0.14	0.64	18
	Perovskite=MAPbI _{3-x} Cl _x	0.03	0.06	0.51	8
	ETL-2=TiO ₂ -ns	0.00	0.01	0.44	1
	Stored humidity=above 60% RH	0.02	0.05	0.37	6
	HTL=P3HT	0.01	0.02	0.36	3
	Back contact=Ag-Al	0.00	0.01	0.31	1
	ETL-2=C60	0.00	0.01	0.22	1

* others: acetonitrile, toluene, p-type polymer with or without (w/wo) molecular fluorination (PF-0, PF-1), n-type polymer w/wo molecular fluorination (N2200, F-N2200)

**others: benzoquinone (BQ), 2-pyridylthiourea, N-Methyl-2-Pyrrolidone (NMP), Pb(SCN)₂, terephthalic acid (TPA)

***others: mZnO, ZnO-SnO₂-nanotube array, Passivated Tin Oxide (PTO), m- α -Fe₂O₃, polystyrene (PS)

****others: thiourea, caprolactam (CPL), PCBM+PEG, PEI, C60/1,2-dichlorobenzene(o-DCB), PDMS-urea, 1,2-dichlorobenzene(o-DCB), 4-TBP

*****others: a novel arylamine-based hole transporting materials with an anthracene p-linker (A102), 2,9,16-triphenoxy-23-nitrophthalocyaninatocobalt (CoPcNO₂-Oph), crosslinked 4,4'-tris(N-carbazolyl)triphenylamine (TCTA-BVP), 2,2',7,7'-tetrakis-(N,N'-di-4-methoxyphenylamine)dispiro[fluorene-9,4'-dithieno[3,2-c:2',3'-e]oxepine-6',9''-fluorene] (DDOF), 2',7'-bis(bis(4-methoxyphenyl)amino)spiro[cyclopenta[2,1-b:3,4-b']dithiophene-4,9'-fluorene] (FDT), poly[bis(4-phenyl)(2,5,6-trimethylphenyl)amine] (PTAA), 5,10,15-trihexyl-3,8,13-tris(4-methoxyphenyl)-10,15-dihydro-5H-diindolo[3,2-a:3',2'-c]carbazole (HMPDI), a benzothiadiazole unit incorporated into the biphenyl core (JY5), p- π conjugated structure that are built up by electron-rich piperazine derivatives N-bridge connecting triarylamine donors (Me-QTPA), octamethyl-substituted palladium(II) phthalocyanine (PdMe₂Pc), a novel dopant-free TPA-based butterfly-shaped HTL (Z1011), two novel thiophene-based HTLs (Z25, Z26), metallophthalocyanine with different metal core 2,9,16-triphenoxy-23-nitrophthalocyaninatozinc (ZnPcNO₂-Oph)

Table D.2. Association Rule Mining For Regular (n-i-p) Cells Stable More Than 30 Days.

Antecedent	Consequent	Support	Confidence	Lift	Data count
Stable more than 30 days	Anti-solvent treatment=ethylacetate	0.00	0.01	3.51	1
	Deposition method=dip-spin	0.00	0.01	3.51	1
	ETL=others (Cd ₂ SnO ₄)	0.00	0.01	3.51	1
	ETL=doped-ZnO	0.00	0.01	3.51	1
	ETL=doped-TiO ₂	0.01	0.03	3.51	2
	ETL-2=PCBM	0.01	0.04	3.51	3
	ETL=α-Fe ₂ O ₃	0.01	0.04	3.51	3
	HTL=inorganic	0.02	0.07	2.93	5
	HTL=PTAA	0.01	0.04	2.64	3
	Anti-solvent treatment=chlorobenzene-others*	0.02	0.08	2.64	6
	Deposition method=spin-drip	0.01	0.03	2.34	2
	HTL=no	0.02	0.07	2.20	5
	Precursor solution=DMF+DMSO+others**	0.03	0.10	2.05	7
	ETL-2=others***	0.02	0.06	2.01	4
	HTL additive=F4TCNQ	0.02	0.06	2.01	4
	Back contact=carbon	0.02	0.07	1.76	5
	Perovskite=C _s ₂ AgBiBr ₆	0.00	0.01	1.76	1
	Precursor solution=na	0.00	0.01	1.76	1
	Perovskite=Cs based	0.00	0.01	1.76	1
	Perovskite=MAPbI _{3-x} Br _x	0.00	0.01	1.76	1
	Perovskite=mixed cation	0.11	0.38	1.58	27
	ETL-2=doped-mTiO ₂	0.02	0.06	1.56	4
	Anti-solvent treatment=chlorobenzene	0.10	0.36	1.47	26
	ETL=SnO ₂	0.02	0.07	1.46	5
	Deposition method=spin 2-3	0.12	0.42	1.44	30
	Stored humidity=0-30% RH	0.19	0.67	1.39	48
	Precursor solution=DMF+DMSO	0.13	0.44	1.39	32
	HTL additive=no	0.09	0.31	1.25	22
	Precursor solution=GBL	0.00	0.01	1.17	1
	Perovskite=FA based	0.01	0.04	1.17	3
	Precursor solution=DMSO+GBL	0.02	0.06	1.17	4
	Stored condition=dark	0.15	0.53	1.17	38
	Back contact=Au	0.23	0.82	1.16	59
	Deposition procedure=one-step	0.21	0.75	1.15	54
	HTL additive=LiTFSI+TBP+FK209	0.04	0.13	1.13	9
	O ₂ =yes	0.27	0.94	1.04	68
	Precursor solution=DMF+others****	0.02	0.07	1.03	5
	ETL-2=mTiO ₂	0.13	0.44	0.97	32
	HTL=spiro-OMeTAD	0.20	0.71	0.95	51
	ETL=TiO ₂	0.23	0.82	0.94	59
	ETL-2=0	0.11	0.38	0.93	27
	Deposition method=spin	0.09	0.33	0.92	24
Anti-solvent treatment=diethyl ether	0.01	0.04	0.88	3	
HTL additive=LiTFSI+TBP	0.14	0.50	0.88	36	
Stored condition=room-light	0.13	0.47	0.86	34	
HTL=others*****	0.03	0.10	0.85	7	
Perovskite=MAPbI ₃	0.13	0.47	0.82	34	

Table D.2. Association Rule Mining For Regular (n-i-p) Cells Stable More Than 30 Days (cont.).

Antecedent	Consequent	Support	Confidence	Lift	Data count
Stable more than 30 days	Anti-solvent treatment=no	0.14	0.49	0.79	35
	Stored humidity=30-60% RH	0.09	0.31	0.77	22
	Deposition method=spin-spin	0.03	0.11	0.76	8
	Deposition procedure=two-step	0.07	0.25	0.72	18
	HTL additive=others (LiTFSI+2-amylpyridine+FK102)	0.00	0.01	0.70	1
	ETL-2=TiO ₂ -ns	0.00	0.01	0.70	1
	Precursor solution=DMF	0.08	0.28	0.64	20
	Deposition method=vasp	0.01	0.03	0.64	2
	O2=no	0.02	0.06	0.59	4
	Perovskite=MAPbI _{3-x} Cl _x	0.02	0.07	0.55	5
	Precursor solution=DMSO	0.01	0.03	0.54	2
	Deposition method=spin-dip	0.02	0.07	0.50	5
	Back contact=Ag	0.03	0.11	0.49	8
	ETL-2=C60	0.00	0.01	0.35	1
	ETL=ZnO	0.00	0.01	0.29	1
	Anti-solvent treatment=toluene	0.00	0.01	0.27	1
	Stored humidity=above 60% RH	0.01	0.03	0.22	2
	HTL=P3HT	0.00	0.01	0.21	1
* others: acetonitrile, toluene, p-type polymer with or without (w/wo) molecular fluorination (PF-0, PF-1), n-type polymer without molecular fluorination (F-N2200)					
**others: benzoquinone (BQ), 2-pyridylthiourea, N-Methyl-2-Pyrrolidone (NMP), Pb(SCN) ₂					
***others: mZnO, Passivated Tin Oxide (PTO)					
****others: thiourea, caprolactam (CPL), PCBM+PEG, C60/1,2-dichlorobenzene(o-DCB), PDMS-urea					
*****others: crosslinked 4,4',4''-tris(N-carbazolyl)triphenylamine (TCTA-BVP), 2,2',7,7'-tetrakis-(N,N'-di-4-methoxyphenylamine)dispiro-[fluorene-9,4'-dithieno[3,2-c:2',3'-e]oxepine-6',9''-fluorene] (DDOF), poly[bis(4-phenyl)(2,5,6-trimethylphenyl)amine (PTAA),5,10,15-trihexyl-3,8,13-tris(4-methoxyphenyl)-10,15-dihydro-5H-diindolo[3,2-a:3',2'-c]carbazole (HMPDI), a novel dopant-free TPA-based butterfly-shaped HTL (Z1011), a novel thiophene-based HTL (Z26), metallophthalocyanine with different metal core 2,9,16-triphenoxy-23-nitrophthalocyaninatozinc (ZnPcNO ₂ -Oph)					

Table D.3. Association Rule Mining for Regular (n-i-p) Cells Stable More Than 60 Days.

Antecedent	Consequent	Support	Confidence	Lift	Data count
Stable more than 60 days	ETL= doped-ZnO	0.00	0.04	8.44	1
	ETL= doped-TiO ₂	0.00	0.04	8.44	1
	HTL=PTAA	0.01	0.08	5.63	2
	Deposition method=spin-drip	0.01	0.08	5.63	2
	HTL=inorganic	0.01	0.08	5.63	2
	Perovskite=Cs based	0.00	0.04	4.22	1
	HTL=no	0.01	0.12	4.22	3
	Back contact=carbon	0.02	0.16	3.75	4
	HTL additive=F4TCNQ	0.01	0.08	3.38	2
	ETL-2=others*	0.01	0.08	3.38	2
	Anti-solvent treatment=chlorobenzene+others (acetonitrile)	0.00	0.04	2.81	1
	Precursor solution=GBL	0.00	0.04	2.81	1
	Precursor solution=DMF+DMSO+others**	0.01	0.08	2.41	2
	ETL-2=doped-mTiO ₂	0.01	0.08	2.41	2

Table D.3. Association Rule Mining for Regular (n-i-p) Cells Stable More Than 60 Days (cont.).

Antecedent	Consequent	Support	Confidence	Lift	Data count
Stable more than 60 days	Anti-solvent treatment=diethyl ether	0.01	0.12	2.11	3
	Precursor solution=DMF+DMSO	0.07	0.56	1.82	14
	Deposition method=spin 2-3	0.06	0.48	1.75	12
	Perovskite=mixed cation	0.04	0.36	1.73	9
	Stored humidity=0-30% RH	0.09	0.76	1.71	19
	HTL additive=LiTFSI+TBP+FK209	0.02	0.20	1.69	5
	HTL additive=no	0.04	0.32	1.41	8
	Anti-solvent treatment=chlorobenzene	0.03	0.28	1.28	7
	Stored condition=dark	0.06	0.48	1.13	12
	Back contact=Au	0.09	0.72	1.07	18
	ETL=SnO ₂	0.00	0.04	1.06	1
	Perovskite=FA based	0.00	0.04	1.06	1
	O ₂ =yes	0.11	0.92	1.03	23
	ETL-2=mTiO ₂	0.06	0.48	1.02	12
	Deposition procedure=one-step	0.08	0.64	1.02	16
	Deposition method=spin-dip	0.02	0.16	0.99	4
	Deposition procedure=two-step	0.04	0.36	0.96	9
	ETL=TiO ₂	0.10	0.84	0.95	21
	Perovskite=MAPbI ₃	0.07	0.56	0.93	14
	Stored condition=room-light	0.06	0.52	0.91	13
	HTL=spiro-OMeTAD	0.08	0.68	0.90	17
	ETL-2=0	0.04	0.36	0.88	9
	Anti-solvent treatment=no	0.07	0.56	0.87	14
	Deposition method=vasp	0.00	0.04	0.84	1
	O ₂ =no	0.01	0.08	0.77	2
	ETL=ZnO	0.00	0.04	0.70	1
	HTL additive=LiTFSI+TBP	0.05	0.40	0.69	10
	Precursor solution=DMF+others***	0.00	0.04	0.60	1
	Precursor solution=DMF	0.03	0.28	0.60	7
	Deposition method=spin-spin	0.01	0.08	0.54	2
	Stored humidity=30-60% RH	0.02	0.20	0.49	5
	Back contact=Ag	0.01	0.12	0.48	3
	Deposition method=spin	0.02	0.16	0.46	4
HTL=others****	0.00	0.04	0.37	1	
Stored humidity=above 60% RH	0.00	0.04	0.27	1	

Table D.4. Association Rule Mining for Inverted (p-i-n) Cells Stable More Than 15 Days.

Antecedent	Consequent	Support	Confidence	Lift	Data count
Stable more than 15 days	Back contact=carbon	0.01	0.02	2.64	1
	Precursor solution=GBL	0.02	0.05	2.64	2
	ETL=others (SnO ₂ , indium-doped zinc oxide (IZO))	0.02	0.05	2.64	2
	Back contact=Cu	0.05	0.14	2.64	6

Table D.4. Association Rule Mining for Inverted (p-i-n) Cells Stable More Than 15 Days (cont.).

Antecedent	Consequent	Support	Confidence	Lift	Data count
Stable more than 15 days	HTL=PTAA	0.05	0.14	2.26	6
	ETL=PCBM+C60	0.04	0.11	2.20	5
	Precursor solution=DMF+others* (CHP, PVP, GO, V ₂ O ₅)	0.04	0.11	1.88	5
	Deposition method=blade coat	0.02	0.05	1.76	2
	Perovskite=mixed cation	0.06	0.16	1.68	7
	O ₂ =no	0.20	0.52	1.64	23
	Back contact=Al	0.08	0.20	1.48	9
	Stored humidity=0-30% RH	0.27	0.70	1.46	31
	ETL-2=BCP	0.14	0.36	1.41	16
	Perovskite=MAPb _{0.5} Sn _{0.5} (I _{0.8} Br _{0.2}) ₃	0.01	0.02	1.32	1
	Precursor solution=na	0.01	0.02	1.32	1
	HTL=GO	0.03	0.07	1.32	3
	HTL-2=others**	0.03	0.09	1.32	4
	Perovskite=MAPbI _{3-x} Cl _x	0.09	0.23	1.32	10
	Precursor solution=DMF+DMSO	0.12	0.32	1.27	14
	Anti-solvent treatment=no	0.18	0.48	1.26	21
	Deposition method=spin-spin	0.05	0.14	1.22	6
	HTL=others***	0.05	0.14	1.22	6
	ETL=C60	0.04	0.11	1.20	5
	ETL-2=others****	0.06	0.16	1.15	7
	HTL= doped-PEDOT:PSS	0.03	0.07	1.13	3
	Deposition procedure=two-step	0.05	0.14	1.05	6
	Stored condition=room-light	0.30	0.80	1.05	35
	Deposition method=spin	0.22	0.57	1.01	25
	Deposition procedure=one-step	0.33	0.86	0.99	38
	HTL-2=0	0.34	0.91	0.99	40
	HTL=NiO _x	0.07	0.18	0.96	8
	Precursor solution=DMF	0.13	0.34	0.94	15
	Precursor solution=2 methoxy ethanol+CHP	0.01	0.02	0.88	1
	HTL=doped-NiO _x	0.02	0.05	0.88	2
	Stored humidity=above 60% RH	0.03	0.09	0.88	4
	Anti-solvent treatment=chlorobenzene	0.09	0.23	0.88	10
	Deposition method=spin 2-3	0.09	0.25	0.88	11
	ETL=PCBM	0.28	0.73	0.88	32
	Anti-solvent treatment=toluene	0.10	0.27	0.88	12
	ETL-2=0	0.18	0.48	0.87	21
	Stored condition=dark	0.08	0.20	0.85	9
	Perovskite=MAPbI ₃	0.22	0.59	0.83	26
	Back contact=Ag	0.24	0.64	0.82	28
	HTL=PEDOT:PSS	0.14	0.36	0.78	16
	O ₂ =yes	0.18	0.48	0.70	21
	Precursor solution=DMF+DMSO+others (ascorbic acid)	0.01	0.02	0.66	1
Precursor solution=DMSO+GBL	0.03	0.09	0.56	4	
Precursor solution=DMSO	0.01	0.02	0.53	1	
stored humidity=30-60% RH	0.08	0.20	0.49	9	

Table D.4. Association Rule Mining for Inverted (p-i-n) Cells Stable More Than 15 Days (cont.).

Antecedent	Consequent	Support	Confidence	Lift	Data count
	Anti-solvent treatment=diethyl ether	0.01	0.02	0.44	1
*others: N-cyclohexyl-2-pyrrolidone (CHP), polyvinylpyrrolidone (PVP), GO, V ₂ O _x **others: diethanolamine (DEA), Al ₂ O ₃ , mNiO _x -Cu, mNiO _x -Li ***others: CuO _x , CoO _x , electropolymerized by targeted monomer M1 tethered bifunctional carbozoyl moieties (PAF-86), polyTPD, NiMgLiO, poly(3,4-ethylenedioxythiophene):sulfonated acetone-formaldehyde (PEDOT:SAF) ****others: phenyl-C61-butyric acid 2-((2-(dimethylamino)ethyl) (methyl)amino) ethyl ester (PCBDAN), polyethylenimine (PEIE), amino-functionalized polymer (PN4N), LiF, PDIN, AZO/SnO _x					

Table D.5. Association Rule Mining for Inverted (p-i-n) Cells Stable More Than 30 Days.

Antecedent	Consequent	Support	Confidence	Lift	Data count
Stable more than 30 days	O ₂ =no	0.18	0.68	2.09	19
	Precursor solution=GBL	0.01	0.04	1.93	1
	Perovskite=MAPb _{0.5} Sn _{0.5} (I _{0.8} Br _{0.2}) ₃	0.01	0.04	1.93	1
	ETL=PCBM+C60	0.02	0.07	1.93	2
	Back contact=Cu	0.02	0.07	1.93	2
	Stored humidity=0-30% RH	0.22	0.86	1.75	24
	Precursor solution=DMF+others* (CHP,PVP, GO)	0.03	0.11	1.65	3
	HTL= doped-PEDOT:PSS	0.03	0.11	1.65	3
	HTL=PTAA	0.02	0.07	1.54	2
	Perovskite=mixed cation	0.03	0.11	1.45	3
	Deposition method=spin-spin	0.04	0.14	1.40	4
	Back contact=Al	0.05	0.18	1.38	5
	Deposition method=blade coat	0.01	0.04	1.29	1
	HTL=GO	0.02	0.07	1.29	2
	HTL-2=others**	0.02	0.07	1.29	2
	HTL=doped-NiO _x	0.02	0.07	1.29	2
	Perovskite=MAPbI _{3-x} Cl _x	0.06	0.21	1.29	6
	Precursor solution=DMF	0.12	0.46	1.22	13
	Anti-solvent treatment=chlorobenzene	0.08	0.32	1.20	9
	Deposition procedure=two-step	0.04	0.14	1.19	4
	HTL=NiO _x	0.06	0.21	1.16	6
	ETL-2=BCP	0.07	0.29	1.14	8
	Anti-solvent treatment=no	0.10	0.39	1.09	11
	ETL-2=0	0.16	0.61	1.07	17
	ETL=C60	0.03	0.11	1.05	3
	HTL=others*** (NiMgLiO, CoO _x , CuO _x)	0.03	0.11	1.05	3
	Stored condition=dark	0.06	0.25	1.00	7
	Stored condition=room-light	0.19	0.75	1.00	21
	HTL-2=0	0.24	0.93	0.99	26
	Deposition procedure=one-step	0.22	0.86	0.97	24
	Precursor solution=DMF+DMSO	0.06	0.21	0.96	6
	Precursor solution=DMF+DMSO+others (ascorbic acid)	0.01	0.04	0.96	1
Deposition method=spin 2-3	0.07	0.29	0.96	8	

Table D.5. Association Rule Mining for Inverted (p-i-n) Cells Stable More Than 30 Days (cont.).

Antecedent	Consequent	Support	Confidence	Lift	Data count
	Deposition method=spin	0.14	0.54	0.96	15
	ETL=PCBM	0.21	0.82	0.96	23
	Back contact=Ag	0.19	0.75	0.93	21
	Perovskite=MAPbI ₃	0.17	0.64	0.87	18
	ETL-2=others****	0.03	0.11	0.83	3
	Anti-solvent treatment=toluene	0.06	0.25	0.79	7
	Precursor solution=DMSO	0.01	0.04	0.77	1
	HTL=PEDOT:PSS	0.09	0.36	0.74	10
	Anti-solvent treatment=diethyl ether	0.01	0.04	0.64	1
	Precursor solution=DMSO+GBL	0.03	0.11	0.64	3
	O ₂ =yes	0.08	0.32	0.48	9
	stored humidity=30-60% RH	0.04	0.14	0.34	4
*others: N-cyclohexyl-2-pyrrolidone (CHP), polyvinylpyrrolidone (PVP), GO **others: diethanolamine (DEA), mNiO _x -Cu ***others: CuO _x , CoO _x , NiMgLiO ****others: phenyl-C61-butyric acid 2-((2-(dimethylamino)ethyl) (methyl)amino) ethyl ester (PCBDAN), polyethylenimine (PEIE), amino-functionalized polymer (PN4N)					

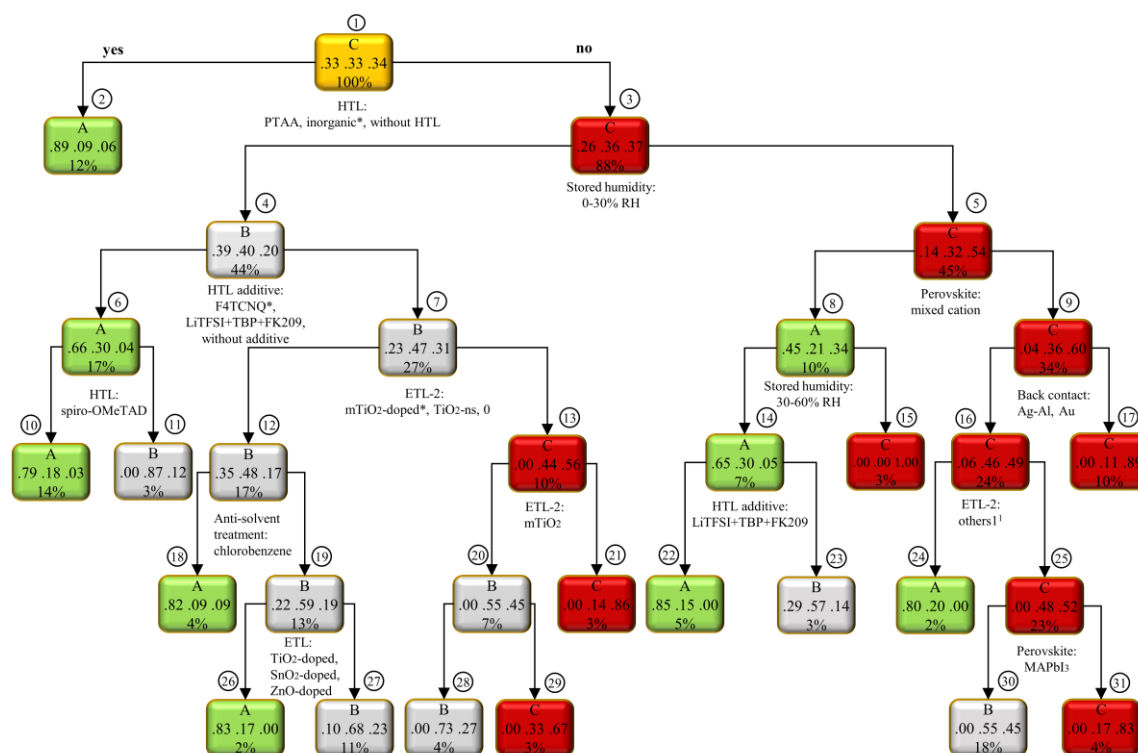
Table D.6. Association Rule Mining for Inverted (p-i-n) Cells Stable More Than 60 Days.

Antecedent	Consequent	Support	Confidence	Lift	Data count
Stable more than 60 days	Precursor solution=DMF+others*	0.02	0.25	3.79	2
	O ₂ =no	0.08	0.88	3.06	7
	HTL-2=others**	0.01	0.13	2.28	1
	Stored humidity=0-30% RH	0.09	1.00	2.28	8
	ETL-2=BCP	0.04	0.50	1.98	4
	HTL=GO	0.01	0.13	1.90	1
	Perovskite=MAPbI _{3-x} Cl _x	0.02	0.25	1.63	2
	Deposition method=spin-spin	0.01	0.13	1.42	1
	Anti-solvent treatment=no	0.04	0.50	1.42	4
	HTL=NiO _x	0.02	0.25	1.34	2
	Precursor solution=DMF	0.04	0.50	1.34	4
	Stored condition=room-light	0.09	1.00	1.28	8
	HTL=PEDOT:PSS	0.05	0.63	1.21	5
	Deposition method=spin 2-3	0.03	0.38	1.18	3
	Deposition procedure=two-step	0.01	0.13	1.14	1
	ETL=PCBM	0.09	1.00	1.14	8
	Back contact=Ag	0.08	0.88	1.06	7
	Back contact=Al	0.01	0.13	1.03	1
	Anti-solvent treatment=chlorobenzene	0.02	0.25	0.99	2
	Deposition procedure=one-step	0.08	0.88	0.98	7
	Perovskite=MAPbI ₃	0.07	0.75	0.96	6
	ETL-2=others****	0.01	0.13	0.95	1
	HTL-2=0	0.08	0.88	0.94	7

Table D.6. Association Rule Mining for Inverted (p-i-n) Cells Stable More Than 60 Days (cont.).

Antecedent	Consequent	Support	Confidence	Lift	Data count
	Deposition method=spin	0.04	0.50	0.91	4
	Anti-solvent treatment=toluene	0.02	0.25	0.73	2
	Precursor solution=DMSO+GBL	0.01	0.13	0.71	1
	ETL-2=0	0.03	0.38	0.68	3
	Precursor solution=DMF+DMSO	0.01	0.13	0.60	1
	O ₂ =yes	0.01	0.13	0.18	1

*others: N-cyclohexyl-2-pyrrolidone (CHP), GO
 **others: diethanolamine (DEA)
 ***others: amino-functionalized polymer (PN4N)



¹ Term of "others" were explained in Table D.9.

Figure D.1. Decision tree model for regular (n-i-p) cells in stability analysis without PCE consideration (minimum split number=5, maximum depth=6, complexity parameter=0).

Table D.7. Confusion Matrix of Regular Cells Without PCE Consideration.

		Actual Class			
		Class A	Class B	Class C	Precision
Predicted Class	Class A	87	15	4	82%
	Class B	5	68	35	63%
	Class C	0	9	55	86%
Accuracy		95%	16%	4%	
Overall accuracy		76%			

Table D.8. Explanation for the Term of “others” in Figure 4.29.

	Article name	Instance	Article name	Instance	Article name	Instance
Others1	Yu, Y. <i>et al.</i> , ChemSusChem 9, 3288–3297 (2016)	Pb(SCN) ₂	Hou, X. <i>et al.</i> , ACS Appl. Mater. Interfaces 9, 35200–35208 (2017)	TPA	Wang, S. <i>et al.</i> , Sol. RRL 2, 1800034 (2018)	thiourea
	Guo, J. J. <i>et al.</i> , Sol. Energy 155, 121–129 (2017)	NMP	Yu, W. <i>et al.</i> , Nano Energy 45, 229–235 (2018)	BQ		
	Article name	Instance	Article name	Instance	Article name	Instance
Others2	Mahmud, M. A. <i>et al.</i> , Electrochim. Acta 222, 1510– 1521 (2016)	TBP	Wei, J. <i>et al.</i> , Nano Energy 26, 139–147 (2016)	PCBM	Liu, C. <i>et al.</i> , J. Phys. Chem. C 121, 6546– 6553 (2017)	TBP
	Chen, H. Bin <i>et al.</i> , ACS Appl. Mater. Interfaces 10, 2603–2611 (2018)	C60/o-DCB	Xiang, W. <i>et al.</i> , J. Mater. Chem. A 5, 5486–5494 (2017)	PDMSurea	Fei, C. <i>et al.</i> , Adv. Energy Mater. 7, 1602017 (2017)	thiourea
	Chen, H. Bin <i>et al.</i> , ACS Appl. Mater. Interfaces 10, 2603–2611 (2018)	o-DCB	Zhao, Y. <i>et al.</i> , Nat. Commun. 7, 10228 (2016)	PEG		

Table D.9. Explanation for the Term of “others” in Figure D.1.

	Article name	Instance	Article name	Instance	Article name	Instance
Others1	Hou, X. <i>et al.</i> , Sol. Energy Mater. Sol. Cells 149, 121– 127 (2016)	ZnGa ₂ O ₄	Dang, V. Q. <i>et al.</i> , Org. Electron. physics, Mater. Appl. 50, 247– 254 (2017)	ZnO-nanorod	Lee, Y. <i>et al.</i> , Adv. Sci. 5, 1800130 (2018)	passivated SnO ₂

Table D.9. Explanation for the Term of “others” in Figure D.1.(cont.).

	Article name	Instance	Article name	Instance	Article name	Instance
	Lei, Y. <i>et al.</i> , J. Mater. Chem. A 4, 5474–5481 (2016)	mZnO	Gao, C. <i>et al.</i> , Chem. Eng. J. 325, 378–385 (2017)	ZnO-nanorod		